ORNL/TM-7777

ornl

OAK RIDGE NATIONAL LABORATORY

UNION CARBIDE

Initial Trade and Design Studies for the Fusion Engineering Device

C. A. Flanagan D. Steiner G. E. Smith
Fusion Engineering Design Center Staff

FEDC

OPERATED BY
UNION CARBIDE CORPORATION
FOR THE UNITED STATES
DEPARTMENT OF ENERGY

Printed in the United States of America. Available from
National Technical Information Service
U.S. Department of Commerce
5285 Port Royal Road, Springfield, Virginia 22161
NTIS price codes—Printed Copy: A15 Microfiche A01

ORNL/TM-7777
Dist. Category UC-20 c, d

Contract No. W-7405-eng-26

FUSION ENERGY DIVISION

INITIAL TRADE AND DESIGN STUDIES FOR THE FUSION ENGINEERING DEVICE

C. A. Flanagan D. Steiner G. E. Smith
Fusion Engineering Design Center Staff

Date Published: June 1981

NOTICE This document contains information of a preliminary nature. It is subject to revision or correction and therefore does not represent a final report.

Prepared by the
OAK RIDGE NATIONAL LABORATORY
Oak Ridge, Tennessee 37830
operated by
UNION CARBIDE CORPORATION
for the
DEPARTMENT OF ENERGY

CONTENTS

FIGURES

TABLES

ABSTRACT

The Magnetic Fusion Energy Engineering Act of 1980 calls for the operation of a Fusion Engineering Device (FED) by 1990. It is the intent of the Act that the FED, in combination with other testing facilities, will establish the engineering feasibility of magnetic fusion energy. The Fusion Engineering Design Center (FEDC), under the guidance of a Technical Management Board (TMB), initiated a program of trade and design studies in October 1980 to support the selection of the FED concept. This document presents the results of these initial trade and design studies. Based on these results, a baseline configuration has been identified and the Design Center effort for the remainder of the fiscal year will be devoted to the development of a self-consistent FED design description.

ACKNOWLEDGMENTS

We wish to acknowledge the dedication and skill of Linda Caldwell, Shirlene Dale, Sandra Vaughan, and Kathie Zell, who provided the secretarial services essential to production of this report. We also wish to thank P. Fogarty, H. Hankins, W. Kunselman, and C. King for the high level of cooperation which they displayed on preparation of the original drawings and figures and E. L. Watkin and staff for preparation of the final artwork for the document. Finally, we express our thanks to M. N. Johnson and her colleagues for the expeditious manner in which they provided editing support. Without their efforts, this report would not have been possible.

C. A. Flanagan
G. E. Smith
D. Steiner — Editors

1. EXECUTIVE SUMMARY

1.1 INTRODUCTION

The Magnetic Fusion Energy Engineering Act of 1980 calls for the operation of a Fusion Engineering Device (FED) by 1990. It is the intent of the Act that the FED, in combination with other facilities, will establish the engineering feasibility of magnetic fusion energy. In order to proceed with planning for the FED program, the Office of Fusion Energy (OFE) established at the beginning of FY 81 a Technical Management Board (TMB) to oversee all FED-related activities. The composition of the TMB and the elements working under the board's direction are shown in Fig. 1.1. The Fusion Engineering Design Center (FEDC), under the direction of Don Steiner, is responsible for FED design activities. The Physics Group, under the direction of Paul Rutherford, establishes the physics basis for the FED and gives physics guidance to the design evolution. The Technology Group, under the direction of Charles Baker, examines the scope of engineering testing which can be accomplished by the FED and by other facilities. The linkage with the U.S. International Tokamak Reactor (INTOR) activity, directed by W. M. Stacey, ensures that the FED effort benefits from the INTOR design effort.

The primary objectives of the FY 81 FED activity are twofold: (1) to select the FED concept and (2) to document the concept and the selection process. During the period from October 1980 to March 1981, the focus of the Design Center has been on trade and design studies. The objectives of these studies have been to develop a baseline concept for the FED and to examine the design space around the baseline. This document describes the current baseline concept and presents the results of the trade and design studies. It is emphasized that the information presented here does not constitute a design description; significant effort remains to develop a self-consistent FED design. This will be accomplished during the period from March 1981 to September 1981.

FED/VU 81-5R

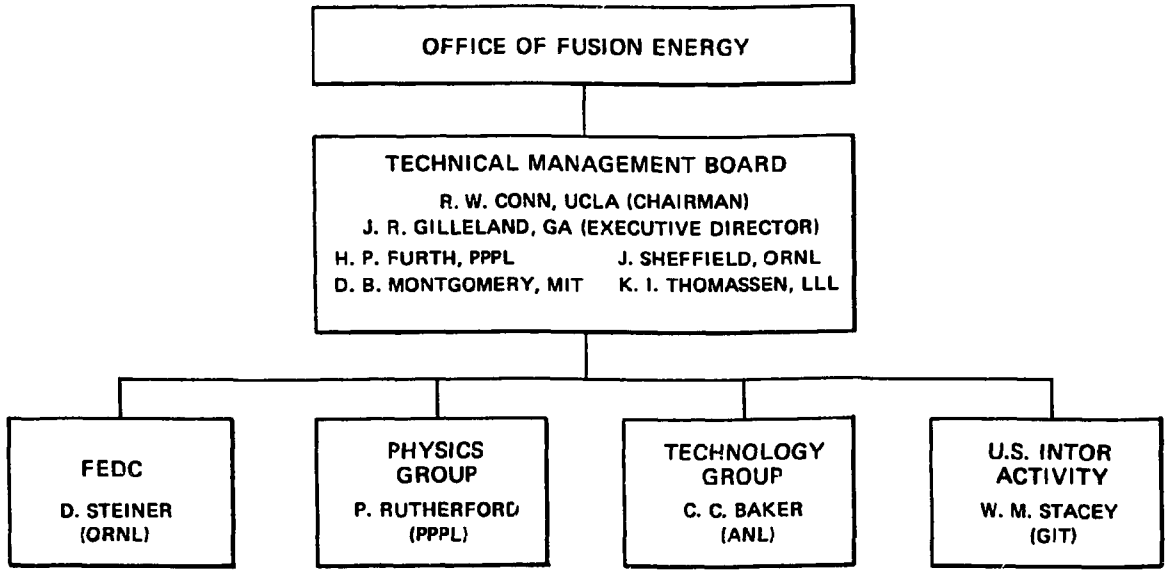

Fig. 1.1. Composition of the TMB established by the OFE to oversee FED-related activities.

1.2 CONTEXT OF STUDIES

As a point of departure for the FED trade and design studies, the TMB with input from its constituent elements established a set of working parameters and guidelines. A precursor to the establishment of the working parameters and guidelines was the TMB's conclusion that at this time the FED should be based on the tokamak concept. These working parameters and guidelines are summarized in Table 1.1 and are based on the following considerations: (1) the requirement to satisfy the general FED technical objectives as articulated in the Magnetic Fusion Energy Engineering Act of 1980, (2) the assessment of the existing and anticipated physics and technology data base supporting the implementation of the FED, and (3) the desire to develop a FED with acceptable costs, engineering requirements, and risks. Although the choices of working parameters and guidelines were influenced by all three considerations, in each individual case certain considerations were dominant, as indicated below.

- The fusion power level, the neutron wall loading, and the burn time specifications were most influenced by the general FED technical objectives and by cost considerations.
- The toroidal field (TF) coil maximum field level was most influenced by the testing goals of the Large Coil Program (LCP).
- The specified plasma elongation reflects physics considerations about beta and confinement.
- The choices of plasma radius and major radius were influenced both by physics considerations (confinement and beta) and by cost considerations.
- The specification of a driven mode of operation ($Q \sim 5$) reflects the desire to reduce the cost and risk related to the ignition requirement.
- The choices of ion cyclotron resonance heating (ICRH) and the pump limiter are an attempt to seek relatively simple engineering solutions for plasma heating and for particle and impurity control, respectively.

Table 1.1. Working parameters and guidelines established by the TMB for FED trade and design studies

Plasma burn mode	Driven, $Q \sim 5$
Plasma radius (m)	1.3
Major radius (m)	4.8
Plasma elongation	1.6
TF coil maximum field (T)	8.0
Bulk heating technique	ICRH
Particle and impurity control	Pump limiter
Fusion power (MW)	~200
Neutron wall loading (MW/m^2)	~0.5
Burn time (s)	~100

Using the parameters and guidelines given in Table 1.1, a full set of system parameters and configuration layouts was developed. These preliminary system parameters and configuration layouts constituted a description of the preliminary FED baseline concept and provided the basis about which trade and design studies were performed. The trade studies focus on cost and performance implications of variations about the baseline; the design studies focus on the engineering feasibility of systems. In developing the scope of the trade and design studies, emphasis was given to those issues and systems that represent major cost drivers, major performance drivers, and major engineering drivers.

1.3 RESULTS

A major initial trade study was directed to the question of a strategy for the goal of demonstrating engineering feasibility. Consistent with this goal, it is possible to define several different fusion engineering devices, each representing differing levels of mission, cost, complexity, and risk. Each device will necessarily have associated with it differing levels of complementary facilities. In Sect. 2 the implications of alternate devices and missions for the FED are examined. It is concluded that the device represented by the working parameters and guidelines (Table 1.1) is an appropriate device based on considerations of cost, complexity, and risk.

As a consequence of the overall study effort, substantial progress was made with regard to the evolution of the FED baseline concept. The current baseline concept is described in Sect. 3. Table 1.2 and Figs. 1.2 and 1.3 summarize the essential features of the baseline.

The plasma engineering analyses described in Sect. 4 suggest that the baseline can achieve its nominal plasma performance goals ($Q \sim 5$, neutron wall loading ~ 0.5 MW/m^2, and burn time ~ 100 s) under a range of reasonable assumptions and eventualities. The engineering design studies described in Sects. 5-8 indicate feasible concepts for key components such as the TF coils, the plasma heating systems, and the limiter. The only key component of the baseline for which a feasible concept does not currently exist is the poloidal field (PF) system.

Table 1.2. Key parameters of current FED baseline concept

Major radius (m)	4.8
Plasma radius (m)	1.3
Plasma elongation	1.6
Fusion power (MW)	180
Neutron wall loading (MW/m^2)	0.4
Heating power (MW)	
Initial	50
Burn	36
Q	5
Burn time (s)	$\geq$100
Duty cycle	0.65
Average D-T density (m^{-3})	0.8×10^{20}
Average ion temperature (keV)	10
Average total beta (%)	5.5
Safety factor at edge	3.2
Poloidal beta/aspect ratio	0.5
Plasma current (MA)	
Low beta	4.8
High beta	5.4
Number of TF coils	10
Clear bore, width times height (m)	7.5×10.9
Field on axis (T)	3.6
Peak field at winding (T)	8.0
Number of full field pulses	3.5×10^5
Availability (%)	10-20

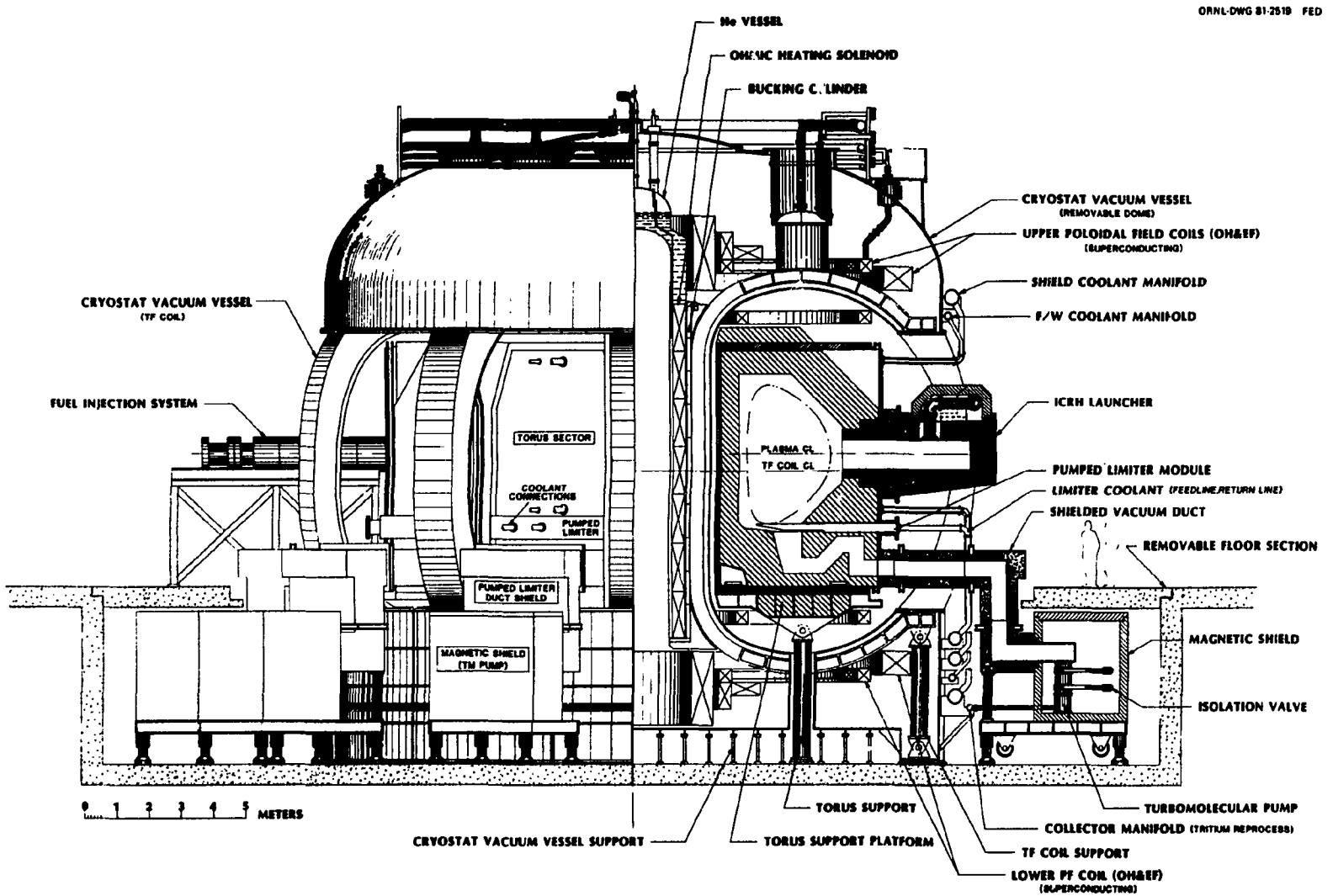

Fig. 1.2. General elevation view of FED.

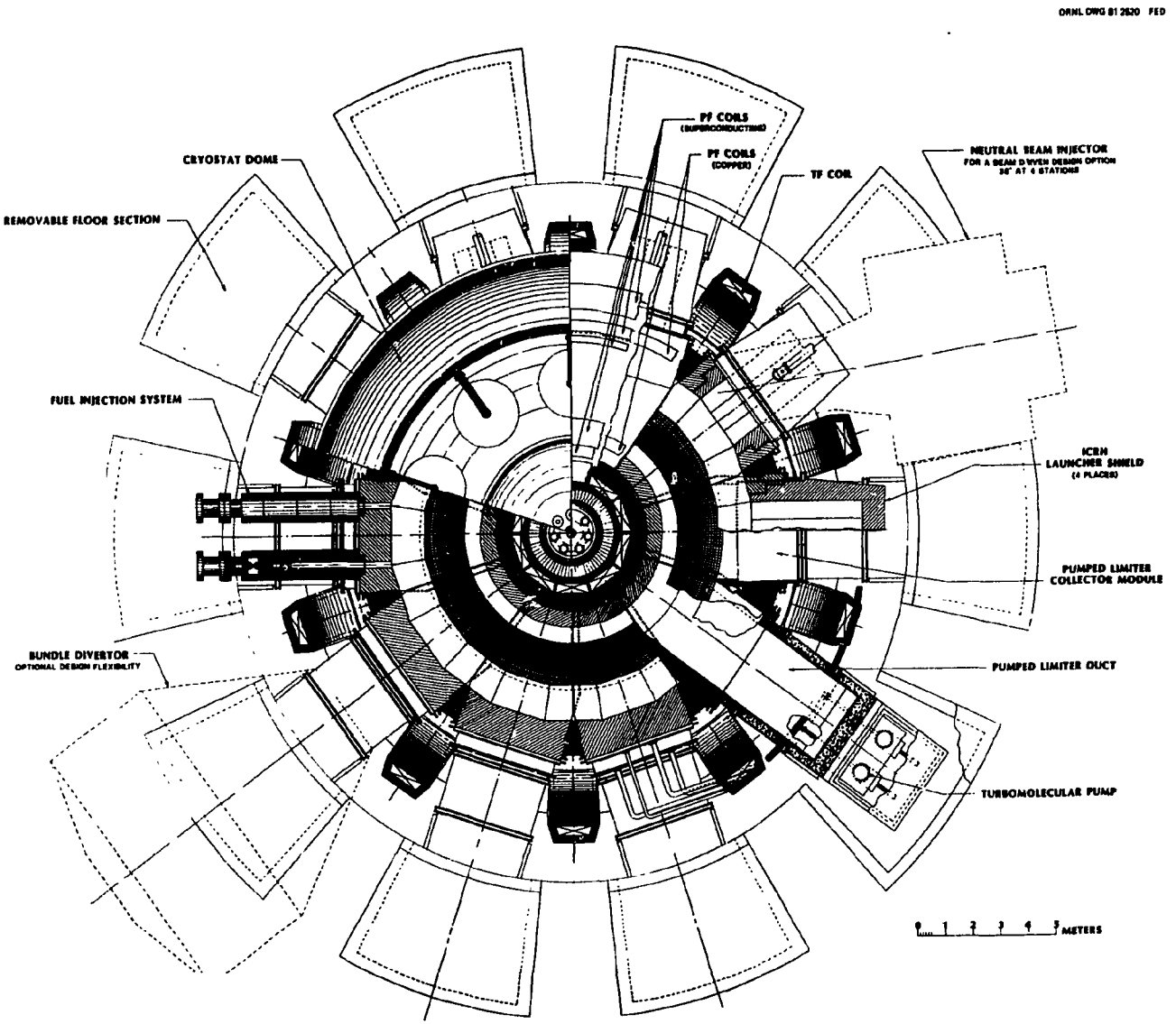

Fig. 1.3. General plan view of FED.

However, several options for the PF system have been identified, and it is expected that at least one of these options will yield a feasible concept.

A number of trade studies was performed to examine cost and performance sensitivity around the baseline. The key results of the trade studies are summarized below.

1. Number of pulses. An assessment of the number of pulses that the FED might sustain over a projected 10-year life was performed. A range of 5×10^4 to 1×10^6 pulses was considered. A value of 3.5×10^5 full field pulses has been recommended as a baseline value for design purposes.

2. Device size. Overall system trade studies suggest that, while the current baseline cannot be viewed as optimized with respect to size, it does approach a minimum cost device for the desired performance goals. Potential reductions in machine size (the key cost driver) relative to the baseline are limited by volt-second requirements necessary to maintain a plasma current of 5.4 MA and achieve the burn time of $\sim$100 s. To retain an adequate performance margin, it is recommended that the baseline values of plasma radius (1.3 m) and major radius (4.8 m) not be reduced.

3. Device flexibility. The cost of incorporating design flexibility necessary to (1) take advantage of better than assumed physics performance and/or (2) meet planned objectives in the face of lower than expected physics performance was estimated to be $\sim$15% relative to the baseline capital cost.

4. Field ripple variation. The impact of varying ripple on cost and access was investigated. Several approaches to modify ripple, both passive and active, were investigated; the approaches included variations in TF coil size, the use of magnetic material in the plane of the TF coil, and the use of trim coils. The results indicated that magnetic material could be used to reduce the ripple with minimal cost increment.

However, the current FED baseline configuration has an edge ripple of ~0.8%, and reduction of the ripple below this level does not appear necessary or warranted at this time.

Although a baseline concept has been developed, it is desirable to retain promising system options in this phase of the FED activity. A number of studies examined system options. The options considered and the recommendations proposed are summarized below.

1. Particle and impurity control. In the plasma engineering investigations, particular emphasis was directed to options in the area of particle and impurity control. The poloidal divertor has been identified as the primary alternative to the pump limiter and will be pursued in future FED design activities.

2. Field enhancement. In order to gain some additional margin with regard to performance, several options for achieving a 1- to 2-T enhancement of the toroidal field on axis were investigated. The results indicated that although these options are feasible, they are likely to result in substantial increases in complexity in the design and may be no less risky than designing the TF coils to higher field strength performance from the outset. It is recommended that these options not be pursued at this point.

3. Bulk heating. The application of neutral beam injection (NBI) for bulk heating in FED was investigated as an alternative to the baseline ICRH system. It was concluded that neutral beam injection appears to be a feasible, practical alternative to rf heating in FED and should be retained as an option.

4. Startup. A number of startup options were considered for FED. The use of small amounts of electron cyclotron resonance heating (ECRH) for plasma initiation appears to be the most efficient option and may also prove to be the most relevant for reactors. Nevertheless, at this

time, other rf options need to be retained for plasma initiation as well as the more conventional approach using the ohmic heating (OH) system.

5. Facilities. The initial studies of the FED facilities were directed toward (1) definitions of the options and major factors influencing the design of tokamak cell and hot cell areas and (2) an assessment of the design and cost impacts imposed by these options. Several feasible approaches have been established. Their development will continue in close coordination with the design of the basic machine.

1.4 FUTURE ACTIVITIES

As a guide to the next phase of FED concept development, a number of key issues require a choice or a statement of position. Table 1.3 summarizes these key issues. In each case, the table indicates the major considerations and identifies the recommended choice for the future design effort. During the remainder of this fiscal year, the Design Center efforts will be directed toward the following activities:

- Develop a point design of FED with feasible solutions for all systems; provide the rationale for the choices made.
- Determine the FED performance over a range of physics assumptions.
- Prepare the necessary configuration layout drawings.
- Prepare a cost projection and associated design and construction schedule.
- Perform an update on the research and development needs for FED.
- Prepare and issue documentation of the effort.

Table 1.3. FED key issues, major considerations, and recommendations

Issue	Major considerations	Recommendations
Mission in terms of device alternatives	Three levels (as discussed in Sect. 2)	Proceed with FED design assuming a Level II mission
Position on cost	Establish FED mission (and therefore device level) and design device to minimize cost (i.e., cost the design) or establish a cost objective and design device to maximize capability within the cost limit (i.e., design to cost)	Design device to achieve mission at minimum cost
Operating schedule	A 10-year operating life and $\sim 3.5 \times 10^5$ pulses (100 s) vs fewer pulses with longer pulse time. A range of 5×10^4 to 1×10^6 pulses was considered	Design to 10-year operating life assuming 3.5×10^5 pulses at 100 s
Power output	Design baseline for currently calculated 180 MW vs incorporating into baseline capability to accommodate significantly increased D-T power	Design to 180 MW, but assess impact of providing first wall and blanket components to handle conditions appropriate to twice the power level
Heating capability	Design to provide capability assuming Q = 5 vs providing capability to operate even if Q = 2	Design heating capability assuming Q = 5
Plasma current capability	Design baseline for present high beta plasma current of 5.4 MA vs providing for capability to operate at higher current ($\geq$6.0 MA) should plasma physics permit	Design for high beta plasma current of 5.4 MA, but assess impact of coil design to provide capability of $\geq$6.0 MA

2. FED MISSION AND DEVICE ALTERNATIVES

2.1 INTRODUCTION

This section examines the implications of mission and device alternatives for the FED. Consistent with the goal of demonstrating engineering feasibility in the 1990s, it is possible to define several different fusion engineering devices, each representing differing levels of mission, cost, complexity, and risk. Each device will necessarily require differing levels of complementary facilities in order to achieve the overall goal of engineering feasibility. In this section the discussion is limited to considerations of device alternatives. The Technology Group (see Fig. 1.1) is addressing the issue of complementary facilities.

In conducting this study, the following approach was adopted.

1. Three alternate missions were defined in terms of test objectives with increasing levels of achievement.
2. Device features and requirements were established for each mission.
3. Capital costs were estimated for each device.

2.2 MISSION ALTERNATIVES FOR THE FED

Using the Engineering Test Facility (ETF) Mission Statement Document[1] and the International Tokamak Reactor (INTOR) Test Plan,[2] three mission alternatives were defined in terms of test objectives with increasing levels of achievement. These alternatives are designated Levels I, II, and III and are summarized in Table 2.1. Note that each subsequent level (i.e., mission) includes the previous level. Thus, the Level II mission includes the Level I mission (plasma engineering and engineering operations) as well as nuclear engineering. The Level III mission includes plasma engineering, engineering operations, and nuclear engineering, as well as component and materials qualification. The Level II mission is that currently envisioned for the FED.

Table 2.1. Mission alternatives for the FED

- Level I = Plasma engineering + engineering operations
  - Demonstrate long-pulse capability of components to control reactor-grade plasma
  - Demonstrate systems integration based on reactor-relevant technologies
  - Demonstrate maintenance operations in a radioactive environment
  - Demonstrate safety of operations
- Level II = Level I + nuclear engineering
  - Demonstrate performance of blanket with significant fusion power
  - Demonstrate total tritium fuel cycle
- Level III = Level II + component and materials qualification
  - Establish high fluence performance
  - Develop reliability data base

Table 1.3 (continued)

Issue	Major considerations	Recommendations
Toroidal field enhancement	Design for field at plasma axis resulting from a maximum field at coil winding of 8 T vs providing for capability to enhance field at plasma by 1-2 T	Design for TF field with field at coil of 8 T and no field enhancement capability
Ripple modification	Accept ripple that naturally results from design or incorporate ripple modification option	Do not design for ripple modification
Startup	Design for rf-assisted startup vs conventional startup approach	Design for rf-assisted startup
Pumping and particle control	Mechanical pump limiter (hot and cold plasma edge) vs poloidal divertor vs bundle divertor	Design for mechanical pump limiter. Also design for poloidal divertor as an alternate
Bulk heating	Ion cyclotron resonant heating vs positive ion neutral beams vs negative ion neutral beams	Design for ion cyclotron resonant heating. Continue to carry neutral beams as an alternate

2.3 DEVICE FEATURES AND REQUIREMENTS

The essential features and requirements of the devices necessary to achieve the alternate missions defined in Table 2.1 are summarized in Table 2.2. Here the Level I device represents a base case and the Level II and Level III device features and requirements are presented as incremental characteristics. The Level I device operates with a catalyzed deuterium-deuterium-tritium (D-D-T) fuel, which provides low fusion power and tritium consumption while at the same time providing a radioactive environment. Thus, neutron shielding, tritium handling equipment, and reactor-relevant maintenance operations are required for the Level I device. The Level II device represents the current FED baseline. The features and requirements of the Level III device are similar to those of ETF/INTOR.

2.4 METHOD OF ANALYSIS AND KEY GROUND RULES

In order to generate a set of consistent device parameters and also to provide preliminary cost estimates, the FEDC systems code was employed (see the Appendix). In order to ensure a common basis for analysis, a number of ground rules were established. These ground rules are summarized below.

1. Beta was held constant for all devices at $\sim$6% and plasma elongation was held constant at 1.6.
2. The toroidal field (TF) coils were assumed to be NbTi operating at a maximum field of 8 T.
3. The pulse length was held constant at $\sim$100 s.
4. The outboard shield was sized to allow hands-on maintenance 24 h after shutdown.
5. Reactor-relevant maintenance assumes that only translational movement of sectors is allowed.

2.5 RESULTS

Table 2.3 summarizes the key parameters which characterize the devices associated with each alternate FED mission. Note that the

Table 2.2. Features and requirements of devices associated with the FED mission alternatives

	Level I (base)		Level II (incremental)	Level III (incremental)
Features	• Long pulse (∿100 s) • Reactor-grade plasma • Reactor technology • Availability ∿ 10-20%	• Remote maintenance • Radioactive environment • Low power and tritium • D-D-T fuel	• Substantial fusion power ∿ 200 MW • L_n ∿ 0.5 MW/m^2 • Availability ∿ 10-20% • ∿1 kg tritium/ year	• $L_n \geq 1$ MW/m^2 • Availability ∿ 50% • ∿10 kg tritium/ year
Plasma requirements	• Control • $\beta \geq 5\%$ • $n\tau$ ∿ few × 10^{13}	• $\bar{T}$ ∿ 5-10 keV • L_p ∿ 20-30 W/cm^2	• Enhanced a, B_t, or β • Burn control	• Enhanced a, B_t, or β
Eng/tech requirements	• Steady-state systems: First wall Armor Limiter Heating • Superconducting TF coils	• Access for maintenance • Neutron shielding • RM equipment • Tritium handling equipment	• Neutron shielding • Blanket test capability • Access for tests • Heat dissipation	• Tritium breeding • Redundancy • Reliability • Shielding

NOTES: L_p is the plasma thermal flux to the wall, L_n is the neutron wall loading, and RM stands for remote maintenance.

Table 2.3. Device parameters for alternative FED missions

	Level I	Level II	Level III
Plasma radius (m)	0.8	1.3	1.5
Major radius (m)	3.5	4.8	6.0
Aspect ratio	4.4	3.7	4.0
Field on axis (T)	4.3	3.6	4.1
Plasma current (MA)	3.2	5.4	6.4
Number of coils	10	10	10
Bore (m x m)	4.5 x 6.4	7.5 x 10.9	8.9 x 12.6
Fusion power (MW)	0.5	180	485
Neutron wall loading (MW/m^2)	0.0025	0.4	0.8
Shield thickness (inner/outer) (cm)	20/80	70/115	80/120
Heating power (MW)	46	36	35

devices characterized in this table do not represent optimizations for each level of mission; rather, they represent devices that nominally satisfy the features and requirements described in Table 2.2. The choice of plasma radius for the Level I device was made on the basis that a reactor-grade plasma should be no smaller in radius than the Tokamak Fusion Test Reactor (TFTR). The major radius of the Level I device is dictated primarily by the volt-seconds required to start up and achieve the 100-s pulse.

The Level II device is the current FED baseline. The Level III device was sized to achieve about twice the neutron wall loading of the Level II device. The Level I and Level II devices operate in a driven mode. The Level III device would achieve ignition with the physics models employed.

Relative capital costs for the three devices were generated by the FEDC systems code. If the Level II device capital cost is normalized to a value of 1.0, then the Level I device relative capital cost is 0.6 and the Level III device relative capital cost is 1.4. It is noted that the key cost drivers in moving from the Level I device to the Level III device are the increases in (1) shielding, (2) size of the TF coils, (3) requirements on the poloidal field (PF) coils and the associated electrical equipment, and (4) building sizes.

The capital costs generated by the FEDC systems code do not reflect the costs associated with availability requirements. Because of the high availability required for component and materials qualification, it is expected that the relative cost of the Level III device will, in fact, be substantially greater than the value of 1.4 derived from the systems code. Also, it is noted that the Level III device has a high tritium consumption rate, ~10 kg/year, and, therefore, will require some level of tritium breeding. This requirement, coupled with the need for some component redundancy (high availability), increases the relative complexity and technological risk of the Level III device.

2.6 CONCLUSIONS

On the bases of relative cost, complexity, and risk, it appears that the Level III device (similar to ETF/INTOR) is too ambitious as a

FED. The Level I device offers attractive relative cost, complexity, and risk. However, it does not provide a demonstration of either blanket performance or the total tritium fuel cycle. These demonstrations are considered to be essential to engineering feasibility and need to be part of the FED mission. Therefore, it is recommended that the Level II mission and device be retained as the context for the FED mission and FED baseline concept.

3. CURRENT FED BASELINE

Fusion Engineering Design Center Staff

This section presents the current FED working parameters and configuration layouts. It is emphasized that the FED design process results in evolutionary changes to many features of the design. The starting point of the FED design effort (October 1980) was a set of guiding parameters established in conjunction with the FED Physics Group under the guidance of P. H. Rutherford. During the intervening months, the work of several Physics Group task teams, in conjunction with the efforts of the FEDC staff, has resulted in revisions to the initial set of working parameters and the associated configuration layouts. As the design effort continues, changes to the working parameters and design configuration will be incorporated as necessary.

The current (March 1981) working parameters for FED are presented in Table 3.1. Information on radial dimensions is given in Table 3.2, on disruption frequency in Table 3.3, and on neutral beam studies in Table 3.4. Performance defined in these tables should be viewed as "nominal."

Associated with the information given in the tables and equally important in constituting the FED baseline are configuration layout drawings that depict the geometrical features of the design and its constituent subsystems. Figures 3.1-3.4 are configuration layout drawings for the current baseline.

As indicated by these data, the baseline FED has a major radius of 4.8 m and a minor radius of 1.3 m and employs a plasma elongation factor of 1.6.

The plasma chamber is assembled by inserting ten 36° shield sectors into a spool support structure. The outer edges of the shield sector are sealed with a support frame of the spool structure and form the vacuum boundary for the plasma chamber.

Table 3.1. FED working parameters

Description	Unit	Value
Geometry		
Major radius, R	m	4.8
Plasma chamber radius, r_w	m	1.5
Plasma radius, a	m	1.3
Plasma elongation, κ	m	1.6
Plasma triangularity, δ		0.5
Aspect ratio, A		3.7
Plasma chamber volume at shield inner surface	m^3	385
Plasma volume	m^3	257
Plasma chamber area	m^2	366
Plasma		
Average ion temperature, $\langle T_i \rangle$	keV	10
Average D-T ion density, $\langle n_i \rangle$	10^{20} m^{-3}	0.78
Average electron density, $\langle n_e \rangle$	10^{20} m^{-3}	0.84
Safety factor (edge), q_ψ (flux surface averaged)		3.2
Effective charge (during burn), Z_{eff}		1.5
Field on axis, B_t	T	3.6
Plasma current, I_p		
Low beta	MA	4.8
High beta	MA	5.4
TF ripple (peak-to-average)		
Center	%	±0.07
Mid-radius	%	±0.27
Edge	%	±0.78
Total beta, $\langle \beta \rangle$	%	5.5
Plasma thermal beta, $\langle \beta_{thermal} \rangle$	%	5.0
Poloidal beta, β_p		1.8

Table 3.1. (continued)

Description	Unit	Value
Operating mode		
Total D-T fusion power, P_{th}	MW(t)	180
Energy confinement time, τ_E	s	1.4
Burn time, t_{burn}	s	$\geq$100
Cycle time, t_{cycle}	s	$\geq$152
Pumpdown time, t_p	s	30
Startup/shutdown time, t_{ss}	s	12/10
Number of full field pulses/lifetime		3.5×10^5
Lifetime	years	10
Plasma thermal power balance (during burn)		
Total D-T fusion power	MW	180
D-T fusion power (neutrons)	MW	144
D-T fusion power (alpha particles)	MW	36
Bulk heating power into plasma during burn	MW	36
Fusion power amplification, Q		5
Total thermal power deposited on plasma chamber surfaces	MW	72
• Power to first wall/armor	MW	16
Charge exchange neutrals	MW	8
Radiation	MW	8
• Power to limiter, charged particles	MW	56
Plasma disruptions		
Probability per pulse (Varies with operating sequence, see later listing)		10^{-1}-10^{-3}
Thermal quench and voltage spike		
Time for thermal quench	ms	5
Thermal energy deposition per disruption	MJ	90

Table 3.1. (continued)

Description	Unit	Value
Region of deposition		
First wall (uniform)	MJ	45
Limiter (uniform)	MJ	45
Peak voltage at plasma	V	1000
Change in plasma magnetic flux	Wb	5
Subsequent current quench		
Time for current decay during disruption	ms	10
Thermal energy deposited during disruption	MJ	10
Region of deposition		Inboard, top, bottom
Extent of region	%	20
Peaking factor		10
Plasma magnetic energy deposited during disruption	MJ	60
Toroidal field coils		
Number		10
Conductor		NbTi or Nb_3Sn
Stabilizer		Cu
Peak design field at winding, B_m	T	8
Clear bore height	m	10.9
Clear bore width	m	7.5
Maximum tolerable radiation, epoxy	rads	10^9
Limiter resistivity change, stabilizer	%	TBD[a]
Overall current density (includes structure/helium)	A/cm^2	1600
Poloidal field coils		
Volt-seconds (total)		89
EF		22
OH		67
OH coil conductor		NbTi
OH maximum field allowable at coil	T	7
OH current ramp time	s	30

Table 3.1. (continued)

Description	Unit	Value
OH current density (internal to coil case)	A/cm^2	1500
EF coil conductor		
Exterior to TF coils		NbTi
Interior to TF coils		Cu
EF current density (internal to case)	A/cm^2	1500
Heating requirements[b]		
Startup		
Type (rf assist)		ECRH
Initiating voltage, with rf assist	V	25
Current rise time	s	6
Time duration for rf assist	s	0.2
Startup rf power	MW	1
Frequency	GHz	∿80
Bulk heating		
Type		ICRH
Species/harmonic		D^+/2nd
Pulse length	s	≥106
Initial	s	6
Burn	s	≥100
Power		
Initial	MW	50
Burn	MW	36
Frequency (B = 3.62 T)	MHz	∿54
Fueling		
Mode		Pellets and gas puff
Number of pellet injectors		2
Pellet velocity	m/s	2000
Injection rate[c]		
Startup	s^{-1}	20
Burn	s^{-1}	4

Table 3.1. (continued)

Description	Unit	Value
Pellet diameter	mm	4
Pellet composition		
Deuterium	%	>90
Tritium	%	>90
Mixed (T/D ratio)		0.5
Number of gas puffers		10
Puffer pulse time	ms	200
Puffer pulse rate	s^{-1}	5
Maximum gas puff rate	s^{-1}	4×10^{22}
Impurity and particle control		
Mode, particle control		Mechanical
Particle flux at edge of plasma	s^{-1}	9×10^{23}
Particle flux (molecular) to be pumped	s^{-1}	2×10^{22}
Pressure at entrance of channel	torr	10^{-2}
First wall/armor		
Material		
First wall material		Stainless steel
Armor material		Graphite
Coolant		H_2O
Average neutron wall load	MW/m^2	0.4
Protective mechanism		
Disruptions		Armor
Runaway electrons		Armor
Location of armor		Inboard, top and bottom surfaces, and surfaces adjacent to pump limiter
Average radiation heat load	W/cm^2	2
Total charge exchange power load to first wall	MW	8
Charge exchange particle energy	eV	1600
Total charge exchange particles	s^{-1}	3.1×10^{22}
Deposition area for charge exchange particles (includes limiter surface)	m^2	~80

Table 3.1. (continued)

Description	Unit	Value
Average charge exchange particle flux	$cm^{-2} \cdot s^{-1}$	4×10^{16}
Limiter		
Function		Pumping
Location		Bottom of chamber
Material, surface		Graphite
Coolant		H_2O
e-fold distance		
Particle flux, λ_n	cm	12
Particle energy, λ_T	cm	24
Heat flux, λ_Q	cm	8
Heat load during burn	MW	56
Associated with ions	MW	43
Associated with electrons	MW	13
Average energy of ions striking limiter	eV	300
Particle (ion) flux at edge of plasma	s^{-1}	9×10^{23}
Shield		
Inboard material (structure)		Stainless steel
Inboard coolant		Borated H_2O
Inboard thickness (excluding spool, armor, gaps, scrapeoff)	m	0.60
Outboard material (structure)		Stainless steel
Outboard coolant		Borated H_2O
Outboard thickness	m	1.15
Maximum structure temperature	°C	200
Dose rate limiter 24 h after shutdown	mrem/h	2.5
Tritium and vacuum		
Initial base pressure	torr	10^{-7}
Preshot base pressure	torr	3×10^{-5}
Postshot base pressure	torr	3×10^{-4}

Table 3.1. (continued)

Description	Unit	Value
Pressure at duct inlet during burn	torr	10^{-2}
External tritium fueling rate	s^{-1}	10^{22}
Helium generation rate	s^{-1}	6.5×10^{19}
Tritium fractional burnup	%	0.33
Tritium consumption, maximum (20% load factor)	kg/year	1.7
Total tritium inventory	kg	1.0
Overall system power balance (average over cycle)		
Thermal output (includes a neutron energy multiplication factor of 1.3)	MW(t)	TBD
Electrical requirements	MW(e)	TBD
Cryogenic requirements		
Liquid helium flow rate	m^3/h	78
Liquid helium inventory	m^3	266
Liquid nitrogen flow rate	m^3/h	13,900
Liquid nitrogen inventory	m^3	TBD

[a]TBD = to be determined.

[b]Parameters for studying neutral beam heating (now an alternate heating mode) are given in Table 3.4.

[c]Includes both deuterium and tritium.

Table 3.2. FED radial dimensions

	Thickness (m)	Radius (m)
Toroidal axis		0
OH bore	1.19	1.19
OH coil	0.40	1.59
Gap	0.04	1.63
Bucking cylinder	0.15	1.78
TF coil	0.42	2.20
Circle/trapezoid effect	0.11	2.31
Cryostat	0.20	2.51
Gap	0.05	2.56
Spool	0.05	2.61
Gap	0.05	2.66
Inboard shield	0.60	3.26
First wall	0.05	3.31
Scrapeoff	0.20	3.51
Plasma radius	1.30	4.81
Plasma radius	1.30	6.11
Scrapeoff	0.20	6.31
First wall	0.15	6.46
Outboard shield	1.15	7.61
Gap	2.35	9.96
Cryostat	0.20	10.16
TF coil	0.42	10.58
Cryostat	0.20	10.78

Table 3.3. FED operating sequence disruption frequency (for design purposes)

Phase	Description	Duration (years)	Disruption frequency	Disruption thermal energy (MJ)
I	Integrated systems checkout	0-1	10^{-1}	10
II	Hydrogen (deuterium) operations	1-3	10^{-1} to 10^{-2}	10-50
III	Initial D-T plasma operations	3-4	10^{-2} to 10^{-3}	100
IV	D-T engineering testing	4-10	10^{-3}	100

Table 3.4. Parameters for use in positive ion neutral beam studies on FED

Energy	150 keV
Power	
Bulk heating	45-50 MW
Steady-state	36 MW
Injection angle[a]	20°
(to normal at magnetic axis; equivalent to 16° at plasma edge)	
Species mix	
Full	60
Half	24
Third	16
Pulse length	
Bulk heating	6 s
Steady-state	Duration of burn

[a]Capable of quasi-tangential injection ($\leq$35°).

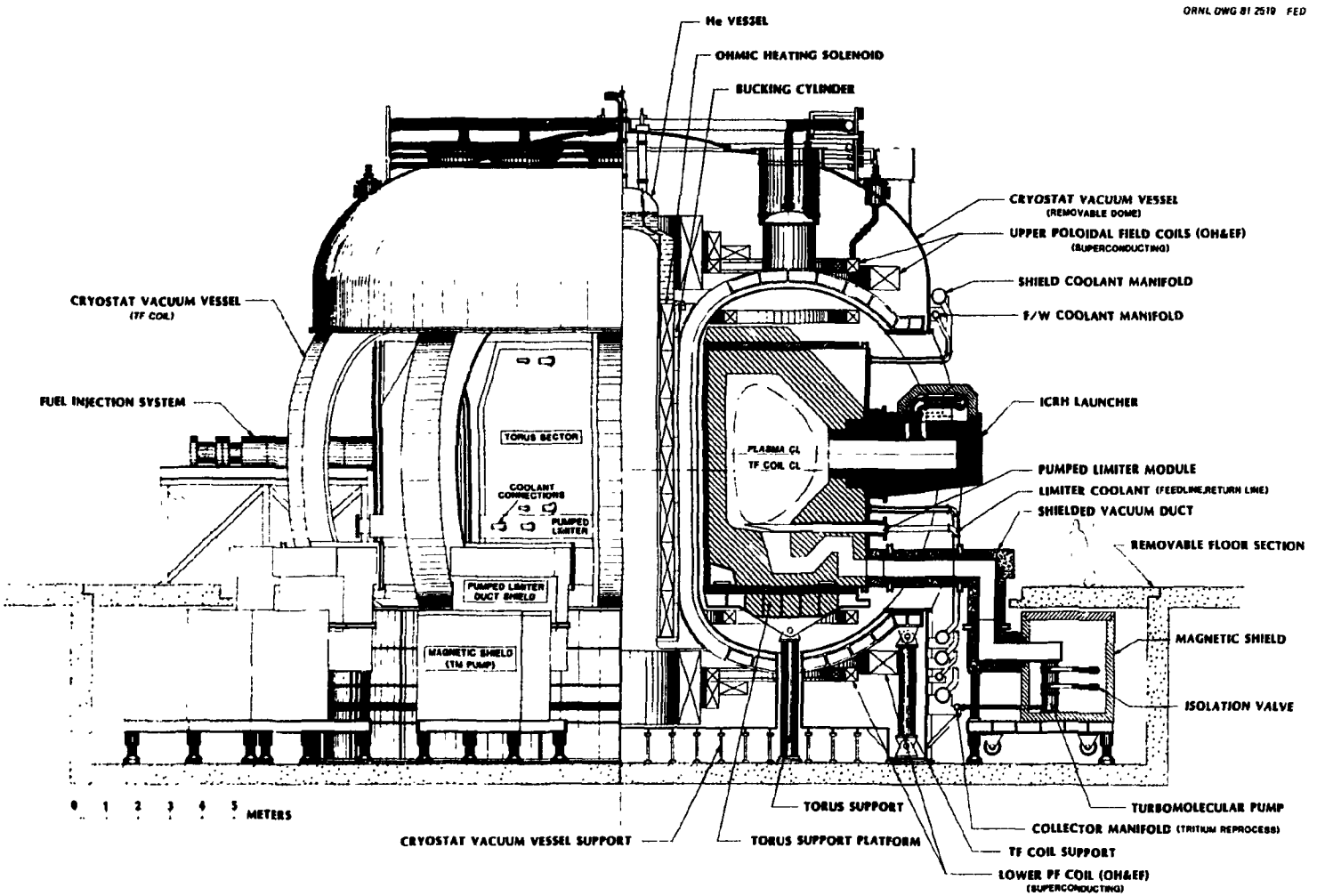

Fig. 3.1. General elevation view of FED.

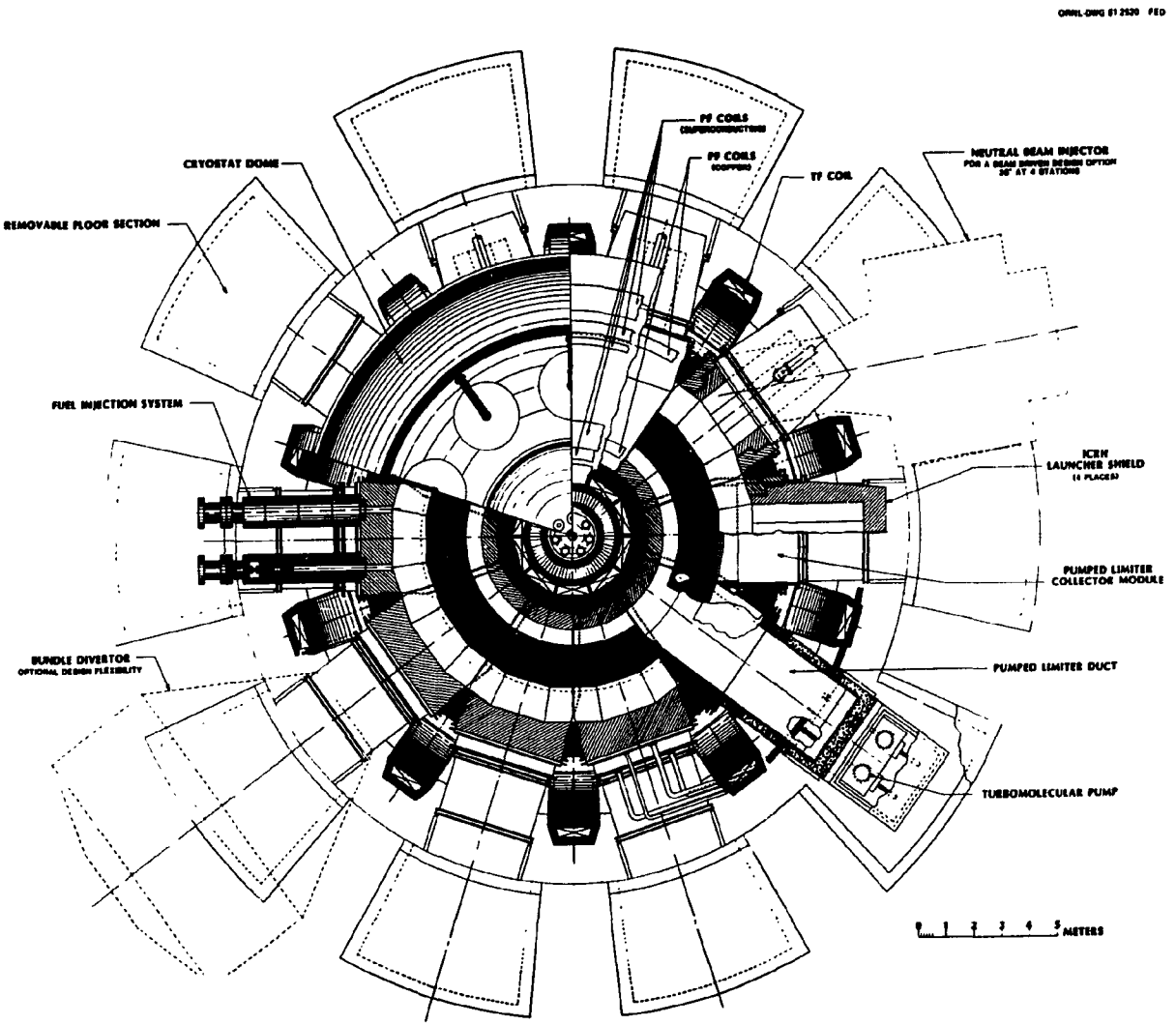

Fig. 3.2. General plan view of FED.

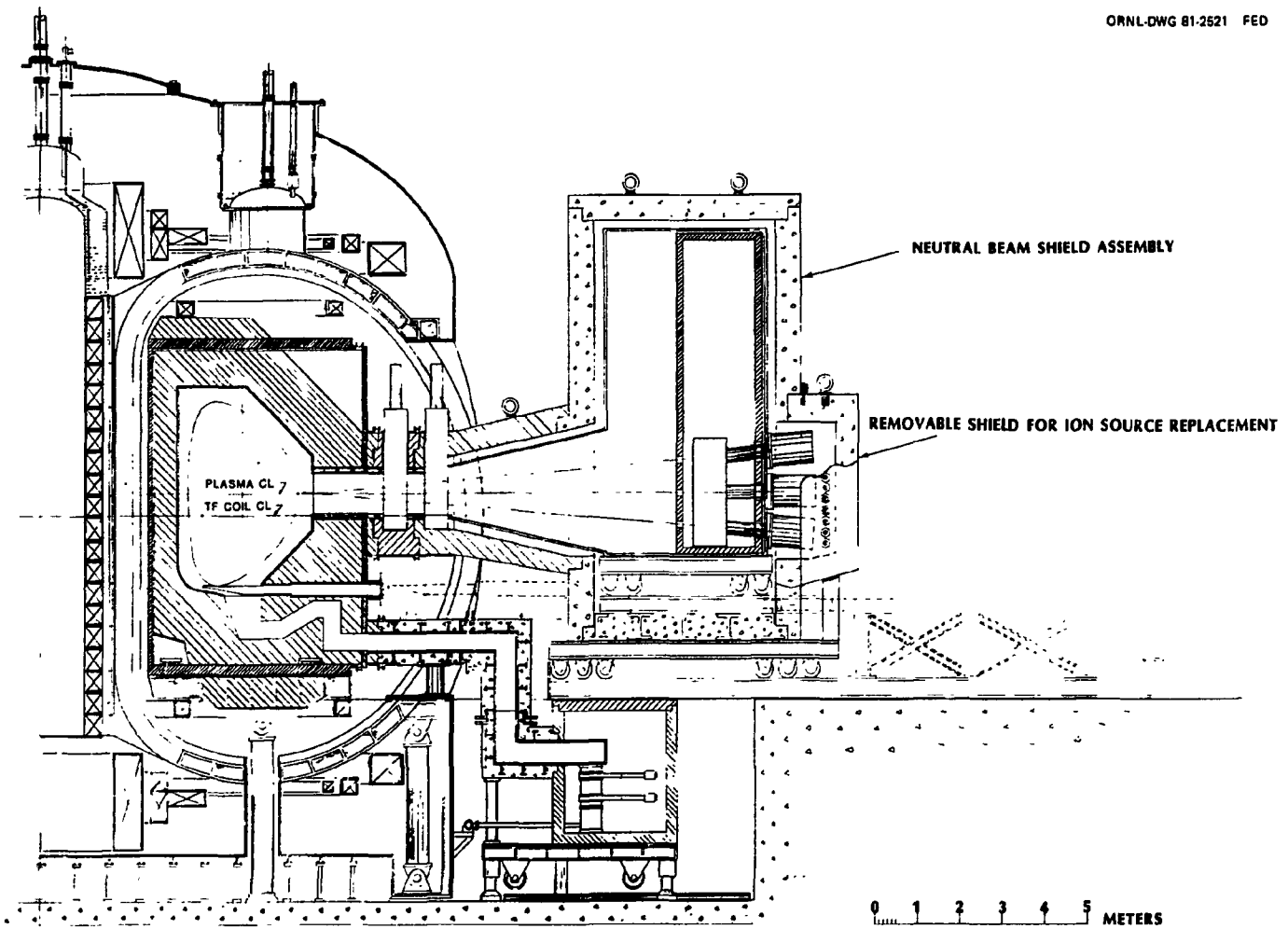

Fig. 3.3. Elevation view of neutral beam system.

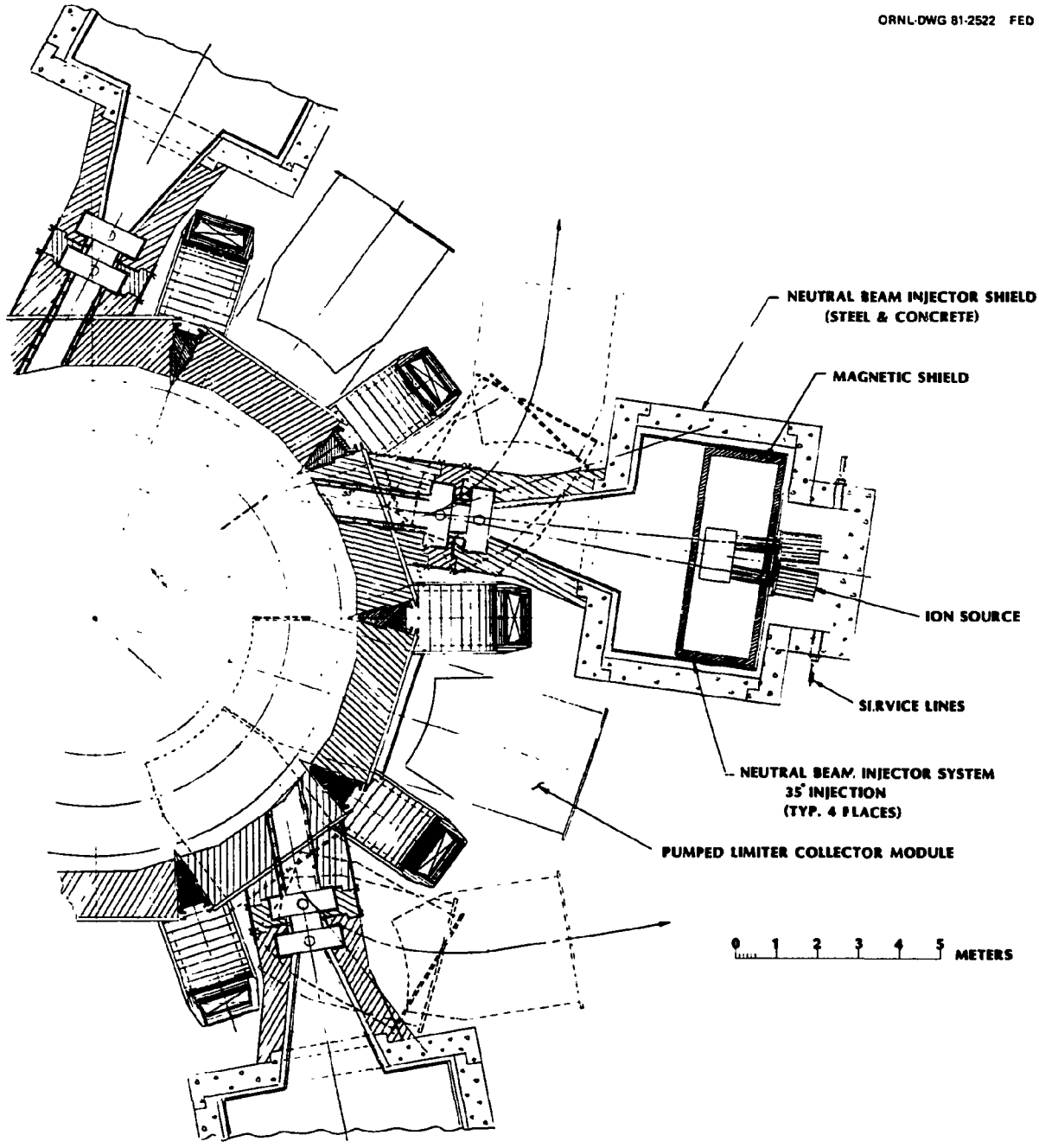

Fig. 3.4. Plan view of neutral beam system.

Access and ripple considerations led to the selection of a 10-coil arrangement for the toroidal field (TF) coil system. The TF coils, which have a 7.5- by 10.9-m bore, require a field of 8.0 T at the coil in order to produce 3.6 T on axis.

The poloidal field (PF) coil system is installed mainly in the poloidal bore and outside the TF coils, but a limited number of low current, fast-response coils are located in the toroidal bore of the TF coil assembly. Those in the poloidal bore and outside the TF coils are superconducting NbTi, whereas those inside the toroidal bore are normal copper.

The TF coils, superconducting PF coils, and bucking cylinder for the TF coils are all enclosed in a common dewar. The dewar is a dome structure that envelops the top and bottom sections of the TF coils and the inboard region of the TF coil toroidal bore with a surface of revolution. The outboard legs of the TF coils are enclosed with individual extensions of the common dewar, providing ten bays for access to the torus.

The plasma is heated using ion cyclotron resonance heating (ICRH). A total of 36 MW is employed and delivered using a ridge-loaded waveguide. Second harmonic deuterium is the currently recommended heating mode. Also carried as an alternate bulk heating approach are positive ion neutral beam injectors. Currently this alternate is represented by 150-keV beams providing a sustaining power of $\sim$36 MW and a heating power of 45-50 MW at an injection angle of up to 35°.

A rf system is provided for startup assist. This electron cyclotron resonance heating (ECRH) system, which supplies a total of 1 MW of power at $\sim$80 GHz, is used for ionization, plasma initiation, and supplemental heating of the plasma during the early phases of startup.

A mechanical pump limiter located at the bottom of the plasma chamber is used to establish the plasma edge and to provide a mechanism to pump hydrogen and helium particles. The construction is water-cooled copper, which was selected to provide high thermal conductivity. The surfaces are protected with graphite tiles. The limiter is designed for removal and replacement.

The present baseline produces a total of 180 MW of deuterium-tritium (D-T) power. The plasma operates at an average temperature of 10 keV and an average D-T ion density of $\sim 8 \times 10^{13}/cm^3$. The average total beta is 5.5%. Of the 180-MW total, 36 MW in the form of alpha particles and an additional 36 MW of injected power are deposited on the plasma chamber surfaces. Of this, it is currently assumed that the major fraction (56 MW) is deposited on the limiter. The remainder (16 MW) is deposited either as radiation or as charge exchange neutrals on the first wall/armor surfaces.

4. PLASMA SYSTEMS*

Y-K. M. Peng[†]
P. H. Rutherford[‡]
D. Blackfield[§]
S. K. Borowski[‖]
D. R. Cohn[§]
L. M. Hively[**]
J. A. Holmes[†]
W. A. Houlberg[††]
H. C. Howe[†]
P. Mioduszewski[††]
M. Murakami[††]
R. L. Reid[†]
J. A. Schmidt[‡]
D. J. Strickler[†]
M. Ulrickson[‡]

4.1 INTRODUCTION

This section addresses the performance and design requirements of FED as derived from our current understanding of plasma physics. The current level of understanding in a number of crucial physics areas has recently been assessed by the FED Physics Group under the direction of P. H. Rutherford. The areas considered include: confinement,[1] pump limiter operation and design concepts,[2] low safety factor operation and plasma shaping,[3] ion cyclotron resonance heating (ICRH),[4] and nonmagnetic impurity control.[5] In addition, FED-relevant input is generated by the physics community on a continuing basis in areas such as startup, plasma performance modeling, neutral beam injection studies, high beta implications and limitations, plasma edge physics, disruption characterization and implications, reactor physics analyses, and machine design and parameters.

---

*The authors gratefully acknowledge useful discussions with S. E. Attenberger, J. F. Lyon, J. A. Rome, D. J. Sigmar, D. W. Swain, K. T. Tsang, and J. B. Wilgen of Oak Ridge National Laboratory; with R. L. Miller of General Atomic Company; with W. Stodiek of Princeton Plasma Physics Laboratory; with L. D. Stewart of Exxon/Princeton Plasma Physics Laboratory; and with K. Evans, M. Kaminsky, J. Norem, and D. L. Smith of Argonne National Laboratory.

[†]Fusion Engineering Design Center/Oak Ridge National Laboratory.

[‡]Princeton Plasma Physics Laboratory.

[§]Massachusetts Institute of Technology.

[‖]Fusion Engineering Design Center/University of Michigan.

[**]Fusion Engineering Design Center/General Electric Company.

[††]Oak Ridge National Laboratory.

Because of the limited time available for preparation of this interim report, a large proportion of the results reported here was produced by scientists at ORNL. While their input has been and will continue to be vital to a sound assessment of the FED plasma properties, new and corroborative input from the fusion physics community will be sought and reported in the final FED design concept description.

The major role of the FED Plasma System Branch is to provide engineering-oriented interpretations of the physics information cited above in order to guide the design evolution. This type of activity is designated "plasma engineering analysis." The plasma engineering analyses presented in this section are of three general categories: (1) analyses that form the basis for the choice of the baseline parameters, (2) analyses that examine the possible range of plasma performance for the given baseline device, and (3) analyses that address potential options relative to the baseline configuration. These three types of analysis are woven through the subsequent discussions.

Section 4.2 provides a description of the operation scenario of a typical FED discharge cycle. Section 4.3 deals with startup and bulk heating. Section 4.4 examines beta implications and limitations. Section 4.5 discusses the possible range of plasma performance anticipated for the FED baseline device. Section 4.6 considers issues associated with particle and impurity control. Section 4.7 deals with the characterization and implications of plasma disruptions. Section 4.8 examines the requirements and constraints of the poloidal field configurations. Section 4.9 provides a summary of the major conclusions of the present plasma engineering analyses.

4.2 OPERATION SCENARIO

The FED plasma operation scenario describes the plasma behavior and the operating approaches through a typical plasma discharge cycle. The scenario serves as a reference to the engineering design trade analyses.

A typical FED plasma discharge cycle involves preionization, current ramp, bulk heating, burn, plasma shutdown, and pumpdown. The proposed scenario of the plasma operation through these phases of a discharge cycle is summarized below and is consistent with the results of the plasma engineering studies presented in Sects. 4.3-4.6.

4.2.1 Preionization (-0.05 s $\leq t \leq 0.15$ s)

About 1 MW of extraordinary mode, electron cyclotron resonant frequency (ECRF) wave at 80 GHz is launched from the high field side for a duration of 0.2 s to preionize and heat the electrons. The heated electrons ($T_e \sim 100$ eV, $n_e \sim 1 \times 10^{13}$ cm^{-3}) are expected to be located at $R = 5.9$ m over a radial width of about 0.4 m. This permits the application of a low toroidal loop voltage ($V_\ell < 25$ V) to initiate and ramp up the plasma current. Additional heating beyond 0.2 s is expected to reduce the volt-seconds expended due to plasma resistance, but achieving this is not as crucial as reducing the initiation voltage. An alternate preionization approach is to apply the ion cyclotron resonant frequency (ICRF) bulk heating capability to obtain significant electron heating near the fundamental frequency of a deliberately introduced proton minority (see Sect. 4.3.1).

4.2.2 Current Ramp (0 s $\leq t \leq$ 6 s)

The plasma minor radius is increased from 0.2 m to 1.3 m. For a pump limiter at the chamber bottom (Sect. 4.6), the elongation κ is also raised to 1.6 to achieve full plasma contact with the pump limiter. For pump limiters 45° from the midplane, a lower value of κ may be adequate. Before this, the small radius plasma leans against startup limiters, which are expected to be located at the outboard midplane. The current is increased so that the safety factor q_ψ at the plasma edge remains constant in time. The plasma reaches about 1 keV, 3×10^{13} cm^{-3}, and 4.8 MA at $t = 6$ s.

4.2.3 Bulk Heating (6 s $\leq$ t $\leq$ 12 s)

Up to 50 MW of ICRH power is applied at a frequency of about 54 MHz for 6 s. The plasma reaches about 10 keV, 8×10^{13} cm^{-3}, and 5.4 MA via pellet fueling and gas puffing, maintaining nearly equal deuterium (D) and tritium (T) content. The contact between plasma and limiter is controlled to achieve adequate particle exhaust through the limiter channels without overheating the leading edge of the pump limiter. The particle source near the plasma edge is dominated by limiter recycling. The value of q_ψ is maintained constant during this phase. A strong alternative to ICRH is neutral beam injection, in which about 50 MW of 150-keV (maximum) D^0 beam is coinjected in the quasi-tangential direction (at an angle of 35° toward parallel, measured at the outer plasma edge). In this case, an enhanced particle exhaust capability and tritium pellet injection are needed to maintain a nearly equal D-T plasma composition. The fusion power reaches about 180 MW at t = 12 s (Sects. 4.3.2 and 4.3.3).

4.2.4 Burn (12 s $\leq$ t $\leq$ 112 s or greater)

A steady-state heating power of about 36 MW is maintained to sustain a controlled fusion burn at $Q \sim 5$. The pump limiter is assumed to adequately exhaust the helium and control the plasma edge, but auxiliary impurity control or reduction schemes may be needed (Sect. 4.6). Backup options include magnetic divertors, externally driven impurity expulsion, and actively maintained plasma edge cooling to minimize impurity production and ingestion at the plasma edge. Assuming adequate helium exhaust and impurity control, the plasma burn time is limited either by volt-second capability of the ohmic heating (OH) coils or by significant resistive diffusion of the plasma poloidal flux. With nearly classical toroidal plasma conductivity, the latter time scale is estimated to be a few hundred seconds (Sect. 4.8.2).

4.2.5 Shutdown (112 s $\leq$ t $\leq$ 122 s)

During shutdown, the fusion burn is quenched before the current is quenched. Under normal conditions, the fusion quench is initiated by termination of fueling while maintaining or possibly enhancing plasma exhaust through the pump limiter. The supplementary heating is decreased while plasma disruption is avoided by staying within the modified Murakami density limit (Sect. 4.7). A plasma density of $<2 \times 10^{13}$ cm^{-3} may be assumed at the end of the fusion quench (at t $\simeq$ 117 s). Conceptually, the current shutdown is the reversal of the current ramp. The value of q_ψ at the plasma edge should be maintained as the plasma radius decreases throughout this phase to avoid disruptive termination of the discharge.

4.2.6 Pumpdown (122 s $\leq$ t $\leq$ 152 s)

The neutral density in the chamber at the end of the current quench is expected to be about 3×10^{-4} torr. It is assumed that the residual gas is relatively clean, with only negligible fractions of helium and low Z impurities. Pumpdown to 3×10^{-5} torr in $\leq$30 s is assumed during this phase.

A characterization of the plasma behavior during major disruptions is presented in Sect. 4.7. The design requirements stemming from the desired plasma poloidal field configurations are discussed in Sect. 4.8.

4.3 PREIONIZATION AND BULK HEATING

4.3.1 RF Heating to Assist Current Startup

Auxiliary rf heating of electrons before and during the current rise phase in the Engineering Test Facility (ETF) and in FED has been suggested to reduce both the initiation loop voltage and the resistive flux expenditure during startup.[6] Lowering the loop voltage requirement is expected to create large engineering benefits in the FED design (Sects. 7.4 and 7.5). Potential rf candidates include heating in the range of the fundamental electron cyclotron resonance (ECRH)[6] and

fundamental proton minority heating (ICRH).[4] Startup assist using the latter technique is being planned on the Princeton Large Torus (PLT) while experiments on the Impurity Study Experiment (ISX-B) have concentrated on ECRH.[7,8]

To date, the FED investigations have focused primarily on the use of ECRH. A two-phase, small radius startup scenario is proposed. An extraordinary wave is first injected from the high field side to preionize and heat the electrons near the upper hybrid resonance (UHR) layer in the absence of toroidal current. The heating is then continued during the current rise phase, while additional rf power could be launched from the low field side. This power input supplements the ohmic heating and eliminates the need for a fast current rise. By producing and maintaining a reasonably high plasma conductivity and extending the startup times, the initial voltage and the resistive volt-second demands can be significantly reduced.

Power and frequency requirements have been calculated for ETF/FED[9] for various levels of electron preheating occurring both on axis and near the outboard torus wall. At $n_e \simeq 10^{13}$ cm^{-3}, estimates indicate that a range of electron temperature ($T_e \simeq$ 50-200 eV) is possible with 0.5-2.0 MW of ECRH power injected from the high field side in the extraordinary mode. The frequency requirements are 130-150 GHz in ETF and 80-100 GHz in FED. Most important, however, is that the maximum required plasma loop voltage is reduced by roughly an order of magnitude (to 25 V or less using 1 MW of power) compared to the purely inductive current startup scenario. The time-averaged inductive loop voltage, $d(L_p I_p)/dt$, is about 10 V during this phase. The initiation plasma parameters are achievable with a "short pulse" ECRH assist ($\tau_{rf} \gtrsim 200$ ms). Additional, longer pulse ECRH up to 4 MW is also considered to reduce the impact of impurities on resistive volt-second consumption. In this case, the estimate of the total resistive volt-seconds dissipated in the plasma is about 13 Wb during the current ramp. The plasma resistive heating power rises monotonically to about 0.5 MW at t = 0.15 s and about 4 MW at t = 6 s.

The physics model describing the UHR heating process includes the formation of ambipolar electric fields and large electron temperature gradients near the UHR region. The predictions are found to compare favorably with preliminary results from ECRH preheating experiments on ISX-B.[7,8] This provides some confidence in the above estimates made for ETF/FED.

Experimental results obtained on PLT[10] and on the Tokamak Fontenay-aux-Roses (TFR) and DIVA[11] indicate that fundamental proton minority heating may also permit a viable ICRF-assisted startup option. In the case of TFR and DIVA, maintaining a sufficient proton minority density has led to strong absorption, attributable to the ion-ion hybrid resonance, and significant electron heating. Predominant electron heating is required to maintain an ambipolar potential for adequate electron confinement in the absence of toroidal plasma current.[6,9] It is not yet certain if such a heating approach will lead to unique design requirements, such as wave launching from the high field side.[12] Further theoretical and experimental study of the ICRF-assisted current startup is required before specific recommendations can be made.

4.3.2 Bulk Heating in the Ion Cyclotron Range of Frequencies

Recent experimental successes[10,11] and the anticipated technology advantages made plasma heating in the ion cyclotron range of frequencies (ICRF) an attractive means of bulk heating in FED.[4] The initial engineering implementations of the wave launching structure appear promising (Sect. 7.2).

Among the several possible regimes of ICRF, heating at the second harmonic of deuterium appears the most promising for the following reasons:

1. At a frequency of about 54 MHz and a half-wavelength of about 2.5 m in FED, the wave can be launched by simple waveguides or loop antennas that fit between two adjacent toroidal field (TF) coils.
2. This same frequency may serve to heat the electrons during preionization and plasma current startup, via minority proton heating at the fundamental frequency (see Sect. 4.3.1).

3. Both heating approaches have the most favorable experimental results so far.[10,11] Heating at the second harmonic of deuterium permits wave launching from the low field side.

As a first step toward simulating this process in FED, a model for power deposition via absorption and mode conversion of a fast magnetosonic wave is developed in a one-dimensional (1-D) slab geometry.[13] Figure 4.1 shows typical results of second harmonic heating of deuterium in an equal mixture of deuterium and tritium and a parallel wave number of $k_{\parallel} = 0.1\ cm^{-1}$. There is a relatively efficient heating of deuterium at low and high values of plasma densities and temperatures. Pending further comparison with existing experimental results,[14] this preliminary model can be used in a 1-D transport simulation of the ICRF bulk heating in FED.

Relative to neutral beam heating (Sect. 4.3.3), the ICRH experimental data base is limited.[2] Successful heating results so far have used antennas rather than waveguides. Much experimental and analytical work is needed to make a reliable assessment of the ICRH launching structure best suited to FED.

4.3.3 Bulk Heating with Neutral Beams

Relative to ICRH, neutral beam heating has a significantly more reliable physics basis for application to FED but has a potentially serious problem of neutron streaming. It remains a strong alternative for bulk heating because it is currently judged to be less risky and better understood. Recent studies of the density buildup scenario during injection[15,16] have suggested the effectiveness of modest energy beams (100-150 keV) in reactor-level tokamaks. However, there remains the question of heating efficiency as a function of injection angle and energy (including the mix of energy species).[17] Some recent work has shed further light on the efficiency of neutral injection heating.

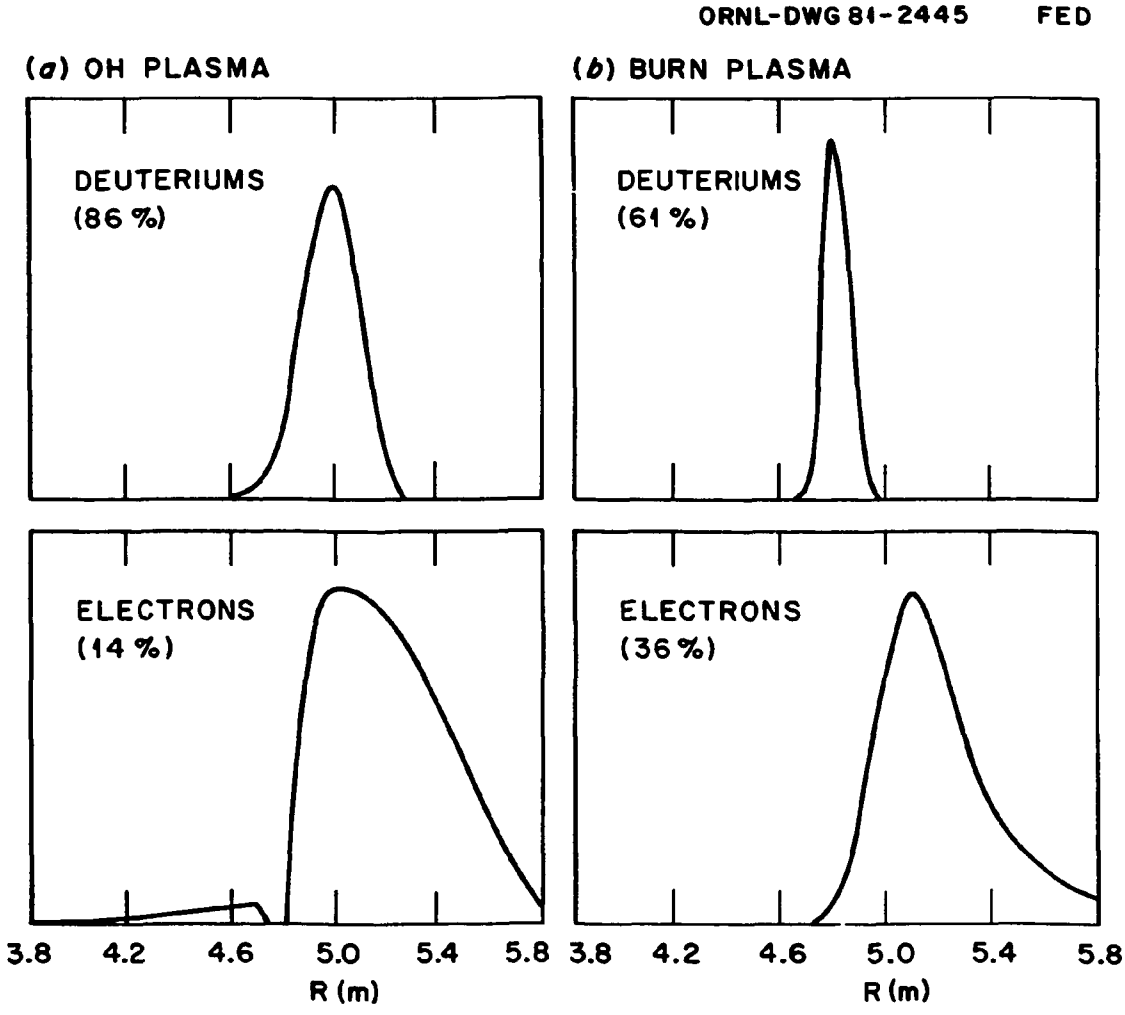

Fig. 4.1. Typical calculated power deposition profiles of a fast magnetosonic wave incident from the low field side near the second harmonic of deuterium: (a) $n_e = 3 \times 10^{13}$ cm^{-3}, T_o = 1 keV, 94% wave absorption per pass and (b) $n_e = 1.5 \times 10^{14}$ cm^{-3}, T_o = 10 keV, 100% wave absorption per pass.

Injection angle

The bounds on injection angle for neutral beam heating are due to constraints on beam line access ($\theta \leq 36°$) (see Sect. 7.3), losses when fast ions become trapped in local magnetic wells, and possible severe loss of plasma confinement via the presence of Debye-shielded potential associated with the space charge density of the banana-trapped beam ions.[1,17,18]

In the presence of a toroidal field ripple, the beam ions with little parallel speed can be collisionlessly trapped in ripple wells,[19] losing the confinement effect of toroidal rotational transform and rapidly drifting outward under local toroidal field curvature. Another collisionless process has to do with the ripple perturbation of the ion banana orbit near its tips,[20] causing an outward drift of some of the banana orbits. The presence of the localized field ripple due to a bundle divertor (which is a backup impurity control option, discussed in Sect. 4.6.2) is expected to enhance the loss of beam ions, especially the banana ions.

Recent experiments on the Poloidal Divertor Experiment (PDX) using nearly perpendicular injection (11° toward parallel at the chamber center) have shown unexplained poor plasma heating efficiencies compared to near-tangential injection results in PLT and ISX-B. This result may be attributable to injection into the banana orbits, which are localized at larger major radius compared to the injected electron population. The resulting Debye-shielded electric field around these ions would be in the direction of the major radius, giving rise to a vertical plasma $\underset{\sim}{E} \times \underset{\sim}{B}$ drift and enhanced plasma loss.[18] These processes all suggest that it is prudent to minimize injection into the ripple-trapped and the banana orbits.

To determine the fraction of fast ions on banana orbits, coinjected deuterium orbits were calculated for injection at 16°, 25°, and 35° into FED-like plasmas (the angle defined at the plasma outboard edge). Positive ion beams at 150 keV (full energy) were assumed. The results are plotted in Fig. 4.2 for $<\beta> = 0.8\%$ and 7.5%. In all cases, the circulating orbits are formed from ions on the inboard portion

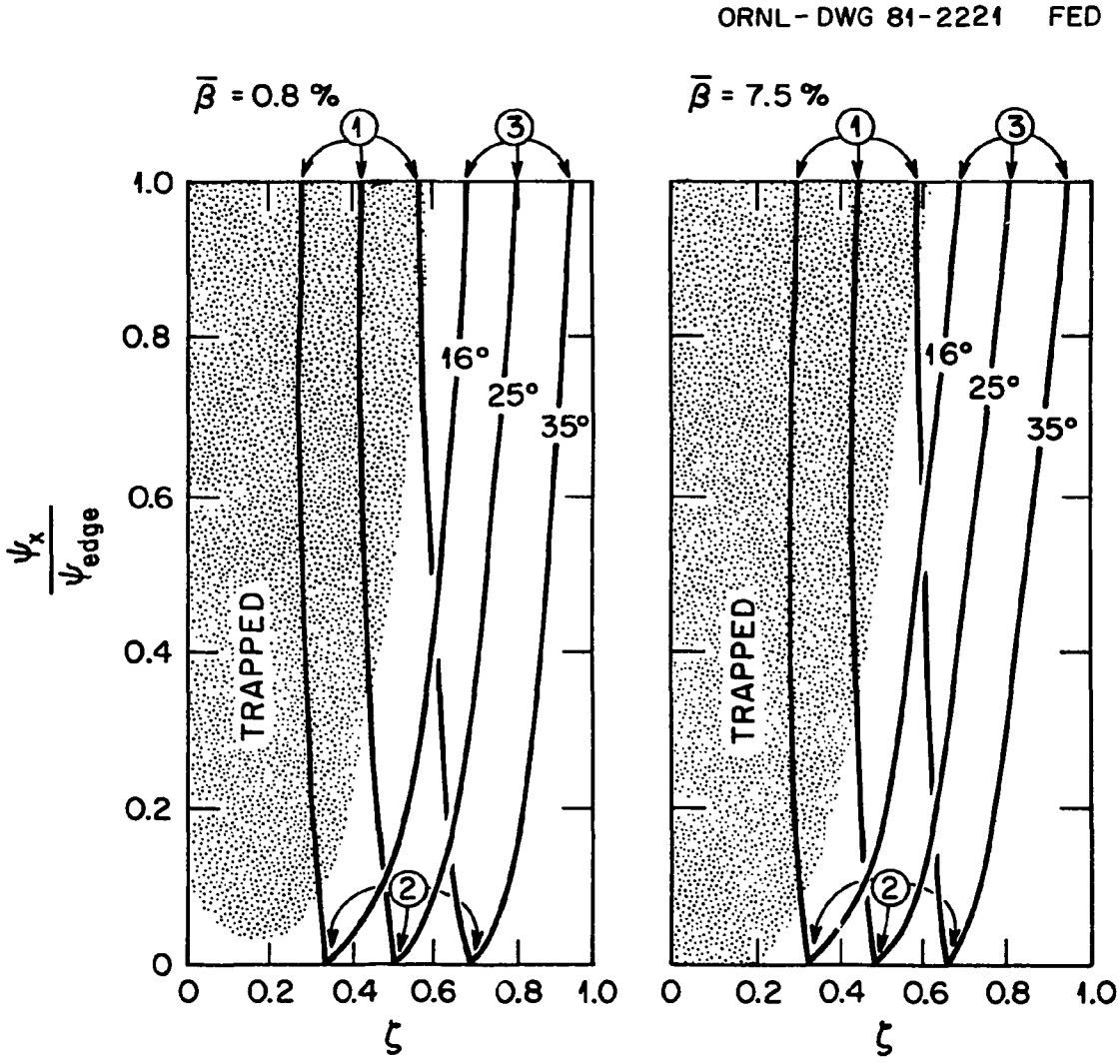

Fig. 4.2. Phase-space loci of 150-keV ion orbits for various coinjection angles into FED-like plasmas for $\langle\beta\rangle$ = 0.8% and 7.5%. The points 1, 2, and 3 correspond to the ion orbits formed at the outboard edge, magnetic axis, and inboard edge, respectively. ψ_x is the maximum value of the poloidal flux function along the guiding center orbit and ζ is the cosine of the pitch angle at ψ_x. The banana-trapped orbits lie in the shaded region.

($R < R_{axis}$) of the beam locus. There is little difference between the low and high beta cases as shown in Fig. 4.2, which was plotted using the constants of motion formulation of Rome and Peng.[21] The fraction of injected ions in banana orbits has also been estimated. They are less than 10%, 65%, and 90% for 35°, 25°, and 16°, respectively. Thus, use of 35° coinjection (or as nearly tangential as possible) will minimize the deleterious effects described here. The maximum angle of the most nearly perpendicular beam line has been estimated to be 36° (Sect. 7.3).

A more sophisticated calculation is currently under way by Fowler and Rome[22] to account for beam ion thermalization in the FED field ripple. Preliminary results show that for injection at an angle of 35°, no beam ions (among a random sampling of a hundred) are lost via ripple trapping, and less than 1% of the injected power goes to the wall and the limiter.

Injection energy

The neutral beam heating power required to maintain a near-thermal steady state in FED has been calculated as a function of plasma density and temperature using the WHIST code.[23] Here the average temperature $\langle T \rangle$ is defined as a per-particle average that includes all thermal particle species and energy ranges. A baseline set of transport models (discussed in Sect. 4.5) is used. The results are plotted in Fig. 4.3 for deuterium beam energies (full) of 100 keV, 150 keV, and 200 keV injected at about 36° toward parallel, so the beam misses the inboard chamber wall. Positive ion beam systems are assumed with the energy species mix and power efficiency listed in Table 4.1. It is seen that the beam efficiency increases by more than a factor of 2 as the beam energy decreases from 200 keV to 100 keV.

Several observations can be made from Fig. 4.3:

1. Variations in beam energy from 100 keV to 200 keV do not significantly alter the nature of the injection heating process of the FED plasma. A saddle point in the contours of the minimum beam power requirement separates the ohmic plasma ($\langle n \rangle \simeq 3 \times 10^{13}$,

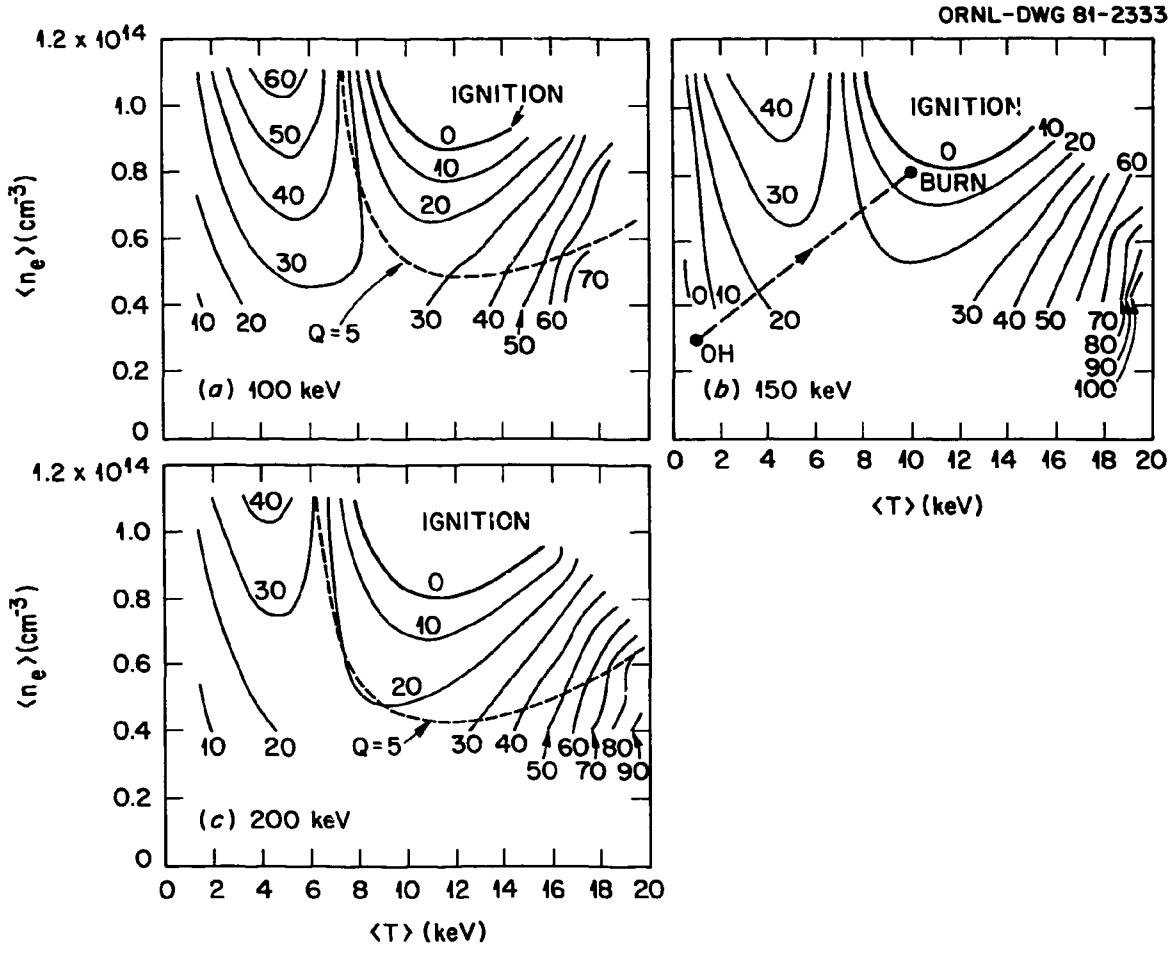

Fig. 4.3. Contours of constant neutral beam power required to maintain a near-steady-state temperature and density, for full deuterium beam energy of (a) 100 keV, (b) 150 keV, and (c) 200 keV. Positive ion beams with beam components listed in Table 4.1 are assumed.

$\langle T \rangle \approx 1$ keV) and the high beta plasma at burn ($\langle n \rangle \approx 8 \times 10^{13}$ cm^{-3}, $\langle T \rangle \approx 10$ keV).[24,25] The desirability of a density buildup scenario for neutral injection heating[16,17] is not altered by this variation in beam energy.

2. The minimum heating power required to surpass the saddle point in a quasi-static fashion decreases from 27 MW to 22 MW with increasing beam energy. The position of the saddle point shifts to slightly larger values of plasma density and temperature as the beam energy is increased.
3. For injection heating at constant density, a decrease in beam power with increasing beam energy is seen. At $\langle n \rangle = 8 \times 10^{13}$ cm^{-3}, the static beam power decreases from 48 MW to 32 MW as the beam energy is increased from 100 keV to 200 keV.
4. The required neutral beam power increases 25-50% as the beam energy is decreased from 200 to 100 keV. Based on the efficiencies given in Table 4.1, the power supply requirement decreases with increasing beam energy.[16]

These results clearly favor low energy (to as low as about 100 keV) positive ion deuterium beams injected in the near-tangential direction to provide bulk heating in a relatively pure FED plasma. However, low energy beams may result in an enhanced burden of particle exhaust via the pump limiter (Sect. 4.6). A beam energy of 150 keV is therefore recommended for the FED neutral beams, consistent with an earlier suggestion by Stewart.[26]

Table 4.1. D^+ neutral beam characteristics used in obtaining the results shown in Fig. 4.3

Energy	Neutral power mix into plasma (full:half:third)	Power efficiency	
		Without recovery	With recovery[a]
100 keV	72:16:12	45%	73%
150 keV	66:19:15	30%	41%
200 keV	56:23:21	21%	31%

[a] See Sect. 7.3.

Injection power

Preliminary dynamic simulations of the neutral injection heating in 6 s have been carried out with the WHIST code (see Sect. 4.5 for more detail on the near-baseline physics assumptions). The results with near-tangential injection of 150 keV are shown in Fig. 4.4. The path chosen for heating, indicated in Fig. 4.4(a), is not optimal for minimum beam power requirements. Thus, the requirement of 50 MW of neutral power shown in Fig. 4.4(b) is pessimistic. Because the plasma thermal energy content at burn is about 100 MJ, a heatup in 6 s will require an average addition of 17 MW over transport losses. The bulk neutral heating power requirement is expected to be close to, if not less than, 40 MW.

4.3.4 Conclusions and Future Work

The requirements of ECRH-assisted current initiation in FED have been estimated based on heating and transport models consistent with the recent experimental results of ISX-B. Only modest levels of power ($\sim$1 MW) at 80 GHz injected from the high field side in extraordinary mode are required to reduce the startup voltage by an order of magnitude. In the case of ICRH-assisted current initiation, it may be necessary to launch the wave from the high field side in order to obtain a predominant electron heating. This may lead to potentially serious design difficulties. Various heating regimes (e.g., fundamental proton minority, second harmonic deuterium majority, etc.) near the ICRF should be examined for their effectiveness in electron heating in the 100-eV and 10^{13}-cm^{-3} range.

Very few ICRF bulk heating calculations for FED have been done so far because of a lack of convincing models of heat deposition. The ICRF heating profile is expected to be more peaked at the plasma center (at 54 MHz) than the 150-keV deuterium beam heating profile. The former is thus expected to require no more power than the latter. The same power requirements for both, initial bulk heating with 50 MW for 6 s followed by a steady-state drive at 36 MW, are currently suggested for the FED design studies.

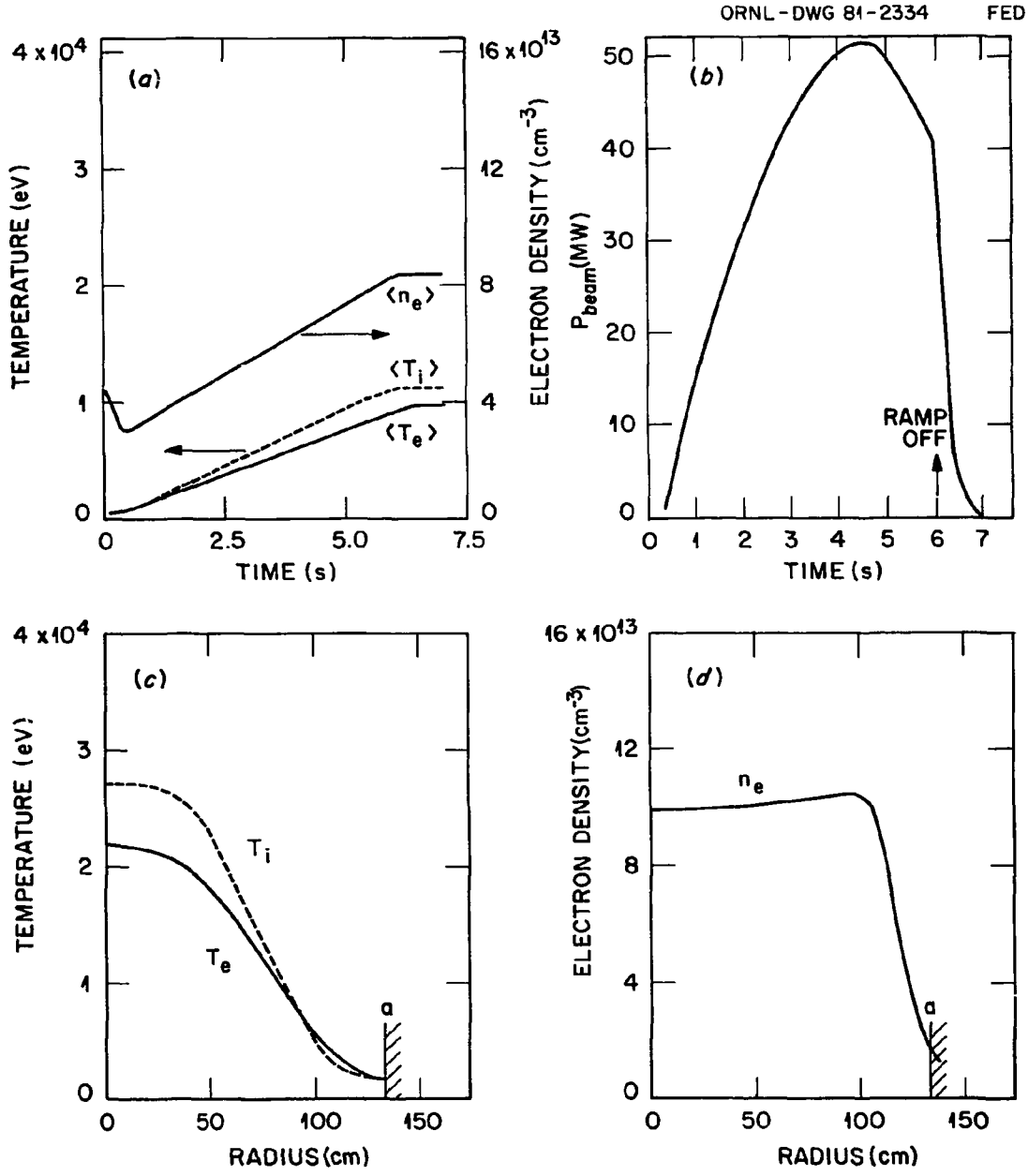

Fig. 4.4. An example of a dynamic neutral injection heating simulation with 150-keV deuterium beams: (a) preprogrammed density and temperature rise as a function of time; (b) the calculated neutral power requirement as a function of time; (c) the final steady-state electron and ion temperature profiles, and (d) the final steady-state electron density profile.

A significantly more sophisticated understanding of neutral beam heating physics is currently available. This has permitted realistic projections of the efficiency of positive ion deuterium beam heating requirements in FED. Our results strongly favor the use of 150-keV beams injected in the near-tangential direction (36° toward parallel at the plasma edge), assuming that the density buildup scenario is used. Current design requirements are calculated as $\lesssim$50 MW for 6 s to heat the plasma from $\langle T \rangle \simeq 1$ keV (at $\langle n \rangle \simeq 3 \times 10^{13}$ cm^{-3}) to $\langle T \rangle \simeq 10$ keV (at $\langle n \rangle \simeq 8 \times 10^{13}$ cm^{-3}), followed by a neutral beam drive power of 36 MW.

Some areas of significant uncertainties still remain in this area and should be investigated. These include the losses of neutral beam ions during thermalization in the presence of field ripples (due to TF coils, bundle divertors, or more exotic forms of coils) and a comparison of heating efficiencies of positive and negative ion deuterium beams in FED. An important deficiency in the current calculations has to do with the assumptions of complete particle exhaust at the plasma edge. A strong particle recycling at the plasma edge [which is appropriate for limiter-pumped plasmas (Sect. 4.6)] is expected to introduce significant difficulties in maintaining the proper plasma density and D-T composition. This potential problem should be investigated in the near future.

4.4 BETA CONSIDERATIONS

Estimates of plasma beta for tokamak reactor studies[27,28] have customarily been based on ideal MHD stability requirements.[15,29,30] However, for the FED baseline these theoretical results would suggest a relatively low beta, $\langle \beta \rangle$, of about 4%, compared to the proposed value of 5.5%. Here the baseline value of $\langle \beta \rangle$ is assessed based on recent experimental indications from ISX-B;[31,32] with intense neutral injection into a nearly circular plasma, the achieved plasma $\langle \beta \rangle$ ($\sim$3%) is about 50% higher than that predicted so far by MHD stability theory. Section 4.4.1 examines these recent experimental results that provide an improved basis for assessing the achievable $\langle \beta \rangle$ values in FED. This new basis suggests the use of explicit expressions for plasma equilibrium parameters,

such as β_p, $\langle\beta\rangle$, I_p, κ, q_ψ, and A (Sect. 4.4.2). The application of the new information is given in Sect. 4.4.3, showing that the current baseline choices of $\langle\beta\rangle = 5.5\%$, $\beta_p = 1.8$, $\kappa = 1.6$, and $q_\psi = 3.2$ are appropriate, despite large uncertainties in the scaling of the electron energy confinement with plasma size and β_p.

4.4.1 Improved Basis for Beta Estimates

Three experimental observations from ISX-B[31,32] are of interest to beta considerations for FED:

1. Using power balance analysis, Murakami has suggested that the electron energy confinement time (normalized to density) decreases with increasing beam power.
2. Using magnetic pickup loop data, Swain has found that the quantity $(\beta_p q^{-1/2})$ is a unique, empirical function of beam power and is satisfied over the typical operating range of ISX-B: $0.8\ T \leq B_t \leq 1.3\ T$, $P_{beam} < 2.5$ MW, and $100\ kA \leq I_p \leq 180\ kA$. The results suggest a poloidal beta limit as the beam power is increased to 2.5 MW.
3. An examination of the $\langle\beta\rangle$ and β_p values achieved shows that $\langle\beta\rangle$ is bounded by two separate constraints. For high values of β_p, the $\langle\beta\rangle$ value achieved appears limited by the impaired electron energy confinement. For low values of β_p, the $\langle\beta\rangle$ value achieved follows the MHD equilibrium condition: $\langle\beta\rangle \propto \beta_p/q^2$.

Based on these observations, the basis for beta considerations in FED involves the following:

1. Figure 4.5 shows how the electron energy confinement time, τ_{Ee}, may vary with $\varepsilon\beta_p$. The solid curve, not inconsistent with ISX-B results, is referred to as a "soft" limit. The dashed curve, referred to as a "stiff" limit, is included to reflect the degree of uncertainty in present results. Based on available data, it is not clear whether the decrease in τ_{Ee} is due to the high beam power density ($\sim$2 MW/m^2) or to the increasing value of $\varepsilon\beta_p$. Because the plasma heating power density in FED is about 0.25 MW/m^3, the

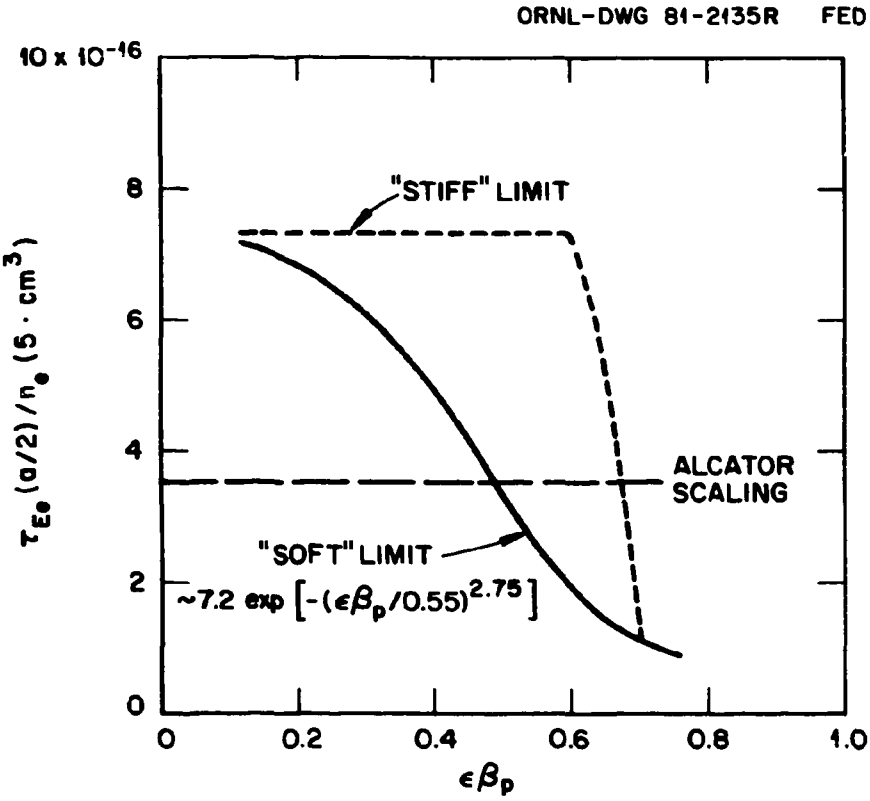

Fig. 4.5. Schematic dependences of τ_{Ee} in $\epsilon\beta_p$, reflecting a soft limit in β_p. The solid (dashed) line indicates a relatively soft (stiff) limit.

former assumption is more pessimistic. Mechanisms that may support this assumption are currently being studied.[33]

2. Within the limits of power balance, the $<\beta>$ values achieved in ISX-B are consistent with MHD equilibria. It is assumed that this will also apply in FED. This means that the achievable $<\beta>$ values are limited either by disruption at low q (Sect. 4.7) or by the available current and size of the OH induction coils.

4.4.2 MHD Equilibrium Formulas

This section presents equations that relate plasma equilibrium parameters, such as I, R, a, κ, $<\beta>$, β_p, and q_ψ, to be used to assess the FED parameters. A number of theoretical[34] and numerical[35] analyses of finite beta MHD equilibria in a flux-conserving tokamak (FCT) serve as the basis for the present formulation. It is convenient to start with an approximation[36] to the flux definition of safety factor q_ψ at the plasma boundary:

$$q_\psi \equiv \frac{\delta\Phi}{\delta\psi} = F\langle R'^{-2}\rangle V'/4\pi^2$$

$$= B_t R \oint d\ell/R'^2 B_p 2\pi$$

$$\simeq 5C(\varepsilon\beta_p, q_\psi)\,\frac{B_t a}{I_p}\,\frac{\varepsilon}{(1-\varepsilon^2)^2}\,\frac{1+\kappa^2}{2}\,, \qquad (4.1)$$

where $F \equiv B_t R$, $R' = R$ at the plasma major radius, B_t is the toroidal field at $R' = R$, $\oint d\ell/R'^2 B_p$ represents the line integral of $(1/R'^2 B_p)$ along the boundary of the plasma cross section, $\varepsilon = a/R$, and $\kappa = b/a$. Here mks units are used with I_p in megamperes.

The coefficient C is somewhat greater than unity and increases as the magnetic axis shifts outward (with increasing $\varepsilon\beta_p$) and the current profile becomes more peaked (with increasing q_ψ). Note that the

influence of triangularity is not explicitly included in Eq. (4.1). At low values of $\varepsilon\beta_p$ and q_ψ, ($\sim$2), the value of C is about 1.1.[36] A set of FCT equilibrium calculations was performed to determine C for a FED tokamak near the baseline; the results are given in Fig. 4.6.

A relatively convenient definition for β_p has been used in plotting Fig. 4.6,

$$\beta_p = 2\mu_o \bar{p}/\bar{B}_p^2 ,$$

$$\bar{B}_p = \oint B_p d\ell / \oint d\ell = \mu_o I_p / \oint d\ell . \tag{4.2}$$

Under the approximation of an elliptical cross section, we find

$$\oint d\ell \simeq 2\pi a[(1 + \kappa)/2](1 + m^2/4) \simeq 2\pi a[(1 + \kappa^2)/2]^{1/2} , \tag{4.3}$$

where $m = (\kappa - 1)/(\kappa + 1)$.

When this is combined with the usual definition of $\langle\beta\rangle = 2\mu_o \bar{p}/B_t^2$, a relatively convenient and accurate relation linking $\langle\beta\rangle$ and β_p is obtained:

$$\langle\beta\rangle = \beta_p \left[\frac{C}{q_\psi} \frac{\varepsilon}{(1 - \varepsilon^2)^2}\right]^2 \frac{1 + \kappa^2}{2}$$

$$= \beta_p \left(\frac{I_p}{5aB_t}\right)^2 \frac{2}{1 + \kappa^2} . \tag{4.4}$$

The value of β_p as defined above is found to be within a few percent of the value of β_I (Ref. 37) for $\beta_p < 2$.

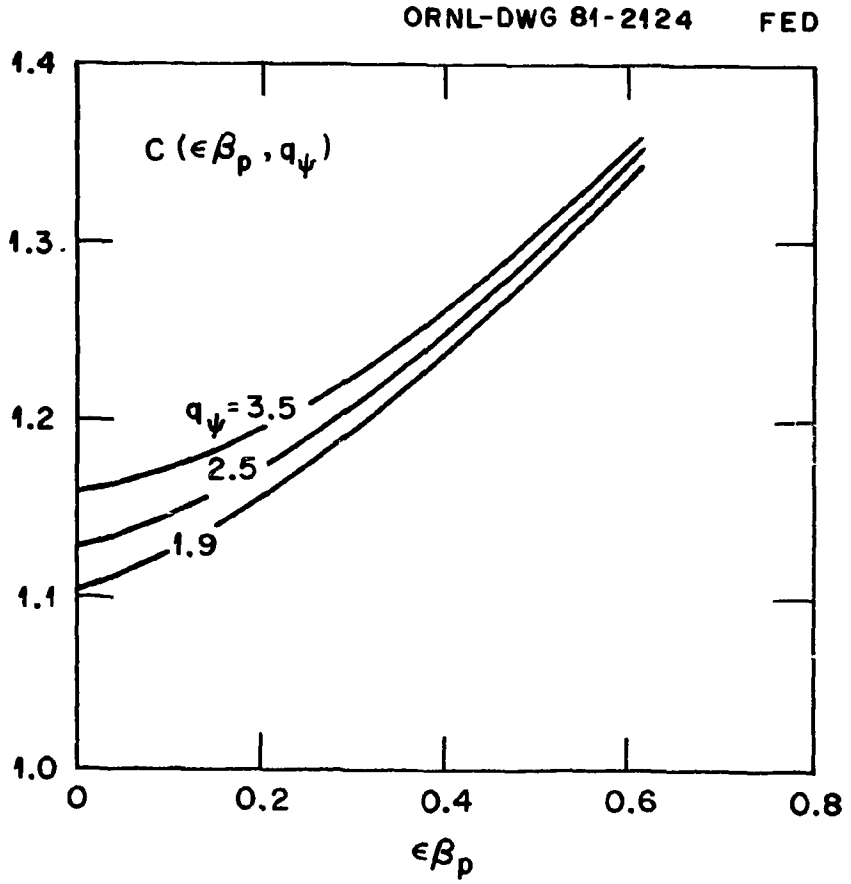

Fig. 4.6. The value of C in Eq. (4.1) as a function of $\varepsilon\beta_p$ and q_ψ for a FED-like flux-conserving tokamak where R = 4.80 m, a = 1.27 m, B_t = 3.62 T, κ = 1.6, and δ = 0.5.

4.4.3 Choices of $\varepsilon\beta_p$ and κ

To assess whether the baseline choices of $\varepsilon\beta_p \lesssim 0.6$ and $\kappa = 1.6$ remain appropriate under the improved assumptions of achievable $<\beta>$, it is convenient to use $n\tau_{Ee}$ as a parameter to reflect potential plasma performance. A maximization of $n\tau_{Ee}$ by appropriate choices of $\varepsilon\beta_p$ and κ, under typical choices of plasma temperature and density (Sect. 4.5), should then lead to an optimization of FED design.

Given the dependences of Fig. 4.5 and the uncertainties in the size scaling of electron confinement,[1] a more general form of the empirical electron energy confinement time can be written as

$$\tau_{Ee} = C_\tau n_e a^s R^t q_\psi^u B_t^v \exp[-(\varepsilon\beta_p/\delta)^\gamma] \ , \tag{4.5}$$

where $\delta \simeq 0.55$ and $\gamma \simeq 2.75$ have been chosen to represent a relatively soft β_p dependence. The values of s, t, u, and v can range from those for Alcator scaling[38] (s = 2, t = v = 0, u = 0.5) to those for Merezhkin scaling[39] (s = 5/24, t = 21/8, u = 7/6, v = -1/3). For constant B_m at the coil, we have

$$B_t = B_m \left(1 - \varepsilon - \frac{\Delta_s}{R}\right) , \tag{4.6}$$

where Δ_s is the distance between the inside TF coil leg and the plasma. Combining Eqs. (4.4)-(4.6) then gives:

$$n\tau_{Ee} = C_\tau \left(\frac{B_m^2}{4\mu_o T_o}\right)^2 B_m^v \alpha^2 q_\psi^{u-4} F(\varepsilon\beta_p) H(\kappa) G(R,a) \ ,$$

$$F(x) = x^2 C^4(x, q_\psi) \exp[-(x/0.55)^{2.75}] \ ,$$

$$H(\kappa) \simeq (1 + \kappa^2)^2/4 \ ,$$

$$G(R,a) = a^{s}R^{t}\varepsilon^{2}\left(1 - \varepsilon - \frac{\Delta_s}{R}\right)^{4+v} \Big/ (1 - \varepsilon^2)^{8} \ , \qquad (4.7)$$

where T_o = 10 keV and α is the fraction of $\langle\beta\rangle$ due to the thermal component of the D-T plasma.

In this equation, the dependence of $n\tau_{Ee}$ (i.e., the plasma performance) on $\varepsilon\beta_p$ and κ is contained solely in the functions $F(\varepsilon\beta_p)$ and $H(\kappa)$. As a result, uncertainties in the size scaling of electron energy confinement do not impact the choice of either $\varepsilon\beta_p$ or κ. Figure 4.7(a) plots $F(\varepsilon\beta_p)$ as a function of $\varepsilon\beta_p$. As indicated, a maximum occurs near $\varepsilon\beta_p$ = 0.55 (soft limit), even though τ_{Ee} increases by a factor of 3 as $\varepsilon\beta_p$ increases from near zero to 0.55. For values of $\varepsilon\beta_p$ in the range 0.4-0.7, it is seen that the function $F(\varepsilon\beta_p)$ remains within 20% of its peak.

Figure 4.7(b) plots the function $H(\kappa)$ versus κ. As indicated, there is more than a threefold increase in $H(\kappa)$ for an elongation of 1.6. This results from the increase in $\langle\beta\rangle$ with increasing κ at constant $\varepsilon\beta_p$ and q_ψ. Thus, the role of elongation in increasing $\langle\beta\rangle$ is via increases in I_p at constant β_p, a, and B [Eq. (4.4)]. This elongation enhancement is much more significant than, and in addition to, the currently perceived dependence of C_τ on κ.[40]

Figure 4.7(a) also shows that the value of $\varepsilon\beta_p$ that maximizes $n\tau_{Ee}$ and plasma performance is not sensitive to the uncertainty in the form of τ_{Ee} as long as a substantial decrease in τ_{Ee} occurs when $\varepsilon\beta_p$ reaches values of 0.6-0.7. As indicated by the plot of the "stiff" limit in β_p in Fig. 4.7(a), a maximum value of $\varepsilon\beta_p$ of $\sim$0.6 remains appropriate.

4.4.4 Conclusions and Future Work

Based on these assessments, it becomes clear that the baseline value of $\varepsilon\beta_p$ = 0.5 is relatively conservative but appropriate. The choice of q_ψ = 3.2 is primarily based on concerns of major plasma disruption (Sect. 4.7). Using Eqs. (4.1) and (4.4), we obtain for q_ψ = 3.2 the baseline FED plasma parameters of β_p = 1.8, $\langle\beta\rangle$ = 5.5%, and I_p = 4.8-5.4 MA as $\langle\beta\rangle$ is increased from 0.2% to 5.5%.

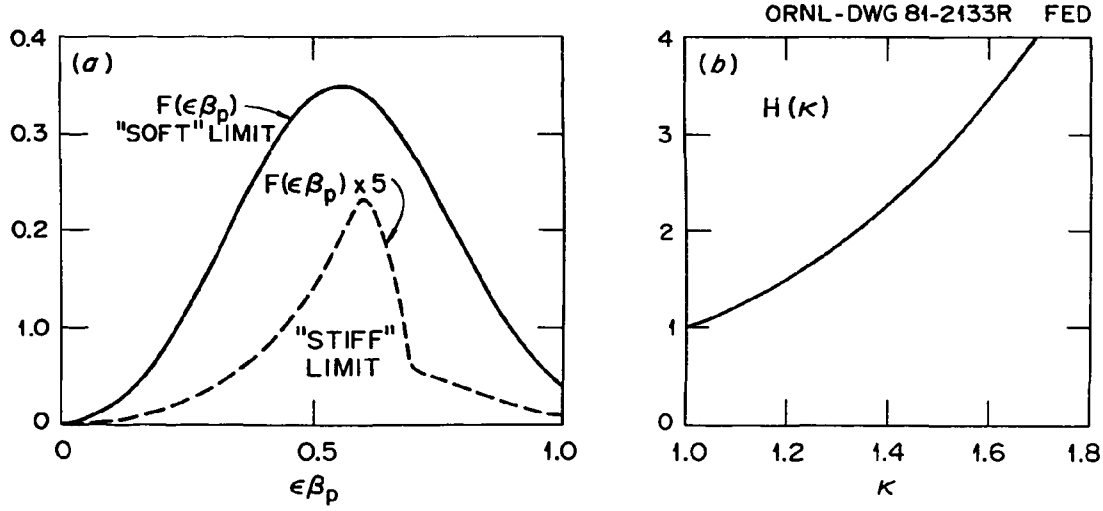

Fig. 4.7. The dependence of $n\tau_{Ee}$ on $\varepsilon\beta_p$ and κ with constant q_ψ as expressed in Eq. (4.3) through (a) $F(\varepsilon\beta_p)$ and (b) $H(\kappa)$. The variations of $F(\varepsilon\beta_p)$ assuming a relatively stiff limit in β_p as shown in Fig. 4.6 are also included.

With a constant q_ψ and B_m, the assumption of a "soft" limit in β_p leads to a strong maximization of the plasma performance $n\tau_{Ee}$, near $\epsilon\beta_p = 0.55\text{-}0.6$, and a threefold enhancement of $n\tau_{Ee}$ by elongation to $\kappa = 1.6$. These results are shown to be invariant to uncertainties in the size scaling of τ_{Ee} and the "stiffness" of the β_p limit.

It is also seen that the plasma performance depends predominantly on B_m and q_ψ, as revealed in Eq. (4.7):

$$n\tau_{Ee} \propto B_m^{4+v}/q_\psi^{4-u} ,$$

aside from the relatively weak dependence through $F(\epsilon\beta_p)$. To achieve high plasma performance, it is thus just as effective to lower q_ψ as it is to raise B_m. Low B_m operation in FED can be offset by a lower q_ψ, as long as plasma disruptions can be avoided (Sect. 4.7.3). This suggests that the disruption-free regime of $q_\psi < 2$ demonstrated in DIVA,[41] if achievable in FED, would permit a highly cost-effective FED design.

The FED performance for a given cost is expected to depend strongly on the achievable $<\beta>$ values. Means to maximize $<\beta>$ should therefore continue to be explored. Also, the effects of triangularity in the improved basis for beta estimates need to be analyzed.

4.5 PLASMA PERFORMANCE

The potential plasma performance for a given FED design can vary over a significant range for three major reasons. First, for a given set of transport assumptions, a given value of q_ψ, and a maximum β_p in a full bore plasma, the plasma density, temperature, and fusion output can be varied significantly while still meeting the basic machine goals. Second, for a given FED design, it may be desirable to operate at a higher q_ψ in exchange for increased pulse length and possibly reduced disruptivity. Third, significant uncertainties still remain in the projection of plasma behavior to FED conditions. Reasonable variation about a given model can significantly alter the expected performance.

Examination of the likely range of plasma burn performance provides valuable information on the available FED plasma design space. Such information, together with its engineering design and cost implications, should aid the development of a flexible FED design.

The preliminary results discussed here have been obtained with the ORNL WHIST code. Similar calculations are needed using the Princeton Plasma Physics Laboratory (PPPL) BALDUR code, the General Atomic Company (GA) transport code, and the ORNL PROCTR code to increase confidence in the estimates of FED performance.

4.5.1 Plasma Performance and Operation Space

The WHIST one-and-one-half-dimensional (1-1/2-D) time-dependent transport code[23] has recently been modified to generate quasi-static plasma operation parameters and profiles as a function of average plasma density and temperature. The information is displayed in the form of Plasma OPeration CONtour (POPCON) plots in density-temperature space[24] for a given set of machine parameters and physics assumptions. A number of POPCON plots have been produced recently for the FED plasma. The basic physics assumptions used include:

1. Injection of 150-keV neutral deuterium beams tangential to the inside edge of the plasma with a neutral power mix of 66:19:15 among full, half, and third energy components (Sect. 4.4.3).
2. An ion conduction model that includes twice neoclassical losses plus flux surface integrated ripple-plateau[42] and ripple-trapped[43] losses for 0.7% peak-to-average ripple at the plasma edge.
3. Alcator scaling for electron conduction.
4. A relatively low q_ψ value of 2.5 (the present baseline value is 3.2).
5. Local fusion alpha heat deposition.
6. Pellet fueling coupled with complete particle exhaust (this leads to peaked density profiles and increased fusion power output compared to a limiter-confined plasma with large recycling).
7. An absence of impurities.

Some examples are shown in Fig. 4.8. The advantages of increasing density during neutral beam heating[16] are illustrated in Fig. 4.8(a) by the occurrence of a saddle point in the heating power requirements.[25] The saddle point lies between a low density ohmic plasma and a higher density burn plasma. The beam power at the saddle point represents the minimum required to reach the operating regime for an indefinite beam pulse time. For the basic physics assumptions, this minimum is about 25 MW. An additional 20 MW or so should be provided to account for the dynamic effects of density buildup (Fig. 4.4) and to heat the plasma in about 6 s, raising the plasma energy content to about 100 MJ.

The fusion power output and the average toroidal beta (including fast beam and alpha contributions) are plotted in Figs. 4.8(a) and 4.8(b), respectively. A reference plasma operating point can be chosen from these results, typically $\langle\beta\rangle \simeq 5.5\%$, $\langle T\rangle \simeq 10$ keV, and $P_{fusion} \simeq 200$ MW at $\langle n\rangle \simeq 7.0 \times 10^{13}$ cm^{-3}. However, under present physics models, this plasma would be thermally unstable at constant beam heating power and plasma density (or beta) [Figs. 4.8(a) and 4.8(c)]. The same $\langle\beta\rangle$ and fusion power conditions can be met with a thermally stable plasma at $\langle T\rangle \simeq 11$ keV and $\langle n\rangle \simeq 6.5 \times 10^{13}$ cm^{-3}. The plasma Q value is plotted in Fig. 4.8(d), indicating $Q \sim 15$ for the thermally stable reference point. Also, it is seen that the condition $Q = 5$ can be achieved with $\langle\beta\rangle \simeq 4\%$ and 100 MW of fusion output.

Thus, under the somewhat ideal assumptions used in the calculations, a domain of plasma densities and temperatures can be found to satisfy the conditions of thermal stability, $Q \geq 5$, $P_{inj} \leq 36$ MW, $\langle\beta\rangle \leq 5.5\%$, and $P_{fusion} \leq 200$ MW. Such a domain is shown in Fig. 4.9. It is seen that the assumptions of thermal stability and a catastrophic beta limit in this case would eliminate plasma operation at densities above 6.5×10^{13} cm^{-3}. However, implementation of thermal burn control or the existence of a benign beta limit would permit operation at densities as high as 1.2×10^{14} cm^{-3} and temperatures as low as 6.5 keV. If an increased range of operation in n and T proves to be desirable, burn control methods for a finite Q device should then be explored.

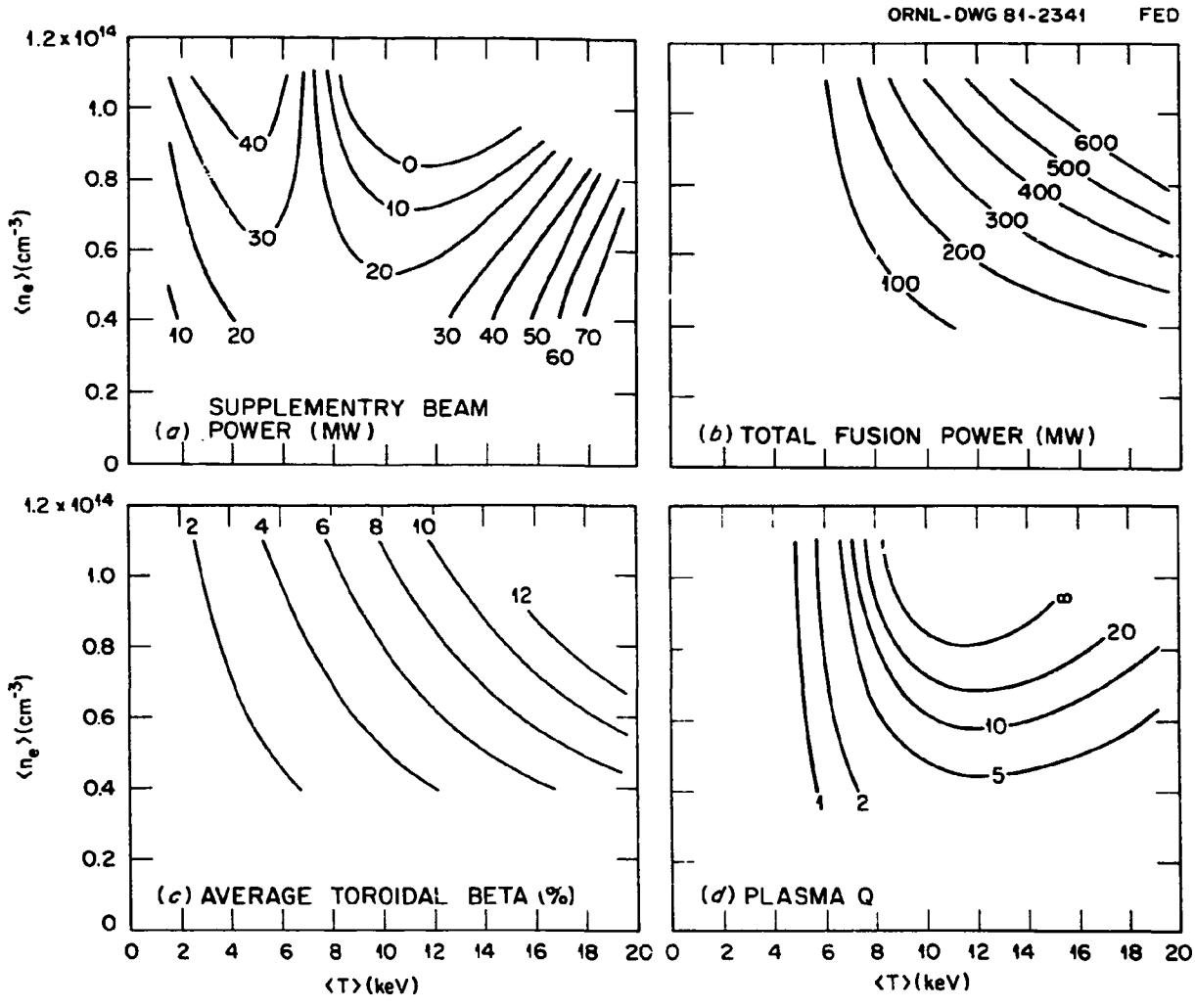

Fig. 4.8. Plasma OPeration CONtours (POPCON) in the density-temperature space for FED based on the physics assumptions listed in Sect. 4.5.1: contours of (a) constant quasi-static heating power, (b) constant fusion power, (c) constant average beta, and (d) constant fusion power amplification Q.

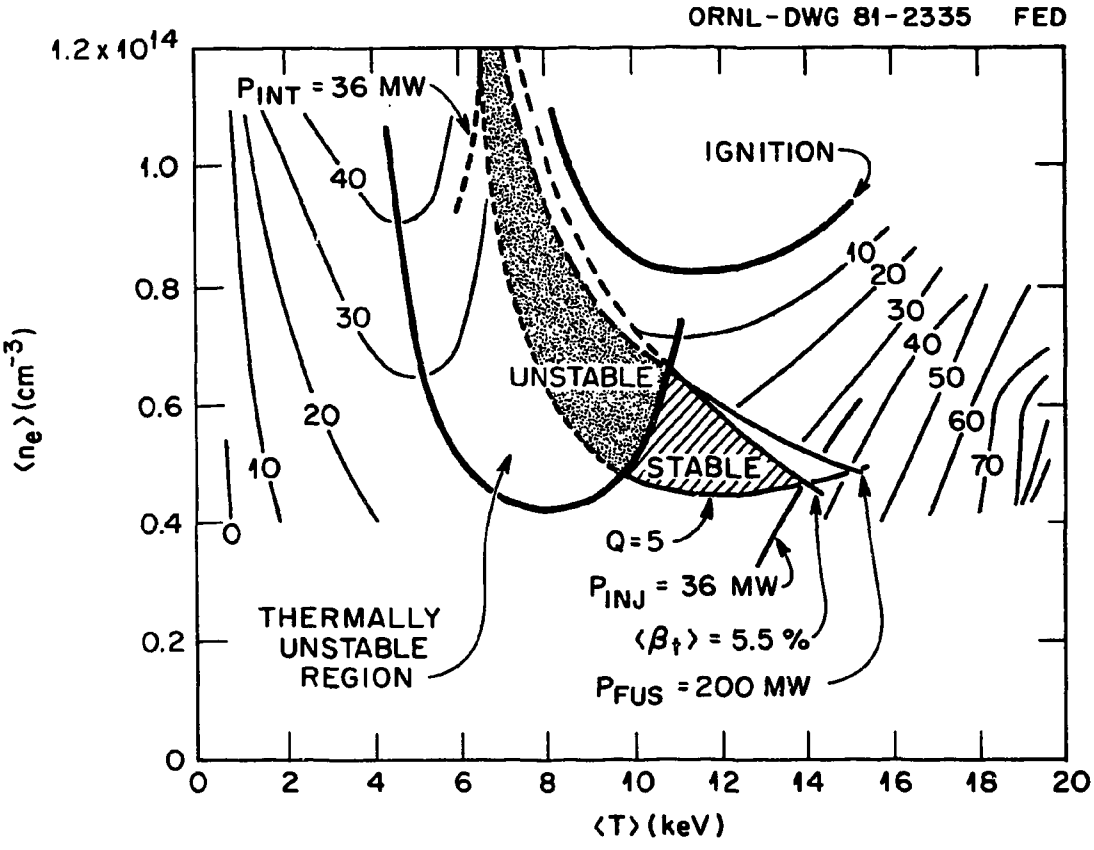

Fig. 4.9. Regimes of densities and temperatures meeting the conditions of $Q \geq 5$, $P_{inj} \leq 36$ MW, $\langle \beta_t \rangle \leq 5.5\%$, and $P_{fusion} \leq 200$ MW.

It should be noted that the parameters suggested in Table 3.1, $\langle T_i \rangle$ = 10 keV and $\langle n_i \rangle = 7.8 \times 10^{13}$ cm^{-3}, depict a point about 10% above the plasma operation domain indicated in Fig. 4.9. However, this inconsistency can be eliminated by improvements to the basic physics assumptions, such as inclusion of some impurities (so that $Z_{eff} = 1.5$) and replacement of pellet fueling by gas puffing and large particle recycling at the limiter. Similar calculations based on contemporary transport codes are needed to provide added confidence in estimates of FED performance.

These POPCON plots prove to be a valuable tool for assessing design requirements, such as the steady-state supplemental heating power and fusion power loads. It is also appropriate to continue design trade analysis with respect to a domain of plasma operations in FED.

4.5.2 Impact of $\varepsilon\beta_p$ and q_ψ Variations

The potential impact of variation in q_ψ on the probability of plasma disruption is discussed in Sect. 4.7. As can be seen from Eqs. (4.1) and (4.4), the values of $\varepsilon\beta_p$ and q_ψ are expected to have a dominating effect on the performance of the FED plasma and the required plasma current. An example of this is given in Table 4.2, which shows that a 20% variation in $\varepsilon\beta_p$ or q_ψ could permit ignition in a clean FED plasma.

The impact of these two parameters on the average beta ($\langle\beta\rangle$), fusion power (P_{fusion}), neutron wall load (L_w), plasma current (I_p), burn pulse length (t_{burn}), and fusion energy production per pulse (W_{fusion}) has been analyzed based on Eqs. (4.1) and (4.4) using the FED Systems Code [discussed in the Appendix (see also Ref. 44)]. The results are plotted in Fig. 4.10. At a low value of $q_\psi \simeq 2.3$, a fusion power of $\sim$1000 MW and a neutron wall loading of $\sim$2.5 MW/m^2 can be produced by the plasma if $\varepsilon\beta_p = 0.6$ is assumed. However, the plasma current is near the limit of the OH flux capability, so only a negligible t_{burn} is obtained, producing little W_{fusion} per pulse. As q_ψ is increased, W_{fusion} rises sharply, reaches a maximum near $q_\psi \simeq 3$,

then falls off relatively slowly. Similar behavior is seen if $\varepsilon\beta_p = 0.4$ is assumed, except that the maxima of P_{fusion} and L_w are 300 MW and 0.8 MW/m^2, respectively.

This rather simple analysis shows that a design limit of $P_{fusion} \lesssim$ 200 MW will determine a lower bound of q_ψ as a function of $\varepsilon\beta_p$. This bound occurs at $q_\psi = 2.6$ for $\varepsilon\beta_p = 0.4$ and at $q_\psi = 3.5$ for $\varepsilon\beta_p = 0.6$. Figure 4.10 also shows that it is possible to operate FED at relatively high q_ψ values without seriously lowering the fusion energy production per pulse, assuming the absence of impurity and ash accumulation (Sect. 4.6) and plasma poloidal flux diffusion (Sect. 4.8).

Table 4.2. Impact of varying q_ψ and $\varepsilon\beta_p$ on global plasma parameters in FED

	Baseline performance	Less favorable performance	More favorable performance
q_ψ	3.2	3.2	2.5
$\varepsilon\beta_p$	0.50	0.40	0.50
I_p (OH)	4.8 MA	4.8 MA	6.0 MA
I_p (during burn)	5.4 MA	5.2 MA	6.8 MA
β_p	1.8	1.5	1.8
$\langle\beta\rangle$ (during burn)	5.5%	4.2%	8.9%
$\langle T\rangle$	10 keV	10 keV	10 keV
$\langle n_e\rangle$	8×10^{13} cm^{-3}	6×10^{13} cm^{-3}	1.3×10^{14} cm^{-3}
Q	5	3	∞
$P_{driving}$	36 MW	40 MW	0
P_I	180 MW	100 MW	$\sim$500 MW

4.5.3 Range of FED Plasma Models and Assumptions

A relatively wide range of plasma physics assumptions was recently suggested by the FED Technical Management Board (TMB) and discussed by the FED Confinement Team[45] as a guideline to the assessment of the FED

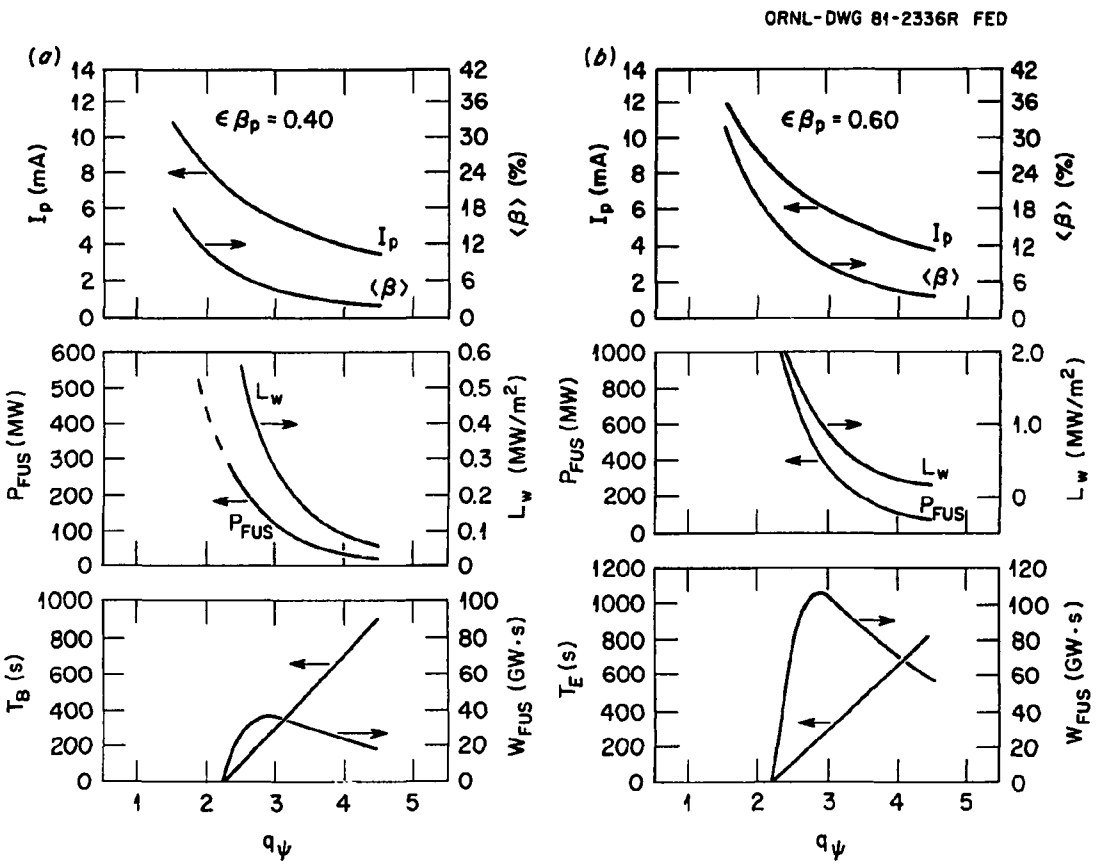

Fig. 4.10. Dependence of plasma current I_p, beta $\langle\beta\rangle$, fusion power P_{fusion}, wall load L_w, burn time t_{burn}, and fusion energy per pulse W_{fusion} on the safety factor q_ψ for (a) $\varepsilon\beta_p = 0.4$ and (b) $\varepsilon\beta_p = 0.6$.

performance. From a baseline model, both optimistic and pessimistic variations are indicated for electron and ion thermal conduction, ripple-induced ion conduction, particle diffusion, beta limitations, high or low q operations, impurity transport, susceptibility to major disruptions, neutral beam and rf heating methods, etc.

The impact of variations in the physics models can be assessed from the POPCON plots, for example, of the supplementary heating power requirements. While significant work in this area is in progress at ORNL[46] and elsewhere, two preliminary examples of interest are discussed here.

Variations in electron heat conduction

The impact of variations in electron heat conduction on the FED performance is studied with the χ_e values from the Alcator scaling doubled and halved. The resulting POPCON plots are shown in Fig. 4.11. One finds that when χ_e is doubled [Fig. 4.11(a)], a minimum beam power (at 150 keV) of 40 MW is needed to sustain operation at $Q \approx 5$ and about 60 MW is needed for heatup in 6 s. Only a minimal domain in $\langle n \rangle$ and $\langle T \rangle$ exists for $Q \geq 5$ and $\langle \beta \rangle \leq 5.5\%$. If χ_e is halved [Fig. 4.11(b)], a minimum beam power of $\lesssim$20 MW would be needed to reach $Q = 5$. The plasma would then ignite with $\langle \beta \rangle \approx 5\%$ and $P_{fusion} < 200$ MW.

Soft limit in β_p

The impact of a soft limit in β_p (Sect. 4.4) is assessed by assuming

$$\chi_e = 0.5\chi_e^{Alc} \exp(2\varepsilon\beta_p)^2 + \chi_e^{NC} ,$$

which is consistent with the recent ISX-B observations.[32,47] The resulting POPCON plots, as shown in Fig. 4.12, reveal a drastically different nature from that of the previous figures. It is seen that, while $Q \geq 5$ is still achievable, ignition is excluded. The supplementary neutral beam power required is also reduced to about 20 MW.

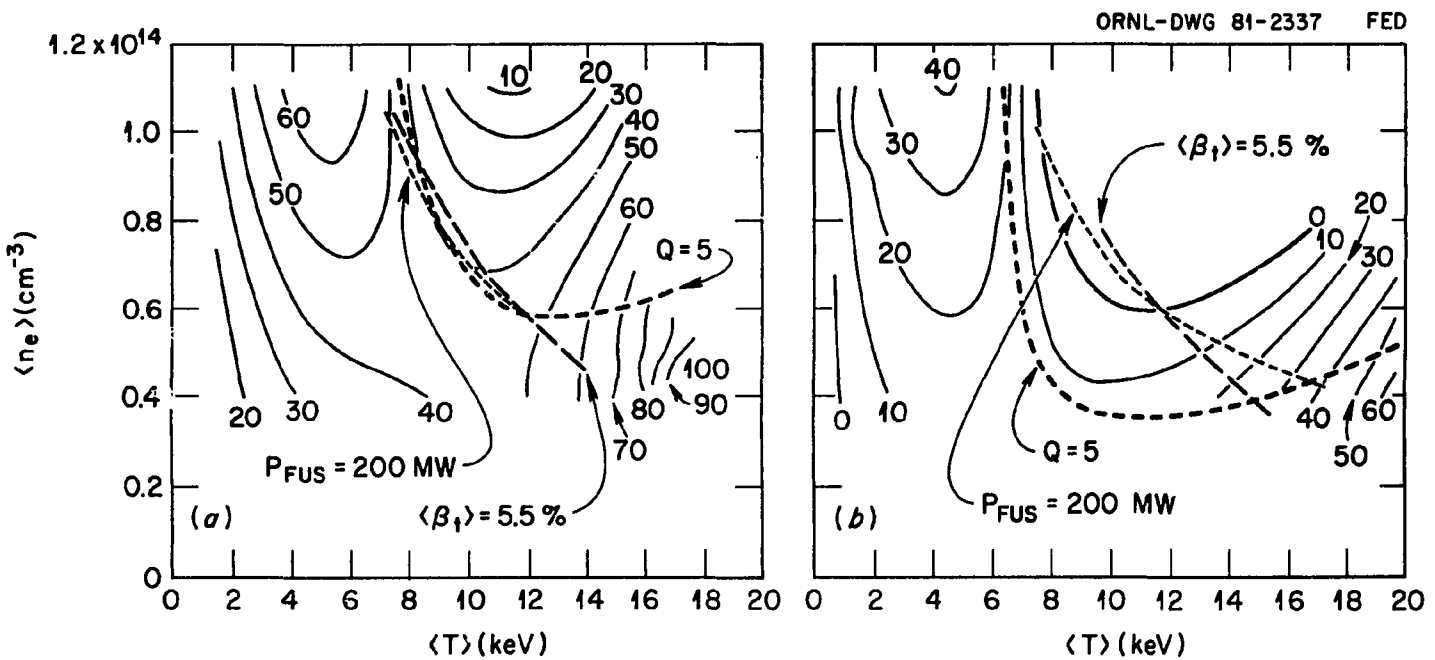

Fig. 4.11. Steady-state beam power requirements as a function of $\langle n_e \rangle$ and $\langle T \rangle$ for (a) $\chi_e = 2\chi_c^{Alc} + \chi_e^{NC}$ and (b) $\chi_e = 0.5\chi_e^{Alc} + \chi_e^{NC}$.

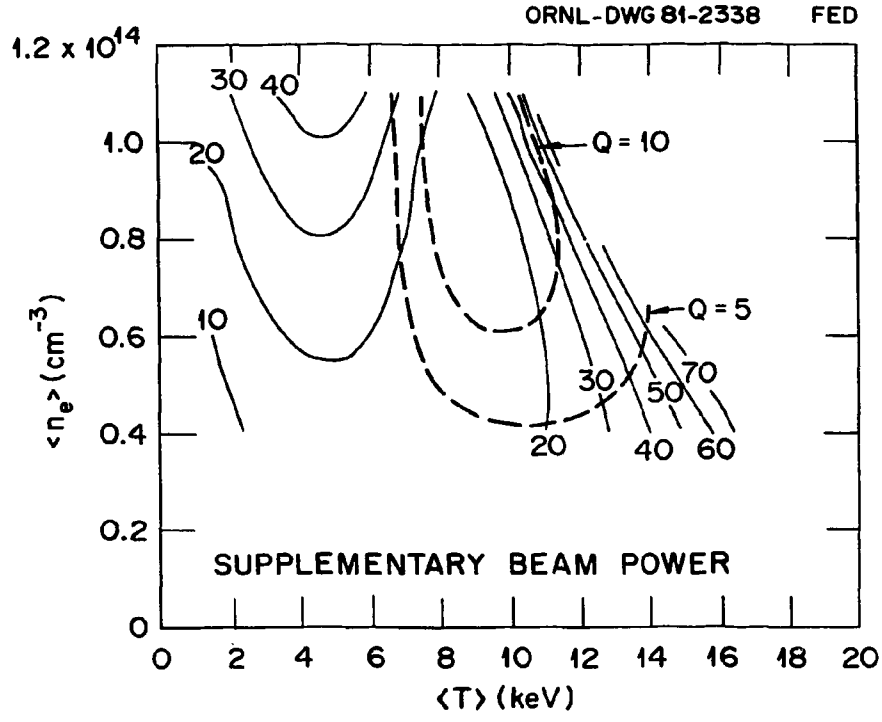

Fig. 4.12. Contours of constant steady-state beam power and plasma power amplification Q as functions of density and temperature in FED assuming $\chi_e = 0.5\chi_e^{Alc}\exp(2\varepsilon\beta_p)^2 + \chi_e^{NC}$.

While the results discussed here should be considered preliminary, a considerable margin exists in the current FED design concept to achieve the basic plasma performance required. The margin can accommodate factor of 2 uncertainties in τ_{Ee} and the assumption of a strongly enhanced χ_e with increasing β_p (a soft β_p limit).

4.5.4 Conclusions and Future Work

It is seen that the assumptions of baseline parameters and physics models lead to a finite domain of clean FED plasma operation to satisfy the conditions of $Q \geq 5$, $P_{inj} \leq 36$ MW, $\langle\beta\rangle \leq 5.5\%$, and $P_{fusion} \leq 200$ MW. Without thermal stability control, the domain ranges from 10 keV to 14 keV in $\langle T\rangle$ and 4.5×10^{13} cm^{-3} to 6.5×10^{13} cm^{-3} in $\langle n\rangle$. With thermal stability control, the domain can be extended to $\langle T\rangle \gtrsim 6.5$ keV and $\langle n\rangle \leq 1.2 \times 10^{14}$ cm^{-3}. The condition of $\langle\beta\rangle \leq 5.5\%$ would exclude achieving $P_{fusion} \geq 200$ MW using the baseline assumptions.

Inclusion of impurity effects and particle recycling is expected to lower the estimated plasma performance and reduce the domain of operation. Compared to these results, the baseline plasma parameters of $\langle n\rangle \simeq 8 \times 10^{13}$ cm^{-3}, $\langle T\rangle \simeq 10$ keV, $P_{fusion} = 180$ MW, and $Q = 5$ are considered reasonable.

It is also seen that a considerable margin exists in the baseline FED concept to achieve the nominal performance parameters. The margin can accommodate factor of 2 uncertainties in τ_{Ee} and the assumption of a strongly enhanced χ_e with increasing β_p (i.e., a soft β_p limit). By deliberately operating a clean FED plasma at higher values of q_ψ, burn times can be increased without a significant reduction in the total fusion energy output per pulse.

These results also suggest that future calculations of FED performance should include improved realism, such as the effects of impurities and large recycling from the pump limiters. Comparisons of FED calculations made with various advanced transport codes from GA, ORNL, and PPPL are indispensable at this stage of the FED concept development. The impact of pessimistic and optimistic physics models should continue to be studied. Also, the efficacy of burn control to expand the FED operation regimes to high density and low temperature should be assessed.

4.6 PARTICLE AND IMPURITY CONTROL

A limiter defining the plasma boundary has recently been observed[48,49] to produce high neutral pressure at pump channels in the vicinity. When the limiter channel configuration is such that a fraction of the incident plasma or neutral particles can also ballistically reach into a pump channel,[50-52] pump limiters are obtained. Thus, a mechanical pump limiter has been proposed as a method to exhaust hydrogen and helium, to handle significant heat load, and to protect the first wall from large particle and energy fluxes. Nevertheless, backup impurity control may be needed, so a number of impurity control options are discussed here. Depending on the outcomes of these impurity control methods, the particle and power loads to the limiter and first wall can vary widely. The range of such variations is also discussed.

4.6.1 Pump Limiter Configurations

Three toroidal belt, pump limiter configurations have been proposed for analysis and comparison before a design choice can be made. They are:

1. single-edge limiters 45° from the midplane (Fig. 4.13),[2]
2. slotted limiters 45° from the midplane (Fig. 4.14),[2] and
3. single-edge limiters at the chamber bottom (Fig. 6.4).[53]

A comparison of these limiter concepts is summarized in Table 4.3. The following observations concerning the particle removal channel, the limiter location, the startup limiter, the necessity of a leading edge, and the choice of limiter surface material are pertinent.

Particle removal channel

Channeled ducts along the field lines behind the limiter have been included in option 1. They result in an increased duct aspect ratio (ratio of length to cross section), reducing the neutral backflow without significantly reducing the charged particle flux into the pump duct. Option 2 could have a similar advantage by orienting the slots and channels along the field lines. However, this approach also limits

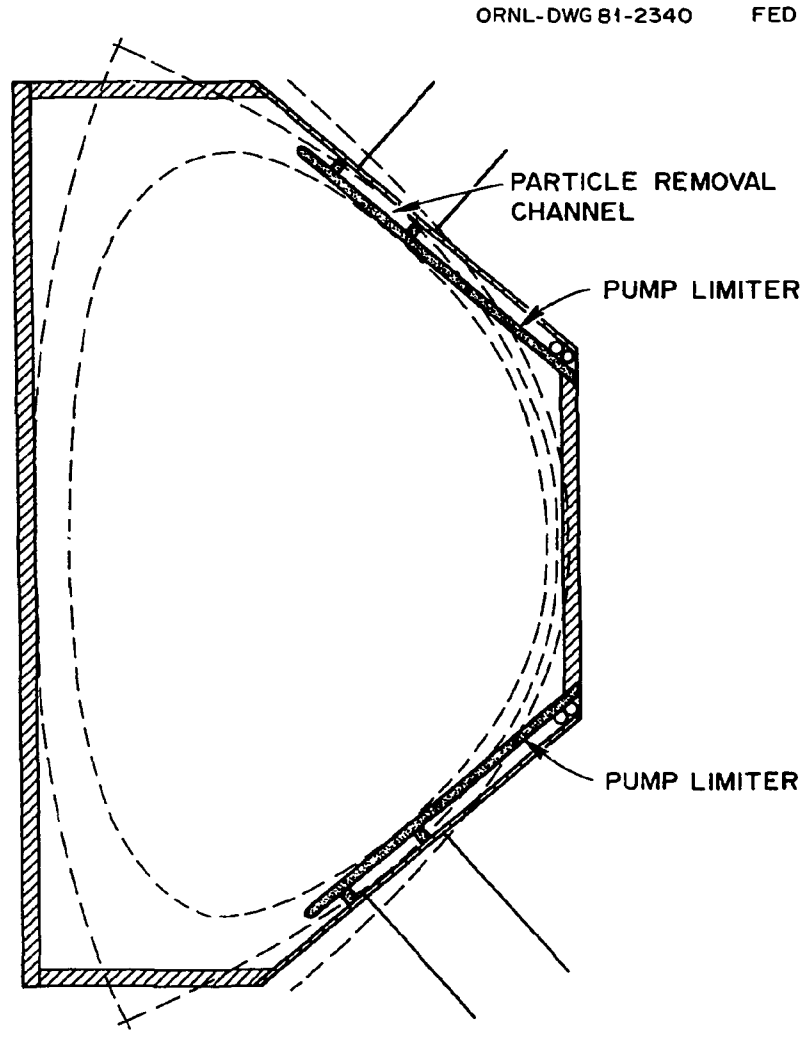

Fig. 4.13. Schematic configuration of single-edge limiters 45° from the midplane.

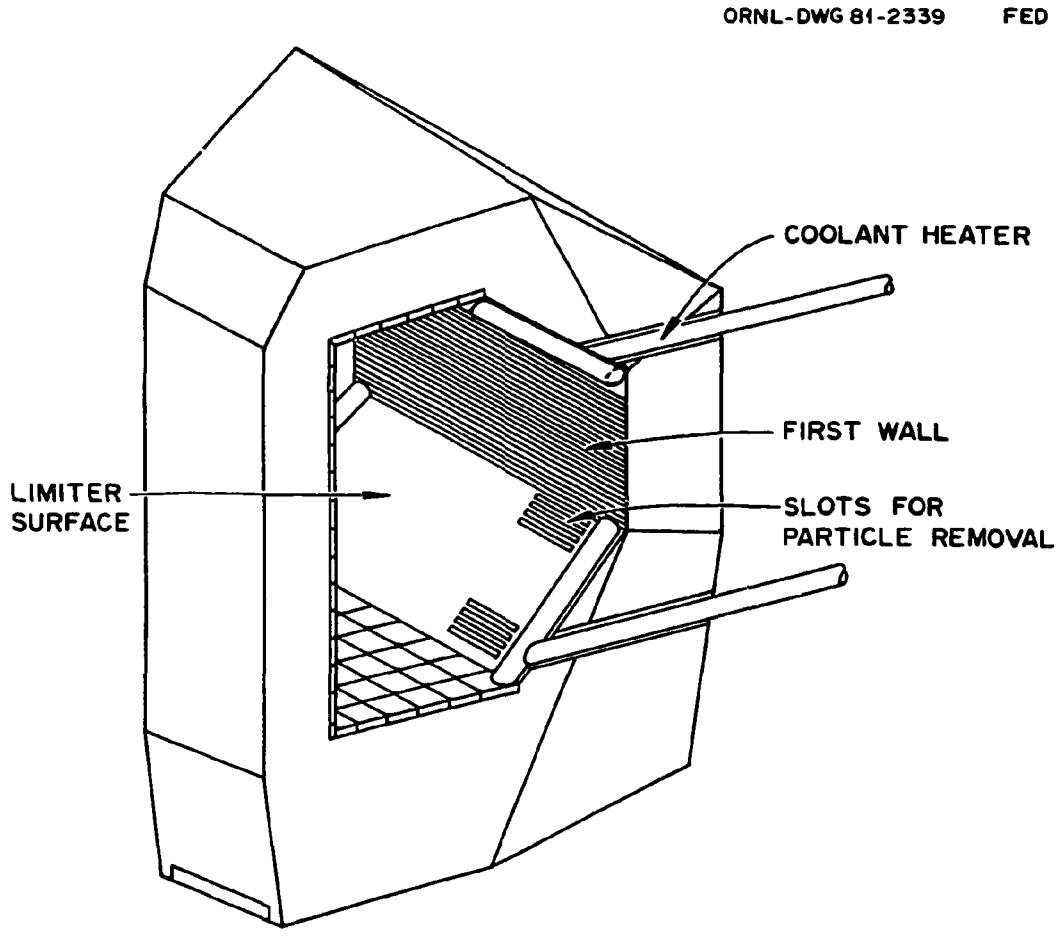

Fig. 4.14. Schematic configuration of slotted limiter 45° from the midplane.

Table 4.3. Comparison of major pump limiter options

Features	Single-edge at 45°	Slotted at 45°	Single-edge at bottom
Curvature of limiter segment	Curved toroidally Flat poloidally	Flat toroidally Flat poloidally	Flat toroidally Flat poloidally
Particle removal channel configuration	Channeled ducts along field lines	Slots in front surface, size and location varied	Currently without channels
Limiter area (percent of chamber area)	18% per limiter	18% per limiter	11%
Estimated particle removal efficiency[a] (λ_n and λ_Q on plasma midplane)	∿10% of plasma particle efflux ($\lambda_n = \lambda_Q = 2$ cm, maximum flux = 100 W/cm^2 on two limiters)	∿3% of plasma particle efflux ($\lambda_n = 4$ cm, $\lambda_Q = 2$ cm, maximum flux = 100 W/cm^2 on two limiters)	∿10% of plasma particle efflux ($\lambda_n = 3.3$ cm, $\lambda_Q = 2.3$ cm, maximum flux = 210 W/cm^2 on one limiter)
Geometric enhancement of λ at leading edge (λ'_n and λ'_Q at leading edge)	∿1.5 ($\lambda'_n = \lambda'_Q = 3$ cm)	∿1.5 ($\lambda'_n = 6$ cm, $\lambda'_Q = 3$ cm)	∿3.5 ($\lambda'_n = 12$ cm, $\lambda'_Q = 8$ cm)
Location of plasma-limiter contact	With two limiters, location controllable by variation in plasma shape. With one limiter, location controllable by movement along 45°		Controllable by radial plasma movement

[a]Assuming clean plasma with large particle heat load to limiter (greater than 52 MW; see Sect. 4.6 and Refs. 48 and 49).

the efficiency of chamber evacuation through the limiter pump ducts during shutdown. A pumpdown time of 30 s between shots is currently assumed. This can be satisfied by options 1 and 3 in the absence of baffle-like channels (Sect. 6.4), but with a potentially large degradation of particle exhaust capability. A careful analysis of the plasma and neutral particle behavior in the pump channel[54] is needed to quantify the particle handling capabilities of the pump limiters and the efficacy of the channeled ducts behind the limiters.

Limiter location

The most desirable location of the pump limiter relative to the plasma is currently unclear. The geometric enhancement of the heat flux decay length λ_Q and the relative ease of controlling the location of plasma-limiter contact apparently favor the bottom limiter (option 3). Enhancement of λ_Q should "soften" the plasma particle flux and heat flux to the limiter face and the leading edge In addition, control of the plasma radial position can help to avoid overheating of the limiter edge while maintaining adequate particle exhaust. However, these potential benefits of the bottom limiter will be mitigated by the relatively curved plasma surface, which tends to increase the angle of field lines incident on the limiter surface, and by the low field line pitch at the bottom, which tends to make it difficult to install channeled ducts behind the limiter. Other potential drawbacks of the bottom limiter relative to options 1 and 2 include the requirements for full plasma elongation and control of the plasma vertical position. Detailed analyses are needed to clarify the trade-off between the two limiter positions.

Startup limiter

The pump limiters become active only when the plasma has attained full (or almost full) elongation. A separate set of limiters at the midplane without pumping capability is therefore needed during small radius startup of the plasma current, although options 1 and 2 could limit the plasma near the end of the startup phase. An alternative

approach (presently judged impractical) is an asymmetric poloidal field (PF) coil system to hold the startup plasma on the pump limiter away from the midplane. The choice between these two approaches seems to depend largely on the need for particle and impurity control during startup and on the difficulties of plasma current startup off the midplane.

Necessity of a leading edge

The configurations proposed so far for FED have been similar in containing a leading edge to "shovel" a stream of plasma toward a pump channel.[50] The heat load at the leading edge can become excessively high when the scrapeoff thickness changes. However, early experimental results related to pump limiters[48] have apparently relied on a ballistic collection process of neutrals reflected from a limiter.[52] It is not clear that an active leading edge is a fundamental requirement of the pump limiter. Configurations without a leading edge were recently proposed by Mioduszewski and Sheffield[55] and have been estimated to have a particle removal efficiency ranging from 2.5% to 8%. In view of the preliminary nature of the pump limiter concept, pump limiters without a leading edge should be seriously pursued for FED.

Limiter and first wall surface material

The material for the limiter and first wall is mainly determined by its interactions with the plasma and its thermomechanical properties during operation and fabrication. The selection criteria discussed here are based on interactions with the plasma. Each material can be assigned a figure of merit based on its sputtering rate and the tolerable level in the FED plasma. Figure 4.15 shows plots of the ratio of the maximum allowable impurity concentration in a burning plasma to the sputtering yield.[56] Deuterium sputtering has been considered here as an example, but the results are similar for tritium and helium sputtering. The figure shows that in the energy range of several hundred electron volts, low Z materials such as carbon and beryllium are superior to all other

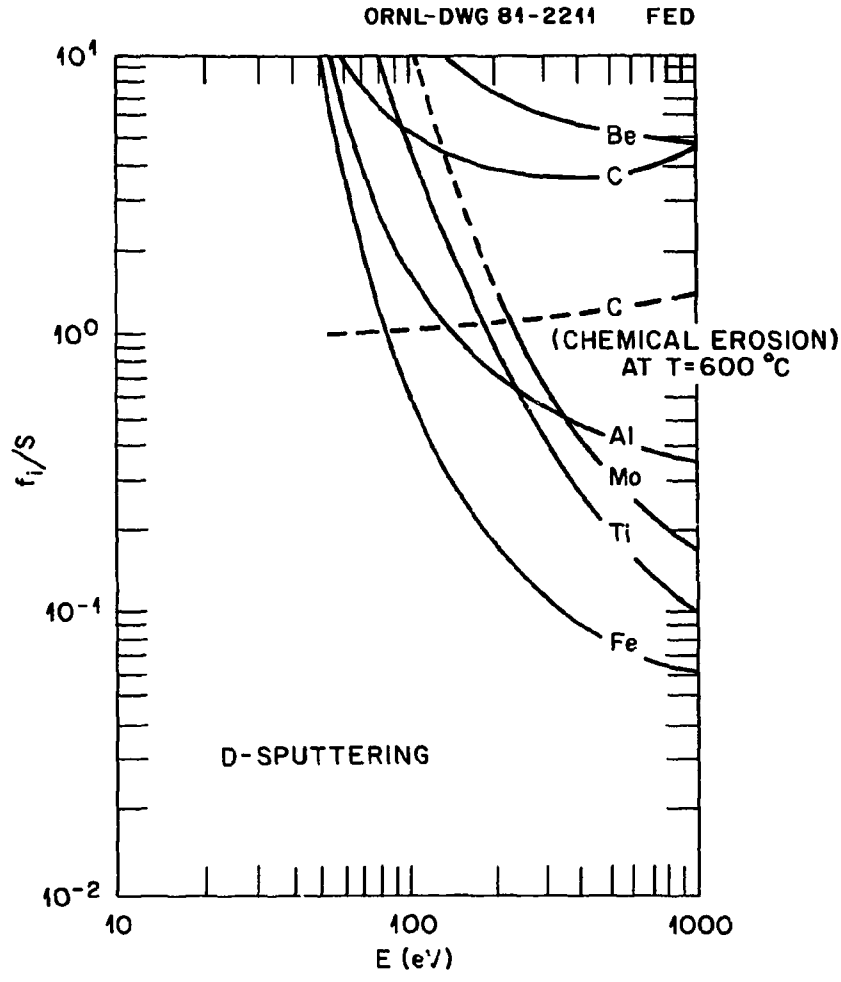

Fig. 4.15. Figures of merit, defined as the ratio of the maximum allowable impurity concentration in plasma (f_i) to the sputtering yield (S) as a function of incident particle energy for candidate limiter and first wall materials.

materials. At particle energies below 100 eV, however, refractory metals like molybdenum appear favorable due to their rather high sputtering threshold. Stainless steel is apparently inferior to almost all other choices over the entire energy range of interest. In the case of carbon, chemical erosion must be taken into account, suggesting the need for a surface coating or a design around the critical temperature.

Low Z coating of the first wall and limiter is apparently an attractive approach to alleviate potential impurity problems of the pump limiter. The technology of precoating before installation or in situ coating during shutdown is being explored[57] and is expected to be highly useful in FED.

4.6.2 Magnetic Divertor Options for Impurity Control

Although the pump limiter has a high potential for particle control, it may not be a viable means of complete impurity control. Limiter-generated impurities resulting from a high plasma edge temperature may be difficult to exclude from the plasma. Although the engineering problems associated with magnetic divertors in ETF[58] were viewed as difficult and complex, the reduced field strength in FED (from 11.4 T to 8 T) is expected to significantly alleviate these difficulties.

Potential advantages of magnetic divertors include placing the source of impurities away from the plasma edge, removing a material leading edge, locating high charge exchange fluxes in the divertor channel, and maintaining a high particle exhaust capability.

Simplified poloidal divertor (primary backup)

Recent experimental results from PDX, ASDEX, and DIVA have provided confidence in the physics basis of poloidal divertors. This divertor option has been assessed in the ETF[58] and International Tokamak Reactor (INTOR)[59] studies. The extensive INTOR studies have suggested feasible poloidal divertor designs with relatively large PF coils external to the TF coils, which are currently perceived to be less than attractive for an eventual reactor. Assessment of the physics requirements of a

simplified FED poloidal divertor with relatively shallow divertor channels will borrow significantly from the INTOR studies.

An example of a single null divertor configuration is depicted in Fig. 4.16. The divertor geometry is configured for the flux surfaces of a high beta equilibrium using PF coils external to the TF coils. The plasma has an elongation of about 1.6 and a triangularity of about 0.3. The inside divertor throat can be quite open and shallow; preliminary studies[54,58] indicate that the neutrals and impurities will be localized near the divertor plate. There is no pumping from the inside divertor throat, since it is sufficient for helium removal to pump only the outside channel. Pumping apparently does not influence the metallic impurity behavior, since these atoms stick readily to the channel walls. The neutral gas fueling appears to be largely confined to the divertor channels; only limited fueling is needed in the main chamber so limited first wall erosion is obtained. Pumping speeds of less than 10^5 L/s should be sufficient to remove the helium from FED.

The entire divertor assembly can in principle be removed by moving the segments radially outward between the TF coils. This allows ready access for replacement of eroded surfaces and surfaces with material buildup. A collaboration with the engineering design is needed to produce a FED-specific magnetic and mechanical configuration. The divertor modeling codes now being developed[54,60] should be used to support the design analysis. However, the need for experimental tests of these new concepts and models should not be underemphasized.

Compact bundle divertor for FED[61]

A compact bundle divertor that fits between two adjacent TF coils can assist the pump limiter in impurity control without significantly altering the FED tokamak configuration. The search for a compact bundle divertor for FED presents a unique challenge of minimizing the deleterious effects of local magnetic field ripple while meeting reasonable engineering constraints.

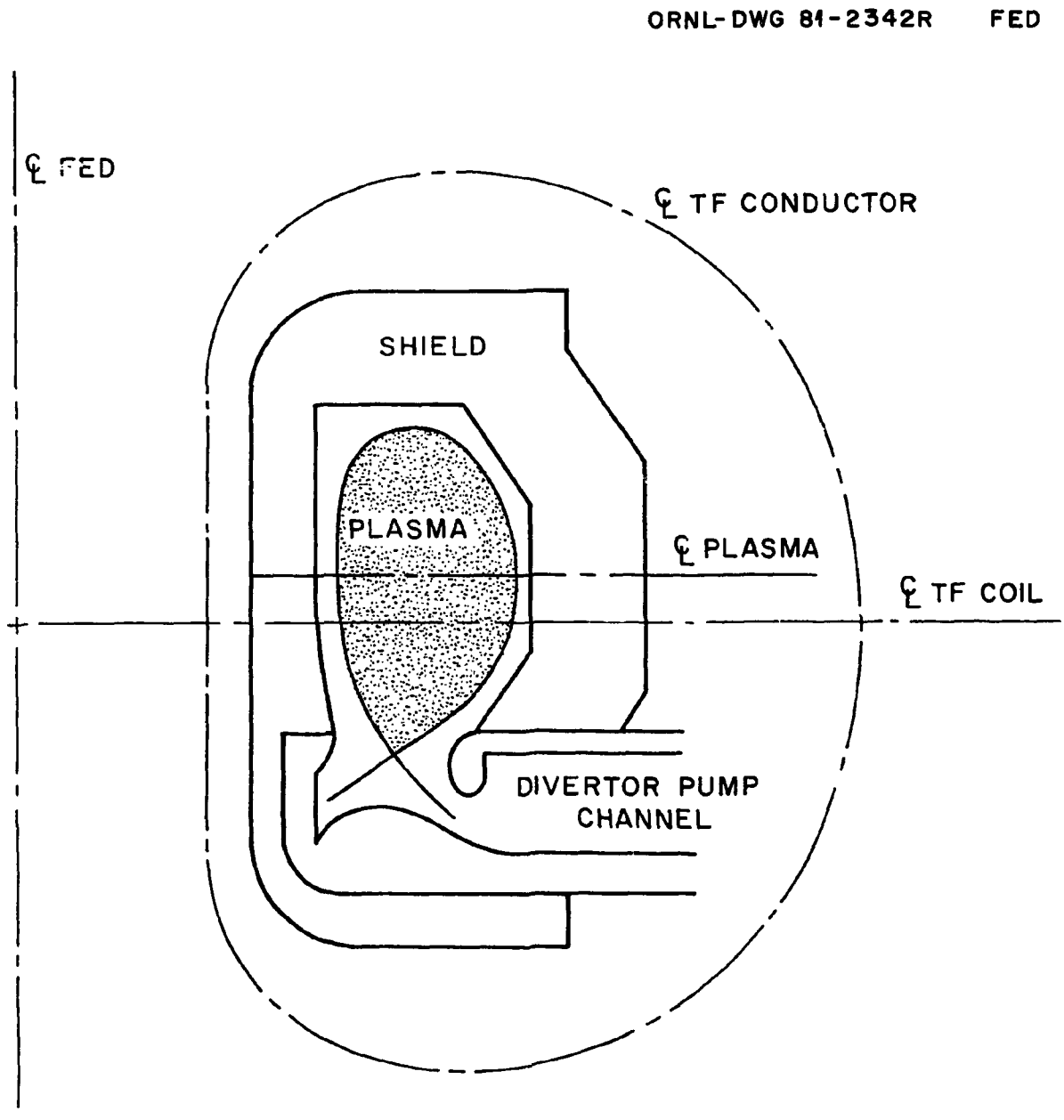

Fig. 4.16. Schematic configuration of a single null poloidal divertor with shallow divertor channels.

When local ripple exists, the toroidal canonical angular momentum, p_ϕ, typically changes near the divertor but is conserved when the ion is far from the divertor. Our work[61] has shown that for fast circulating ions, p_ϕ is quasi-periodic and bounded, implying good confinement in the presence of a new invariant. Most banana-trapped fast ions, however, cannot maintain quasi-periodicity when these particles mirror off the local maxima flanking the divertor. The radial step size at the mirror point can be estimated by

$$|\Delta\psi|/\psi \sim 2(\Delta B/B)^{1/2}(vRB_\phi/\omega_c)/\psi \sim (qA\rho_i/\pi a)(\Delta B/B)^{1/2} .$$

This gives a value on the order of 0.01 for FED, meaning that bananas walk out in ~100 bounces or ~1 ms.

High beta worsens the effect of ripple due to the outward shift of the magnetic axis into a higher ripple region. Also, a global minimum in $|\vec{B}|$ usually forms for $\langle\beta\rangle > 6\%$ (Ref. 62), causing the toroidal drift of bananas to stagnate where $\nabla B \to 0$, increasing their interaction time with the ripple and thus increasing the radial step size per bounce. Furthermore, large local ripple will make the outer flux surfaces ergodic and reduce confinement of the bulk plasma. For these reasons, a maximum on-axis ripple of 0.3% has been set as a design requirement.[63]

Our work[61] focuses on the double-T divertor (first proposed by T. Yang[64]) because 2- and 4-coil designs appear unacceptable from an engineering viewpoint. The divertor coil geometry is illustrated in Fig. 4.17. An optimization model is used to minimize on-axis ripple subject to the following constraints: power dissipation < 100 MW; current < 6 kA/cm^2; magnetic scrapeoff thickness < 10-15 cm; horizontal and vertical hole clearances > 30 and 40 cm, respectively; no interference between the front and back T-coils; and the innermost edge of the flux bundle lying beyond the back T-coil. The current density chosen is similar to the steady-state current density used in the ELMO Bumpy Torus (EBT) coils with organic insulation.[65] The coil currents are calculated so that the separatrix joins the plasma edge far from the divertor. The total magnetic field is composed of the vacuum

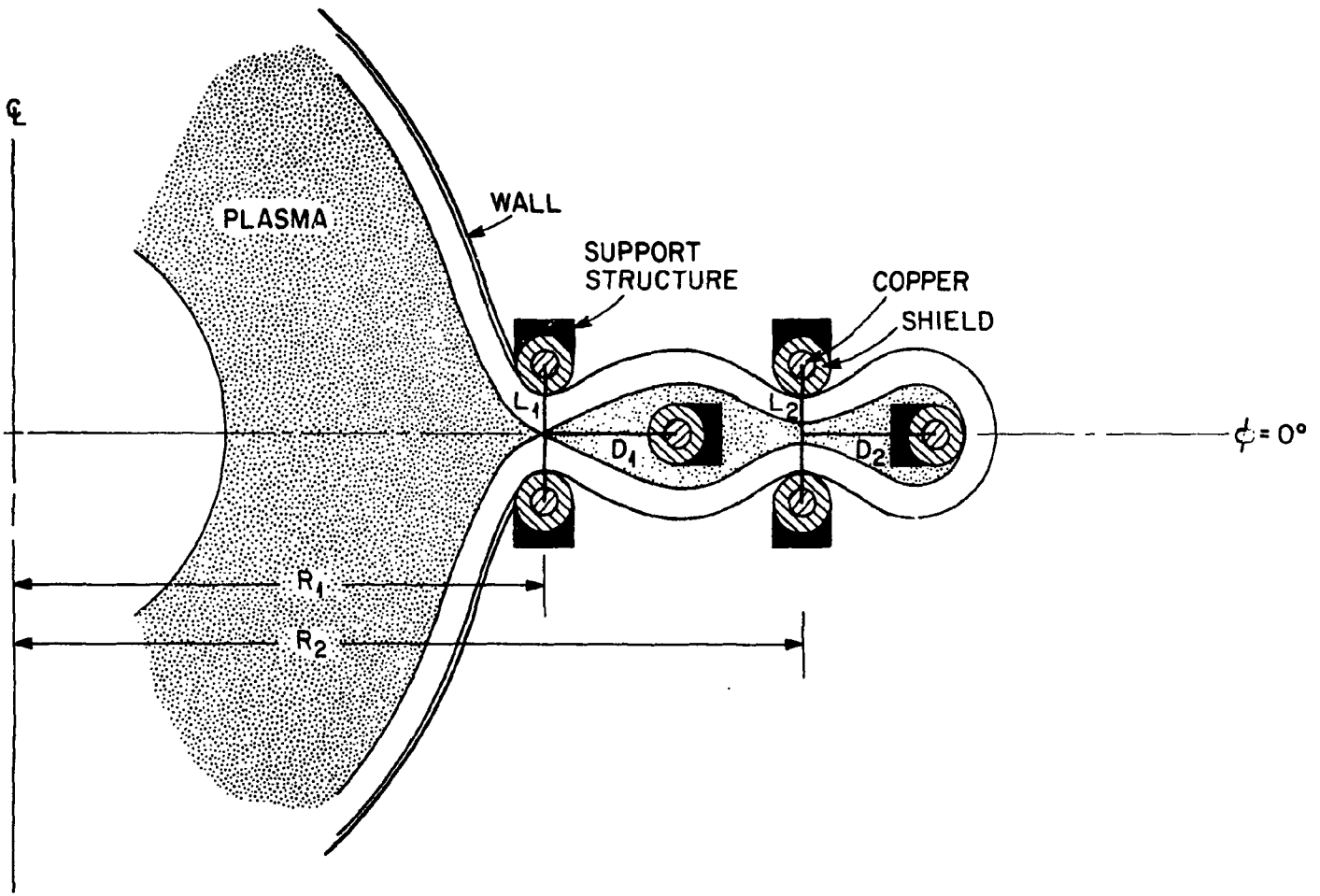

Fig. 4.17. Schematic coil configuration for a compact bundle divertor.

divertor field superimposed on an axisymmetric FED equilibrium; a single wire filament models each coil leg. The TF ripple is presently excluded, so these results tend to be somewhat pessimistic in space requirements but optimistic in total ripple magnitude.

Our results indicate that the ripple and coil currents increase strongly with larger scrapeoff thickness. Since the front T-coil contributes 75-80% of the local ripple at the plasma axis, it is optimized first in the absence of the back T-coil. The back T-coil is then optimized with the front one fixed. Our results for the ETF (B_m = 11.4 T) and for a low field version similar to FED (B_m = 8 T) are summarized in Table 4.4.

The optimization of a nuclear-shielded (30 cm at the front and 20 cm at the back of each coil), double-T divertor on FED yields unacceptably high ripple (∿1%). This is due to the high coil currents necessary for proper location of the separatrix, now that the conductor cross section and the shield cause the divertor to be relatively removed from the plasma. The ripple is found to be acceptable (∿0.25%) for a smaller, unshielded divertor that can be placed relatively close to the plasma with much lower currents. Since FED is expected to be a subignition tokamak with a low neutron fluence, an unshielded divertor with ceramic insulation is expected to last several years. In this case, a coil casing cooling of more than 8 W/cm^3 is needed to handle nuclear heating.

This example indicates that a compact bundle divertor may be a viable backup for impurity control in FED. Further improvements resulting from the hybrid bundle divertor concept[66] may be possible and should be examined. The longer-range importance of the bundle divertor concept depends largely on the experimental outcome of plasma confinement in the presence of local ripple and on the advantages of bundle divertors over competing impurity control and reduction schemes.

4.6.3 Nonmagnetic Approaches to Impurity Control

Significant impurity contamination of the FED plasma is considered highly probable when a pump limiter handles large particle and power loads from the plasma. The limiter face serves as the location of a

Table 4.4. Optimized divertor parameters

Parameter	ETF		Low field version	
R_o (m)	5.42		5.60	
R_{axis} of plasma (m)	5.50		5.66	
R_{edge} (m)	6.72		6.90	
a (m)	1.26		1.30	
b/a	1.6		1.6	
q_s	4.3		2.5	
I_p (MA)	4.9		5.3	
β_p	0.53		0.52	
B_o (T)	5.5		3.91	
	Shielded	Unshielded	Shielded	Unshielded
R_1 (m)	7.268	6.937	7.424	7.178
L_1 (m)	1.853	0.927	0.941	0.903
D_1 (m)	1.876	0.865	0.948	0.761
H_1 (m)	1.442	0.690	1.482	0.653
R_2 (m)	10.040	7.945	9.271	8.127
L_2 (m)	1.786	0.901	9.992	0.975
D_2 (m)	0.152	0.255	0.972	0.100
H_2 (m)	1.498	0.838	1.461	0.860
I_1 (MA)	4.406	1.910	5.711	1.420
I_2/I_1	1.341	0.764	0.875	0.655
δ at plasma axis (%)	1.83	0.27	0.96	0.24
r_{cu} (m)	0.177	0.088	0.174	0.070

dominating source of neutrals as well as impurities. The transport mechanism that brings recycled particles into the plasma core is also expected to bring in significant impurities. It is therefore of interest to explore methods to reduce the impurity contamination to a tolerable level in the fusion plasma core, complementing the particle exhaust capabilities of the pump limiter.

Several nonmagnetic approaches to impurity control have recently been reviewed[5] and suggested.[67] Here the discussion is limited to methods that introduce momentum, particles, or heat into the plasma to modify the flow or the source of impurities. These approaches are summarized in Table 4.5, together with some key properties and preliminary estimates. When the impurity ions are confined to the edge region, where the electron temperature is less than 1 keV, significant radiation is expected to cool the plasma edge even further. The reduced flux of particles and power striking the limiter then leads to a significantly reduced rate of impurity production.

Among these approaches, only impurity flow reversal by momentum[8] and by particle sources[68] has obtained preliminary, but encouraging, experimental indications. A significant amount of research is needed in these promising areas before more reliable projections to FED can be made. Fortunately, none of the proposed schemes is expected to create a need for major modifications in the FED design.

4.6.4 Particle and Power Loads During Burn

Particle and power loads to the limiter and first wall depend strongly on the fraction of thermal power lost through impurity radiation. The radiation power density P_{rad} [$= n_e n_z f(T_e)$] in turn depends strongly on the electron and impurity densities and the electron temperature. The steady-state "emissivity" $f(T_e)$ for several elements is shown in Fig. 4.18 (Ref. 69). The range of $f(T_e)$ as a function of T_e and Z and the uncertainties in the n_e and n_z profiles due to uncertainties in the particle diffusion process are seen to be large, making reliable predictions for FED unattainable at present.

Table 4.5. Comparison of nonmagnetic impurity control concepts in FED

Concept	External supply	Affected region	Estimated requirements	Estimated effectiveness	Potential impact on plasma
Flow reversal by momentum sources[a-c]	Coinjected neutral beam (possibly also ICRF)	Flexible, dependent on beam energy (ICRF dependent on frequency)	Injected power of ~25-50 MW at 150 keV	To be calculated	May require more heating power than needed for burn
Flow reversal by particle sources[a,d,e]	Gas injection	Asymmetric at plasma edge	Injection rate of $\gtrsim 4 \times 10^{22}$/s	Two orders of magnitude reduction in impurity influx[f]	May result in strong steepening of edge density profile
Flow reversal by heat sources[g]	ICRF heating	Asymmetric at plasma edge	Injected power of $\gtrsim$5 MW, using quarter-turn antenna	Two orders of magnitude reduction in impurity influx[f]	May result in steepening of edge temperature profile
Deuterium plasma flush[h]	Deuterium pellet injection	Within 10-20 cm of plasma edge	Pellet injection and particle exhaust a significant fraction of plasma efflux at edge (the latter being $\sim 10^{24}$/s)	To be calculated	May result in radiation cooling of edge by limiting the impurities to the edge region

[a] See Ref. 5.

[b] W. M. Stacey and D. J. Sigmar, Phys. Fluids 22, 2000 (1979); Nucl. Fusion 19, 1665 (1979).

[c] K. H. Burrell, Phys. Fluids 23, 1526 (1980); P. B. Parks, K. H. Burrell, and S. K. Wong, Nucl. Fusion 20, 27 (1980); K. H. Burrell, T. Ohkawa, and S. K. Wong, GA-A16082, General Atomic Company (September 1980).

[d] T. Ohkawa, Kakuyugo Kenkyu 32, 67 (1974).

[e] K. H. Burrell, Phys. Fluids 19, 401 (1976); K. H. Burrell, Phys. Fluids 20, 342 (1977); K. H. Burrell, S. K. Wong, and T. Amano, Nucl. Fusion 20, 1021 (1980).

[f] Assuming no strong steepening of the plasma density and temperature profile at edge. A steepened profile is expected to lead to an enhanced inward transport of the impurity ions, significantly reducing the effectiveness of flow reversal.

[g] J. Y. Hsu, S. C. Chin, and S. K. Wong, "Impurity Flow Reversal by Poloidally Asymmetric ICRF Heating," paper presented at the 4th Topical Conference on Radio Frequency Plasma Heating, Austin, Texas, February 9-10, 1981.

[h] See Ref. 67.

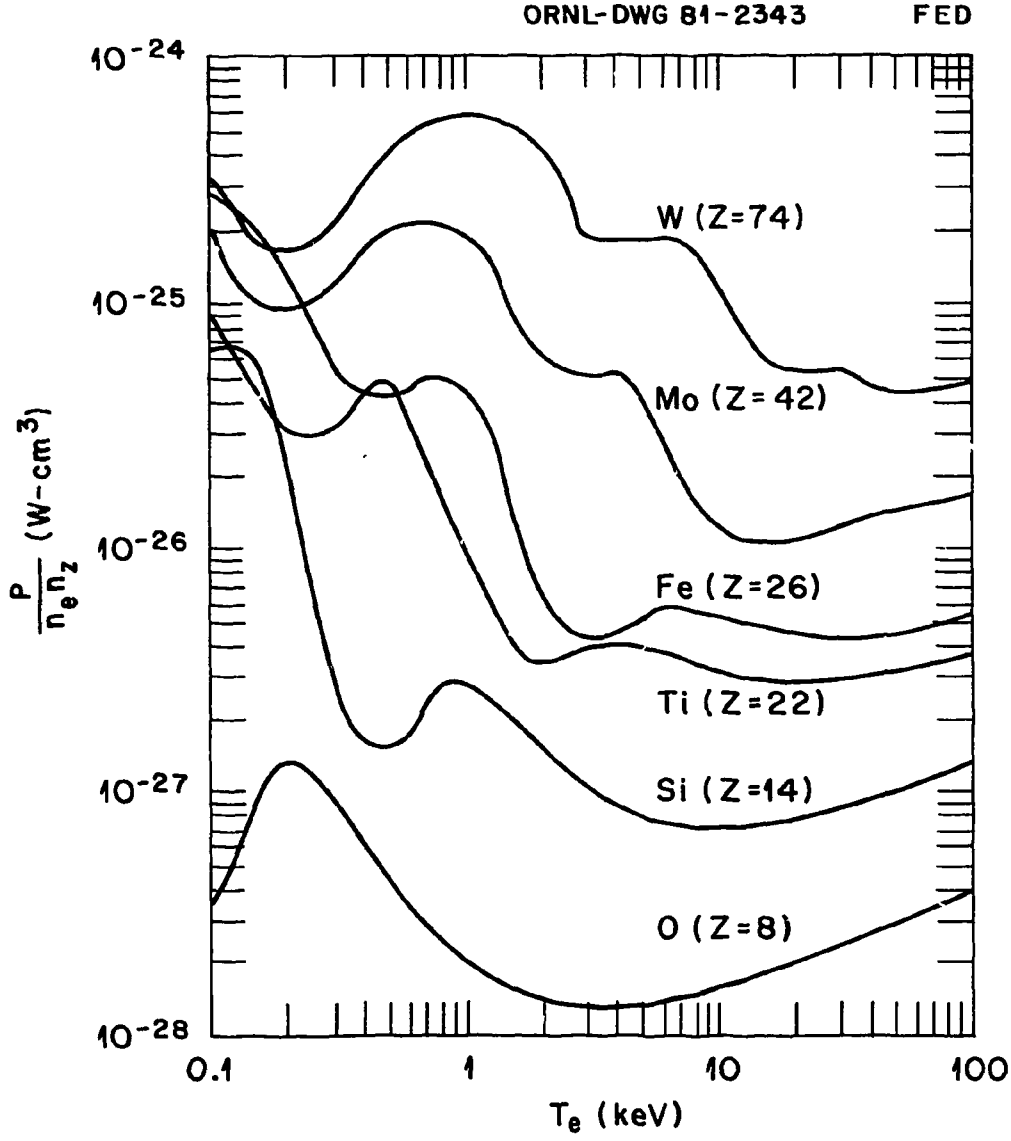

Fig. 4.18. Steady-state impurity radiation power intensity as a function of T_e for various impurity ions.

For the purpose of assessing the impact on the limiter and first wall design, three distinct regimes that span the possible range of particle and power loads are discussed here:

1. Clean plasma (present FED baseline): The plasma contains no more than a small fraction of relatively uniform low Z impurities (e.g., less than 1% oxygen and $Z_{eff} \leq 1.5$) with relatively little impurity radiation. An impurity radiation of about 4 MW is estimated in addition to about 4 MW from cyclotron and bremsstrahlung radiation.
2. Mildly contaminated plasma: The plasma contains a tolerable level of relatively uniform, medium Z impurities (e.g., less than 0.15% iron and $Z_{eff} \leq 1.8\%$), with large impurity radiation loss, perhaps using a mild form of impurity control. With $n_z \sim 1.1 \times 10^{11}$ cm^{-3} and an edge regime of 25 cm where $T_e \sim 200$ eV and $n_e \sim 4 \times 10^{13}$ cm^{-3}, a radiation power of 55 MW would be lost by the edge region. The radiation lost from the plasma core is estimated to be about 10 MW.
3. Plasma with cold edge: The plasma contains a high level of rapidly recycling medium Z and low Z impurities in the edge region. Essentially all the thermal power is radiated from the plasma edge. A highly effective impurity expulsion mechanism, such as the "plasma flush,"[67] is assumed (Table 4.5).

From these assumptions, rough estimates of the particle and power loads for the three regimes can be obtained and are listed in Table 4.6. It is seen that the clean plasma assumption leads to a set of severe design requirements for the pump limiter (Sect. 6.4). A relatively modest success in the nonmagnetic approaches to impurity control to obtain a mildly contaminated plasma is expected to drastically reduce the particle flux and its power loads to the limiter and first wall. The relatively large exhaust in the cold edge scenario is expected to be difficult to achieve with the pump limiters discussed in this document. Thus, the mildly contaminated case seems to represent a workable compromise in the particle pumping and power handling achievable by the pump limiter. One-dimensional transport calculations of the FED, with careful modeling of the edge plasma and impurity transport, are needed to obtain more reliable estimates.

Table 4.6. Rough estimates of particle and power loads on the FED limiter and first wall in three representative edge regimes

	Clean (baseline)	Mildly contaminated	Cold edge
Power to limiter (MW)			
Via electrons	13	2	0.2
Via ions	43	5	0.6
Average ion energy hitting the limiter (eV)	300	50	10
Ion flux to limiter (s^{-1})	9×10^{23}	6×10^{23}	4×10^{23}
Atomic flux to be pumped and fueled (s^{-1})	4×10^{22}	4×10^{22}	10^{23}
Power lost via radiation (MW)	8	65	71
Power to a 3-m strip centered at the limiter via charge exchange neutrals (MW)	8	1	0.2
Average energy of charge exchange neutrals (eV)	1600	200	20
Average charge exchange particle flux ($cm^{-2} \cdot s^{-1}$)	4×10^{16}	4×10^{16}	8×10^{16}

4.6.5 Conclusions and Future Work

Impurity control in FED is an area where large uncertainties and design impacts remain. Much scientific and developmental work in this area is needed before a reliable basis can be obtained for FED design considerations. The ideas discussed here are considered preliminary and the estimates of design requirements crude.

Several particle and impurity control options have been discussed. It is seen that the concept of a single-belt pump limiter at the chamber bottom has some apparent advantages relative to other configurations of pump limiter in FED. However, more analyses are needed for a proper comparison of the merits of all options, including the configuration without a leading edge. Particle exhaust efficiencies ranging from 3% to 10% seem feasible. New concepts to increase this efficiency beyond 25% should be seriously explored to support the concept of impurity control via particle flushing.

A number of nonmagnetic impurity control schemes have been reviewed. None of them is expected to impose major modifications to the current FED design. A wide range of energy and particle loads is deemed possible, depending on the success of nonmagnetic impurity control. It is seen that success in maintaining relatively flat impurity and plasma profiles at a tolerable impurity content will also drastically reduce the particle and power loads to the limiter. A middle ground between engineering feasibility and plasma requirements may exist with the mildly contaminated plasma for FED. This is presently a little explored area in transport simulation. Models of impurity sources, sinks, and transport, albeit crude initially, need to be identified and applied together with realistic plasma scrapeoff models.

A simplified poloidal divertor and a compact bundle divertor both seem feasible in FED. Examples of the latter have been found to achieve a ripple of <0.3% at the plasma center and to satisfy engineering requirements of dissipated power, current density, and clearance for scrapeoff and divertor channels. Work is needed to determine whether a poloidal divertor (currently developed for INTOR) can be adapted in FED.

4.7 DISRUPTION CONSTRAINTS AND CHARACTERISTICS

The consequences of major plasma disruptions are critical in the design of FED. The maximum plasma currents and densities at which stable tokamak operation is possible are limited by the onset of a major disruption.[70] The resulting abrupt termination of the plasma discharge produces large electromagnetic and thermal loads on the device. It is therefore important to have realistic assessments of the achievable values of plasma currents and densities, the likely behavior of the plasma during disruption, and the expected probability of disruption over the operating range of the FED plasma. This discussion benefits from recent reports by the Disruption Control Task Force[71] and the FED Low q/Shaping Team[3] and from an earlier ETF Plasma Disruption Workshop Report.[72]

4.7.1 Maximum Achievable Density

In ohmically heated discharges with typical operating conditions ($q_a \simeq 2.5$-5.0), the maximum achievable line average density for a given q has been found to follow the form $\bar{n}_e^{max} = k \times (B_T/R)$ (Ref. 73). The value of the coefficient k has increased due to improvements in experimental techniques, mainly carefully programmed gas puffing and the maintenance of a relatively pure hydrogen plasma. Disruptions can also be prevented by broadening the current channel, as shown in the Japanese Institute of Plasma Physics (JIPP) T-2, and by combining the gas injection with a positive ramp in plasma current to promote edge heating, as shown in Alcator-A. Furthermore, k increases with a lowered safety factor (q_a), presumably because of a broadened current profile.

It is useful to indicate the maximum achieved density in a plot of $1/q_a$ versus k (Ref. 70), as shown in Fig. 4.19. In beam-heated discharges, the beam power tends to broaden the current density, thereby extending the operational range of $\bar{n}_e$ and q_a. However, there does not seem to be a unique relationship between k and beam power. The best values of $\bar{n}_e$ in ohmically heated and beam-heated circular plasmas in various existing tokamaks are given by the diagonal line in the figure:

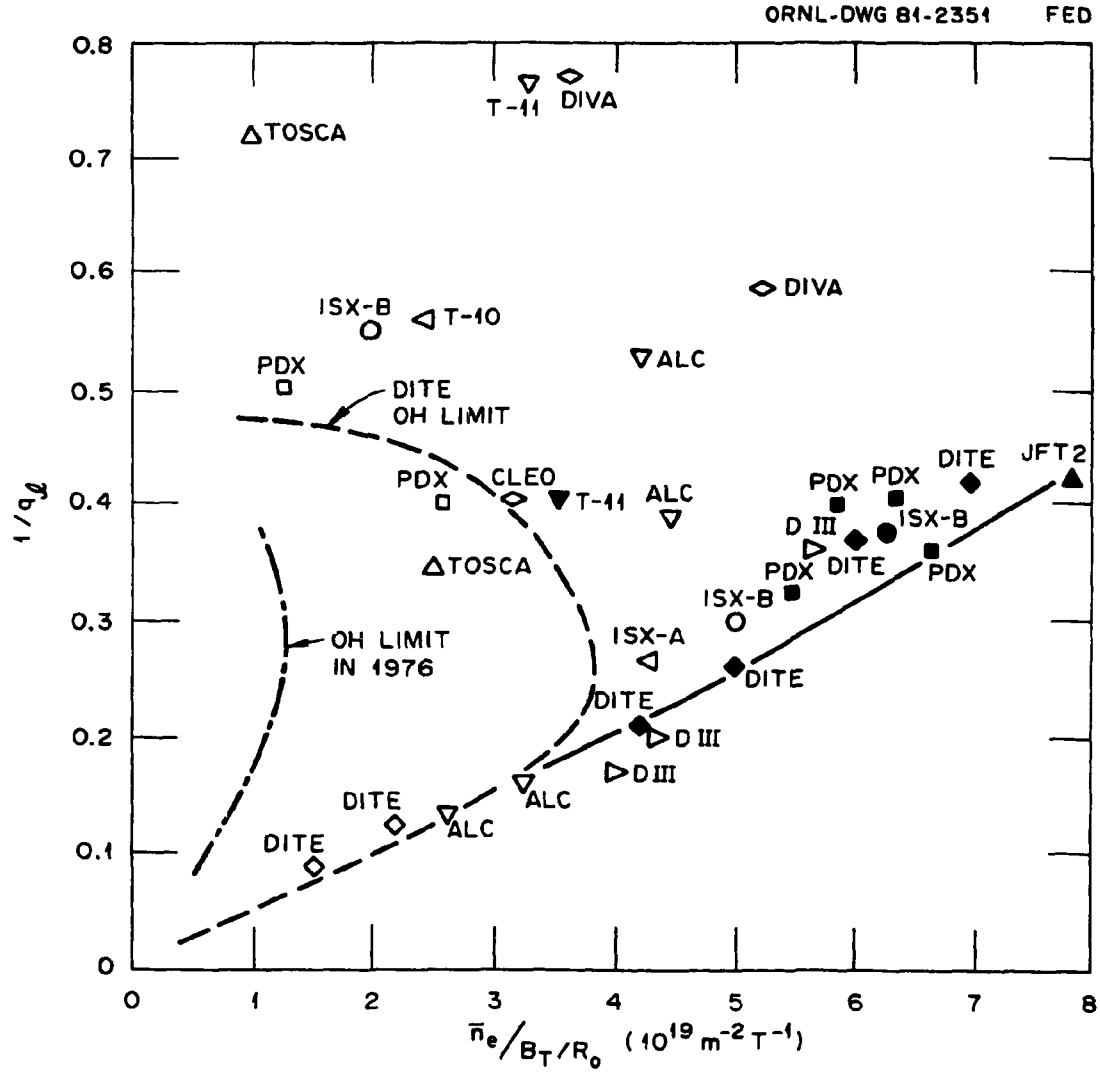

Fig. 4.19. The achieved values of the line average electron density $\bar{n}_e$ and the safety factor at the limiter q_ℓ in present-day tokamaks in ohmically heated (open symbols) and beam-heated (solid symbols) plasmas.

$$\bar{n}_e^{max} = k \frac{B_T}{R_o} \cdot \frac{1}{q_\ell} , \quad k = 2 \times 10^{20} \ m^{-2}T^{-1} ,$$

which suggests that $\bar{n}_e^{max}$ is proportional to the average current density.

Using the proposed parameters for the FED device (B_T = 3.62 T, R_o = 4.8 m, and $q_\ell = 5B_T ab/I_p R_o$ = 1.9), we obtain $\bar{n}_e^{max} = 0.8 \times 10^{14}$ cm^{-3}. Recent experiments in ISX-B and Doublet III indicated that the achievable densities increase with plasma elongation, achieving $k = 3.3 \times 10^{20}$ m^{-2}T^{-1}. The calculated operational densities of 3-4 $\times 10^{13}$ cm^{-3} during ohmic heating and 6-12 $\times 10^{13}$ cm^{-3} during burn (Sect. 4.5.1) are therefore consistent with the empirical limitations of disruption.

4.7.2 Disruption Characterization

Experimental observations[71]

Common features of disruptions include an initial slight current increase accompanied by a negative voltage spike, an abrupt plasma cooling, and a broadening of the current density profile. The plasma then shifts radially inward, and plasma-wall or plasma-limiter interactions increase dramatically. Disruptions are usually preceded by a rapid growth of m = 2, n = 1 helical activity, although this is not observed in all cases. In noncircular plasmas, major disruptions frequently result in a loss of vertical stability, with rapid vertical plasma motion. The magnitude of the negative voltage spike varies; it seems to decrease with increasing toroidal conductance of the vacuum vessel and with more nearby passive conductors. The subsequent current decay apparently depends on a number of factors, including the wall conditions and the effectiveness of the radial and vertical position control systems. In machines with relatively fast feedback control (e.g., Doublet III), abrupt termination of the plasma current does not occur unless vertical stability is lost. A schematic of plasma behavior during disruption is shown in Fig. 4.20.

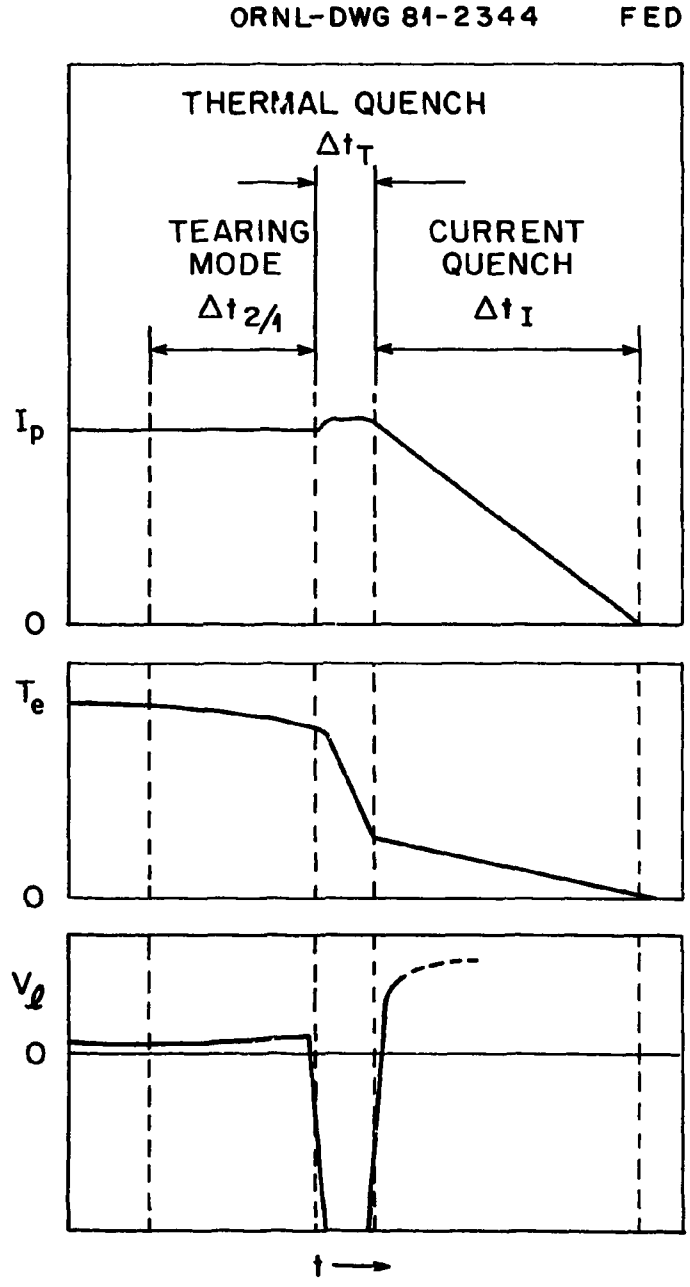

Fig. 4.20. Schematic plasma behavior during a typical major disruption. The disruption is currently assumed to be preceded by increased activities of m = 2/n = 1 and other tearing modes in a time scale of $\Delta t_{2/1}$, to proceed with a thermal quench in a time scale of Δt_T, and to terminate with a current quench and loss of plasma position in Δt_I.

Theoretical models and interpretation

The theoretical studies of major disruptions to date are limited to low beta, large-aspect-ratio tokamak plasmas and are in the form of two- and three-dimensional, nonlinear calculations of interacting tearing modes.[74-76] Through comparison with experiments, these studies strongly suggest that a prerequisite for a "typical" major disruption is the presence of a large magnetic island resulting from an unstable m = 2, n = 1 tearing mode. The island's explosive interaction with overlapping magnetic islands leads to a sudden onset of stochastic magnetic field lines, a large plasma heat loss, and a significant broadening of the plasma current profile.[75] This causes a large drop in plasma pressure and some reduction in plasma self-inductance. Because of the flux trapped by the torus vessel, the plasma position and shape should suffer little change over the vessel eddy current decay time. This does not necessarily rule out, however, strong plasma contamination via ablation of limiter materials.

For a time scale longer than the skin time of a nearby vessel, if the poloidal field system does not respond adequately, the plasma current begins to decay. There is also a progressive loss of plasma position, an increasing amount of plasma-wall interaction, and further plasma cooling. The plasma usually moves inward because of the reduced pressure and internal inductance. It seems reasonable to assume that the time scale of current quench Δt_I is determined mainly by the electromagnetic and thermal interactions between the plasma and its environment.

These qualitative descriptions of the major disruption can be considered appropriate for nearly circular plasmas at low beta. The effects of finite beta and large noncircularity are now being studied.[33] Preliminary results in higher beta, neutral-beam-heated plasmas have not revealed fundamentally new pathologies.[77] A significant theoretical effort is under way to model the current quench phase.[78]

Recommended plasma disruption parameters

A set of tentative plasma disruption parameters is summarized in Table 4.7 for use in the ongoing engineering analysis, together with additional assumptions and comments. Care has been taken to preserve some pessimism in the assumptions (Sect. 4.7.4). These parameters and descriptions will be updated as additional information becomes available.

Table 4.7. Working plasma disruption parameters for FED

Parameter	Value	Assumptions/comments
Thermal quench phase		
Time scale, Δt_T	5 ms	About 5% of τ_{Ee} under normal conditions
Thermal energy deposition	90 MJ	Concomitant fusion quench and stopping supplementary heating
Deposition region		
Limiter (via particle)	45 MJ	Little change in plasma position and shape
First wall (via radiation)	45 MJ	Due to ablated impurities
Voltage spike	1 kV	
Plasma flux reduction	5 Wb	
Current quench phase		
Time scale, Δt_I	10 ms	Short compared with the first wall eddy current decay time
Thermal energy deposition	10 MJ	Ohmic plasma energy
Region of plasma impact		Inboard, top, or bottom
Affected area/chamber wall	10%	Uncertain
Energy deposition peaking factor	10	To retain some pessimism
Plasma magnetic energy	60 MJ	Dissipated via eddy currents in nearby conductors

4.7.3 Probability of Disruption

Our current understanding of the causes of plasma disruptions and of the techniques to avoid or control them is limited and does not provide an adequate basis for predicting the probability of disruption in FED. Experiments indicate that the plasma disrupts more frequently (approach 100% probability) as $q_\psi(a)$ is reduced toward 2 (Refs. 3 and 66). However, for $1.3 < q_\psi(a) < 2$, a complete absence of disruptions has been observed in DIVA,[41] consistent with the theoretical suggestions.[75,76] This may also be attributed to the presence of a conducting shell at $r = 1.2a$.[3,71] The latter condition apparently could be satisfied by the first wall in FED at $r = 1.15a$ and a resistive skin time greater than 30 ms. Extensive work is needed to explore the accessibility of this regime in FED.

Without overlooking the need for extensive experimentation and analysis on plasma disruptions, we have made the following assumptions about plasma disruptions in FED:

1. Successful schemes of disruption avoidance or control in finite beta, noncircular plasmas will have been demonstrated before the operation of FED, at least with relatively conservative values of q_ψ.[3,66] Figure 4.10 shows that the fusion energy per pulse drops only by a factor of 2 when q_ψ is raised to 4, but possibly at an unacceptably large reduction in fusion power.
2. There will be an extensive period of time (during hydrogen, deuterium, and initial D-T operations) to experiment with disruption-related processes in FED at low energy and current levels. A regime of plasma operation essentially free from disruptions will be mapped out before repeated long pulse, full power operations are carried out.
3. Even if major disruptions can be avoided under normal conditions of FED operation, there will be a 10^{-3} probability of disruption under abnormal or error conditions.

This assumed progressive improvement in plasma disruptivity in FED is summarized in Table 3.3.

4.7.4 Energy and Particle Loads During Disruption

At present there is at best a qualitative agreement between theory and experiment as to what consitutes a "typical disruption." As discussed in Sect. 4.7.2, a substantial fraction of the plasma energy is lost to the wall in an early phase while the plasma position is still essentially unchanged. After this "thermal quench" the current starts to decay and the plasma moves toward the inboard wall. For FED the time scales for these processes have been estimated by scaling laws[78] to be approximately 5 ms for the thermal quench and 10 ms for the current decay. Only crude estimates can presently be given for the corresponding energy losses (Table 4.7). It is therefore of interest to consider the two extreme cases: either the total thermal plasma energy is deposited on the limiter during the thermal quench, or it is deposited on the inner first wall due to the inward movement of the plasma column. In both cases it is assumed that impurities are generated and protect the limiter and first wall against further damage via strong radiation.

Assuming that the thermal plasma energy of 100 MJ is deposited on the bottom FED limiter in 5 ms, the average power density would be 10^3 MW/m^2 with a peaking factor of 1.5, due to the power deposition profile.[53] At this level of power flux, the surface of a graphite limiter would reach sublimation temperature after absorbing only about 10-20% of the total power. The number of atoms of ablated limiter material corresponding to this fraction of total energy would be larger than the number of hydrogen plasma particles. The remaining fraction of the thermal plasma energy would probably be radiated to the first wall, reducing the thermal load to the limiter by at least an order of magnitude. This concept of combined ablation and radiation cooling has been introduced as a "virtual limiter."[79]

An estimate is needed for the heat load on the inner wall due to the inward shift of the plasma during the current decay phase of the disruption. The model assumes conserved flux tubes that are scraped off consecutively at the inboard first wall.[80] Assuming a thermal energy of 100 MJ and a decay time of 10 ms, the power flux density is again on the order of 10^3 MW/m^2. Thus, the same considerations of ablation and radiation cooling used for the limiter can be applied.

If this self-protective mechanism works, the exact amount of energy lost in the various phases of the disruption would not be very critical. To calculate the thermal response and surface erosion of the affected first wall components, only about 20% of the total released thermal energy would have to be taken into account. There is, however, no clear experimental evidence that this mechanism dominates during disruptions.

The total number of particles incident either on the limiter or on the inboard armor is estimated to be about 2×10^{22}, with an average fluence of $F = 10^{21}$ m^{-2}. The estimated surface erosion due to sputtering by these particles is only a few monolayers and is negligible compared to erosion by evaporation. The plasma particles impinging on the surface will be either reflected or trapped. The saturation dose for trapping is on the order of 10^{21} m^{-2} (Ref. 81). Surface erosion due to blistering does not seem to be a problem, probably because of the preconditioning of the surface and the energy distribution of the particles.[82] These rough estimates suggest that the parameters used in Table 4.7 may be pessimistic.

4.7.5 Conclusions and Future Work

A review of the achieved densities in existing tokamaks suggests that the baseline densities of $3\text{-}4 \times 10^{13}$ cm^{-3} before bulk heating and 8×10^{13} cm^{-3} during burn are reasonable. The up-to-date experimental and theoretical results from disruption studies have led to a two-phase plasma quench model. The plasma first loses a large fraction of thermal energy in about 5 ms (thermal quench) with little change in plasma shape and position. A current quench then follows, simultaneous with a progressive loss of plasma position in about 10 ms. Baseline disruption assumptions are listed in Table 4.7.

If it is assumed that radiation plasma cooling from ablation-generated impurities halts further thermal load to the limiter and armor, then only 10-20% of the plasma thermal energy is deposited over the region of plasma contact. If this ablation process proves to be dominant during disruption, the thermal loads will be significantly lower than those listed in Table 4.7.

Disruption is an area of major concern in large tokamaks and can strongly influence the limiter and armor design of FED. Improved estimates of the disruption time scale and energy loads are of vital importance to the FED concept development. Exploration of concepts to avoid or slow down a current quench after the thermal quench via electromagnetic means is highly worthwhile. The implications of the $q_\psi < 2$ disruption-free regime of operation demonstrated on DIVA should be explored.

4.8 POLOIDAL FIELD CONFIGURATION

The poloidal field configuration external to the plasma deals with the coil locations and currents that produce and maintain the plasma shape and position over the ranges of interest for the plasma beta and the safety factor. The poloidal field configuration within the plasma deals with the plasma current profile that is consistent with the ranges of interest for the MHD equilibrium pressure and the safety factor throughout the burn pulse.

The basic concept of a PF coil system that is well coupled to high beta, D-shaped plasmas has been proposed recently[15] and used in the ISX-B device[83] and in the study of The Next Step (TNS) tokamak concept.[84] An assessment of the FED PF coil configuration based on the same approach is summarized in Sect. 4.8.1. Assessments of a decoupled FED coil system, such as that used in PDX,[85] and of a coil system with quasi-steady-state exterior superconducting coils[86] are currently in progress.

The dependence of coil currents on the variation in safety factor has been studied for the TNS tokamak concept.[84] These studies showed that increases in q_ψ do not introduce additional requirements on the PF coil current. Here we estimate the time scale in which the internal plasma field configuration (and hence the safety factor) can evolve significantly because of finite plasma resistivity. Work is in progress to translate the resistive evolution of the plasma poloidal field into requirements for the coil currents.

4.8.1 Poloidal Field Coil Configurations

The PF coils consist of equilibrium field (EF) and ohmic heating (OH) coil sets. Many engineering design issues are directly related to the configuration of these coil sets. These issues arise, for example, from the conflict between the desirable coil location (so that the total ampere-turns can be minimized) and the space and access requirements of other components of FED, the relatively large pulsed poloidal fields and out-of-plane forces on the TF coils, and the excessive local fields resulting from a juxtaposition of large coil bundles and currents. The major options and difficulties that have been examined recently for the OH and EF coil configurations are summarized. Work is in progress to obtain a PF coil configuration in FED that satisfies the physics requirements and permits a feasible engineering solution.

Ohmic heating coils

The OH coils consist of a central solenoid, to be sized by volt-second requirements, and a few coils necessary to minimize or eliminate the stray OH field in the plasma. Coil locations may be determined by assuming a uniform current totaling 20 MAT in the central solenoid and computing a corresponding current distribution in another set of equally spaced coils so that the field is minimized in the plasma region. Figure 4.21(a) shows this current distribution as a function of distance along the solenoid and across the top of the TF coils, assuming symmetry about the midplane. The poloidal magnetic field on the midplane that is created by these coils is shown in Fig. 4.21(b). The average magnitude of this field along the plasma midplane is about 5 G. In practice, this current distribution would be replaced by a smaller number of coils, as in Fig. 4.22 and Table 4.8.

A second option that has been considered is that of a split, or discontinuous, OH solenoid, leaving space near the midplane for inner EF coils (Sect. 5.5). Figure 4.23(a) shows the current distribution of such a system, and Fig. 4.23(b) gives the poloidal field along the midplane. We see that if the central solenoid is assumed to have a

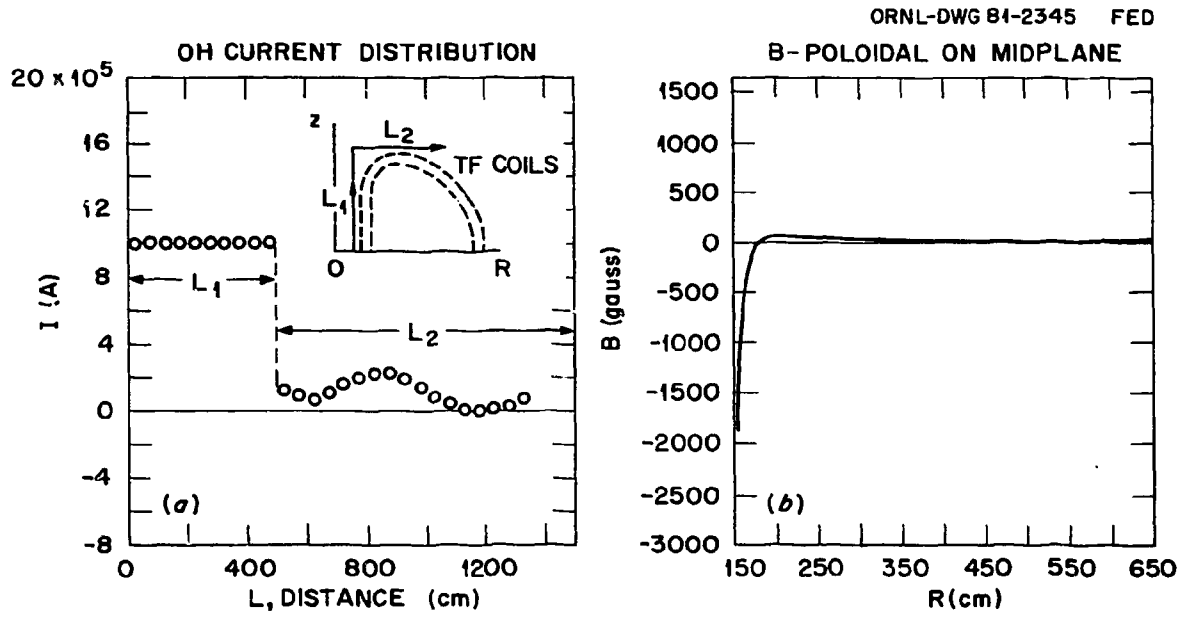

Fig. 4.21. (a) OH current distribution as a function of distance along the solenoid and across the top of the TF coil, assuming a uniform current in a continuous solenoid, and (b) the poloidal magnetic field on the midplane.

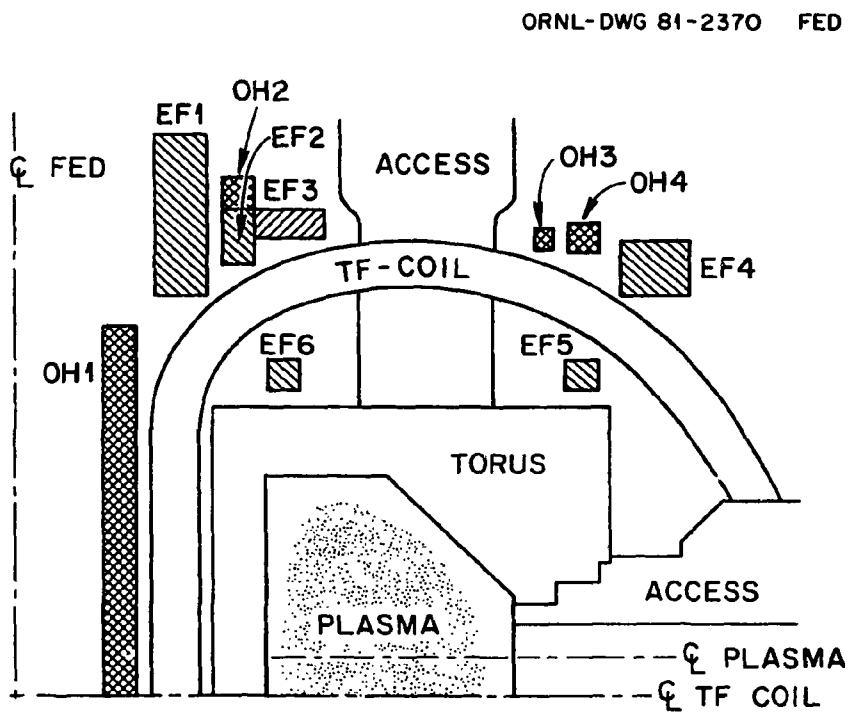

Fig. 4.22. The current distribution of Fig. 4.21 may be replaced by a continuous solenoid (OH1) and three decoupling coils (OH2-OH4). The EF coils listed in Table 4.11 are also implemented here.

2-m gap at the midplane and again to carry a total of 20 MAT, the field can be minimized in the region of the plasma, but large fields tend to intersect the TF coil region. The average magnitude of the poloidal field along the plasma midplane in this case is about 18 G. Note that ampere-turns in the decoupling coils rise by about a factor of 2.1 and currents change direction relative to the solenoid. This is expected to severely reduce the inductive capability of the OH coil system with a split solenoid.

Table 4.8. OH coil locations and currents assuming 20 MA in the continuous central solenoid and the split solenoid

		Coil currents (MA)	
R (m)	Z (m)	In continuous central solenoid	In split solenoid
1.35	0.25	1.00	0.00
1.35	0.75	1.00	0.00
1.35	1.25	1.00	1.25
1.35	1.75	1.00	1.25
1.35	2.25	1.00	1.25
1.35	2.75	1.00	1.25
1.35	3.25	1.00	1.25
1.35	3.75	1.00	1.25
1.35	4.25	1.00	1.25
1.35	4.75	1.00	1.25
1.35	5.65	0.34	0.00
3.40	6.25	1.20	0.00
7.95	6.25	0.27	0.00
1.35	5.60	0.00	-0.92
2.90	6.25	0.00	-0.25
6.40	6.25	0.00	0.77

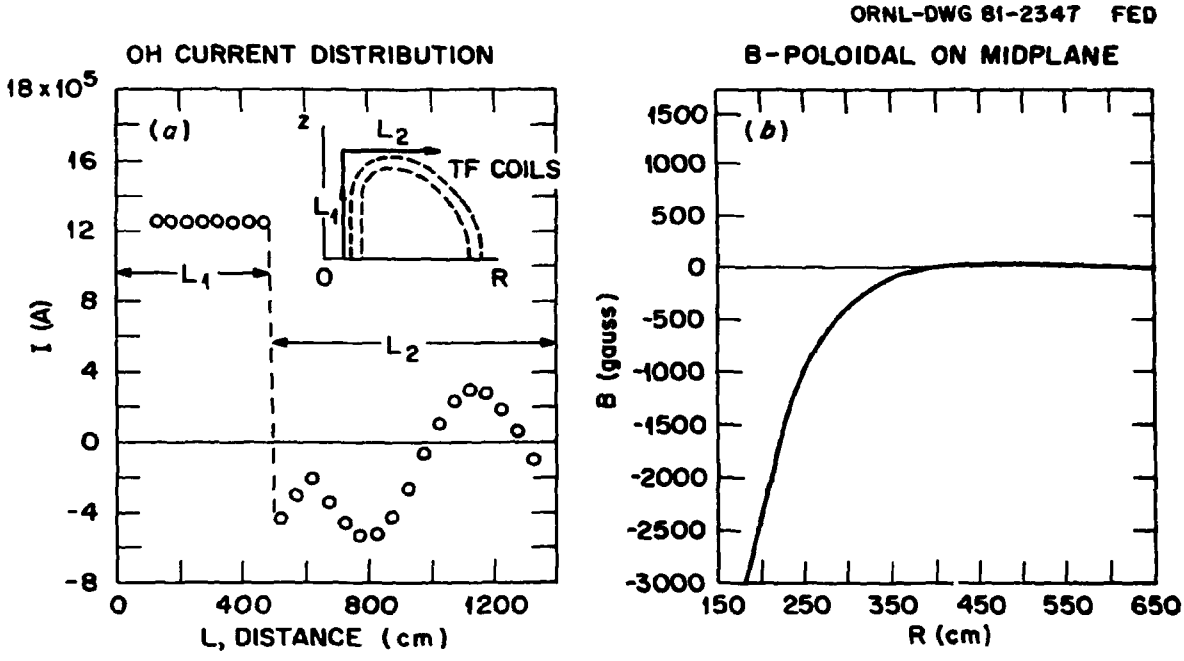

Fig. 4.23. (a) OH current distribution as a function of distance along the solenoid and across the top of the TF coil, assuming a uniform current in a split (discontinuous) solenoid, and (b) the poloidal magnetic field on the midplane.

Equilibrium field coils

Through numerical MHD equilibrium calculations we compare two options for the EF coil configuration. The first is a set of EF coils that includes coils on the inboard side of the torus. These coil locations and currents are summarized in Table 4.9 and Fig. 4.22. Note that two normal conducting coils are located internal to the TF coils and are assumed to carry 1 MA in a low beta, D-shaped plasma with elongation $\kappa = 1.6$ and triangularity $\delta = 0.4$ (defined as the inward shift of the tips of the D-shape relative to the minor radius). The largest currents, totaling 15.5 MA, are concentrated in the inboard coils. As beta rises to 6% and the triangularity is increased to 0.5, the ampere-turns are 61 MA, with about 18 MA in the inboard coils and 11 MA in each set of shaping coils.

Table 4.9. Coil locations and currents for an EF coil system including inboard coils at $B_t = 3.6$ T for the $q_\psi = 2.5$ design

		Coil currents (MA)	
		$\langle\beta\rangle = 0.4\%$,	$\langle\beta\rangle = 6.0\%$,
R (m)	Z (m)	$I_p = 4.6$ MA	$I_p = 6.5$ MA
1.35	0.45	-7.73	-8.99
4.00	4.30	1.00	2.00
2.00	6.15	3.58	5.63
2.50	6.15	3.58	5.63
7.40	4.30	-1.00	-2.00
8.20	5.55	-3.74	-6.11
	Total ampere-turns	41.3	60.7

Because of this magnitude of current in the inboard EF coils in the form of a short solenoid, a local field of about 2 T is produced. This field is added to the 7-T field produced by the OH solenoid near the end of the burn pulse. The 7-T limit of the OH superconducting coils will thus be exceeded locally. Splitting the OH solenoid will not substantially reduce the local field maximum, and in view of the deleterious effects of splitting the OH solenoid such an EF coil configuration does not appear promising.

The second option is to eliminate the inner EF coils and use an OH system with a continuous solenoid. Such a system has been calculated and is summarized in Table 4.10. Ampere-turns in this system are about 60 MA for a low beta plasma with elongation $\kappa = 1.6$ and triangularity $\delta = 0.3$; they increase to 86 MA for a high beta plasma with $\kappa = 1.6$ and $\delta = 0.4$. The plasma equilibrium flux surfaces that include the stray fields of the continuous OH system (Table 4.9) are presented in Figs. 4.24 and 4.25. The results indicate that large local fields, created by the shaping coils with total ampere-turns of 32 MAT, will intersect the TF coils and create large out-of-plane forces. The local field produced by these coils has been estimated to be about 10 T, again exceeding the current design limit of NbTi superconducting coils.

Table 4.10. Coil locations and currents for an EF coil system excluding inboard coils at $B_t = 3.6$ T

		Coil currents (MA)	
R (m)	Z (m)	$\langle\beta\rangle = 0.4\%$, $I_p = 4.6$ MA	$\langle\beta\rangle = 6.0\%$, $I_p = 6.5$ MA
3.50	4.30	1.00	2.00
2.40	6.15	23.78	32.34
7.40	4.30	-1.00	-2.00
8.20	5.55	-4.18	-6.73
	Total ampere-turns	59.9	86.1

Dependence on plasma elongation

Recent MHD stability analyses have shown that the stable beta value increases with increasing plasma elongation and triangularity.[29,87] Recent experimental results in ISX-B[31] have suggested that the ideal MHD stability limit on beta may not be applicable. A soft β_p limit in the form of progressively enhanced electron heat conduction may be responsible for the achievable beta values.[32] The impact of this soft limit in β_p has been assessed recently[88] and is discussed in Sect. 4.4.3. There it is shown that plasma elongation to $\kappa = 1.6$ for fixed

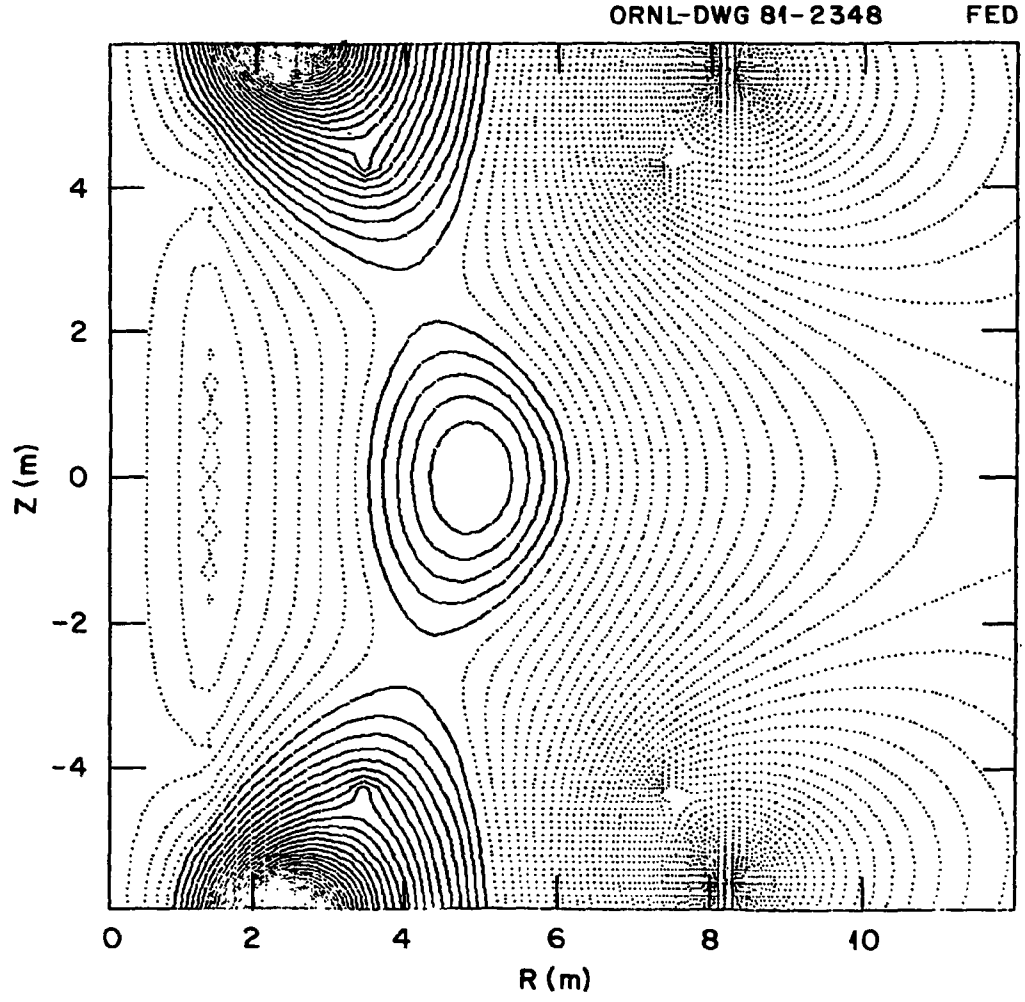

Fig. 4.24. Poloidal flux contours of a low beta (<β> = 0.4%, I_p = 4.6 MA, B_t = 3.6 T) equilibrium using the OH system of Table 4.9 and the EF coils of Table 4.11.

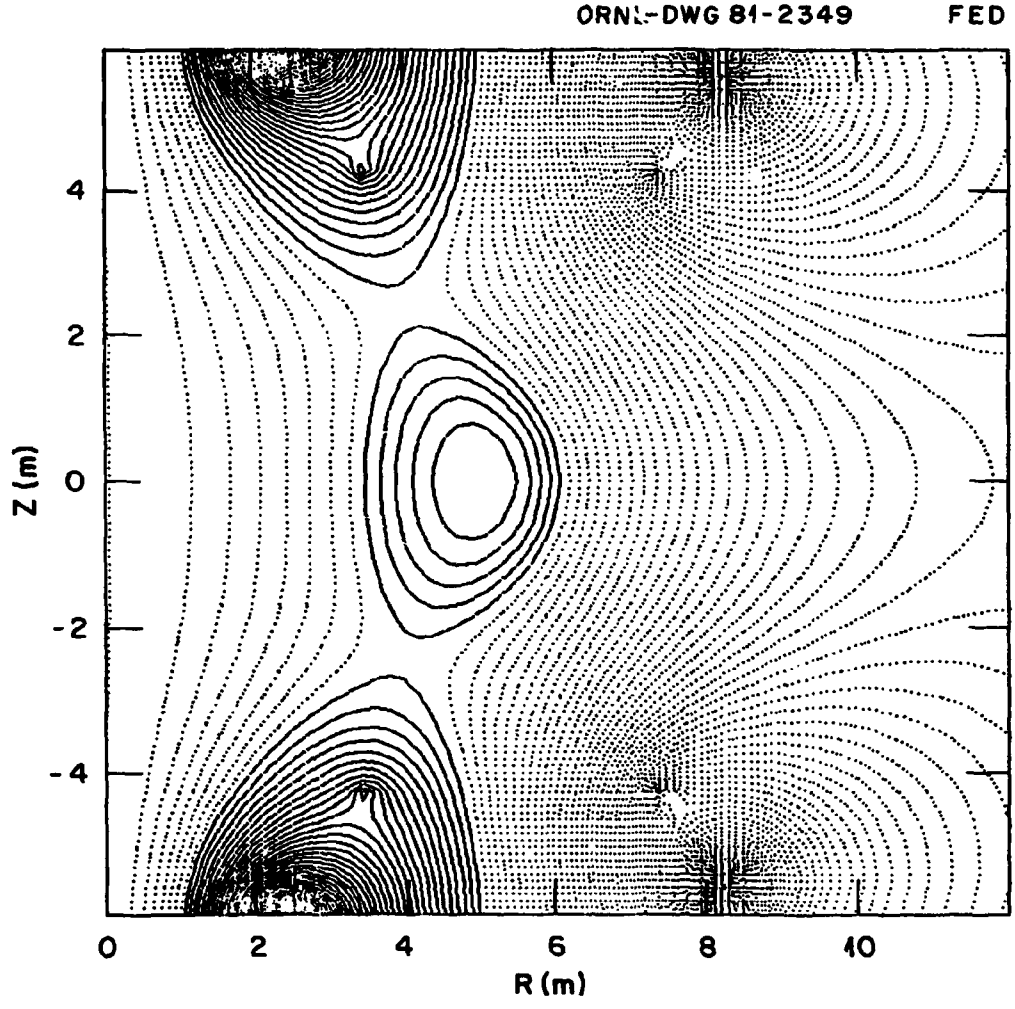

Fig. 4.25. Poloidal flux contours of a high beta ($<\beta> = 6.0\%$, $I_p = 6.5$ MA, $B_t = 3.6$ T) equilibrium using the EF coils of Table 4.11.

values of β_p and q_ψ enhances beta by a factor of 1.8 and the plasma performance by more than a factor of 3. These potential benefits have to be balanced by the incremental engineering difficulties of obtaining elongation and triangularity in FED. It is of interest to assess the impact on the poloidal field systems of relaxing the plasma shaping requirements.

In Table 4.11 and Fig. 4.26 we present the coil currents for a high beta equilibrium with $\kappa = 1.2$, $I_p = 5.6$ MA, and $\delta = 0.1$, using the coil locations of Table 4.10. It is seen that for $\langle\beta\rangle = 6\%$ and a system without inboard EF coils, relaxing the plasma shape can mean a 60% reduction in shaping coil currents and a 50% reduction in total ampere-turns. Further reductions could probably be realized by adjusting coil locations after a reduction in the torus vertical height. However, the assumptions of $\langle\beta\rangle = 6\%$ in a plasma with $\kappa = 1.2$ may not be realistic, because q_ψ and β_p are estimated to be 1.9 and 2.4, respectively, according to Eqs. (4.1) and (4.4).

Table 4.11. Coil currents for a high beta equilibrium using the coil locations of Table 4.10. Plasma parameters are $\langle\beta\rangle = 6.1\%$, $I_p = 5.6$ MA, $B_t = 3.6$ T, $\kappa = 1.2$, and $\delta = 0.1$

R (m)	Z (m)	Coil current (MA)
3.50	4.30	2.00
2.40	6.15	13.61
7.40	4.30	-2.00
8.20	5.55	-4.54
	Total ampere-turns	44.3

More work is in progress to determine whether a feasible poloidal field configuration can be obtained for D-shaped plasmas with full elongation without creating a large local field and whether an acceptable compromise is necessary between plasma shaping and engineering difficulties.

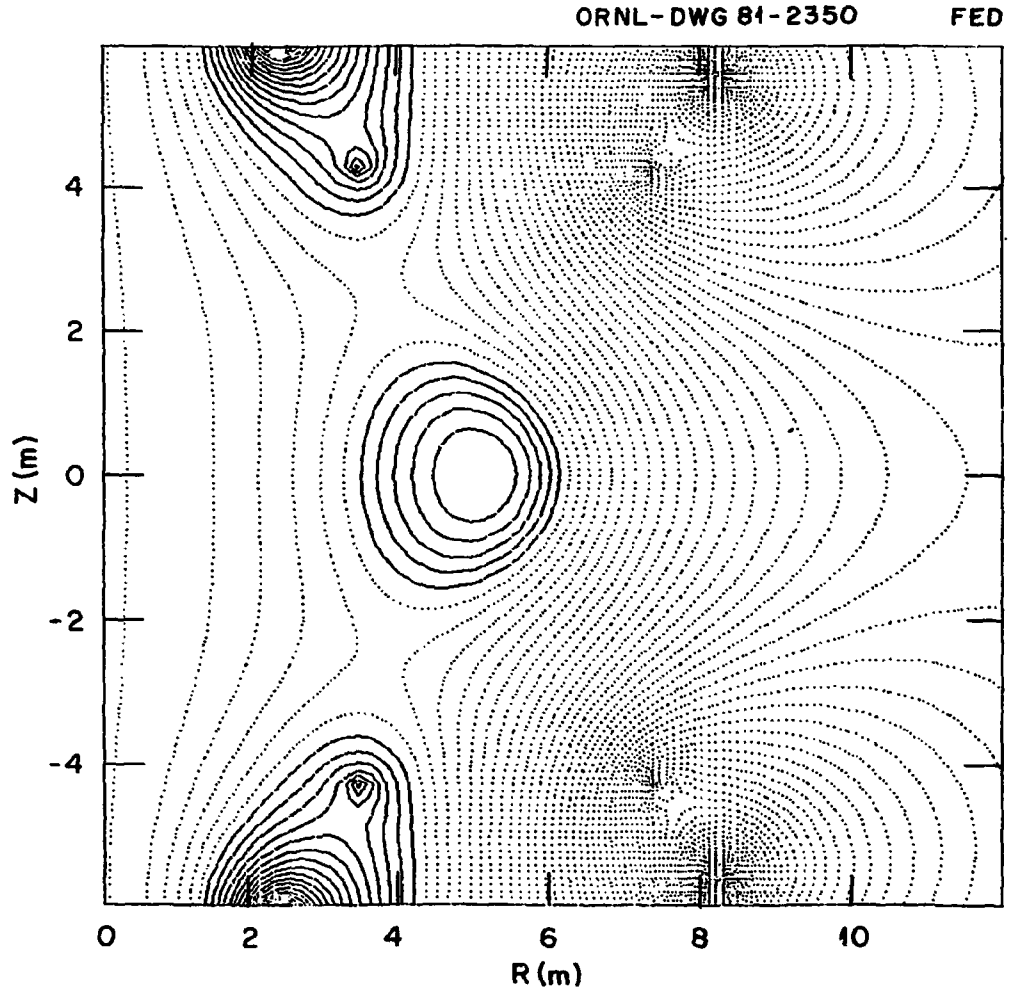

Fig. 4.26. Poloidal flux contours of a high beta ($\langle\beta\rangle$ = 6.1%, I_p = 5.6 MA, B_t = 3.6 T) equilibrium of low elongation (κ = 1.2) and triangularity (δ = 0.1) using the EF coils and currents of Table 4.12.

4.8.2 Time Scale of Resistive Evolution of Plasma Poloidal Field

In the operation of FED it may be necessary, for reasons of MHD stability and plasma disruption prevention, to control the evolution of the plasma poloidal field and the safety factor profile over the pulse duration. The FED pulse length is expected to be on the order of 100 s, which may be comparable to the resistive time scale governing the evolution of the q profile. Recently, this evolution has been explored numerically[89] using a 1-1/2-D single fluid transport code.[90] This code couples 1-D particle balance, energy balance, and magnetic flux diffusion equations to a 2-D axisymmetric MHD equilibrium equation through the pressure p, the poloidal flux function ψ, and the safety factor q. The diffusion and conduction coefficients include Alcator electron, neoclassical ion, and field ripple ion contributions. The classical Spitzer resistivity was used, together with source terms including particle fueling, neutral injection, ohmic heating, and fusion alpha heating.

Two high beta cases were considered for a device having tokamak reactor conditions: a beam-driven hydrogen plasma and an ignited D-T plasma. The resistive steady-state q profiles for various heating sources are plotted in Fig. 4.27. Using the neutral injection energy as a device to control the temperature profile in the beam-driven cases, we found that, in resistive steady state, broad temperature profiles resulting from relatively hollow heating profiles lead to flat q profiles, while peaked temperature profiles result in deep q profiles. For the peaked temperature profiles expected in an ignited plasma, the evolution toward resistive steady state involved decreasing q_o (safety factor at plasma center), decreasing B_ϕ, and increasing $\langle\beta\rangle$. The time scale of this evolution is shown in Fig. 4.28. It is seen that the plasma burn time in a device the size of FED may be limited by magnetic flux diffusion and MHD stability considerations to possibly as little as 250 s. Based on Fig. 4.28, a FED with a burn at Q = 5 and 150-keV positive ion beam heating may not have any significant extension of pulse length beyond 250 s.

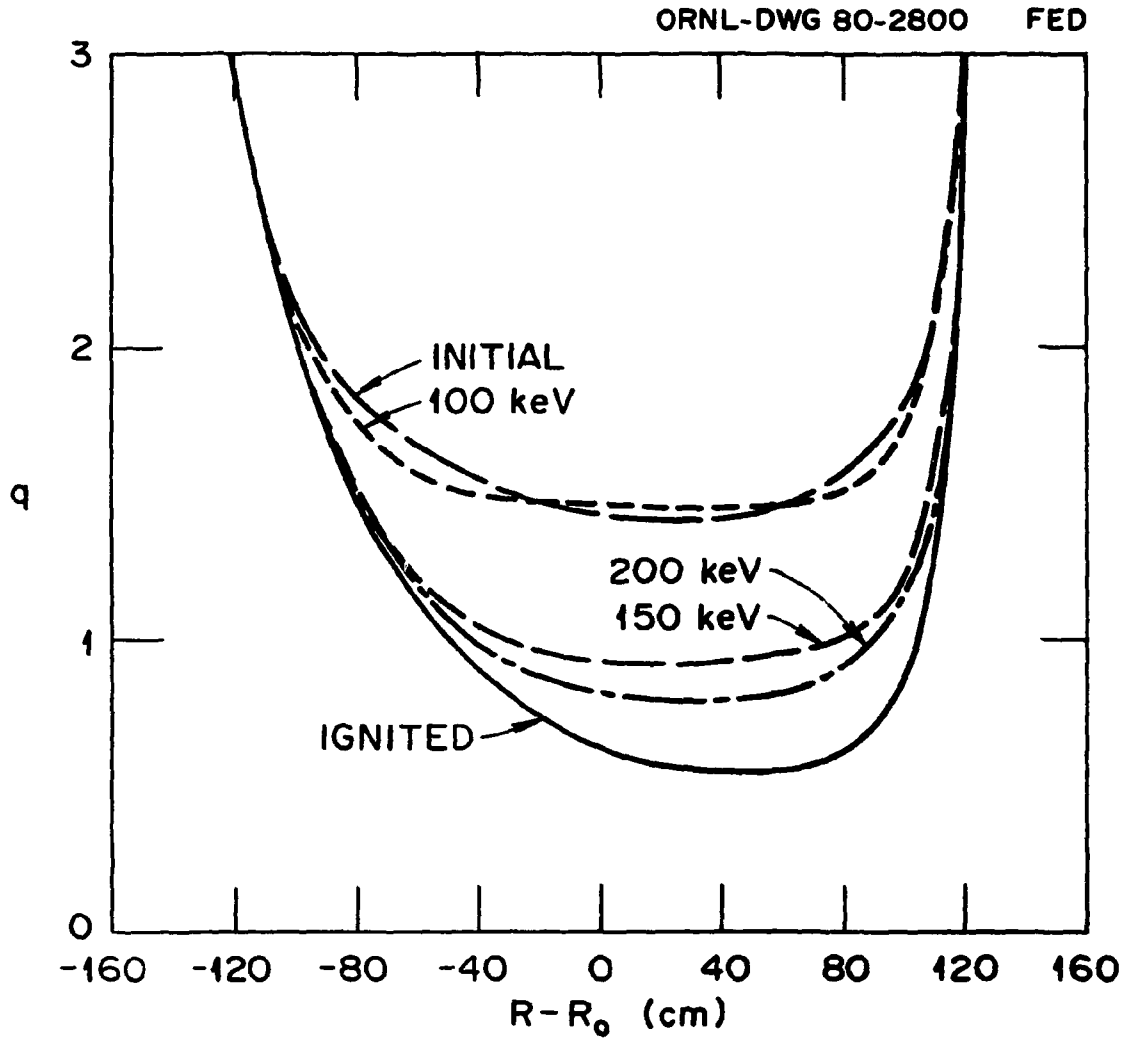

Fig. 4.27. Resistive steady-state toroidal current profiles compared with the initial toroidal current profile for an ignited D-T plasma.

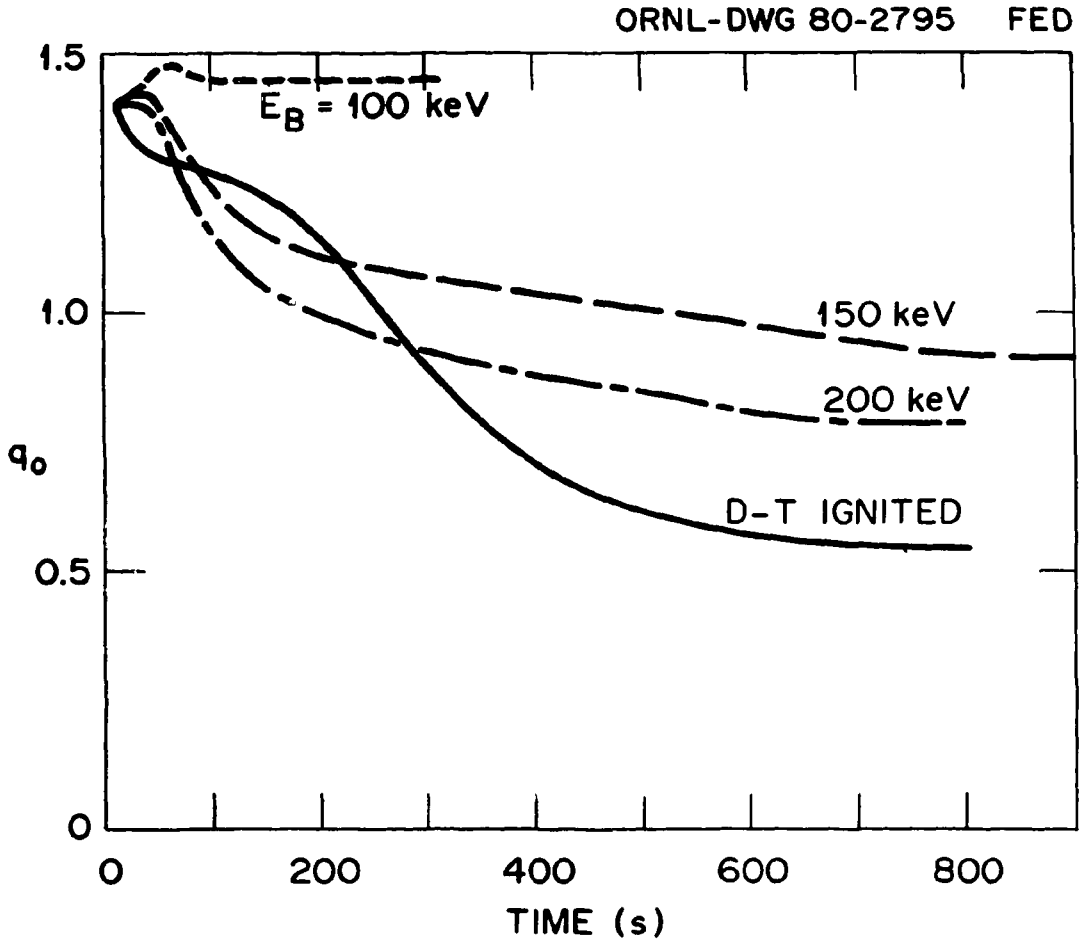

Fig. 4.28. The safety factor at the magnetic axis, q_o, as a function of time for beam-driven plasmas with injection energies of 100 keV, 150 keV, and 200 keV and for an ignited D-T plasma.

4.8.3 Conclusions and Future Work

The considerations of poloidal field configuration in FED have dealt with the concerns of access and clearance. Excessive local fields are seen at the OH solenoid and the EF coil bundles external to the TF coils. A tentative, less-than-ideal system is proposed (Fig. 4.22) for current design studies, while work continues on a search for an attractive PF configuration.

The tentative EF coil system carrying a maximum of 60 MAT, with some interior copper coils carrying up to 8 MAT, is required. The size and capability of these coils are thus comparable to those of the TF coils. The engineering design required to handle the interactions between the two coil sets is currently considered feasible but difficult (Sects. 5.2 and 5.5). The factor of 2 reduction in ampere-turns in the EF coils is shown by relaxing the plasma to $\kappa = 1.2$ and $\delta = 0.1$, at the cost of a less conservative q_ψ value of 1.9. Analysis is needed to assess the trade-offs among plasma shaping requirements, plasma performance, and engineering difficulties in the coil systems. Different combinations of interior and exterior coils should also be explored.

Our preliminary work with a relatively empirical transport model supports the conclusions of Charlton et al.,[91] which were obtained using a classical transport model with fixed temperature and density profiles. The estimated time scale of 250 s is significantly shorter than previously anticipated. However, to the extent that neoclassical corrections could increase the resistivity, this time could be decreased still further. The effects of tearing modes and their nonlinear manifestations in enhancing loss of poloidal flux may also alter the present results significantly. Work is in progress to use more realistic transport models in assessing the extent and the consequences of poloidal flux diffusion in FED discharges.

4.9 SUMMARY

The plasma engineering analyses presented here suggest that the current FED baseline concept can achieve its nominal plasma performance goals under a range of reasonable assumptions and eventualities. Considerable uncertainty exists in the areas of impurity control and disruption characterization and implications. However, options in these areas have been identified. The range of options appears promising, not only because the options can be studied through the U.S. tokamak research program, but also because they are not expected to lead to fundamental FED design modifications.

The major results of the FED plasma engineering analyses are summarized below.

1. RF-assisted Current Initiation and ICRF Heating. Based on heating and transport models that are consistent with recent experimental results from ISX-B, the requirements of ECRH-assisted current initiation in FED are estimated to be modest ($\sim$1 MW at $\sim$80 GHz for a fraction of a second) and can reduce the startup loop voltage by an order of magnitude. The requirement of a predominant electron heating near the ion cyclotron resonant frequency to successfully assist low voltage current initiation in FED suggests the need to launch waves from the high field side. Consistency of this with the ICRF bulk heating requirements needs to be examined.

2. Neutral Beam Bulk Heating. Studies of D^+ neutral beam heating (as a backup to ICRH) have been carried out for varying injection energy, angle, and power. The results favor the use of 150-keV beams injected in the near-tangential direction (36° toward parallel at the plasma edge) for bulk heating in FED, assuming that the density buildup heating scenario is utilized.

3. Beta Considerations. The assumption of a soft limit in β_p (as preliminary experimental results in ISX-B recently suggested) leads to a maximization of $n\tau_{Ee}$ near $\varepsilon\beta_p \simeq 0.6$. At the same time an elongation of 1.6 leads to a factor of 3 enhancement of $n\tau_{Ee}$, assuming a constant safety factor q_ψ and a fixed maximum toroidal field at the coil B_m. These results are invariant to large uncertainties in the size scaling

of τ_{Ee} and in the stiffness of the β_p limit. Also, for a given device, $n\tau_{Ee} \propto (B_m/q_\psi)^4$; thus a lowered B_m can be compensated by lowering q_ψ. The disruption-free regime of $q_\psi < 2$ demonstrated in DIVA, if achievable in FED, would permit a more cost-effective FED design.

4. FED Plasma Operation Space. Under the assumptions of baseline device parameters and physics models, a clean, beam-driven FED plasma can operate over a finite domain in <T> and <n> and satisfy the conditions of $Q \geq 5$, $P_{inj} \leq 36$ MW, $<\beta> \leq 5.5\%$, and $P_{fusion} \leq 200$ MW. Without thermal stability control or a benign beta limit, the domain ranges from 10 keV to 14 keV in <T> and 4.5×10^{13} cm^{-3} to 6.5×10^{13} cm^{-3} in <n>. Otherwise, the domain can be extended to $<T> \gtrsim 6.5$ keV and $<n> \lesssim 1.2 \times 10^{14}$ cm^{-3}.

5. Performance Margin of FED Concept. A considerable margin exists in the baseline FED concept to achieve the nominal performance parameters. The margin can accommodate a factor of 2 uncertainty in τ_{Ee} and the assumption of a strongly enhanced χ_e with increasing β_p (i.e., a soft β_p limit).

6. Pump Limiter Configuration. The concept of a single-belt pump limiter at the chamber bottom may have some advantages over other options for the pump limiter configuration in FED. However, more analyses are needed to properly compare the merits of all options.

7. Magnetic Divertor Options. A simplified poloidal divertor and a compact bundle divertor both seem feasible in FED. A compact bundle divertor has been found that satisfies the physics requirement of <0.3% ripple at the plasma center and the engineering requirements of dissipated power, current density, and clearance for scrapeoff and divertor channel. Work to adapt the poloidal divertor developed for INTOR to FED will continue in the next period.

8. Nonmagnetic Backup for Impurity Control. A preliminary review of several nonmagnetic impurity control schemes suggests that none of the schemes would impose major modifications to the FED design. A wide range of energy and particle loads may be possible, depending on the success of nonmagnetic impurity control. However, a relatively modest success in impurity expulsion that permits mild impurity contamination will drastically reduce the particle and power loads to the limiter without requiring a large particle exhaust rate.

9. Disruption Constraints and Characteristics. A review of the achieved densities in present-day tokamaks suggests that the baseline densities of 3-4 $\times 10^{13}$ cm^{-3} before bulk heating and 6-8 $\times 10^{13}$ cm^{-3} during burn are reasonable. A review of up-to-date experimental and theoretical results from disruption studies has led to a two-phase plasma quench model consisting of a thermal quench in about 5 ms with little change in plasma shape and position, followed by a current quench accompanied by a progressive loss of plasma position in about 10 ms. If it is assumed that radiation from ablation-generated impurities halts further thermal damage to the limiter and armor during a disruption, then less than 20% of the plasma thermal energy is deposited over the region of plasma contact. If this assumption proves to be valid for disruptions in FED, thermal loads could be greatly reduced relative to the current baseline values.

10. Poloidal Field Configuration. It is necessary to explore for designs that avoid excessively large local fields at the small bore poloidal coil bundles external to the TF coils. Variations in plasma shaping are seen to have a major impact on poloidal field requirements. Based on preliminary 1-1/2-D transport and flux diffusion calculations and assuming classical resistivity, significant flux diffusion in high beta FED plasmas occurs in about 300 s. This may prove to be a limiting time scale for the burn pulse. However, the consequences of this process are still relatively uncertain.

REFERENCES

1. R. Goldston, J. D. Callen, A. Gondelekhar, F. Marcus, M. Murakami, and Y-K. M. Peng, *FED Confinement Team Report*, to be published.
2. D. O. Overskei, R. Conn, A. Prinja, H. Mantz, P. H. Rutherford, R. Taylor, W. Stodiek, and M. Ulrickson, *FED Mechanical Divertor Proposals*, to be published.
3. J. T. Hogan, T. Brown, K. McGuire, J. Wesley, M. Nagami, D. Overskei, and A. Todd, *FED Low-q/Shaping Team Report*, to be published.
4. J. Hosea, D. Cohn, D. Hwang, J. Lyon, F. Perkins, J. Rawls, J. Sharer, and D. Metzler, *FED Ion Cyclotron Heating Team Report*, to be published.
5. K. H. Burrell, R. J. Hawryluk, F. L. Hinton, Y-K. M. Peng, P. H. Rutherford, and D. J. Sigmar, *FED Non-divertor Active Impurity Control Team Report*, to be published.
6. Y-K. M. Peng, S. K. Borowski, and T. Kammash, Nucl. Fusion 18, 1489 (1978).
7. R. M. Gilgenbach et al., *Electron Cyclotron/Upper Hybrid Resonant Preionization in the ISX-B Tokamak*, NRL Memorandum Report 4248, Naval Research Laboratory (June 1980), to be published in Nucl. Fusion.
8. R. C. Isler et al., "Experiments in the ISX-B Tokamak: ECH, Ripple Studies, Pellet Fueling, Impurity Flow Reversal, and Surface Physics," paper IAEA-CN-38/A-5 in *Plasma Physics and Controlled Nuclear Fusion Research 1980*, to be published.
9. S. K. Borowski, Y-K. M. Peng, and T. Kammash, *RF Assisted Current Startup of ETF/INTOR-Size Tokamak Plasmas*, to be published.
10. J. C. Hosea et al., "Fast Wave Ion Cyclotron Heating in the Princeton Large Torus," paper IAEA-CN-38/D-5-1 in *Plasma Physics and Controlled Nuclear Fusion Research 1980*, to be published.
11. TFR Group, "ICRF Heating in TFR 600," paper IAEA-CN-38/D-3 in *Plasma Physics and Controlled Nuclear Fusion Research 1980*, to be published; H. Kimura et al., "High Efficiency ICRF Heating Experiment in DIVA," paper IAEA-CN-38/D-5-2 in *Plasma Physics and Controlled Nuclear Fusion Research 1980*, to be published.

12. J. Adam, J. Jacquinot, Y. Lapierre, and D. Marty, "ICRF Theoretical Progress in Fontenay-aux-Roses," paper presented at the Fourth Topical Conference on RF Heating in Plasma, Austin, Texas, February 9-10, 1981.
13. D. Blackfield, *Numerical Simulations of ICRF Heated Tokamak Plasmas*, UWFDM-353, University of Wisconsin (May 1980).
14. D. Blackfield and D. Cohn, private communications.
15. D. Steiner et al., *Oak Ridge TNS Program, Summary of FY 1978 Activities*, ORNL/TM-6720, Oak Ridge National Laboratory (July 1979).
16. J. A. Holmes, J. A. Rome, W. A. Houlberg, Y-K. M. Peng, and S. J. Lynch, Nucl. Fusion 20, 59 (1980).
17. L. D. Stewart et al., *Merits of D^--Based Neutral Beam Injectors for Tokamaks*, PPPL-1756, Princeton Plasma Physics Laboratory (February 1980); H. P. Eubank et al., "Neutral Beam Heating Task Force Report," to be published.
18. J. D. Callen, J. F. Clarke, and J. A. Rome, "Theory of Neutral Beam Injection into a Tokamak," paper E14 presented at the 3rd International Symposium on Toroidal Plasma Confinement, Garching, Federal Republic of Germany, March 26-30, 1973.
19. T. E. Stringer, Nucl. Fusion 12, 689 (1972).
20. J. N. Davidson, Nucl. Fusion 16, 73 (1976).
21. J. A. Rome and Y-K. M. Peng, Nucl. Fusion 19, 1193 (1979).
22. R. H. Fowler and J. A. Rome, *Effects of Toroidal Field Ripple on Injected Deuterons in the FED Device*, ORNL/TM-7774, Oak Ridge National Laboratory, to be published.
23. W. A. Houlberg, S. E. Attenberger, and L. L. Lao, "Developments in Tokamak Transport Modeling," paper presented at ANS/ENS Topical Meeting on Advances in Mathematical Methods for Nuclear Engineering Problems, Munich, Federal Republic of Germany, April 27-29, 1981.
24. S. E. Attenberger and W. A. Houlberg, "Heating Power Contours for the FED Tokamak," to be presented at the 1981 IEEE International Conference on Plasma Science, Santa Fe, New Mexico, May 18-20, 1981.
25. M. L. Watkins et al., "Considerations on the Approach to Ignition in Large Tokamaks," paper IAEA-CN-38/W-3 in *Plasma Physics and Controlled Nuclear Fusion Research 1980*, to be published.

26. L. D. Stewart, "Tokamak Neutral Beam System Power Efficiency and Cost," paper presented at the IEEE International Conference on Plasma Science, Montreal, Canada, June 4-6, 1976.
27. Recent examples include: *ETF Interim Design Description Document*, ETF Design Center (July 1980); *International Tokamak Reactor: Zero Phase*, International Atomic Energy Agency (1980).
28. Recent examples of this large body of work include: Y-K. M. Peng et al., Phys. Fluids 21, 467 (1978) and Refs. 29 and 30.
29. A. M. M. Todd et al., Phys. Fluids 19, 743 (1979).
30. L. A. Charlton et al., Phys. Rev. Lett. 43, 1395 (1979).
31. M. Murakami et al., "Neutral Injection Experiments in the ISX-B Tokamak," paper IAEA-CN-38/M-1 in *Plasma Physics and Controlled Nuclear Fusion Research 1980*, to be published.
32. D. Swain, M. Murakami et al., "High Power Neutral Beam Injection Experiments on the ISX-B Tokamak," to be published.
33. J. A. Holmes, B. Carreras et al., "Nonlinear Tearing Mode Evolution in Moderate Beta Tokamaks," Bull. Am. Phys. Soc. 25, 930 (1980).
34. J. F. Clarke and D. J. Sigmar, Phys. Rev. Lett. 38, 70 (1977); D. J. Sigmar and G. Vahala, Phys. Fluids 21, 2280 (1978); T. Mizoguchi, T. Kammash, and D. J. Sigmar, Phys. Fluids 21, 2086 (1978).
35. R. A. Dory and Y-K. M. Peng, Nucl. Fusion 17, 21 (1977); J. L. Johnson et al., J. Comput. Phys. 32, 212 (1979); J. A. Holmes, Y-K. M. Peng, and S. J. Lynch, J. Comput. Phys. 36, 35 (1980).
36. Section II.1.1 in *JET Design Report*, EUR5516e, Euratom (1976).
37. V. S. Mukhovatov and V. D. Shafranov, Nucl. Fusion 11, 605 (1971).
38. D. L. Jassby, D. R. Cohn, and R. R. Parker, Nucl. Fusion 16, 1045 (1976).
39. V. M. Leonov, V. G. Merezhkin et al., "Ohmic-heating and Neutral-beam Injection Studies on the T-11 Tokamak," paper IAEA-CN-38/N-2 in *Plasma Physics and Controlled Nuclear Fusion Research 1980*, to be published.
40. J. C. Wesley et al., "Shaping and Characteristics of Ohmically Heated Noncircular Plasmas in Doublet III," paper IAEA-CN-38/A-3 in *Plasma Physics and Controlled Nuclear Fusion Research 1980*, to be published.

41. DIVA Group, Nucl. Fusion 20, 271 (1980).

42. A. Boozer, *Enhanced Transport in Tokamaks Due to Toroidal Ripple*, PPPL-1619, Princeton Plasma Physics Laboratory (1980); R. J. Goldston and H. H. Towner, *Effects of Toroidal Field Ripple on Superthermal Ions in Tokamak Plasmas*, PPPL-1637, Princeton Plasma Physics Laboratory (1980).

43. R. J. Goldston and H. H. Towner, Nucl. Fusion 20, 781 (1980).

44. R. L. Reid et al., "ETF Systems Code — Composition and Application," paper presented at the Fourth ANS Topical Conference on the Technology of Controlled Nuclear Fusion, King of Prussia, Pennsylvania, October 14-17, 1980.

45. Minutes of the FED Technical Management Board Meeting, Los Angeles, California, December 18-19, 1980; R. Goldston et al., *FED Confinement Team Report*, to be published.

46. S. E. Attenberger, J. A. Holmes, W. A. Houlberg, and S. D. Scott, "Toroidal Field Ripple Conduction Losses in the FED Tokamak," to be presented at the 1981 IEEE Conference on Plasma Science, Santa Fe, New Mexico, May 18-20, 1981.

47. M. Murakami et al., "Neutral Injection Experiments in the ISX-B Tokamak," paper IAEA-CN-31/N-1 in *Plasma Physics and Controlled Nuclear Fusion Research 1980*, to be published.

48. D. Overskei, Phys. Rev. Lett. 46, 177 (1980).

49. S. Talmadge and R. J. Taylor, Bull. Am. Phys. Soc. 25, 1033 (1980).

50. J. F. Schivell, *Methods of Plasma Purity Control Without Magnetic Divertor*, PPPL-1342, Princeton Plasma Physics Laboratory (June 1977).

51. R. Jacobsen, paper presented at the Non-magnetic Divertor Workshop, Massachusetts Institute of Technology, Cambridge, Massachusetts, October 1980.

52. Y-K. M. Peng, R. R. Parker, and D. Overskei, *An Option of Limiter Pumping Approach for ETF*, ETF-R-80-PS-023, ETF Design Center (July 1980).

53. H. C. Howe, "Physics Considerations for the FED Limiter," to be published.

54. D. E. Post et al., "INTOR Plasma Edge and Divertor Characteristics," to be published.

55. P. Mioduszewski and J. Sheffield, "Pump Limiter Studies at Oak Ridge," paper presented at the Japan-U.S. Workshop on Impurity Control, Divertors, and Plasma-Wall Interactions, Princeton, New Jersey, February 2-6, 1981.

56. J. Bohdansky et al., J. Nucl. Mater. 76&77, 163 (1978).

57. D. L. Smith, M. Kaminsky, and J. Norem, "Low Z Coating Technology for FED First Wall and Limiter," to be published.

58. *ETF Interim Design Description Document*, ETF Design Center (July 1980).

59. J. A. Schmidt et al., *INTOR Phase I Poloidal Divertor Studies*, to be published.

60. M. Petravic et al., "Plasma Flow and Neutral-plasma Interaction in Poloidal Divertors," abstract published in Bull. Am. Phys. Soc. 25, 1033 (1980); D. Heifetz et al., "Monte Carlo Calculation of Neutral Particle Transport in Poloidal Divertors," abstract published in Bull. Am. Phys. Soc. 25, 1033 (1980).

61. L. M. Hively et al., "Physics Optimization of Bundle Divertors," to be published.

62. J. A. Rome and Y-K. M. Peng, Nucl. Fusion 19, 1193 (1979).

63. D. R. Cohn, D. Jassby, and Y-K. M. Peng, "ETF Ripple Workshop Recommendations," October 25, 1979.

64. T. F. Yang et al., "In Search of Optimized Bundle Divertor," abstract published in Bull. Am. Phys. Soc. 25, 1032 (1980).

65. R. A. Dandl et al., *The ELMO Bumpy Torus Experiments*, ORNL/TM-3694, Oak Ridge National Laboratory (November 1977).

66. G. Bateman and P. Theriault, *Hybrid Bundle Divertor Design*, GTFR-23, Georgia Institute of Technology (February 1981).

67. H. P. Furth, "Heat Outflow, Particle Outflow and Impurity Control in FED," to be published.

68. D. R. Eames et al., Bull. Am. Phys. Soc. 25, 998 (1980).

69. D. E. Post, R. V. Jensen et al., *Steady-state Radiation Cooling Rates for Low-density, High-temperature Plasmas*, PPPL-1352, Princeton Plasma Physics Laboratory (July 1977).

70. K. B. Axon et al., "Results from the Divertor Injection Tokamak Experiment (DITE)," in *Plasma Physics and Controlled Nuclear Fusion Research 1978*, p. 51 (1979).

71. J. Wesley et al., "Disruption Control Task Force Report," to be published.

72. R. L. Miller et al., *Plasma Disruption Characteristics and Protection Requirements in ETF/INTOR*, ETF-R-80-PS-025, Fusion Engineering Design Center (July 1980).

73. M. Murakami, Nucl. Fusion 16, 347 (1976).

74. R. B. White, D. A. Monticello, M. N. Rosenbluth, and B. V. Waddell, Phys. Fluids 20, 800 (1977); R. B. White, D. A. Monticello, and M. N. Rosenbluth, Phys. Rev. Lett. 39, 1678 (1977).

75. B. Carreras, H. R. Hicks, J. A. Holmes, and B. V. Waddell, Phys. Fluids 23, 1811 (1980); H. R. Hicks, J. A. Holmes, D. K. Lee, B. A. Carreras, and B. V. Waddell, *3-D Nonlinear Calculations of Resistive Tearing Modes*, ORNL/TM-7132, Oak Ridge National Laboratory (1981).

76. A. Sykes and J. A. Wesson, Phys. Rev. Lett. 44, 1215 (1980).

77. J. Dunlap, private communication.

78. B. Carreras, private communication.

79. A. Sestero, in *Proc. Int. Symp. on Plasma-Wall Interaction*, p. 131 (1976).

80. P. Mioduszewski, "Surface Heat Loads During Major Disruptions in INTOR," paper presented at the 11th Symposium on Fusion Technology, Oxford, England, September 15-19, 1980.

81. B. L. Doyle et al., J. Nucl. Mater. 93&94, 551 (1980).

82. W. Bauer, J. Nucl. Mater. 76&77, 3 (1978).

83. Y-K. M. Peng et al., in *Proc. 7th Symp. on Engineering Problems in Fusion Research*, p. 186 (1977).

84. *Fusion Energy Division Annual Progress Report*, ORNL-5405, Oak Ridge National Laboratory (August 1978), p. 87.

85. PDX poloidal field system.

86. This idea was brought to our attention recently by D. B. Montgomery.

87. Y-K. M. Peng et al., Phys. Fluids 21, 467 (1978).

88. Y-K. M. Peng, *Influence of a Soft β_p Limit on Choices of FED Parameters*, FEDC-R-81-PS-001, Fusion Engineering Design Center, to be published.

89. J. A. Holmes, Y-K. M. Peng, and K. E. Rothe, *Equilibrium Evolution on the Resistive Time Scale in a Tokamak Reactor*, ORNL/TM-7678, Oak Ridge National Laboratory (in press).

90. J. A. Holmes, Y-K. M. Peng, and S. J. Lynch, J. Comput. Phys. 36, 35 (1980).

91. L. A. Charlton, D. B. Nelson, and R. A. Dory, Phys. Rev. Lett. 45, 24 (1980).

5. MAGNETICS SYSTEMS

R. W. Derby*

S. S. Kalsi[†]
R. J. Hooper[†]
B. L. Hunter[†]
P. T. Spampinato[‡]
V. C. Srivastava[†]
J. Schultz[§]

5.1 INTRODUCTION

The magnetics systems of the FED, as in any magnetic confinement device, not only will consume a large part of the capital investment required, but also will require long lead times. The successful design and fabrication of these systems represent a major technical challenge.

Because resistive coils large enough to satisfy the FED mission requirements would use prohibitive amounts of electric power, the toroidal field (TF) coils will be superconducting. The design of these coils will make maximum use of the designs and associated development information currently being generated within the Large Coil Program (LCP). The design and development of the FED TF coils will, however, present additional questions beyond those that can be easily answered in LCP. The first is that the FED mission will require the TF coils to be approximately three times as large as the LCP coils. Accordingly, scaling of this technology must be understood. Other areas requiring resolution are the degree to which eddy currents will play a major role in driving the design and the degree to which they can be studied in LCP. Finally, there is the matter of structural design requirements and fatigue. The cyclic, out-of-plane loads in FED will be more severe than

---

*Fusion Engineering Design Center/Massachusetts Institute of Technology.

[†]Fusion Engineering Design Center/General Electric Company.

[‡]Fusion Engineering Design Center/Grumman Aerospace Corporation.

[§]Massachusetts Institute of Technology.

those in the LCP coils. These subjects are all receiving careful attention during the trade and design studies to be described in this section.

As challenging as the design of the TF system is that of the ohmic heating (OH) and equilibrium field (EF) systems. Although ongoing development programs are small compared to those for the TF system, maximum advantage will be taken of the design and performance information from the Los Alamos National Laboratory (LANL) 20-MJ coil program and from ancillary programs at Argonne National Laboratory (ANL).

In any major technological undertaking, insurance in the form of backup or upgrade options will invariably come up for consideration. The FED is no exception. A substantial portion of the work described in this section is devoted to magnetics-related options that might be exercised if the current baseline concept requires enhancement. In short, the three major themes of feasibility, cost, and insurance run through the discussions presented below.

Section 5.2, which deals with TF coil structural design, and Sect. 5.5, which deals with poloidal field (PF) coil design, are primarily devoted to feasibility issues. Section 5.4, which deals with ripple control, was motivated by economic and maintenance issues. Section 5.3, which deals with field strength enhancement, and Sect. 5.6, which deals with inorganic insulators, were motivated by insurance concerns.

5.2 TF COIL STRUCTURAL DESIGN

5.2.1 Purpose

The purpose of this effort is to develop a feasible structural design of superconducting 8-T TF coils, including coil case and inter-coil support structure (ISS), as a function of the number of pulses N in the range $5 \times 10^4 \leq N \leq 1 \times 10^6$.

Figure 5.1 shows a TF coil along with the bucking post and ISS. The TF coils are subjected to forces both in and normal to the plane of the coil. The in-plane force results from the interaction of the toroidal magnetic field (produced by the TF coil) and the current in the TF coil; it varies in magnitude around the coil periphery and is everywhere

ORNL-DWG 84-2526 FED

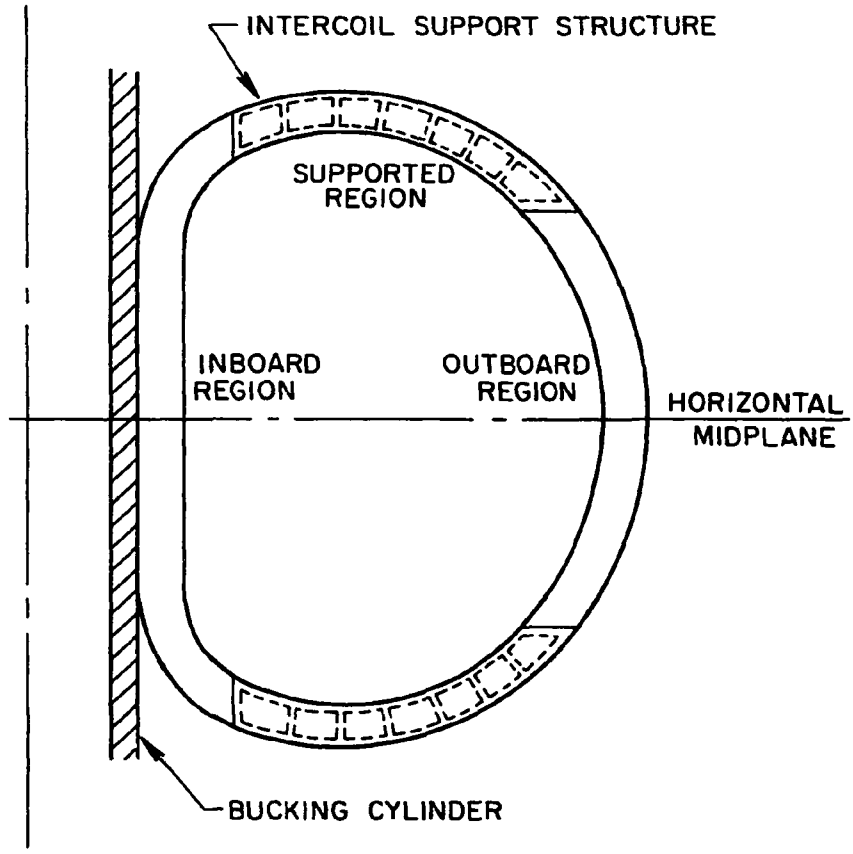

Fig. 5.1. TF coil, bucking cylinder, and ISS.

directed along an outward normal to the TF coil. Once the TF coils are energized, this force remains constant with time. The net resultant in-plane force is radially inward and is equilibrated by the bucking post. An additional force, acting normal to the plane of the coil, results from the interaction of the TF coil current and the field produced by the PF coils. Because the PF coil operation is typically pulsed, the out-of-plane force is typically cyclic. It varies in magnitude and sign around the periphery of the coil but is antisymmetrical (or nearly so) about the horizontal midplane. While there is little or no net resultant out-of-plane force, there is an out-of-plane moment tending to overturn the TF coil about its horizontal midplane. The ISS is provided to equilibrate the overturning moment.

Earlier design efforts on generically similar devices [the Engineering Test Facility (ETF) and the International Tokamak Reactor (INTOR)] have exhibited severe TF coil structural support problems that are a direct consequence of the pulsed nature of the out-of-plane loads. Crack growth and fracture mechanics considerations lead to allowable working stresses far below those which would be used for a steady-state device. Consequently, the resulting thickness and weight of structural components such as coil case and ISS are so large that the ability to fabricate, weld, and inspect these components appears questionable.

Given the more modest TF requirements of FED, the loads on the TF coils are lower, with an attendant decrease in the amount of structure needed to equilibrate the loads. Furthermore, the number of full field pulses currently adopted for FED is lower than the figure used in the earlier ETF and INTOR studies, resulting in somewhat higher fracture mechanics allowable stresses.

5.2.2 Assumptions and Guidelines

The structural design criteria used in the present study include conventional limits on primary membrane and bending stress intensities to preclude large-scale yielding or rupture due to gross overloading, as well as a limit on peak normal stress that is based on crack growth and fracture mechanics considerations. This limit is considered in basic

sizing calculations because the large number of design pulses tends to lead to very restrictive design allowances for cyclic stresses. The structural criteria are determined using the same formalism as used in recent INTOR studies, although the fracture mechanics allowable stress is higher in FED than in INTOR because of the smaller number of pulses.

The conventional design allowable stresses are stated as multiples of the quantity S_m, defined as the lesser of two-thirds yield stress or one-third ultimate stress, at operating temperature. The conventional design allowables are as follows:

1. Normal operation:
   primary membrane stress intensity $\leq S_m$,
   primary membrane plus bending stress intensity $\leq 1.5S_m$.
2. Abnormal operation:
   primary membrane stress intensity $\leq 1.5S_m$,
   primary membrane plus bending stress intensity $\leq 2.25S_m$.

Table 5.1 summarizes the material properties used for 316 LN stainless steel.

The limit on peak normal stress is derived from linear elastic fracture mechanics concepts. In general, the stress σ acting normal to the plane of an assumed flaw is composed of a steady-state component plus a cyclic component that varies from zero to $f\sigma$ ($0 \leq f \leq 1$). Potential fracture in the vicinity of the flaw is dependent upon the full stress σ, whereas only the component $f\sigma$ causes the flaw to grow with each cycle. Given an assumed initial flaw size a_o and a specified number of applications N_o of the cyclic stress $f\sigma$, a Paris crack growth law is used to determine the final crack size a_f in terms of σ, N_o, and a_o. Furthermore, a well-known fracture mechanics equation relates the failure stress to a_f and the material fracture toughness K_{IC}. By mathematically eliminating the explicit dependence upon a_f, the failure stress may be expressed in terms of a_o, K_{IC}, N_o, and the empirical parameters C_o and n in the Paris equation.

An allowable stress is obtained by applying the analytical result for two combinations of parameters and choosing the more conservative of the two results. On the one hand, it is desired to maintain a safety

Table 5.1. Properties of 316 LN stainless steel

	Plate		Weld	
	293 K	4 K	293 K	4 K
Yield stress, ksi	30	125	30	100
Ultimate stress, ksi	75	200	70	161
Fracture toughness, ksi·in.$^{1/2}$		150		100
Crack growth constants[a]				
n	3.26		3.36	
C_o	4.5×10^{11}		7.6×10^{11}	

[a] $\frac{da}{dN} = C_o(\Delta K)^n$; $\frac{da}{dN}$ in inches per cycle, ΔK in ksi·in.$^{1/2}$

factor of S_s on stress after N applications of load, where N is the number of cycles for which the device is to be designed. A stress level σ results by setting the failure stress equal to $S_s\sigma$ and $N_o = N$. On the other hand, it is desired to maintain a safety factor S_n on cycles by ensuring that the stress level would remain below the predicted failure stress if the device were to be operated for S_n design lives. A second stress level results by setting the failure stress equal to σ and $N_o = S_nN$. The allowable stress is then taken as the lesser of the two stress levels.

Figure 5.2 shows a family of design curves used in the present study. The curves are based on the properties for 316 LN stainless steel listed in Table 5.1, on safety factors of either 2 on stress or 4 on cycles (whichever is more conservative), and on an initial flaw diameter $2a_o = 0.2$ in. The assumed defect size is considered an aggressive, but realistic, estimate of the smallest flaw that can be guaranteed to be detected by ultrasonic testing in thick sections. The safety factors (2 on stress and 4 on cycles) are considered consistent with good engineering practice — reasonable yet not unduly conservative — and are comparable to those used in the design of the Mirror Fusion Test

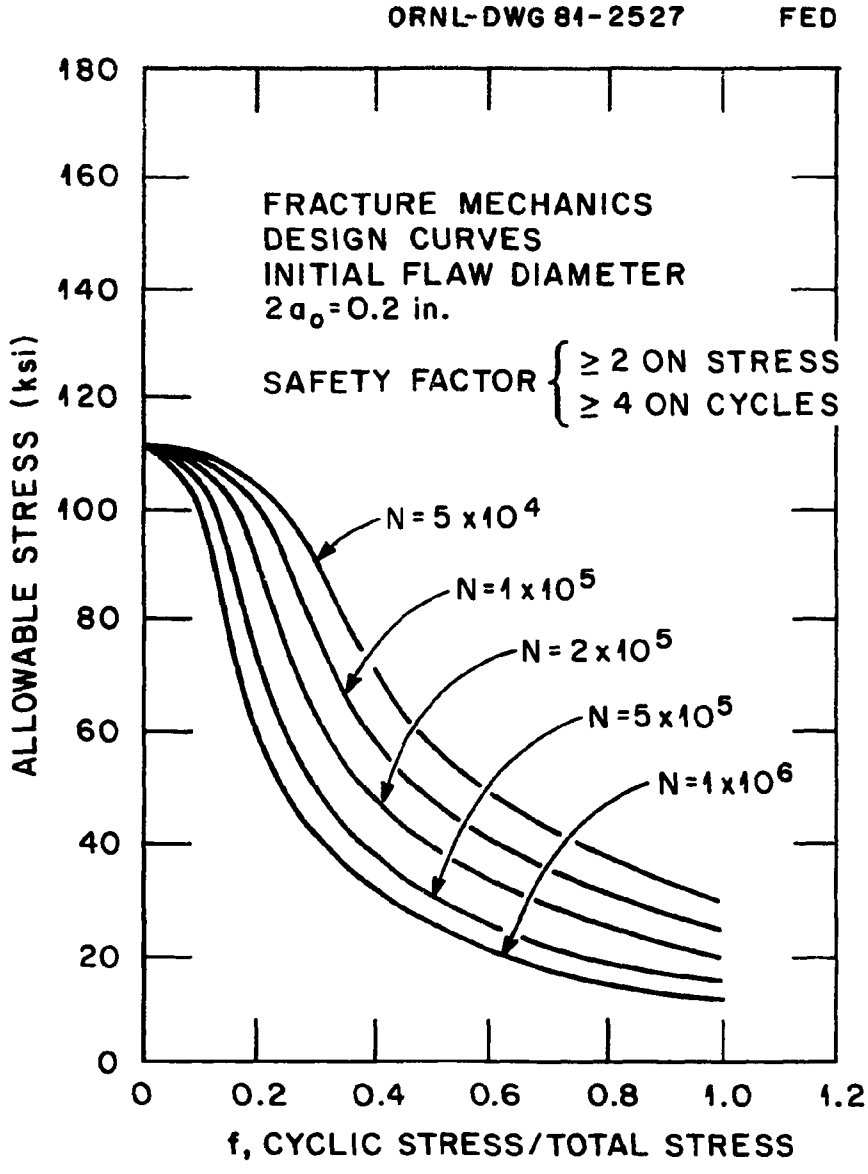

Fig. 5.2. Allowable stress for 316 LN stainless steel.

Facility (MFTF) superconducting yin-yang magnets.[1] The limiting value of allowable stress at f = 0 is $K_{IC}/2.4\ \pi a_o$, which is the basic fracture mechanics limit in the absence of cyclic loading and crack growth. As the stress ratio f increases, the allowable stress drops to a small fraction of the value at f = 0.

5.2.3 Description of Design Effort

The present effort involves sizing the TF coil case wall thickness and the ISS based on a peak field of 8 T in the TF coil winding and for N ranging from 5×10^4 to 1×10^6. The baseline value of N for FED is 3.5×10^5 pulses.

The final configuration of the PF coils for FED has not yet been determined. Consequently, the out-of-plane load profile shown in Fig. 5.3 is based on a preliminary PF coil design and is used here for design purposes. While the design effort is based on tentative loads and is therefore still preliminary, results to date indicate that the more modest requirements of FED (relative to ETF/INTOR) lead to a significant reduction in the severity of the structural support problems.

Since the fracture mechanics allowable stress and the resulting thickness and weight of structural support members are a function of the required number of pulses, this study considers the variation of the structural weights with number of pulses; structural weight is directly related to the capital cost of the coils.

Figure 5.4 shows the fracture mechanics allowable stress as a function of N, based on a fully cyclic load (f = 1.0) and an assumed initial defect diameter of 0.2 in. This defect size is considered a realistic quality control goal and is used as a baseline value. As indicated, the allowable stress varies from 30 ksi at $N = 5 \times 10^4$ pulses to 12 ksi at $N = 1 \times 10^6$ pulses. Figure 5.5 shows the fracture mechanics allowable stress (assuming a fully cyclic load) as a function of the assumed initial flaw size for discrete values of N ranging from 5×10^4 to 1×10^6.

Table 5.2 shows the results to date, based on the available estimate of the out-of-plane load profile around the TF coil periphery. This

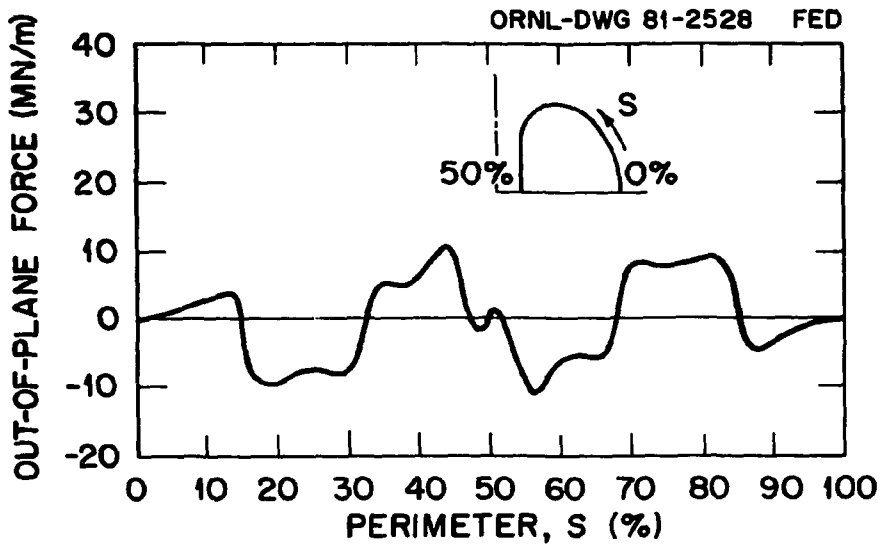

Fig. 5.3. Out-of-plane force distribution on TF coil.

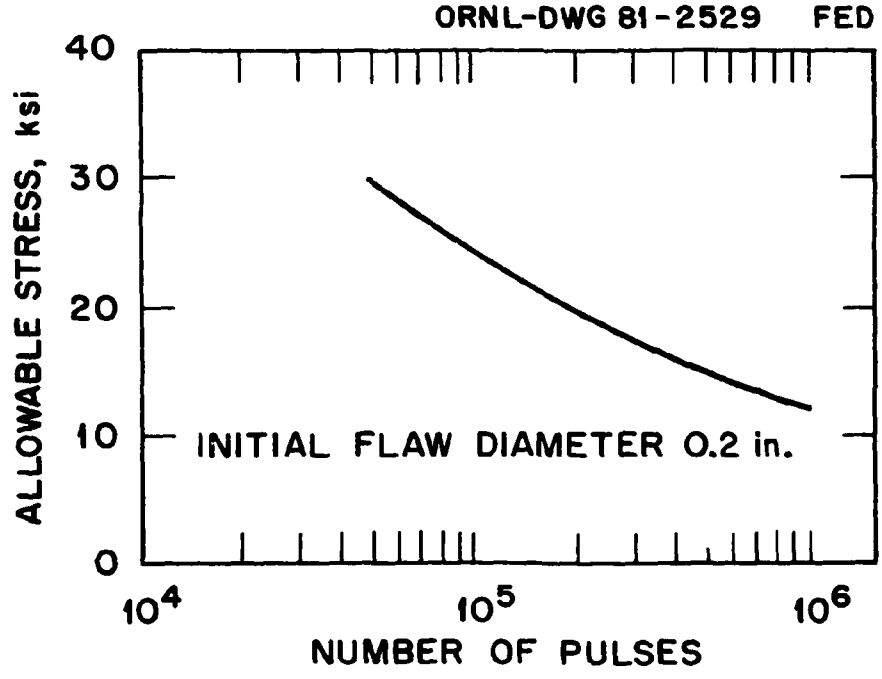

Fig. 5.4. Fracture mechanics allowable stress vs number of pulses.

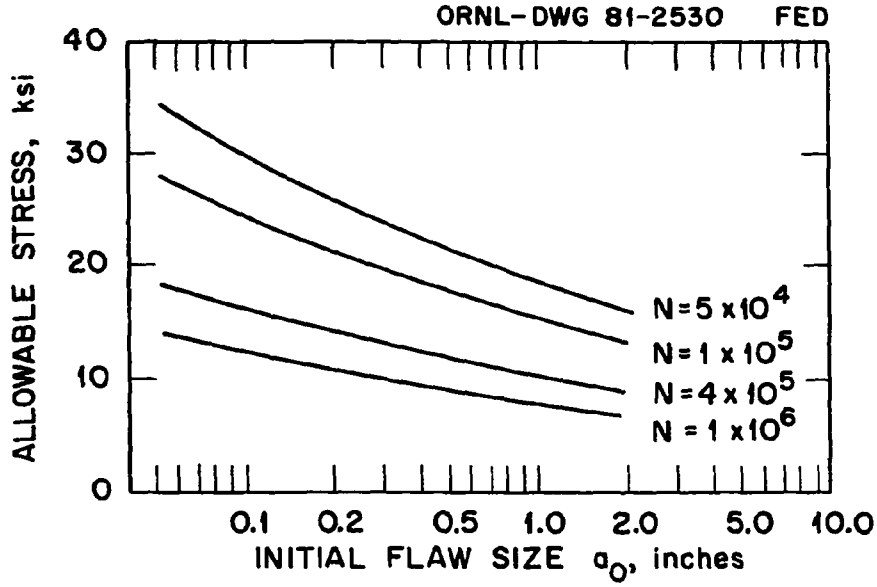

Fig. 5.5. Fracture mechanics allowable stress vs initial flaw size.

Table 5.2. FED coil case data versus number of pulses

	INTOR	FED		
Number of cycles	1×10^6	1×10^5	4×10^5	8×10^5
Fracture mechanics allowable stress, assuming fully cyclic load (ksi)	12	24	16	13
Inboard region				
Maximum out-of-plane load (MN/m)	10.0	10.8	10.8	10.8
Wall thickness per plate bending allowance (cm)	15.0	8.6	10.5	11.7
Case cross section (m^2)	0.558	0.305	0.380	0.429
Supported region				
Maximum out-of-plane load (MN/m)	27.6	9.5	9.5	9.5
Wall thickness per plate bending allowance (cm)	20.0	7.0	8.6	9.5
Case cross section (m^2)	0.784	0.244	0.305	0.340
Outboard region				
Maximum out-of-plane load (MN/m)	24.0	4.2	4.2	4.2
Wall thickness per plate bending allowance (cm)	30.2	7.6	9.3	10.3
Case cross section (m^2)	1.307	0.266	0.332	0.372
Total coil perimeter (m)	34.0	32.6	32.6	32.6
Case weight per TF coil (kg)	2.2×10^5	6.7×10^4	8.4×10^4	9.4×10^4

table shows the TF coil case wall thickness and resulting coil case weight, based on limiting the plate bending stress in the case sidewall to the fracture mechanics design allowance corresponding to an initial flaw diameter of 0.2 in. This bending stress results from the winding being thrust against the case sidewall by the out-of-plane pulsed field load. (While not part of the present study, corresponding results from the latest INTOR design are shown to illustrate the large difference between INTOR results and the present FED results.)

It is apparent that the more modest fields and forces associated with FED, as well as the reduced cycles, lead to large reductions in coil case thickness and weight. Whereas the INTOR thicknesses appear near or beyond existing fabrication capabilities, the FED thicknesses appear practical to build. The table shows that a reduction in cycles from 4×10^5 to 1×10^5 would reduce the coil case weight by about 20%, which would result in a cost savings for the TF coil case of approximately the same percentage. On the other hand, increasing the cycles from 4×10^5 to 8×10^5 would increase the weight, and therefore the TF coil case cost, by about 12%.

Figure 5.6 shows the TF coil case weight as a function of the number of pulses, for $5 \times 10^4 \leq N \leq 1 \times 10^6$. On the assumption that cost is proportional to weight, the axis is also labeled to show the relative cost of the TF coil case with the cost at 3.5×10^5 pulses (FED baseline value) normalized to 1.0. Because the weights of some parts of the TF coil system (e.g., the winding and the bucking cylinder) are not affected by the number of pulses, the sensitivity of the overall TF coil system cost to number of pulses is more modest. Between 5×10^4 and 1×10^6 pulses, the overall TF system cost varies from about 96% to 103% of its value at 3.5×10^5 pulses.

5.2.4 Conclusions and Recommendations

While the present results are based upon a preliminary estimate of the out-of-plane loads acting on the TF coil, the coil case thicknesses computed for FED are in the range that is practical to fabricate, weld, and inspect.

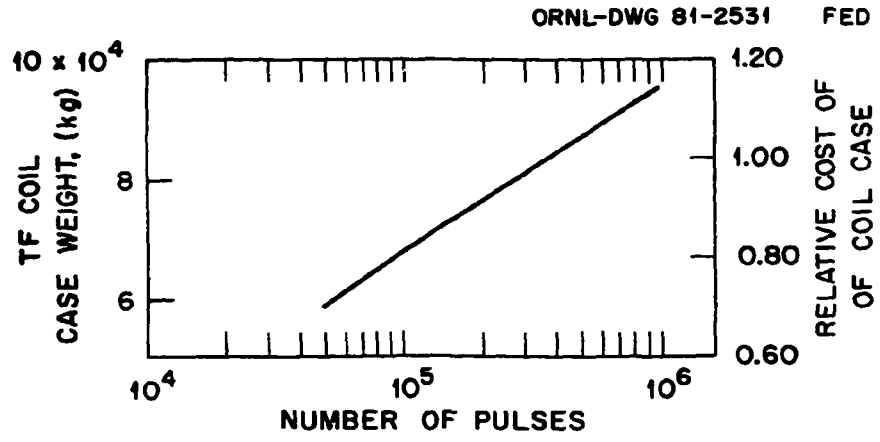

Fig. 5.6. Weight and relative cost of TF coil case vs number of pulses.

The reduced structural requirements, relative to the ETF/INTOR designs, are attributable principally to the lower forces associated with the reduced field strength (8 T in FED versus 11-12 T in ETF/INTOR). Furthermore, while the number of pulses for FED has not been finalized, it will be less than that specified for INTOR (3.5×10^5 cycles for FED versus $0.6\text{-}1.0 \times 10^6$ cycles for INTOR); this reduction in cycles leads to somewhat higher fracture mechanics allowable stress levels and, therefore, lower structural weights.

Future effort in this area will proceed once the configuration of the PF coil system has been determined, along with the out-of-plane load profile corresponding to this configuration. This information is needed to properly size the ISS and to determine what additional stiffening of the outboard leg of the coil is required to resist the beam bending loads that arise, as the top and bottom halves of the TF coil system tend to rotate in opposite directions due to the antisymmetrical out-of-plane loads. Since the use of fracture mechanics leads to allowable working stresses far below those that would be used for a steady-state device, the structural requirements for the TF coil design will be examined with and without the application of fracture mechanics to identify the impact on the design. Conceptual design of the total TF coil system will then be performed, after which structural designs will be developed for the coil case and ISS.

5.3 TOROIDAL FIELD ENHANCEMENT

5.3.1 Purpose

The present FED baseline design assumes a maximum toroidal field of 8 T at the coil winding and 3.6 T on the plasma axis. The present superconducting TF coil R&D program will provide the technology basis for 8-T coil design; however, design for peak fields above 8 T incurs increased risk. It may be desirable to provide for field enhancement ($\sim$1-2 T) on the plasma axis subsequent to initial operations depending on the physics performance achieved. Alternatively, the device performance could be improved from the outset by an enhancement of the

toroidal field. The purpose of this study is to explore various techniques for achieving a 1- to 2-T toroidal field enhancement of FED, given the assumption that the TF coils are designed for 8-T operation.

5.3.2 Concepts Considered

Generally, it is difficult to effectively enhance the magnetic field on the plasma axis after the TF system has been designed, in this case using superconducting magnets to provide an 8-T field at the windings. However, some concepts considered for generating higher fields at the plasma axis are:

1. NbTi main TF coils supplemented with copper insert coils,
2. NbTi TF coils cooled with superfluid helium,
3. NbTi main coils supplemented with Nb_3Sn insert coils,
4. Hybrid NbTi and Nb_3Sn coils.

Each of these options was examined relative to an 8-T NbTi superconducting TF system. It should be recognized that the enhanced field, in general, also increases the magnetic forces, resulting in additional structural requirements. This additional structural need must be accommodated in each concept.

5.3.3 Description of Concepts Studied

The concepts were examined to determine their technical feasibility. The considerations for each concept are briefly described.

NbTi main TF coils supplemented with copper insert coils

In this concept, additional field on the plasma axis is obtained by incorporating auxiliary copper coils around the plasma chamber and inside the bore of the superconducting TF coils (see Fig. 5.7). To provide a field enhancement of 1.5 T on the plasma axis, the power requirement for the copper coil set would be on the order of 160 MW for a duty factor of 66%. Operating cost at reduced field enhancement will

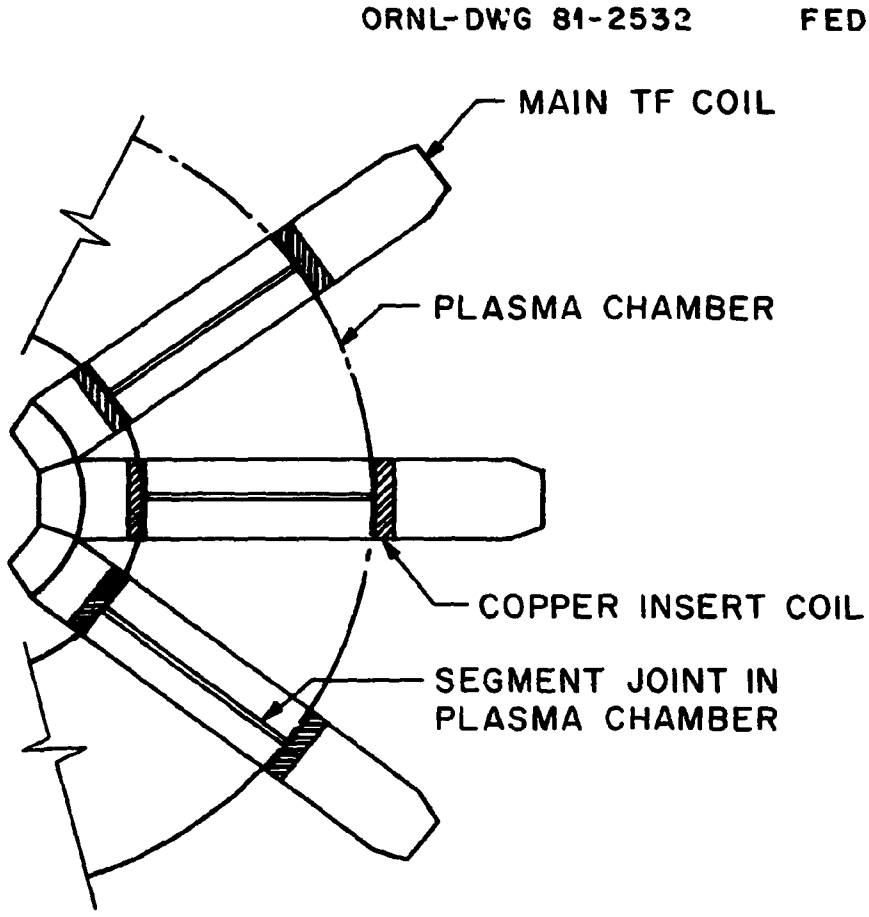

Fig. 5.7. Relative location of main and copper insert TF coils.

be proportional to the square of the field enhancement ratios. For example, the operating cost for 0.5-T field enhancement would be 18 MW. If these coils were made from aluminum, approximately 60% more power would be required for the same winding cross section.

Another consideration of this approach is that if the copper insert coils are located in the positions shown in Fig. 5.7, a higher toroidal field ripple would result. The ripple could be reduced if the insert coils were located midway between the main TF coils. However, this is likely to interfere with penetrations. Determining the optimum location of the copper insert coils relative to the superconducting TF coils would require additional design work.

A very rough estimate was made of the cost of these copper insert coils, and it appears to be about 10% of the cost of the 8-T superconducting coils. Although it appears that such a design approach is technically feasible, considerable design effort would be required to demonstrate that this is an attractive concept.

NbTi superconducting coils cooled with superfluid helium

The TF system would initially be designed for 8-T operation using NbTi superconductor cooled with 4.2 K helium. The operating field capability of this winding could be enhanced to 10 T by cooling it with 1.8 K superfluid helium. However, such a TF system would need additional refrigeration capability for cooling the magnet system from 4.2 K to 1.8 K. Additional structure would also have to be provided to accommodate the increased electromagnetic forces at the higher fields.

The cryogenic design of TF coils operating at 4.2 K is significantly different from that of coils operating at 1.8 K. The system must be designed for 1.8 K. Coils could be operated at 4.2 K, with additional refrigeration added later for operating the coils at 1.8 K to achieve a 10-T field. Nevertheless, magnets designed for such dual temperature operation could be more expensive than if they were designed for operation at either 1.8 K or 4.2 K.

The additional structure needed for operation at 10 T would be required from the beginning. This structure cannot be efficiently added

at a later date because an optimally designed 8-T system would not have space for the additional structure required for this concept. Moreover, the incorporation of additional structure at a later date might be more expensive. Thus, if this concept were followed, the TF coils would have to be designed for 10-T operation using NbTi superconductor cooled with 1.8 K superfluid helium. Alternatively, it might be feasible to design the coils for 8-T operation but, if higher field operation became desirable, to operate at 9-10 T and accept a lifetime with a decreased number of full field pulses. Such operation requires evaluation.

At this time the additional cost of this TF coil system, relative to the 8-T system at 4.2 K, appears uncertain. Not only will there be the cost of doubling the refrigeration system capacity and the addition of complicated structure, but also allowances must be made for more complex plumbing needed for operation with the superfluid helium system. For example, the current leads and heat exchanger associated with each coil would be complex and would increase the cost of the TF system. Additional development work is needed on the magnet design and the superfluid helium refrigeration system design. Superfluid-helium-cooled coils will not be tested in the Large Coil Test Facility. However, a 1-m-diam circular coil will be tested in the Lawrence Livermore National Laboratory's High Field Test Facility, as part of the 12-T Program.

NbTi main coils supplemented with Nb_3Sn insert

In this approach, a Nb_3Sn superconducting coil would be installed inside the 8-T NbTi coils (see Fig. 5.8). The Nb_3Sn coil would be designed for operation at fields above 8 T. The torus sectors would have to be modified to provide space for the Nb_3Sn coil, and this could require that the major radius be increased. The Nb_3Sn coil would have its own coil case and intercoil structure for accommodating out-of-plane loads. However, it may be difficult to react in-plane forces of the Nb_3Sn magnet inserts. One possible option is to increase the thickness of the bucking cylinder by adding material at its inside surface. This would, however, reduce the available room for the ohmic heating solenoid, which would lead to lower volt-second capability.

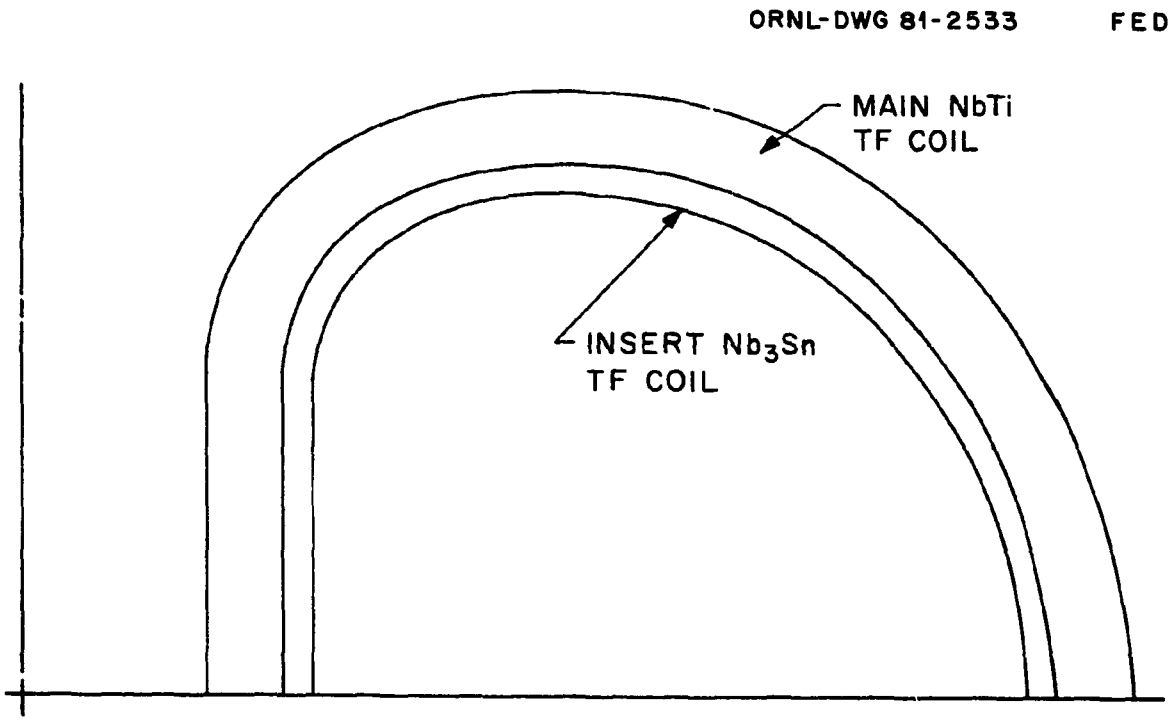

Fig. 5.8. Location of main and Nb_3Sn insert TF coils.

Hybrid NbTi and Nb_3Sn TF coils

This approach appears attractive if it is certain that a 10-T TF system is needed at the outset of the design process. In this concept, the 10-T TF coils are designed with a hybrid winding, using NbTi for fields up to 8 T and Nb_3Sn for fields above 8 T. One consideration of this approach is the price of the Nb_3Sn conductor, which costs approximately twice as much as the NbTi conductor.

The initial cost of this system appears to be 40% higher than an 8-T NbTi baseline design. This system is expensive in terms of initial cost, but it will not interfere with the other subsystems of the tokamak. The system can be operated initially at a peak field of 8 T if necessary.

5.3.4 Conclusions and Recommendations

The various options discussed above are summarized in Table 5.3. Suitability of any concept would have to be evaluated with respect to the FED needs, including (1) the amount of field enhancement desired, (2) the extent of physics parameters relaxation for simplifying magnetics system problems, (3) the type and size of the various penetrations, and (4) the worth of the field enhancement option to the program.

However, all field enhancement options involve substantial costs and complexity. Increased complexity will, of course, present a threat to both the construction schedule and the reliability of operation. Hence, it is recommended that if the need for 10-T operation appears probable, such capacity should be designed and built into the machine from the very beginning. If, however, this course of action is impossible due to financial or programmatic considerations, then a much more extensive and detailed comparison of upgrade options should be initiated.

5.4 RIPPLE CONTROL

5.4.1 Purpose

This trade study assesses the impact of varying ripple on cost and performance. In this study, performance is defined as configurational

Table 5.3. Summary of field strength enhancement options

Concept	Comments	Approximate cost
NbTi main TF coils supplemented with copper insert coils	Copper coils placed around plasma chamber will enhance ripple if placed in shadow of main TF coils; will reduce ripple if placed between TF coils but will interfere with penetrations into the plasma chamber.	Capital cost of copper coils ∿10% of 8-T superconducting coils. Operating cost ∿$8M/year for 1.5-T field enhancement, assuming $0.05/kWh electricity charge.
NbTi TF coils cooled with superfluid helium	System should be initially designed for superfluid helium operation. Superfluid helium plumbing could be very complex and expensive. Superfluid helium coils will not be tested in LCTF.	Uncertain, but will be greater than 10% (relative to 8-T case).
NbTi main coils supplemented with Nb_3Sn insert coils	Nb_3Sn costs twice as much as NbTi. Major changes in the FED configuration would be needed to accommodate Nb_3Sn insert coil. OH coil flux swing capability would be reduced.	Cost of the Nb_3Sn insert coils will be greater than 40% compared with the cost of 8-T main TF coils.
Hybrid NbTi and Nb_3Sn coils	Nb_3Sn costs twice as much as NbTi. Will not interfere with other subsystems of FED.	Hybrid coil system would cost 40% more than the 8-T NbTi TF system.

performance, i.e., reasonable access for torus sector penetrations and disassembly. Assessing the impact of ripple on the configuration and its cost involves a threefold approach, which is partly based on earlier work reported in the literature. The three aspects of this approach are:

1. Variation of the size of the TF coil for various device configurations and ripple limits.
2. Addition of magnetic material to the torus in the plane of the TF coil.
3. Addition of normal copper trim coils to the torus sectors.

5.4.2 Assumptions and Guidelines

The first aspect provides a fixed solution to ripple reduction but does not allow for ripple variation. The second aspect, in addition to reducing ripple, allows ripple variation through physical adding or subtracting of the amount of magnetic material used. The third aspect could provide a "knob" on ripple reduction by controlling the current in the trim coils. The calculations for aspects 2 and 3 were done by W. G. Langton of MIT, and the systems code data were provided by R. L. Reid of the Design Center.

5.4.3 Description of Design

TF coil size

The TF coil size was studied for four device configurations (8-, 9-, 10-, and 12-coil arrangements), each having an edge ripple of 2%, 1%, and 0.5% (see Fig. 5.9). The ripple is the peak-to-average value measured at the plasma edge. The systems code provided the parameters used for comparing the twelve cases. Relevant parameters are summarized in Table 5.4.

Figure 5.10 is a plot of the data relating cost to ripple for the 12 configurations.

Some interesting data can be observed from the table. Six of the configurations are access-limited, which means that the minimum TF coil

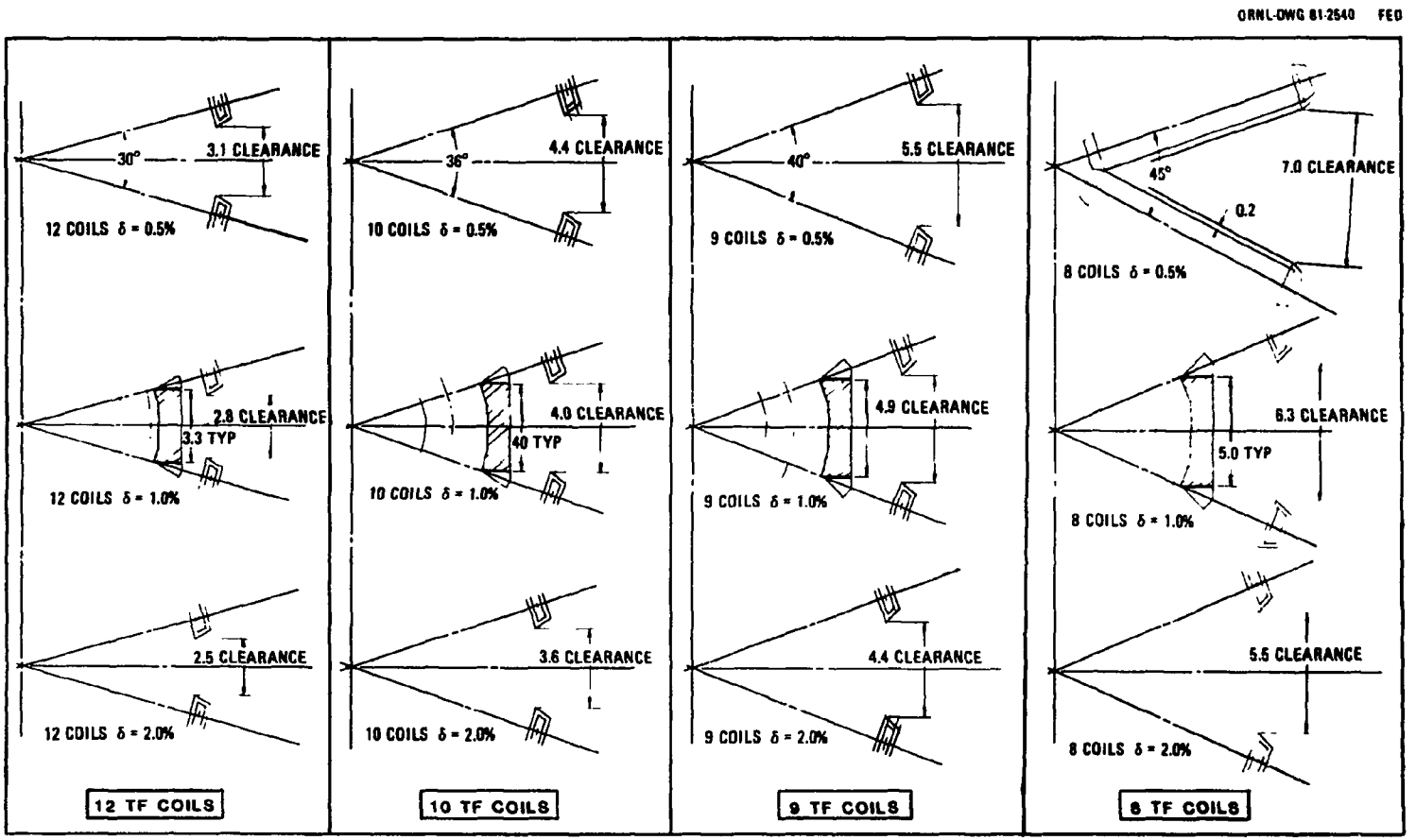

Fig. 5.9. Device configurations investigated for ripple control.

Table 5.4. Relevant systems code parameters

Number of TF coils	8			9			10			12			10[a]
Ripple (%)	0.5	1.0	2.0	0.5	1.0	2.0	0.5	1.0	2.0	0.5	1.0	2.0	0.78
Cost[b]	1.65	1.48	1.33	1.16	1.07	0.98	1.08	1.00	0.93	0.97	0.92	0.79	1.07
Available access[c] (m)	7.0	6.3	5.5	5.5	4.9	4.4	4.4	4.0	3.6	3.1	2.8	2.5	4.3
Required access[d] (m)	5.0	5.0	5.0	4.4	4.4	4.4[e]	4.0	4.0	4.0	3.3	3.3	3.3	4.0
TF coil weight (thousands of pounds)	0.57	0.50	0.43	0.42	0.36	0.32	0.32	0.29	0.26	0.22	0.20	0.18	0.30
Centering force (thousands of pounds)	74	63	51	54	46	39	42	36	30	28	24	21	37

[a] FED baseline case.

[b] Total relative capital cost for the device.

[c] Measured at the horizontal midplane.

[d] Measured across the torus sector.

[e] Underlining indicates an access-limited configuration.

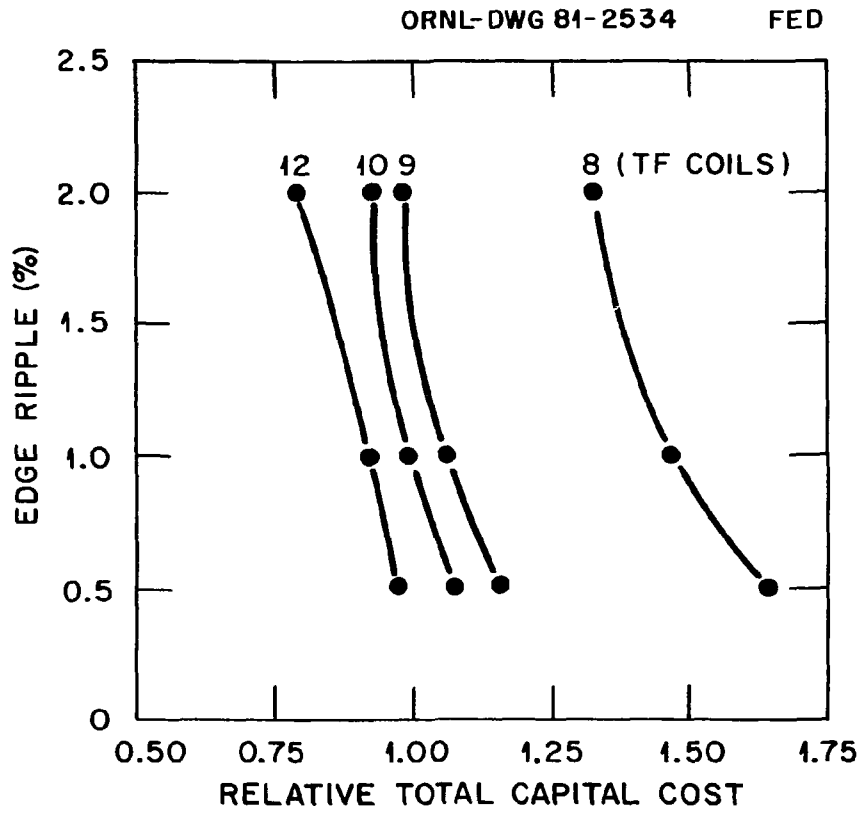

Fig. 5.10. Relation of total capital cost to variations in TF coils for ripple reduction (R = 4.8 m, B_{max} = 8 T, $t_{burn} \geq 100$ s).

size is not defined by the particular ripple limit, but by the need to allow for torus sector removal. For example, it is not possible to have a 10-coil arrangement at 2% ripple. The 9-coil configuration was included in the study as a means of investigating an arrangement with an odd number of TF coils. It is worth noting that the cost of this arrangement is the same as the FED baseline case, and the disadvantage of higher coil loads may be offset by the increased TF system reliability resulting from having one less coil.

Use of magnetic material

For this second part of the study it was assumed that magnetic material (iron) is added to the torus sector as shown in Fig. 5.11 for the 8-, 9-, and 10-coil configurations. (The 12-coil configurations are access-limited and therefore not relevant to this case.) The magnetic iron is located at the torus sector frame in the shadow of the TF coil, 7.6 m from the device center. It has a thickness of 1 m in the radial direction, a width t in the azimuthal direction, and a constant height of 2.6 m above and below the midplane.

The magnetic material has no deleterious effects on the TF or PF coil fields because the material is in a field greater than 2 T and is therefore saturated. The additional vertical field created by the iron is always less than 20 G at the plasma edge.

As indicated in Fig. 5.11, 40 tonnes of magnetic material is sufficient to reduce edge ripple from 2% to 0.5% for each of the eight coil locations. It is also possible to vary the ripple by controlling the amount of iron at these locations. The cost for this method of ripple control is minimal compared to total cost and is estimated to be less than $10 million plus the cost of the downtime needed to add or subtract iron. Table 5.5 is a summary of the magnetic material data.

As indicated, the interactive force between the iron and the TF coil is largest (464,000 lb) for the 9-coil configuration, with the final ripple equal to 0.5%. The distribution of this load along the torus frame yields 60 lb/in.^{2}, which can easily be reacted by this structure.

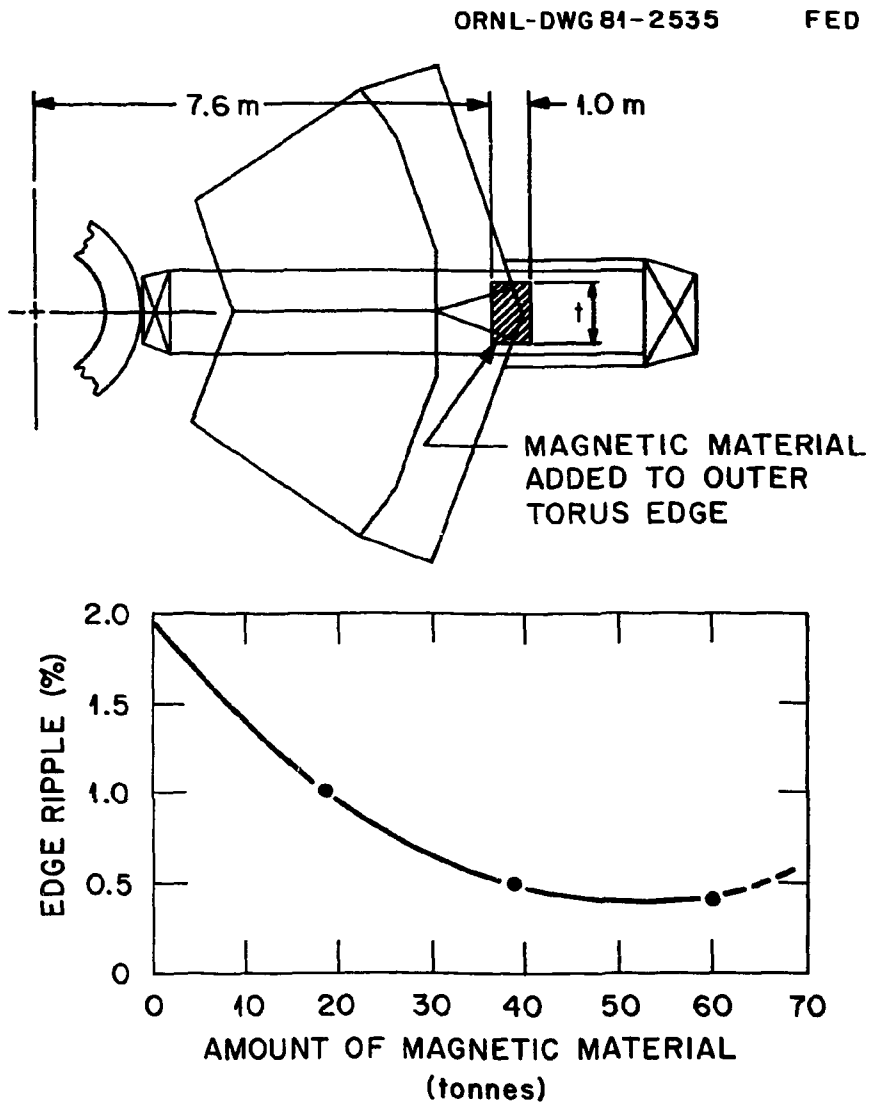

Fig. 5.11. Ripple reduction vs required magnetic material for the 8-coil case.

Table 5.5. Summary of the magnetic material requirements for ripple reduction

Number of coils	Initial ripple (%)	Final ripple (%)	Magnetic material per coil location (tonnes)	Attractive force[a] (lb)
8	2.0	1.0	19	54,000
		0.5	39	86,000
9	2.0	1.0	21	308,000
		0.5	35	464,000
10	1.0	0.5	11	61,000

[a]The attractive force is a function of the proximity of the iron to the TF coils; the iron is closest to the coils for the 9-coil cases.

Use of trim coils

The third aspect of the study assumes that the magnetic material is replaced with an equivalent coil in the same location. Saddle coils, which are typically mounted to the torus sector instead of the fixed frame, were not considered because they impose restrictions on the major penetrations into the plasma chamber. The use of trim coils has the advantage of providing a "knob" on ripple by varying the field produced by the coils. For the case shown in Fig. 5.11, each trim coil would weigh 17 tonnes and require 3.4 MW of power.

5.4.4 Conclusions and Recommendations

Ripple reduction from 2% to 0.5% can be accomplished by adjusting the TF coil size; this results in an average increase of about 20% in total capital cost for the four cases shown in Table 5.4. (For this comparison, we ignore the fact that some of the configurations are access-limited.) Therefore, adjusting the TF coil size to achieve a desired ripple may not be cost-effective compared to the addition of magnetic material. The use of iron for ripple reduction allows the configuration design to proceed with the least costly option (provided it is not access-limited); the iron cost quoted previously is not an

additional capital cost because this material would simply replace nonmagnetic structure which supports the torus sectors. Replacing the iron with an equivalent magnetic coil is an effective way to vary ripple, if this is desirable. However, a system such as this requires power supplies totaling ∿27 MW. A combination of iron and copper coils may provide ripple variance in a cost-effective manner.

The present FED configuration has an edge ripple of ∿0.8%. If reducing this value has physics and engineering advantages, then the recommendation, based on this study, is to incorporate magnetic material in the design as the least costly option for reducing ripple. Such a design should also incorporate the possibility of changing the amount of material installed as a simple means of ripple variation.

5.5 PF SYSTEM

5.5.1 Purpose

The design of the PF system is determined by the requirements to satisfy plasma performance goals and by the limitations of engineering constraints. The PF system consists of two subsystems, the ohmic heating (OH) coils and the equilibrium field (EF) coils. The purpose of the study is to develop a reference PF system design that satisfies the requirements of ohmic heating startup, the magnetic limitations on currents and fields, plasma stability, and the physical limitations on coil sizes and locations. Figure 5.12 shows the interaction required to develop the PF coil system.

5.5.2 Assumptions and Guidelines

Figure 5.13 is a schematic representation of the relative coil positions for the combined OH and EF coils. In this study, it is assumed that the OH solenoid and the EF coils around the outside of the TF coils are superconducting and that the EF coils within the bore of the TF coil are resistive copper coils.

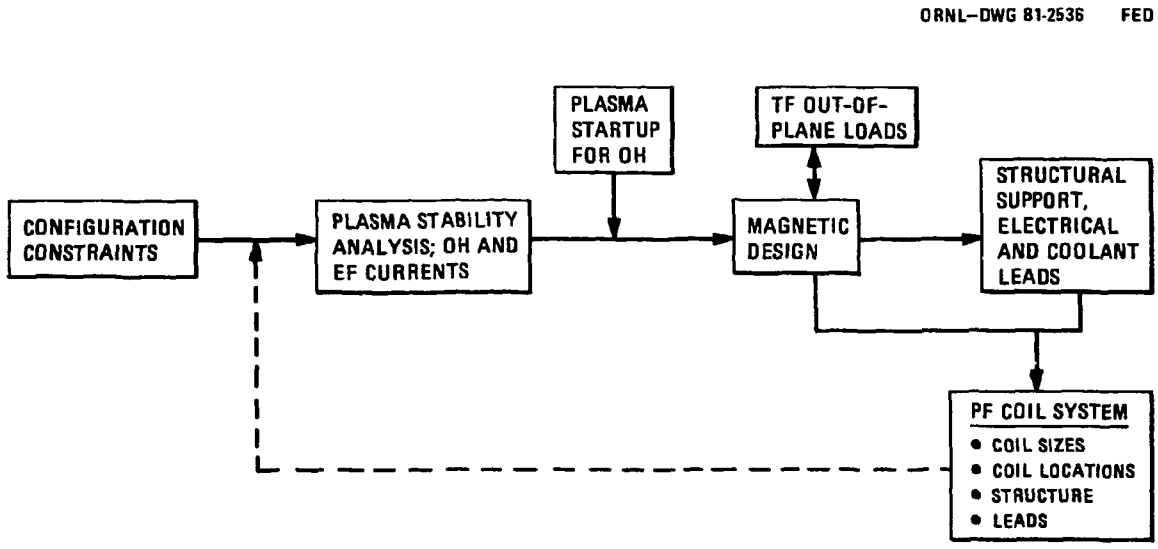

Fig. 5.12. Interaction between physics and engineering for development of the PF coil system.

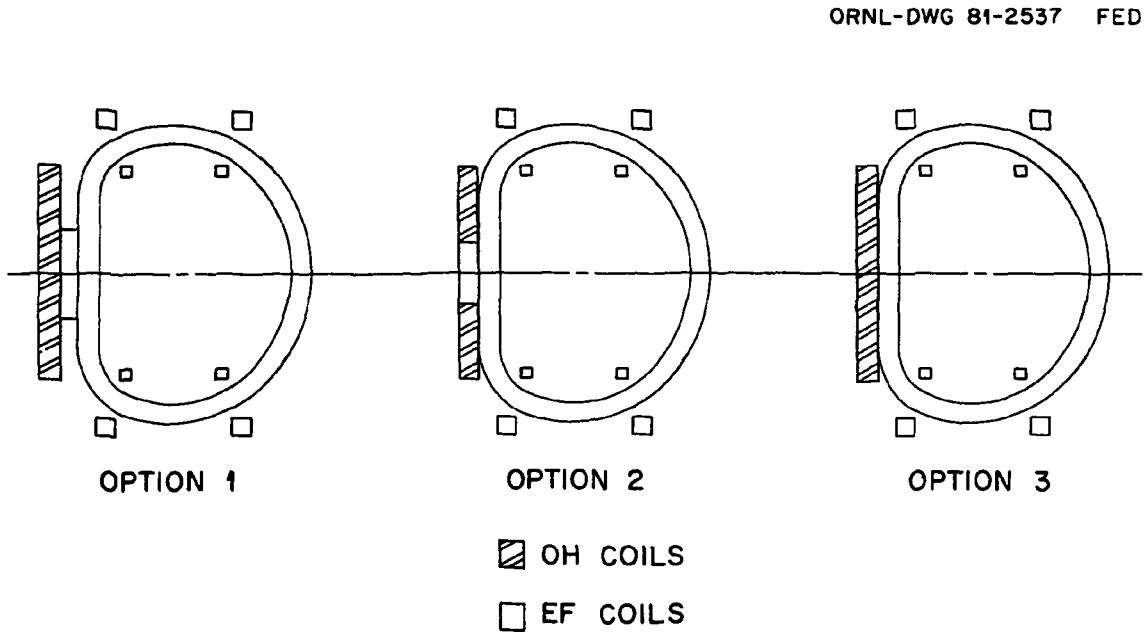

Fig. 5.13. Three PF coil arrangements under consideration.

5.5.3 Description of Design Effort

The unique functions of the EF and OH coil sets result in distinctly different locations and currents for each coil set. These differences in turn manifest themselves in distinctly different structural problems. The PF coils are assumed to be semi-permanent; i.e., they are to be designed to remain functional for the life of the machine without planned periodic replacement or repair. The structural design criteria are identical to those being adopted for the TF coils. As documented in Refs. 2 and 3, safety factors of either 1.5 against yield or 3 against ultimate, whichever is more limiting, are the basic primary membrane stress limits with bending limits being 50% higher. These limits, based on yield and ultimate, are supplemented by a limit based on fracture mechanics and crack growth data to reflect the cyclic nature of the loads. Another criterion imposed on the structural design of the PF coils is that the induced eddy current losses must be small during pulsing of these coils.

Most of the OH coils are stacked together into an approximately 11-m-long cylinder or solenoid. The cylinder has thick walls, a mean radius of approximately 1.35 m, and a radial build of approximately 0.4 m. The OH solenoid is located in the central bore of the machine, inside the TF coil bucking cylinder. By virtue of its location, the solenoid is subjected to axisymmetric magnetic loads. The radial loads are directed outward and are axially uniform except near the ends, where there is a slight diminution of amplitude due to end effects. End effects also cause axially compressive forces on the solenoid that are maximum at the ends and quickly decay to zero away from the ends.

A viable design for the PF system has not yet been developed, so detailed structural analysis has not yet been done. However, enough work has been accomplished to indicate that the conductor and structural concepts developed by the Los Alamos National Laboratory for the Department of Energy 20-MJ Pulsed Coil Program will be applicable to the pulsed solenoid of FED. Design studies on devices similar to FED (e.g., ETF and INTOR) have shown that the conductor itself has sufficient hoop strength (the conductor is a series of cables spiraling around a flat

steel strap that provides structural support to the superconducting cables) to be capable of equilibrating the radial magnetic loads without the need for additional support. The conductor is not well suited to equilibrate axial load in the solenoid (load parallel to the long dimension of the cross section of the strap), and it has been found necessary in previous design studies to provide axial support to the pancakes near the ends to prevent accumulation of axial load.

The EF coils differ from the OH coils in both form and location. They are rings rather than long cylinders (diameter in the range 5-10 m and a coil cross section approximately 1 m by 1 m) and are located outside and within the TF coils, both above and below the horizontal midplane. As a result of their location, they have a larger radius of curvature than the OH coils and therefore require proportionately more structural steel to equilibrate the radial loads (hoop stress due to radial load is proportional to radial load, inversely proportional to cross-sectional area). It is impractical to thicken the steel strap sufficiently for this purpose, and therefore the additional structural steel will be provided in the form of a case around the winding. Because of location, the magnetic loads in the EF coils are not axisymmetric and cause bending of the coils. The case serves to equilibrate bending loads as well.

A resistive water-cooled copper coil for application to EF coils located in the bore of the TF coils has been conceptualized. Coils in this location must be either jointed, so they can be assembled within the bore of the TF coils, or wound in place. The baseline design for FED is a jointed coil. A conceptual design has been developed for a 2-MAT coil, a current-carrying capability considered to be representative of FED needs. The design concept selected is a 10-turn copper coil. The current density is 1600 A/cm^2, resulting in a coil cross-sectional area of 1250 cm^2 and a power consumption of 13.8 MW, both of which are considered reasonable and acceptable. The coil would be assembled by connecting half-turn segments, fastened together by bolted lap joints.

Coil locations and ampere-turn requirements have been derived through MHD equilibrium calculations for the system shown schematically

in Fig. 5.13. In these calculations, it was assumed that each of the four resistive copper coils carries 2 MA. Figure 5.14 shows the approximate coil locations and currents for the EF coils. Note that the total EF current is ∿88 MA. Of particular concern are the large currents associated with the superconducting EF coils (33 MA). In the baseline configuration, there is not sufficient space to accommodate such coils.

5.5.4. Conclusions and Recommendations

Several promising paths have been identified for developing a viable PF coil design. One path that will be examined is that of increasing the currents in the inner (normal) EF coils as a means of reducing the currents required for the outer (superconducting) coils. Another is that of reducing the requirements on plasma shaping. Future work will also be directed toward developing specific support concepts for the EF coils and performing detailed structural analysis when a viable PF system design is available.

5.6 FEASIBILITY OF USING INORGANIC INSULATION

5.6.1 Purpose

Because of the possibility (Sect. 4.6) that radiation damage might make organic insulators unsuitable for use in bundle divertors, an investigation of inorganic systems was initiated.

5.6.2 Assumptions and Guidelines

An extensive literature search was conducted and magnesium oxide (MgO) emerged as the most promising inorganic candidate. Hence its use became a basic premise of the study.

Magnesium oxide insulation is used in commercial stove elements, in thermocouples for nuclear reactors, and as a magnet insulation for accelerator magnets in a high gamma flux environment. Approximately 40 such magnets have been built by A. Harvey's group at the LANL and 20 for accelerators operated by the Suisse Institut Nucleaire (SIN) in Switzerland.[4]

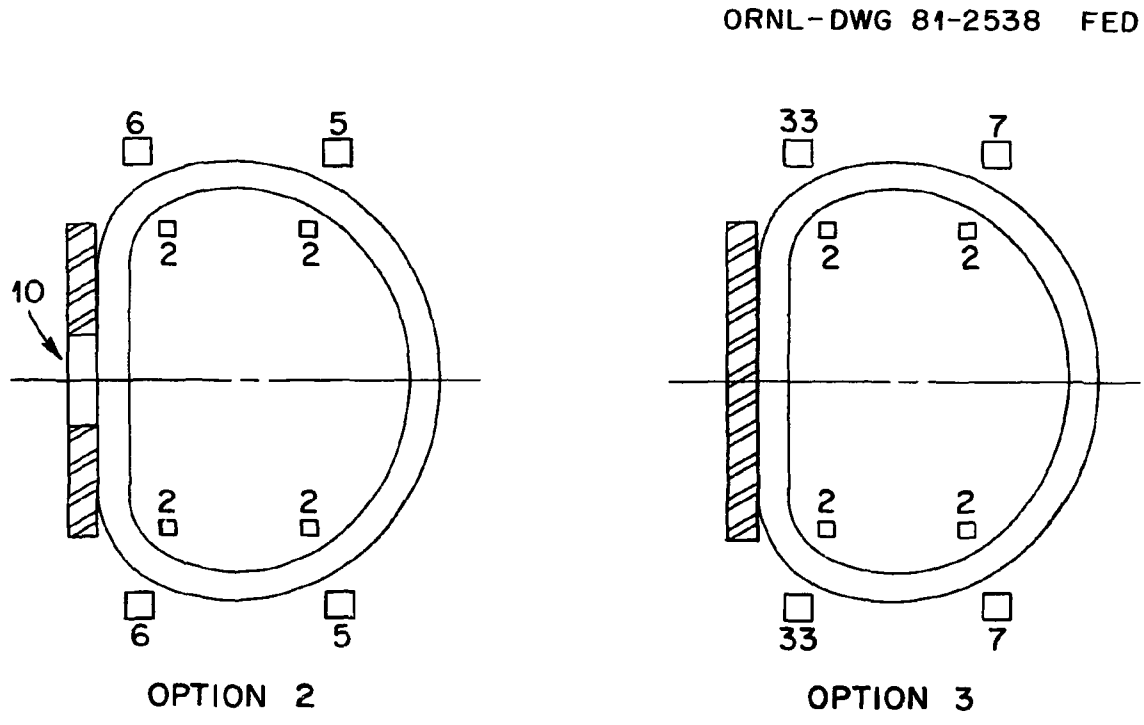

Fig. 5.14. Approximate EF current distribution (in megamperes) for high beta.

There have been no failures related to insulation degradation in the several dozen magnets using ceramic powder insulation in a high gamma irradiation environment. The world's record for irradiation is not known, but it is believed to be greater than 10^{10} rad in one of the SIN magnets. Some of the magnets at LANL have logged over 30,000 hours of failure-free dc operation.

Operational experience with organic insulations in radiation environments is difficult to obtain, partly because failure reports appear infrequently in the open literature.[5] Few magnets have failed because of radiation damage to the insulation, since most accelerators never achieve their original design specification radiation dosages. Insulations are routinely inspected at laboratories such as the Stanford Linear Accelerator (SLAC) and Brookhaven National Laboratory (BNL) and are replaced when significant discoloration or delamination of the insulation is observed. According to D. Hay[6] at SLAC, magnets with Al_2O_3-filled epoxy glass insulation are routinely replaced after irradiations of 10^9 rad because of depolymerization. Therefore, magnets subjected to successful preventive maintenance cannot be used to test the hypothesis that thin insulations will continue to function successfully at irradiations well beyond those causing visible damage. The most spectacular unreported magnet failure, which was unambiguously due to radiation damage, was the failure of dozens of ring magnets in the DESY device at radiation doses of about 10^8 rad. These magnets used aliphatic amine-cured epoxies with mica and glass fillers. It is believed that the failure mechanism was bubble rupture, bubbles being prevented from diffusing out of the insulation by the mica fillers. The most encouraging example of nonfailure that has been identified is that of the NINA bending magnets in Darsbury, England. R. Sheldon[7] believes that these insulations have been irradiated to greater than 10^{10} rad with no magnet failures. The insulations are S-glass-filled imide epoxies, cured with NMA, and are relatively thin, thus avoiding trapped gas formation.

5.6.3 Conclusions and Recommendations

While no spectacularly high magnet irradiations have been reported for MgO insulation, the insulation of the neutron flux detectors in the Canadian Pickrell reactors is known to have been irradiated to 10^{14} rad in the first three full power runs.[8] No insulation failures occurred. When the detectors were removed from service, the insulation resistance had changed from 10^9 Ω to 10^8 Ω at 100 V. This contrasts with the order of magnitude reduction in the resistivity of G-10 after an irradiation of 10^{10} rad reported by Coltman.[9] Brechna[10] reported a decrease in the unirradiated resistivity of wet-wound epoxy DER 332 of five orders of magnitude at an irradiation of 10^{10} rad. Therefore, the electrical properties of MgO insulation appear to be far more stable under irradiation than those of organic insulations. A conductor suitable for a divertor in FED was conceptualized[11] and is shown in Fig. 5.15. Future efforts could be profitably committed to the refinements of a divertor design incorporating the conductor shown in the figure.

5.7 SUMMARY

The major conclusions of the magnetics systems analysis are summarized below.

1. Poloidal Field System. Several approaches have been examined to define a viable PF system, and the impacts of these various approaches on the physics and engineering considerations have been evaluated.

Continued effort is required to obtain configurations for both the OH and the EF coils that simultaneously satisfy the physics requirements for appropriate plasma conditions and the engineering requirements associated with coil locations and structural support.

2. Toroidal Field Coil Structural Design. Using out-of-plane loads based on a preliminary but representative PF coil system, an evaluation of the structural requirements on the TF system as a function of the number of pulses in a range from 5×10^4 to 1×10^6 resulted in TF coil case thicknesses ($\sim$10 cm) that are practical to fabricate, weld, and inspect.

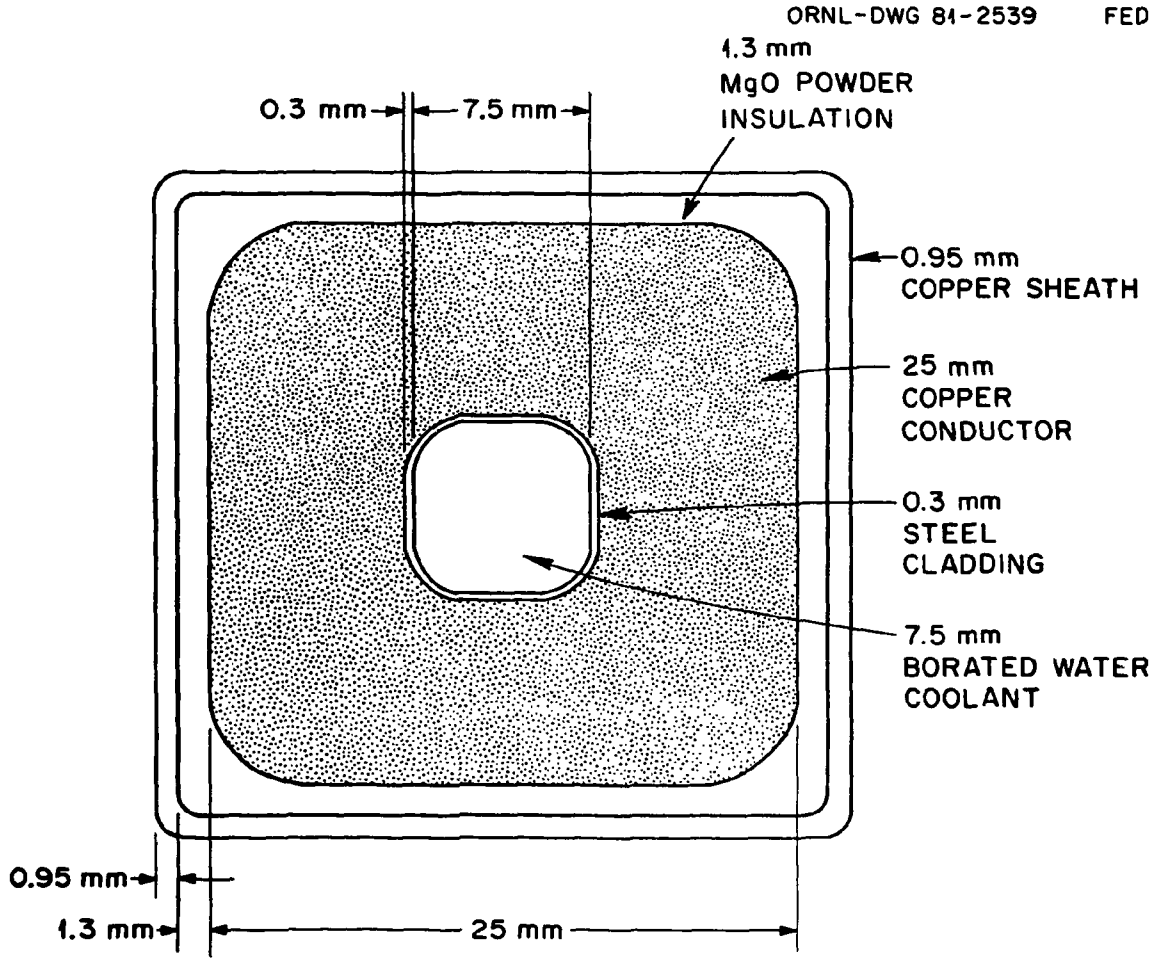

Fig. 5.15. Conceptual conductor design for a bundle divertor coil.

3. Enhancement of Toroidal Field. Several methods of achieving a 1- to 2-T enhancement of the toroidal field on axis were investigated. These methods include supplemental coil inserts, the use of superfluid helium, and hybrid NbTi and Nb_3Sn coils. The results indicate that although these approaches are feasible, they are likely to result in substantial increases in the complexity of the design and may be no less risky than designing the TF coils to higher field strength performance from the outset.

4. Control of Toroidal Field Ripple. Several approaches, both passive and active, were investigated as a means of varying the TF ripple; the approaches included the use of magnetic material in the plane of the TF coil and the use of trim coils. The results indicate that these methods can be used to alter the ripple at a reasonable cost. However, the present FED baseline configuration has an edge ripple of $\sim$0.8%, so reduction of the ripple below this level does not appear necessary or warranted at this time.

5. Use of Inorganic Insulators. In studies related to continuing efforts to investigate the development of a bundle divertor for FED, magnesium oxide emerged as a promising inorganic insulator.

6. NUCLEAR SYSTEMS

P. H. Sager*

G. M. Fuller†
J. N. Brooks‡
B. A. Cramer†
J. P. Davisson†
B. A. Engholm§
J. R. Haines†
W. G. Homeyer§
J. Kirchner†
H. C. Mantz†

6.1 INTRODUCTION

Many of the FED nuclear system components have evolved from the Engineering Test Facility (ETF) designs reviewed by the fusion community in July 1980. For instance, the number of torus sectors is ten for FED and is equal to the number of toroidal field (TF) coils, permitting direct radial extraction of the torus sectors.

The major differences from the ETF designs are due to the change from an ignited machine to a driven machine (smaller major radius), the lower power (smaller neutron wall loading), the consideration of rf bulk heating [ion cyclotron resonance heating (ICRH)], and the incorporation of a mechanical pump limiter for helium ash control.

The design philosophy for the FED first wall is that components should have relatively thick surfaces (>1 cm) and be capable of accepting locally severe conditions. This approach provides a high degree of confidence in reactor operation for a reasonable length of time.

The following discussion summarizes the design features of the major components: the torus, the first wall/armor, and the mechanical pump limiter. Guidelines and assumptions are presented, and design options are identified. The major emphasis, however, is to achieve

---

* Fusion Engineering Design Center/General Atomic Company.

† Fusion Engineering Design Center/McDonnell Douglas Astronautics Company.

‡ Argonne National Laboratory.

§ General Atomic Company.

feasible solutions for the selected baseline features. Finally, for each of the major components, the conclusions are stated and the direction and focus for the future design effort are described.

6.2 TORUS SECTOR DESIGN

6.2.1 Purpose

The purposes of the torus sector design studies were to (1) incorporate the latest FED plasma geometry and operating environments, (2) review and select a segmentation approach, (3) review shield material selection, (4) select a vacuum seal technique, (5) integrate a pump limiter design, (6) provide an interface for the rf waveguides, (7) identify a sector extraction/transport concept, and (8) achieve the highest possible electrical resistance in the torus support structure (spool).

6.2.2 Assumptions and Guidelines

The following guidelines were established for the torus design studies:

1. A vacuum boundary on the outer boundary of the shield.
2. Ten TF coils and ten equal-size torus sector modules.
3. Direct radial extraction of each of the sector modules.
4. A welded vacuum seal for each torus sector using the simplest configuration possible.
5. Incorporation of a pump limiter to be removed independently of sector removal.
6. Use of rf heating for startup and operation (driven machine).
7. Location of all seal welds on ducts, etc., on the outside of the shielding.
8. A thin-skinned spool structure to provide a resistance of ≥ 1 mΩ.

6.2.3 Description of Design Effort

The following discussion presents the options considered in three areas: (1) shield segmentation, (2) integration of the pump limiter, and (3) the primary vacuum seal concept.

Shield segmentation

In considering how to configure the torus sector, it was recognized, based on earlier ETF studies, that at least two approaches are possible relative to the bulk shielding configuration. The two shield segmentation options that were examined were major shield removal (Fig. 6.1) and partial shield removal (Fig. 6.2).

The major shield removal concept features actively cooled radial frames that serve as semipermanent structure and a noncooled spool structure. All of the required shield thickness is incorporated in the replaceable shield module, which is designed for periodic removal as required. This design approach employs a complex sealing surface on the outboard wall.

The partial shield removal concept features a combined floor, radial frame, and partial shield structure, an outer shield module (which is semipermanent), and a replaceable inner shield module designed for periodic removal as required. This design approach involves a complicated joining of the adjacent outer shield wall.

The preferred arrangement for FED combines features of both concepts. The outer face is defined as a single planar surface to simplify the vacuum sealing problem. The radial frames are simplified to single vertical posts spanning the structural spool rims. Cooling is, therefore, present only in the vertical posts and in the replaceable module. This preferred arrangement is shown schematically in Fig. 6.3.

Mechanical pump limiter

A toroidal belt-type limiter was selected based on considerations of accessibility and availability of space for other subsystems, such as the rf auxiliary heating system and test module installation. Two locations for the pump limiter were considered. The preferred location is at the bottom of the vacuum chamber, as shown in Fig. 6.4. An alternate concept locates the pump limiter on the lower 45° surface of the outboard wall, as shown in Fig. 6.5.

Locating the limiter at the bottom of the plasma chamber has substantial maintenance advantages. The limiter blade, where most of the

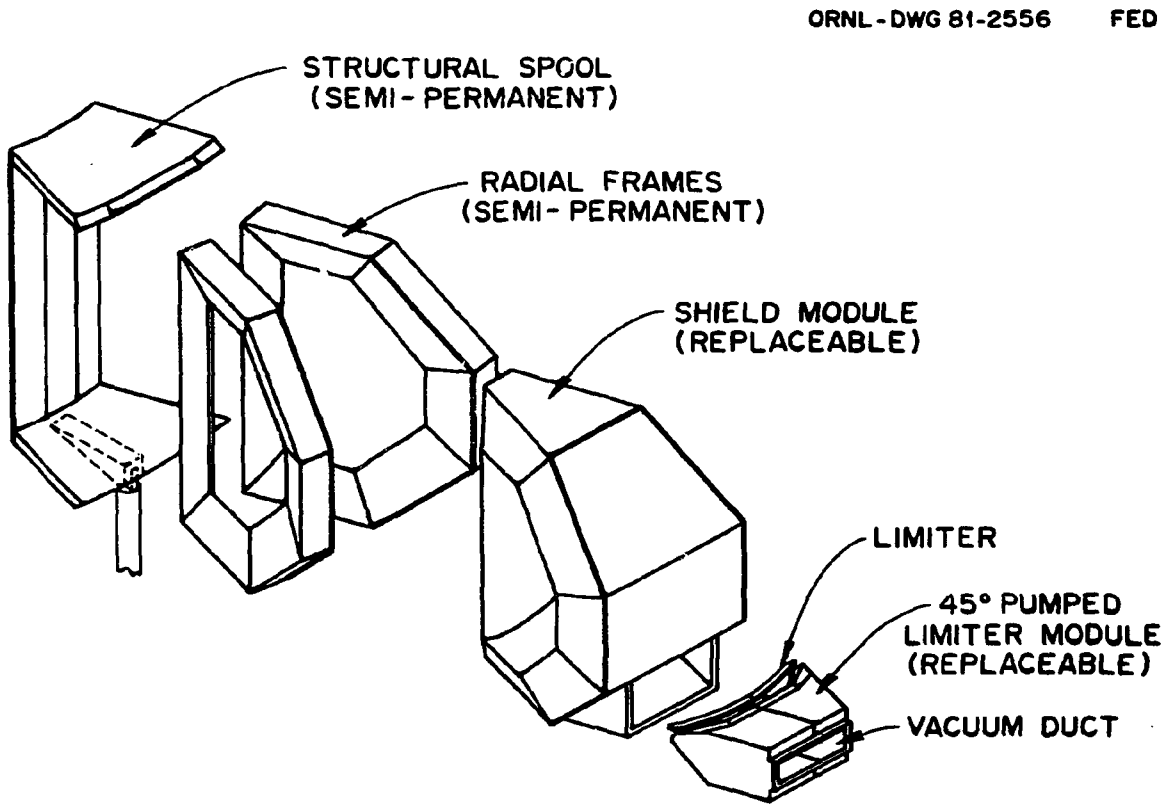

Fig. 6.1. Major shield removal concept. Channel-type seal edges are shown in heavy outline. See Fig. 6.6 for details.

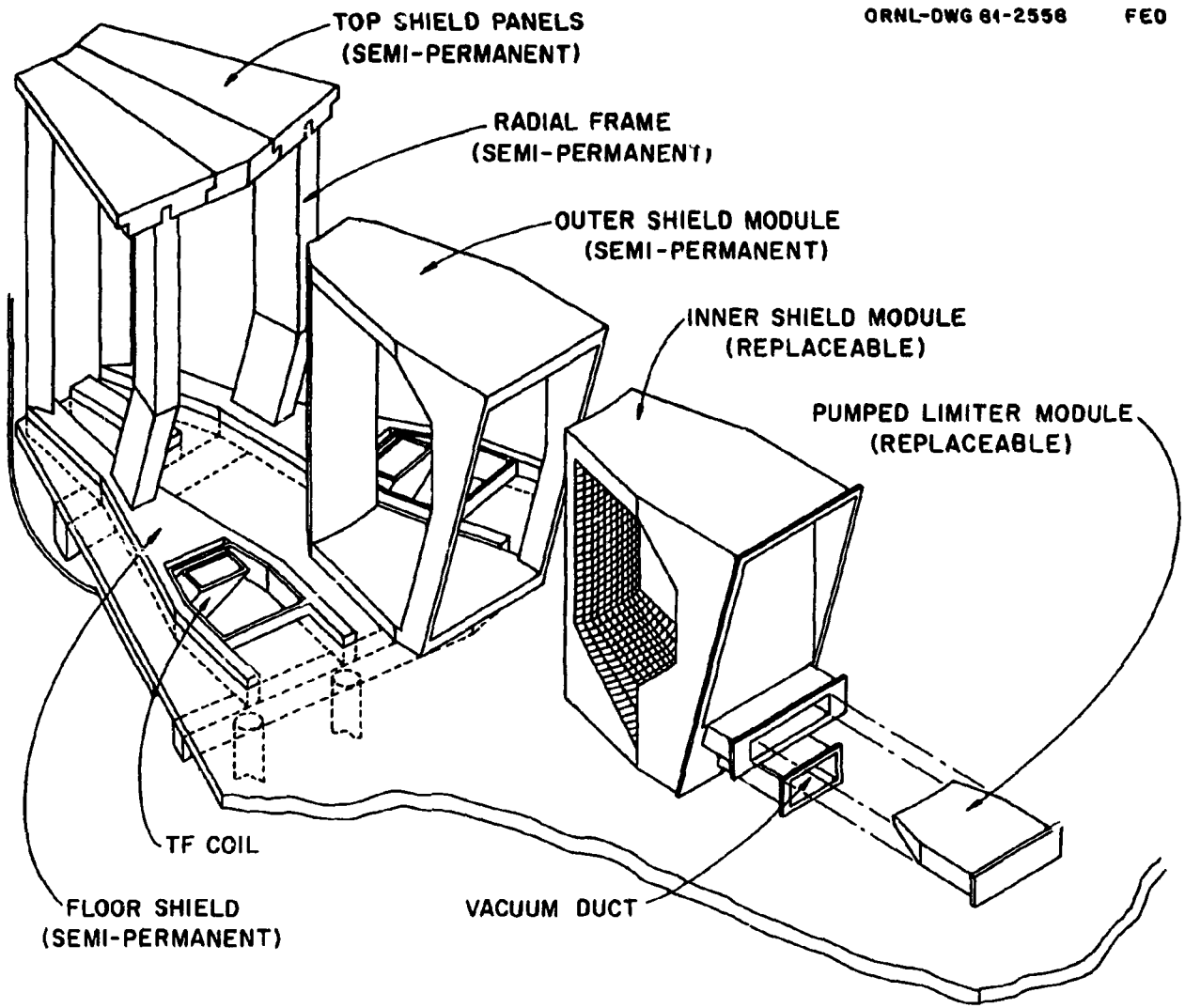

Fig. 6.2. Partial shield removal concept.

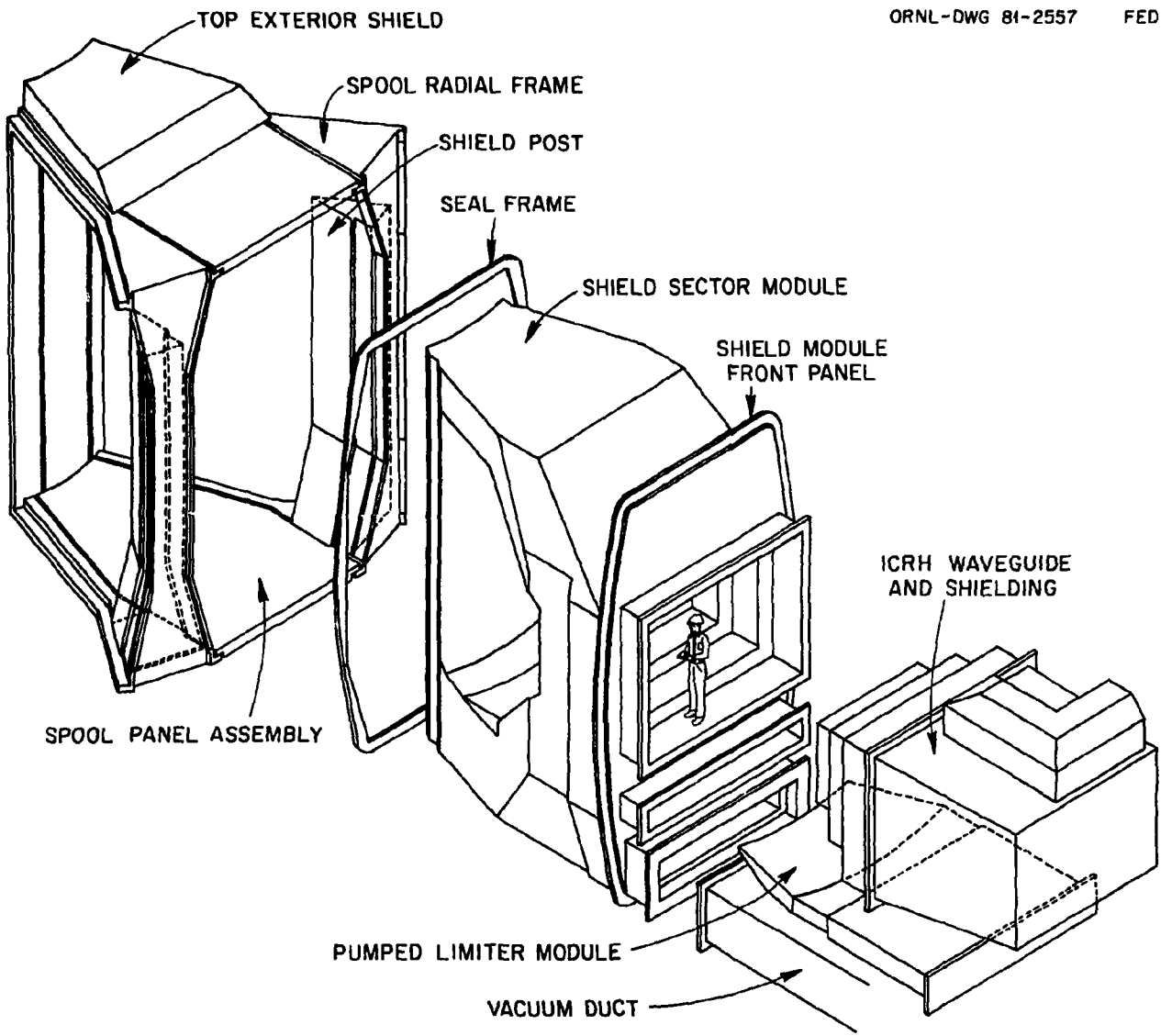

Fig. 6.3. FED assembly sequence.

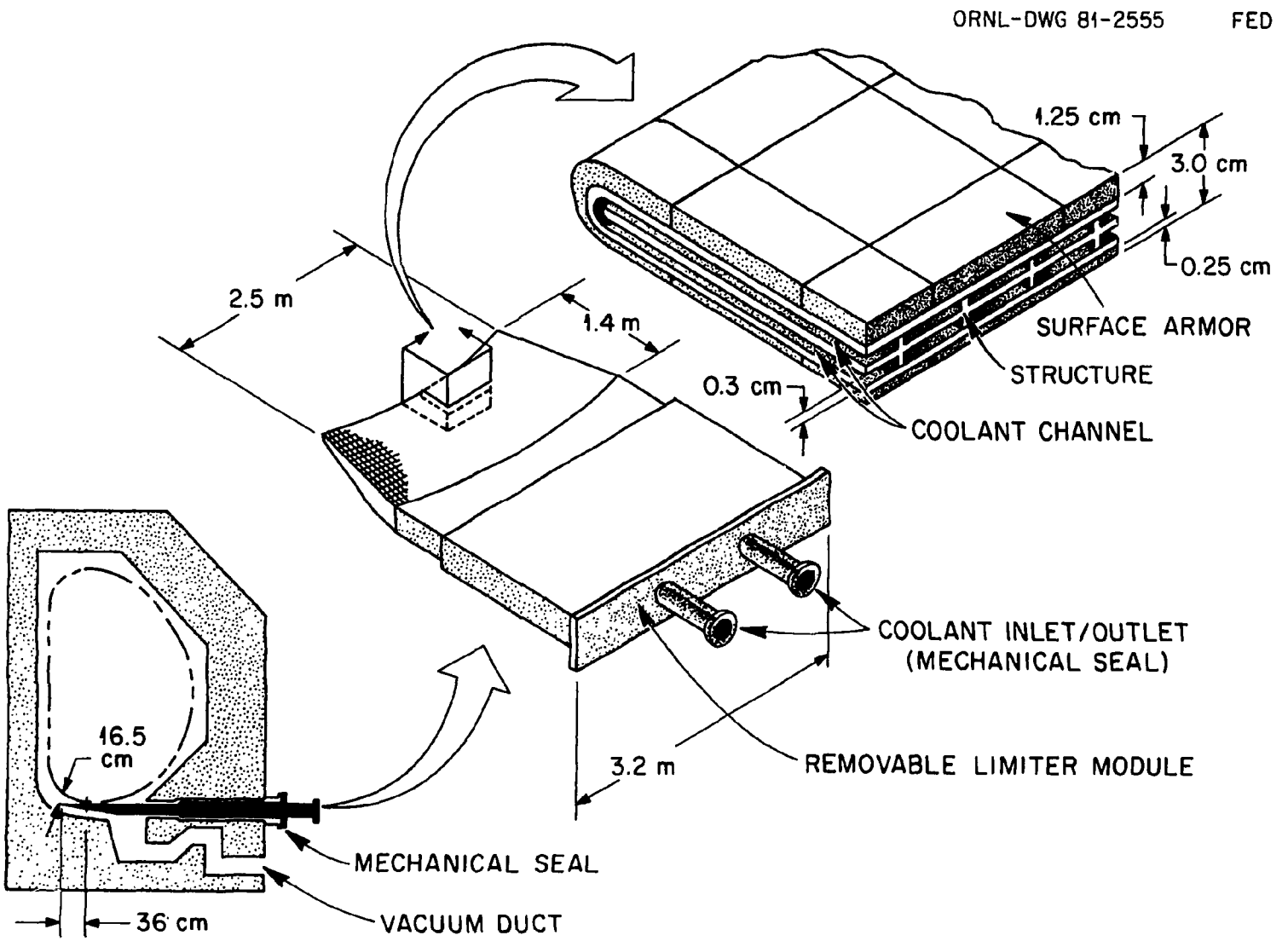

Fig. 6.4. FED pump limiter.

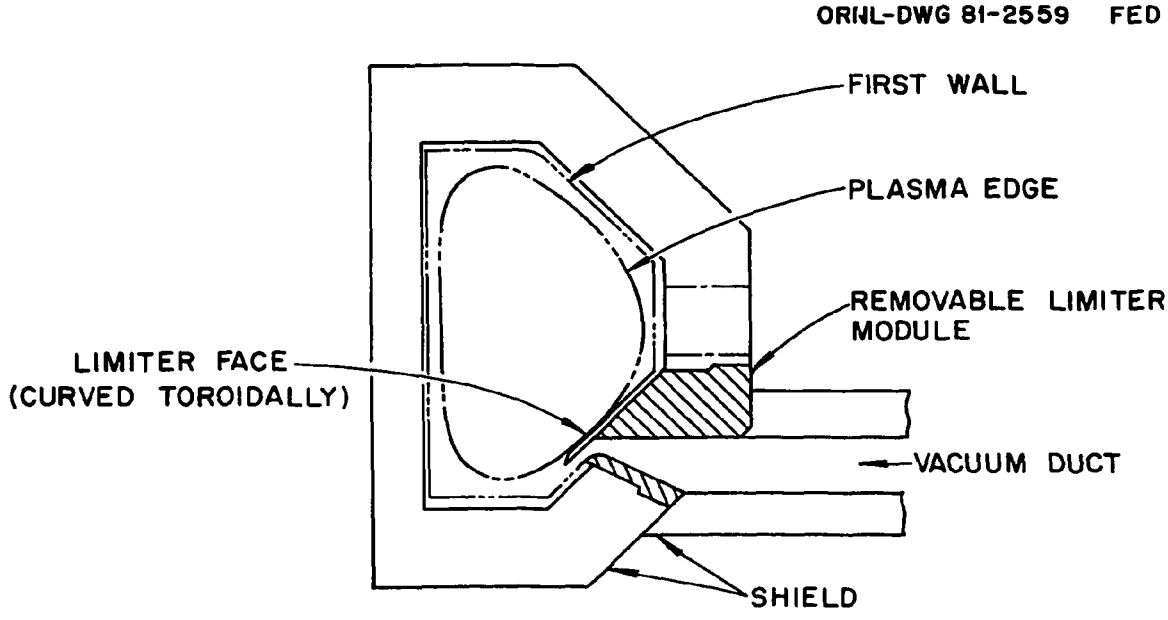

Fig. 6.5. Alternative pump limiter configuration.

damage from erosion is likely to occur, can be replaced without removing the vacuum duct. In addition, it is much smaller and easier to handle remotely. The limiter vacuum seal is a mechanical one and there is the potential for incorporating valves which would permit exchanging the limiter blade without breaking the plasma chamber vacuum.

Primary vacuum seal concepts

The channel seal developed for ETF is one of two seal concepts considered. The channel seal follows the D-shaped outside contour of the torus. A cross-sectional view of this seal concept is shown in Fig. 6.6. The second seal concept is a single, convoluted bellows flat in the outboard plane. A cross-sectional view of this concept is shown in Fig. 6.7.

This second seal concept possesses two advantageous features. The first is the single planar seal surface, which greatly simplifies the welder/cutter machine design. The second is the single convolution seal geometry. The seal weld may first be made to attach the seal to the spool structure. A second seal weld is made after the sector flanges are mated to the seal and is the only seal weld made or cut for subsequent replacement. This is basically simpler than the channel-type seal, which requires that both weld seams must be made after the torus sector is in place and every time a sector is replaced. The second seal concept is preferred for the FED baseline.

6.2.4 Design Description

The torus consists of a spool structure and ten shield sectors. The sectors are supported by the thin-skinned (high resistance) spool structure. Each sector is designed to be removed radially outward. A mechanical pump limiter is located at the bottom of the vacuum chamber and can be removed independently of the torus sector. A schematic of an assembly sequence is shown in Fig. 6.3. The radial buildup is as shown in Fig. 6.8.

The thin-skinned spool structure consists of two outer skins with internal stiffeners, Fig. 6.9. The overall thickness is 4 cm. The

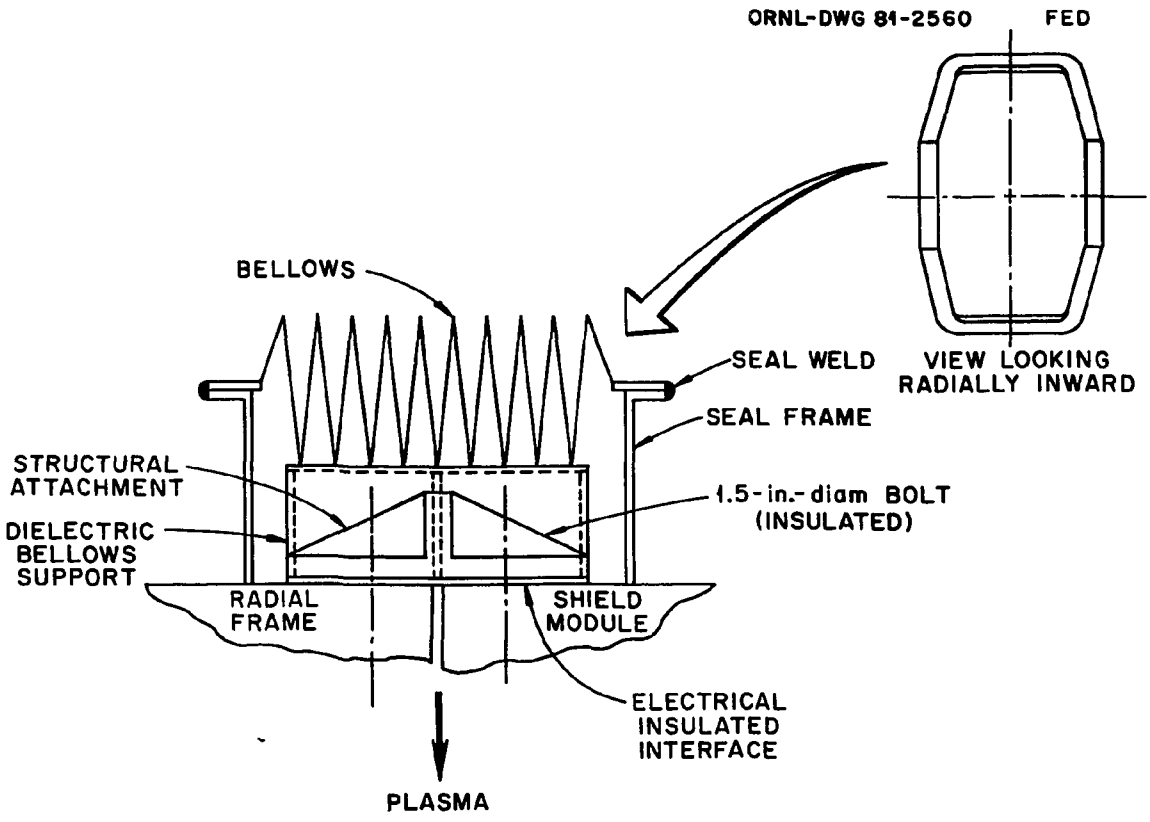

Fig. 6.6. Channel-type seal.

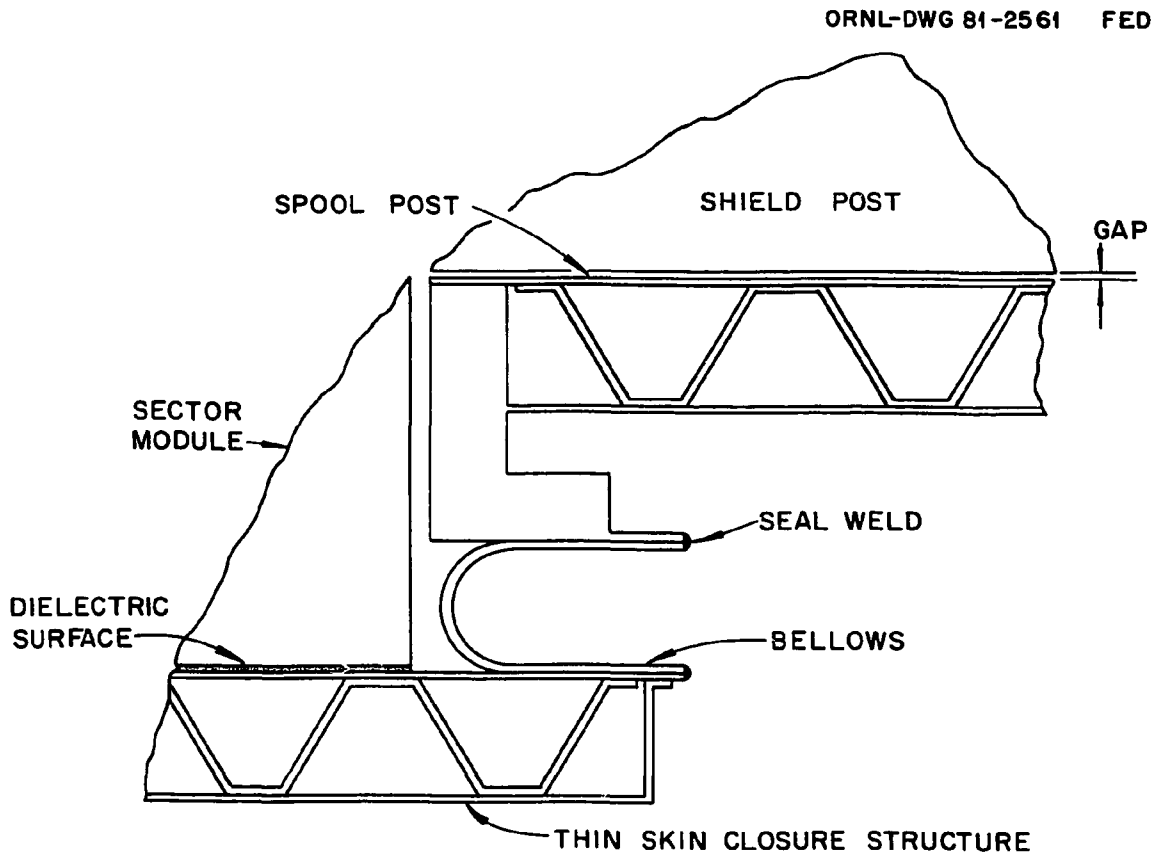

Fig. 6.7. Single convolution bellows vacuum seal.

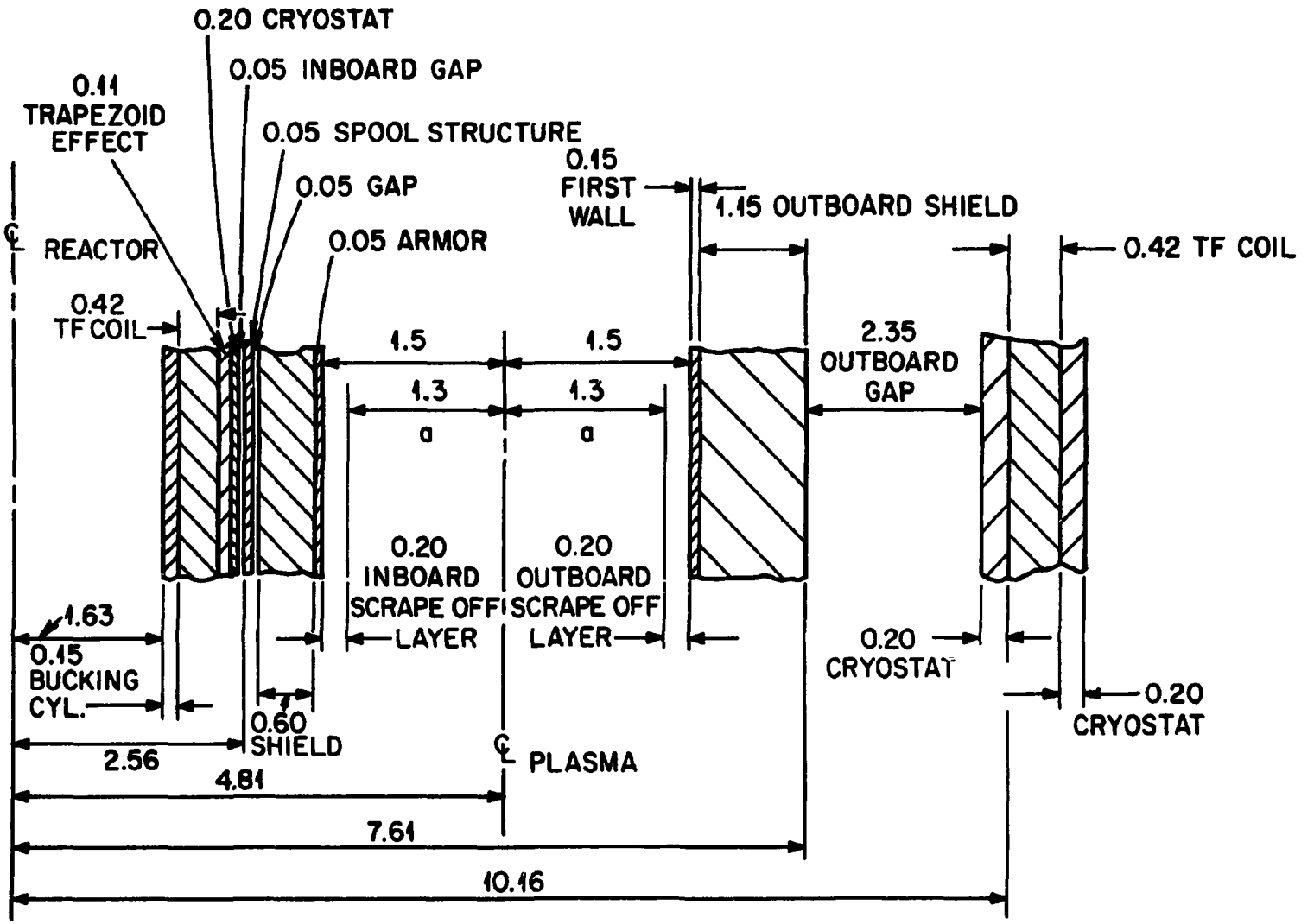

Fig. 6.8. FED radial build.

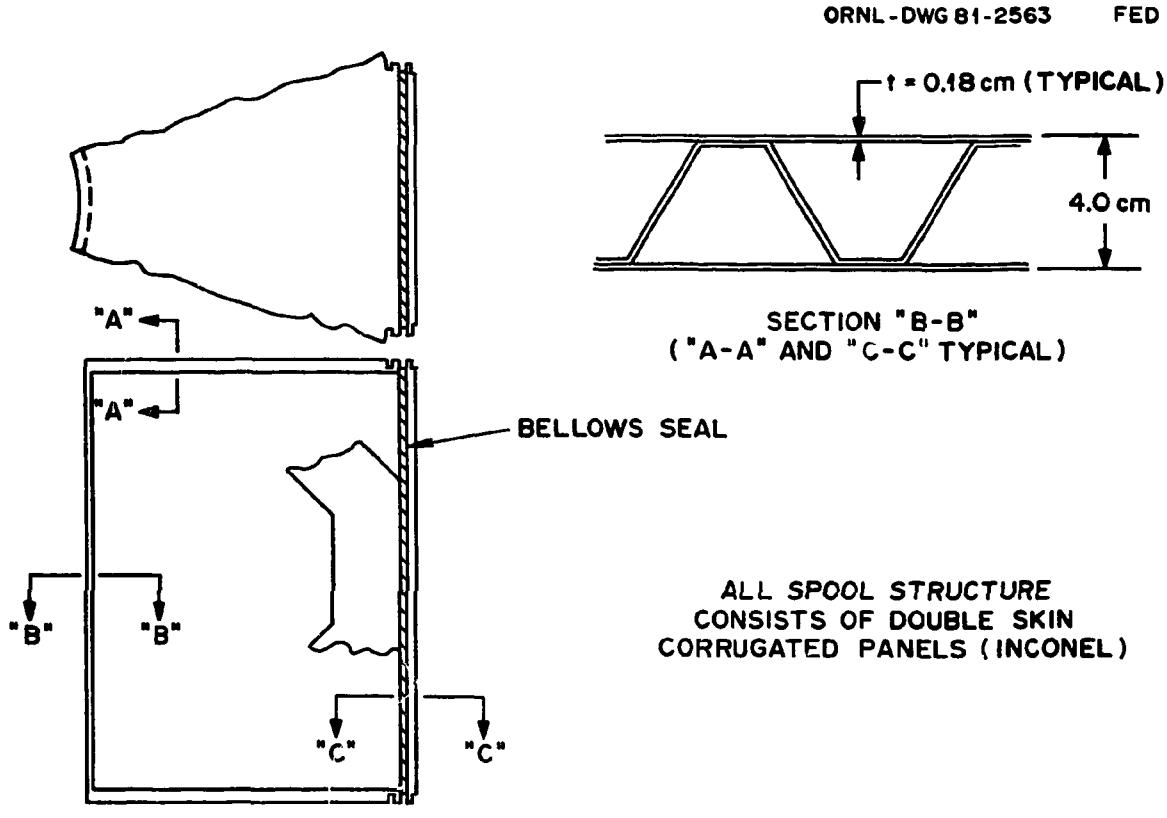

Fig. 6.9. Spool structure.

material is Inconel. The spool structure is considered semipermanent (good for the life of the reactor) and does not require active cooling. The upper and lower spool flanges are connected with a thin-skinned (high resistance) post. This design provides a window for sector module insertion and has provision for seal welding. The bottom spool flange (inside and outside surface) and top flange (outside surface) must be coated with a dielectric material, such as Al_2O_3, to provide electrical isolation. The calculated resistance of the Inconel spool structure is 2.3×10^{-4} Ω. While this resistance is below the desired level (1 mΩ) it is close enough to merit retention as a feasible approach. Control of sector-to-sector electrical properties is discussed in Sect. 7.

Preliminary sizing of the shield spool cylindrical structure is based on a 1.0-atm hoop tension (vacuum) load, a 0.2-MPa (30-psi) plasma disruption load (tension initially), and a possible 1.0-atm hoop compression load for leak checking. The Inconel membrane thickness of 0.36 cm is required to resist local instability from the 1-atm compression load, resulting from either the leak check condition or a combination of 1-atm tension and 0.2-MPa (net 1-atm) compression occurring when the cylindrical spool responds dynamically during disruption. The skin spacing is based on preventing general instability of the spool under these same compression loads. Axial loads also result from the 1-atm external pressure and deadweight of portions of the shield. However, these loads are not critical.

The shield segmentation concept provides for interfacing offsets between adjacent sectors on top, bottom, and inboard sides to minimize neutron streaming, Fig. 6.10. The outboard shielding between sectors is provided by an independent triangular shield post that is actively water cooled. The shield post is considered semipermanent. Stepoffs are provided in the sector module and shield post to minimize neutron streaming.

The shield sector consists of a 1-cm-thick structural box internally stiffened with both transverse and radial members. Each of the members is electrically isolated from the box. The inside of the casing is filled with low nickel alloy steel plates and cooling water. The steel plates are laminated and coated with a dielectric (Al_2O_3) to provide

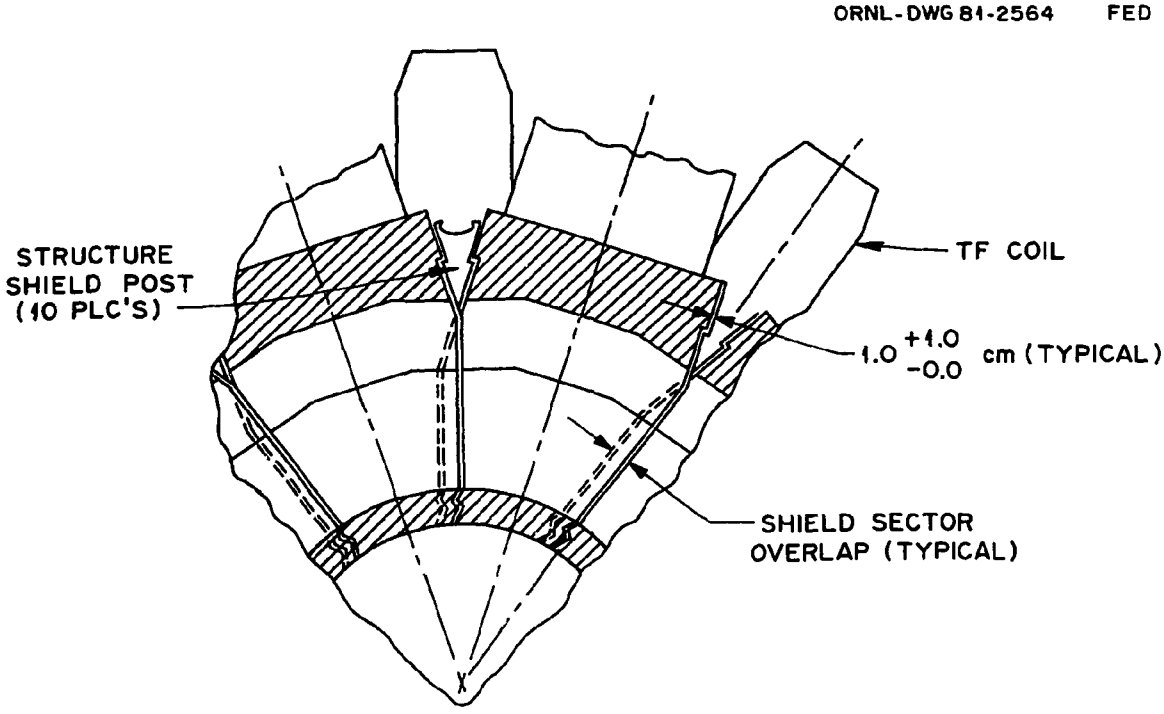

Fig. 6.10. Plan view of sector-to-sector interface.

eddy current breaks and to increase resistance. The bui' shield lamination concept is schematically shown in Fig. 6.11. The inboard shield thickness is 60 cm. The outboard thickness is 1.15 m. The inboard shield is sized to limit the lifetime exposure of TF coil insulators to $<10^9$ rad and to limit refrigeration requirements. The outboard shield is designed to limit the dose rate at the external surface to 2.5 mrem 24 h after shutdown.

The sector-to-spool structure vacuum seal consists of a single convoluted metal bellows. The bellows is welded to the spool rim and posts and to the front panel of the shield sector. The front panel is electrically insulated from the bulk shield material to maintain a high resistance path.

The pump limiter is installed as a single module, allowing for independent radial extraction. The vacuum seal is a mechanical type, since it has a high frequency of replacement. A separate coolant inlet and outlet are required. The vacuum duct for the pump limiter is independent of the limiter, with a welded seal on the outside of the shielding. Additional discussion of the pump limiter design is presented in Sect. 6.4.

The ICRH waveguides are designed as plug-in modules with a vacuum seal consisting of a single convoluted bellows located on the outside of the shielding.

The shield sector module removal is accomplished with the use of an extractor pallet, Fig. 6.12. After the vacuum seal is cut, the extractor/transporter pallet is rolled into position. The sector is mechanically coupled to the pallet and extraction is initiated. The pallet contains recessed roller assemblies that are raised into position after the seal flange is clear. This provides a stable rolling surface to complete extraction.

6.2.5 Conclusions and Recommendations

Technically feasible approaches have been conceptually developed for the key aspects of the torus sector design. Based on preliminary studies, a number of preferred approaches have been identified. However,

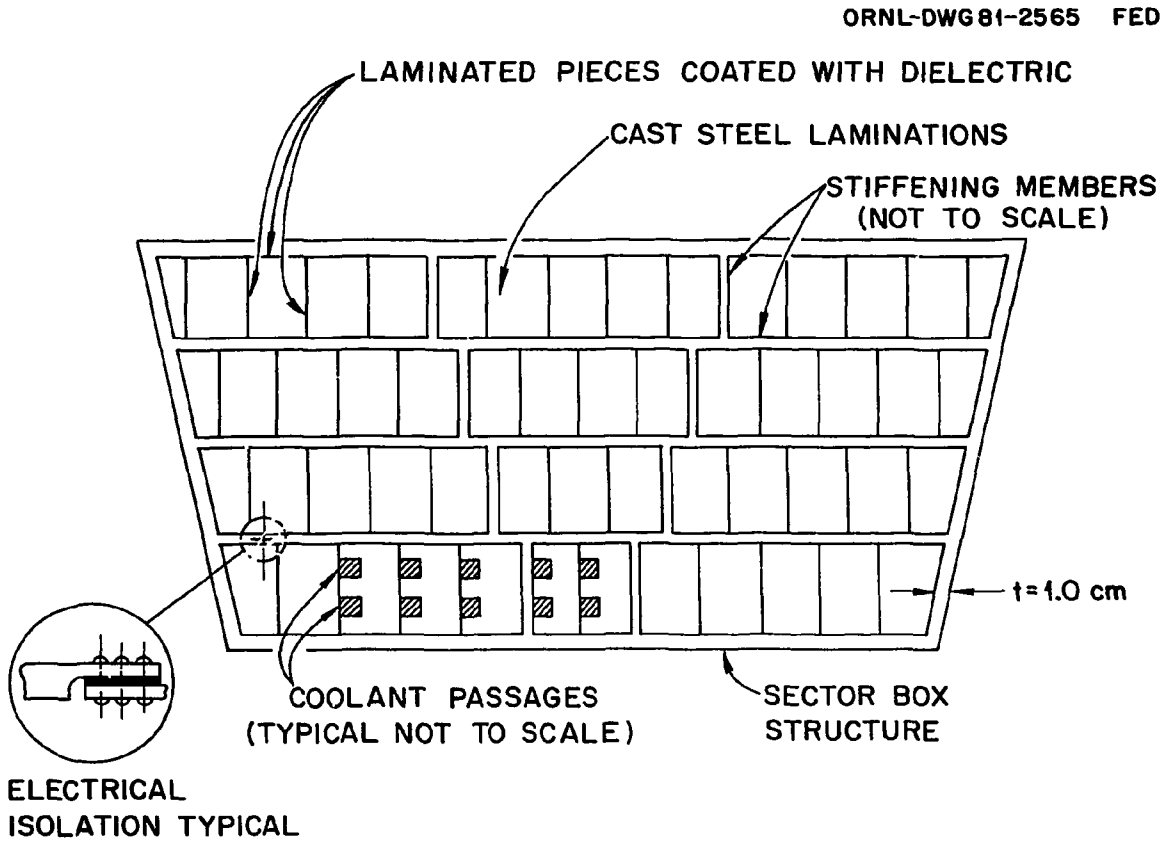

Fig. 6.11. Bulk shield internal arrangement.

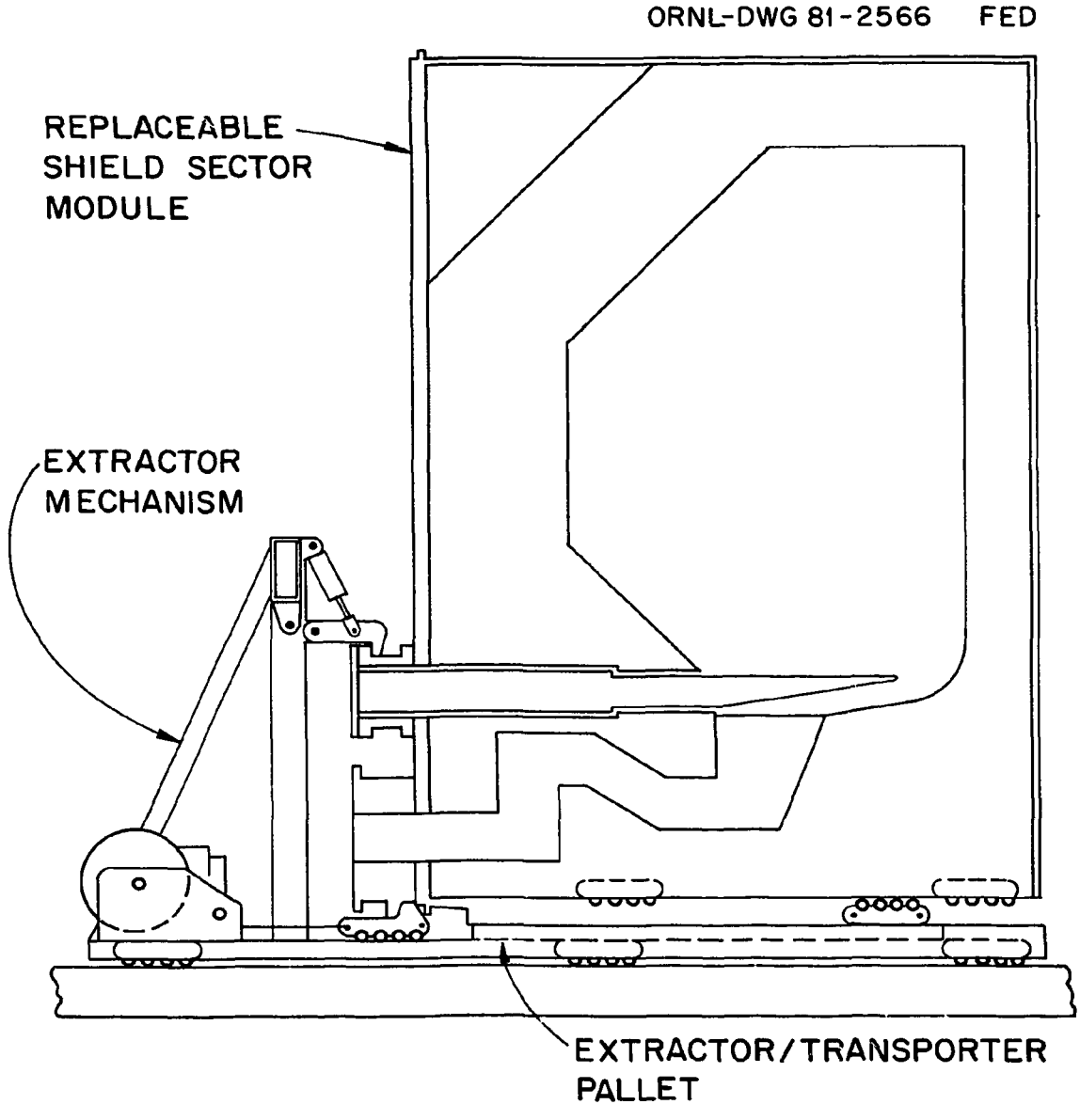

Fig. 6.12. Shield sector removal.

numerous aspects of the torus design remain to be addressed. More fully developed subsystem designs are required in each area. Future efforts will address these development design issues; examine interface problems; address removal and transport techniques; begin investigation of incorporating service connections, instrumentation, and diagnostic equipment; and define the support system accounting for seismic events. Component costs will also be assembled.

6.3 FIRST WALL/ARMOR

6.3.1 Purpose

The primary objective of first wall studies has been to define baseline materials facing the plasma and to develop preliminary design approaches that appear feasible in meeting FED objectives. Material definitions and design approaches have allowed assessments of structural temperatures and erosion rates. These preliminary results form the basis for assessing plasma-wall interactions and developing a more detailed design.

6.3.2 Assumptions and Guidelines

Operating conditions for the first wall components are based on the FED parameters defined in Sect. 3. In addition to these parameters, considerable effort has been directed toward developing design factors consistent with sound engineering practice and with the uncertainties associated with many of the parameters. The studies have been guided by the results of tests conducted in support of the Tokamak Fusion Test Reactor (TFTR) design and the desirability of low Z materials from a physics viewpoint.

6.3.3 Design Description

The first wall baseline design for FED is based on consideration of three regions. These regions, shown in Fig. 6.13, are (1) an actively cooled stainless steel wall occupying the 45° and outboard shield facets, (2) passively cooled graphite armor occupying the top and

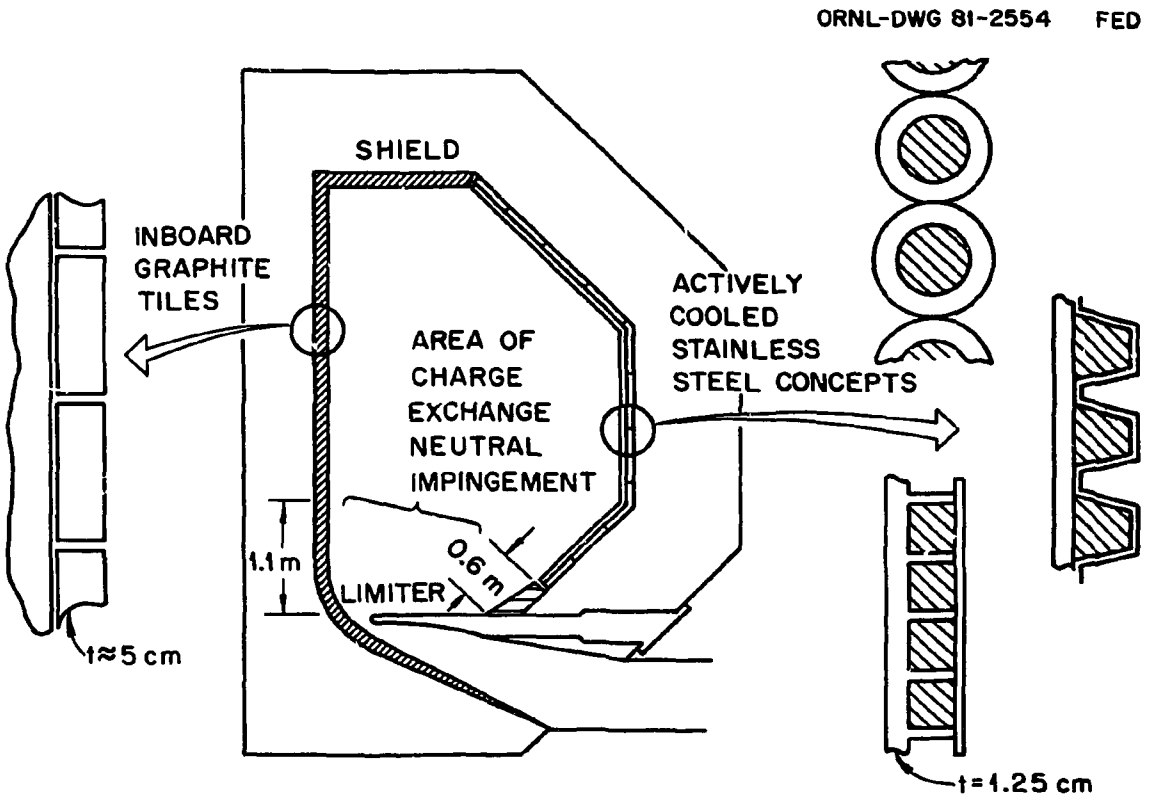

Fig. 6.13. First wall protection. It is assumed that all components can tolerate plasma disruptions and runaway electrons.

inboard walls, and (3) passively cooled graphite armor bands on each side of the limiter. The graphite armor is coated with titanium carbide (TiC). Design conditions for each of these first wall regions are given in Table 6.1.

The design philosophy for the FED first wall is that components should have relatively thick surfaces (>1 cm) and be capable of accepting locally severe conditions. This approach provides a maximum degree of confidence in reactor operation for a reasonable length of time. Thus, no special protection is provided for runaway electrons, as it is intended that they be taken anywhere.

Graphite tiles on the inboard and top surfaces provide maximum protection capability for shock and heat load conditions associated with plasma disruption and neutral beam dumps. Although bare stainless steel may be adequate for the inboard wall, uncertainties associated with the surface melt layer during disruptions push the design to include graphite tiles. Additionally, graphite satisfies the demand for low Z material over a significant portion of the first wall. The TiC coating is intended to control chemical erosion as much as possible. The actively cooled stainless steel outboard wall provides a cool surface to which the graphite tiles can radiate heat.

Requirements for attachment of first wall tiles and coolant panels are based on thermal expansions and plasma disruption electromagnetic loads. For the outboard wall coolant panels, electromagnetic loads have been calculated to be approximately 0.2 MPa (29 psi). For a 1.0-m panel support spacing, panel bending stresses under electromagnetic loads can be kept to 100 MPa (15 ksi). The attachment approach is shown conceptually in Fig. 6.14. Each first wall panel includes a multipass tube system extending from the edge to the middle of the sector. These panels have pin connections that allow for free in-plane thermal expansions. A gap of approximately 1.0 cm is required at the sector midplane for thermal expansion. Out-of-plane deflection is not required and is constrained by the pin/lug attachments. Electromagnetic loads on the graphite tiles are only 0.04 MPa (6 psi). Thus, no problems are anticipated in developing appropriate attachment concepts.

Table 6.1. First wall operating and plasma disruption conditions

First wall region	Baseline protection	Normal operating conditions	Plasma disruption conditions
Outboard wall and 45° facets	Actively cooled stainless steel	7.5-W/cm^2 surface heat load[a] 4.0-W/cm^3 neutron heat load 314,500 full field pulses	2056 thermal quench disruptions at 0.6 MJ/m^2, 5 ms No current quenches expected[b]
Top and inboard wall	Passively cooled graphite armor (TiC coated)	2.2-W/cm^2 surface heat load[c] 2.8-W/cm^3 neutron heat load 314,500 full field pulses	2056 full power disruptions Thermal quench at 0.6 MJ/m^2, 5 ms, followed by current quench at 2.48 MJ/m^2, 10 ms
Armor bands near limiter	Passively cooled graphite armor (TiC coated)	22.2-W/cm^2 surface heat load[d] 2.8-W/cm^3 neutron heat load 314,500 full field pulses	Inboard band same as for inboard wall Outboard band same as for outboard wall

[a] Radiation from plasma, 2.2 W/cm^2; radiation from armor, 5.3 W/cm^2.

[b] Design condition is ten current quenches at 2.48 MJ/m^2, 10 ms.

[c] Radiation from plasma.

[d] Radiation from plasma, 2.2 W/cm^2; charge exchange heat flux with peaking factor of 2, 20 W/cm^2.

ORNL-DWG 81-2567 FED

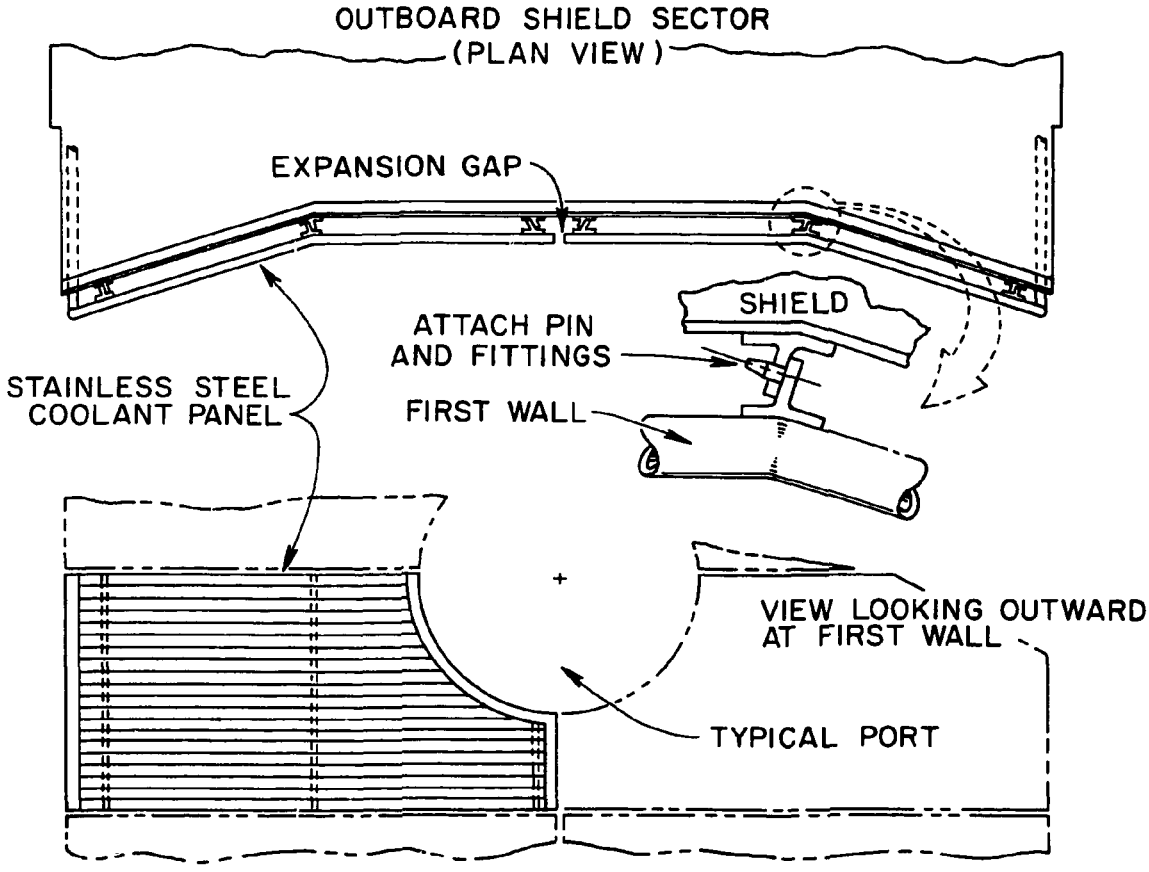

Fig. 6.14. Coolant panel attachment.

6.3.4 Analysis of First Wall Performance

The graphite armor will be coated with titanium carbide. This coating may be ineffective in regions subjected to physical erosion or vaporization. Therefore, it is desirable to avoid extensive periods of time with graphite surface temperatures in the methane generation range of 400°C to 800°C. Maximum tile surface temperatures during normal plasma operation are shown as a function of tile thickness in Fig. 6.15. For the baseline tile thickness of 5 cm, all armored surfaces will operate with maximum surface temperatures between 800°C and 1400°C. During cooldown between burns, inboard and top armor surface temperatures will drop within the methane generation range, thus resulting in some chemical erosion. Since erosion of these surfaces is small, however, the coating may adequately protect most tiles from chemical erosion. The charge exchange neutral armor will pass through the methane generation range for a period of approximately 4.5 min during the first three cycles of a series of burns with the nominal 52-s cooldown time between burns. If the cooldown time between burns is increased significantly during normal operations, the charge exchange armor will pass through the methane generation range during every burn.

Because of the relatively low heat loads, the stainless steel first surface (on outboard and 45° facets) is 1.25 cm thick with maximum structural temperatures of 200°C and associated maximum thermal stresses of 130 MPa (20 ksi). Alternating stress intensities associated with these thermal cycles are below the endurance limit for 316 stainless steel and, therefore, fatigue is not considered to be a problem. This provides a capability for potential disruption load conditions and unexpected erosion, while using a reactor-relevant material with as good an irradiation data base as possible. Coolant flow conditions for the first wall panels are:

Coolant inlet temperature	60°C
Coolant outlet temperature	100°C
Coolant inlet pressure	100 psi
Coolant outlet pressure	90 psi
Total coolant flow	239 kg/s

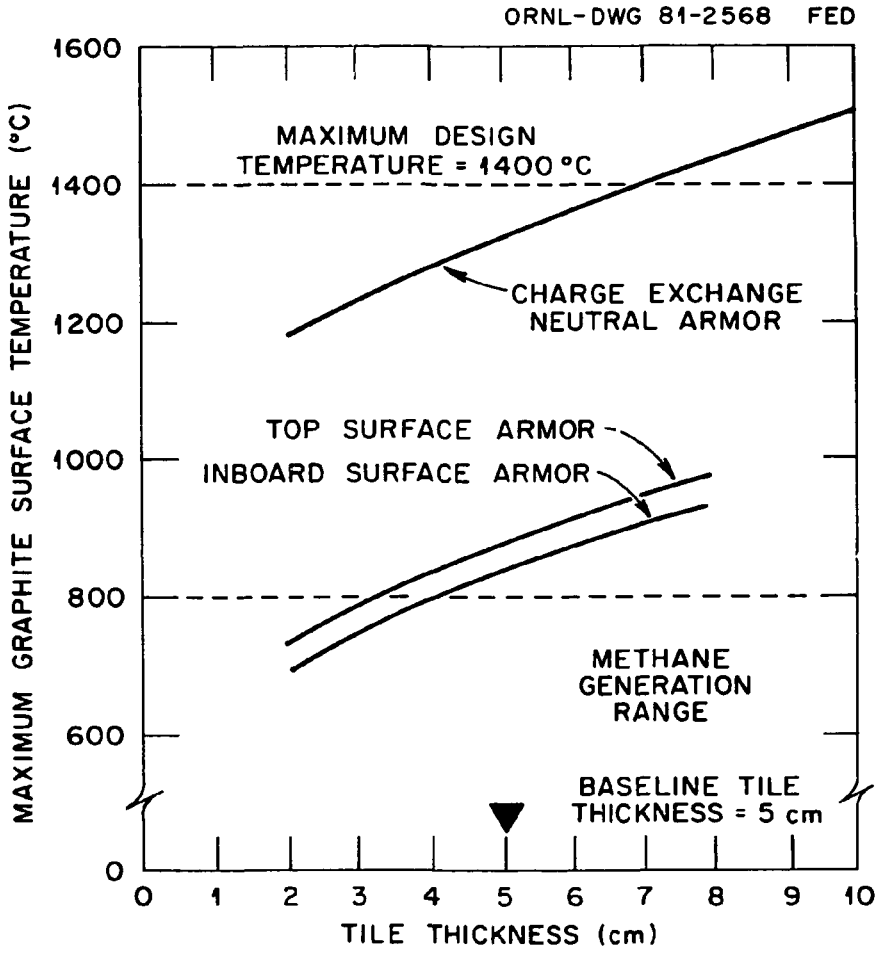

Fig. 6.15. FED first wall/armor temperature.

Erosion over a ten-year period of the first wall graphite and stainless steel surfaces is based on the four-phase operating scenario shown in Table 6.2. This scenario results in the total erosion shown in Table 6.3. Each disruption is assumed to consist of a thermal quench followed by a current quench. The energy flux and time duration of each of these disruption phases are presented in Table 6.1. Although no current quench disruptions are expected on the outboard wall, ten are assumed for design purposes. Erosion for ten full field disruptions on the stainless steel outboard wall is $\sim$0.2 cm. This assumes that all of the melt layer formed by the disruption is removed. For this rate of erosion, the stainless steel first wall lasts the full reactor life with an adequate end-of-life (EOL) thickness in excess of 1.0 cm. Erosion of the graphite tiles covering the top and majority of the inboard wall results from vaporization only. This calculated total erosion over the reactor life is 0.5 cm. Erosion rates are higher where the charge exchange neutrals impinge (primarily on surfaces adjacent to the limiter). The erosion in these regions is 2.6 cm. Thus, approximately half of the original tile thickness remains at end of life. The erosion of these graphite surfaces over the operating life of the reactor is shown graphically in Fig. 6.16. The erosion values shown in this figure assume no redeposition of the sputtered material. No accounting for the sputtered material has been considered in the studies. The importance of developing an understanding of the phenomenon is recognized, however.

6.3.5 Conclusions and Recommendations

The FED operating environment for the first wall is relatively mild when compared to that of previous reactor studies. This allows use of thick wall structures capable of lasting the reactor life. Electromagnetic loads appear manageable, although iterative analysis between the design and the loads will continue to be needed. However, the design of first wall components remains one of the critical considerations for fusion reactors because of the interaction between materials and its association with plasma performance and because of the first wall's vulnerability to locally severe damage and associated maintenance requirements. Key

Table 6.2. FED operating scenario for first wall erosion calculations

Phase	Years	Pulses	Full field pulses	Disruption frequency	Disruptions
I	0-1	16,000	4,000	10^{-1}	400
II	1-3	46,000	11,500	10^{-1}	1,150
III	3-4	23,000	23,000	10^{-2}	230
IV	4-10	276,000	276,000	10^{-3}	276
Total	10	361,000	314,500	—	2,056

Table 6.3. First wall surface erosion

Location	Approximate surface area	Erosion, ten-year life (cm)		
		Charged particles	Charge exchange neutrals	Disruptions
Outboard (stainless steel)	208 m^2	None	None	0.2
Outboard (graphite band)	20 m^2	None	2.1	—
Inboard and top (graphite)	120 m^2	None	None	0.5
Inboard (graphite band)	20 m^2	None	2.1	0.5

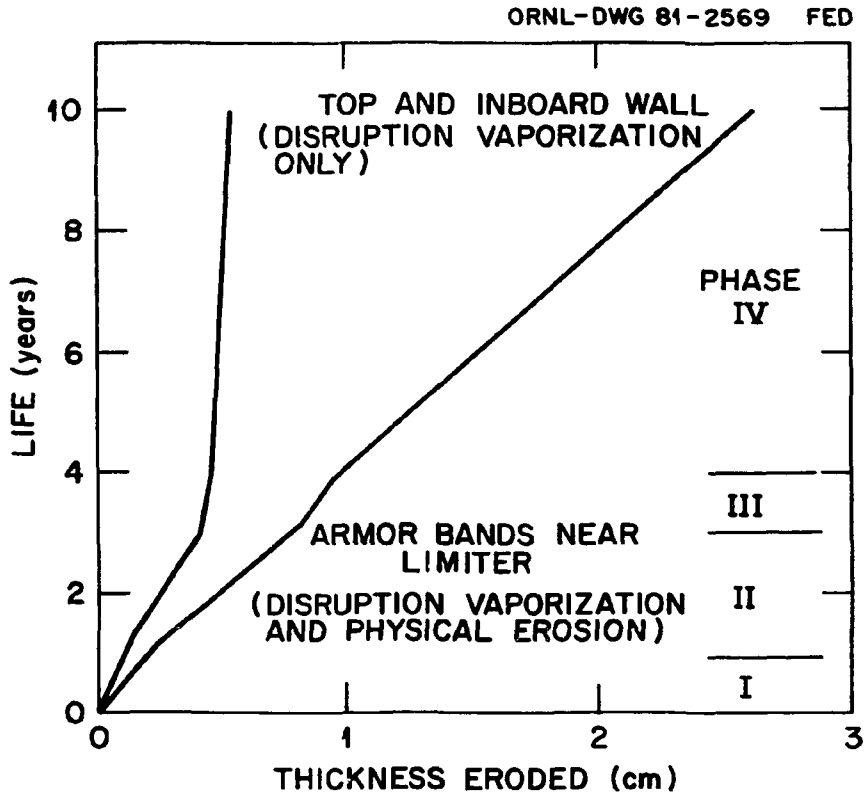

Fig. 6.16. Erosion of graphite surfaces.

issues in preliminary assessment of the present FED baseline design include (1) plasma-wall interaction phenomena, including self-sputtering, and (2) plasma disruption effects, including melt layer response. These two key issues will not be adequately resolved in the near future.

Remaining efforts that can be accomplished in the FED conceptual design phases include:

1. Studies of the desirability of active versus passive cooling of various components.
2. Graphite tile attachment schemes.
3. Graphite/TiC coating considerations, including consideration for entire tiles of TiC.
4. Definition of operating parameter ranges where no first wall would be required (shield surface would act as first wall).
5. Detailed considerations of outboard wall attachment and manifolding requirements, including consideration of regions around ports.
6. Limiter dynamic response analysis.

Additionally, recent equations for irradiation creep of steel indicate significant creep at displacement per atom (dpa) levels in the FED operating range. Study of the response of FED structures, including these phenomena, is recommended.

6.4 MECHANICAL PUMP LIMITER STUDIES

6.4.1 Purpose

This study was conducted to investigate the feasibility of incorporating a mechanical pump limiter into the FED design. The purposes of the limiter are to establish the plasma edge, to exhaust plasma particles, to handle a significant fraction of the plasma heat load, and to protect the first wall from large particle and energy fluxes. Specific objectives were to (1) identify alternative limiter concepts, (2) evaluate the applicability of these concepts to FED, and (3) develop a baseline design.

6.4.2 Assumptions and Guidelines

Maintainability was a prime consideration. It was assumed that the limiter would require frequent replacement. This places constraints on the number of limiters, their size, and their configuration: they must be easily removable and replaceable with a minimum impact on the overall design.

Parameters used in the analysis of the limiter are shown in Table 6.4 and are consistent with the current FED working parameters (see Sect. 3).

6.4.3 Description of Design Effort

A survey of literature and knowledgeable individuals was conducted to define the status of pump limiter assessments and to identify candidate design concepts.

One of the more familiar configurations for a pump limiter is the T-shaped toroidal belt limiter[1] with continuous pumping channels on either side of the T-leg. A belt limiter with perforations has been proposed by Conn et al.[2] and consists of a perforated belt extending around the complete toroidal periphery of the torus chamber. The use of a large area limiter to reduce the average heat load has also been proposed in the form of a global limiter.[2] In this approach, the entire torus wall area is used as a limiter. Plasma rotation is required with this technique to evenly distribute the heat over the large area.

Several other concepts have been proposed, e.g., a poloidal limiter,[3] oscillating limiters to distribute heat and particle load,[4] lithium pellet injection,[5] multiple small ablation limiters ("cigarette limiters"),[6] and integration of limiters with rf antennas.[6]

A number of physics task teams were formed to address critical physics-related issues in formulation of the FED concept. One of these task teams was formed for the purpose of addressing the pump limiter issue. A report[7] was prepared by this task team and identifies two pump limiter concepts for potential FED application. Both concepts consist of two toroidal limiters, one each on the upper and lower 45° facets of the outboard wall. Both concepts feature a limiter face that

Table 6.4. Parameters for FED limiter analyses

Parameter	Value
Particle flux e-fold distance, λ_n	12.0 cm
Heat flux e-fold distance, λ_Q	8.0 cm
Particle flux at edge of plasma	9×10^{23} s^{-1}
Particle flux to be pumped	2×10^{22} s^{-1}
Total transport heat load	56 MW
Average energy of ions striking limiter	300 eV
Number of pulses/lifetime	361,000
Number of full field disruptions	2,056
Disruption: energy flux and duration	
Thermal quench	5.0 MJ/m^2, 5 ms
Current quench	2.48 MJ/m^2, 10 ms

is flat in the poloidal direction. One concept uses a single continuous channel for pumping particles, while the other uses discrete localized slots. Attractive features of these concepts are their flat faces, leading to ease of fabrication, and the ability to attach them rigidly to the shield structure. It is from these concepts that the baseline design described below evolved.

Incorporating two limiter surfaces on the top and bottom of the plasma chamber presents problems from an overall reactor configuration and maintenance standpoint. Both the top and the bottom locations require vacuum ducting. The ducting must be routed to vacuum pumps at a common location, such as the bottom, or pumps must be located at both top and bottom of the torus. Removal and replacement of the limiters could require a major disassembly of the shield sectors.

To alleviate the space problem, an arrangement using only one limiter, located on the lower 45° facet, was examined. This reduces the access and maintenance problems but also increases the maximum heat and particle fluxes on the limiter face by a factor of approximately 1.7. Analysis shows, however, that these heat loads are still acceptable.

The removal and replacement problem can be further simplified by locating the limiter at the bottom of the torus chamber with the face in a horizontal position. This is the design approach which is recommended as the baseline design for FED. The primary features of the design are:

1. Ease of fabrication due to flat face (no poloidal or toroidal curvature).
2. Minimum size module required for removal and replacement.
3. Direct access of external manifolding to limiter.
4. Direct structural attachment to shielding.
5. Control of the position of the leading edge with respect to the plasma edge by changing the horizontal location of the plasma major radius.
6. Decoupling of limiter structure and vacuum duct.

The disadvantage of the bottom location is that the plasma edge characteristics are less well defined near the bottom. The heat and particle loads on a bottom limiter are higher than for a location nearer the

plasma horizontal centerline because of the small radius of curvature of the plasma edge; however, the leading edge loads are smaller at the bottom location due to spreading of the magnetic flux surfaces in this area.

6.4.4 Baseline Design Description and Analysis

The baseline configuration is shown in Fig. 6.4. The system consists of one limiter located at the bottom of the torus chamber. The limiter extends around the entire torus and consists of ten removable segments, one for each torus sector. The limiter surface is flat in both the toroidal and poloidal directions. A particle collection/vacuum channel extends around the torus on the underside of the limiter blade. This continuous channel diverges to ten separate vacuum ducts that extend outward through the TF coils. Each removable limiter segment weighs approximately 15 tonnes.

The leading edge of the limiter is nominally located 36 cm inboard of the tangency point (see Fig. 6.4). This location positions the limiter leading edge far enough from the plasma edge to assure a low heat and particle load but close enough to allow enough particles to pass behind the limiter to be pumped. This location places the limiter leading edge 16.5 cm radially from the plasma edge.

The particle trapping and vacuum pumping channel, located immediately below the limiter, is 10 cm high. This 10-cm height is maintained radially for a distance of 55 cm from the limiter tip. Beyond this location the channel height gradually increases until the transition into the individual ducts for each sector.

The construction of the limiter blade is shown in Fig. 6.4. The basic structure is copper with integral coolant channels. Copper was chosen because its high thermal conductivity results in low temperature gradients when subjected to the limiter heat loads. The surface material is graphite in the form of 5- by 5-cm tiles, 1.25 cm thick on the top side and 0.25 cm thick on the underside of the limiter. As the limiter blade depth increases with increasing distance from the leading edge, shielding is added to fill the void volumes.

The baseline design is for a fixed position limiter. Adjustment of the plasma point of tangency relative to the limiter's leading edge is accomplished by horizontal positioning of the plasma centerline. If desired, an active control system can be incorporated that measures the leading edge temperature and positions the plasma accordingly.

The heat flux and particle flux distributions vary significantly with position along the top and leading edge of the limiter surface. Profiles of these distributions are shown in Fig. 6.17. The magnitude of the flux in this figure is the perpendicular distance from the limiter surface to the plotted curve.

The leading edge is located so that 5.5% of the total particle flux at the plasma edge will pass through a 1.0-cm-high slot formed by the first wall and the lower surface of a 3.0-cm-thick limiter. Pumping efficiency calculations indicate that essentially 100% of the particles entering the slot are pumped. This results in a total particle pumping rate of 5×10^{22} particles/s, a factor of 2.5 times greater than that required for adequate pumping.

A two-dimensional (2-D) finite difference thermal model of the limiter was used to determine the transient temperature distribution throughout the limiter. The copper substrate maximum temperature is maintained below 200°C. Using an upper temperature limit of 1200°C, the maximum graphite tile thickness was determined to be 1.25 cm. Because of large temperature differences along the graphite surface exposed to the plasma, some regions of the graphite surface will operate in the chemical erosion zone of 400°C to 800°C. Because the surface temperatures will decrease as the tile erodes, the region of the graphite surface that is subjected to chemical erosion will change. A comprehensive analysis of this time-dependent process remains to be done.

Thermal-hydraulic analyses of the limiter water coolant system were performed. The characteristics of this coolant system are:

Coolant inlet temperature	60°C
Coolant outlet temperature	84°C
Coolant inlet pressure	1 MPa (150 psi)

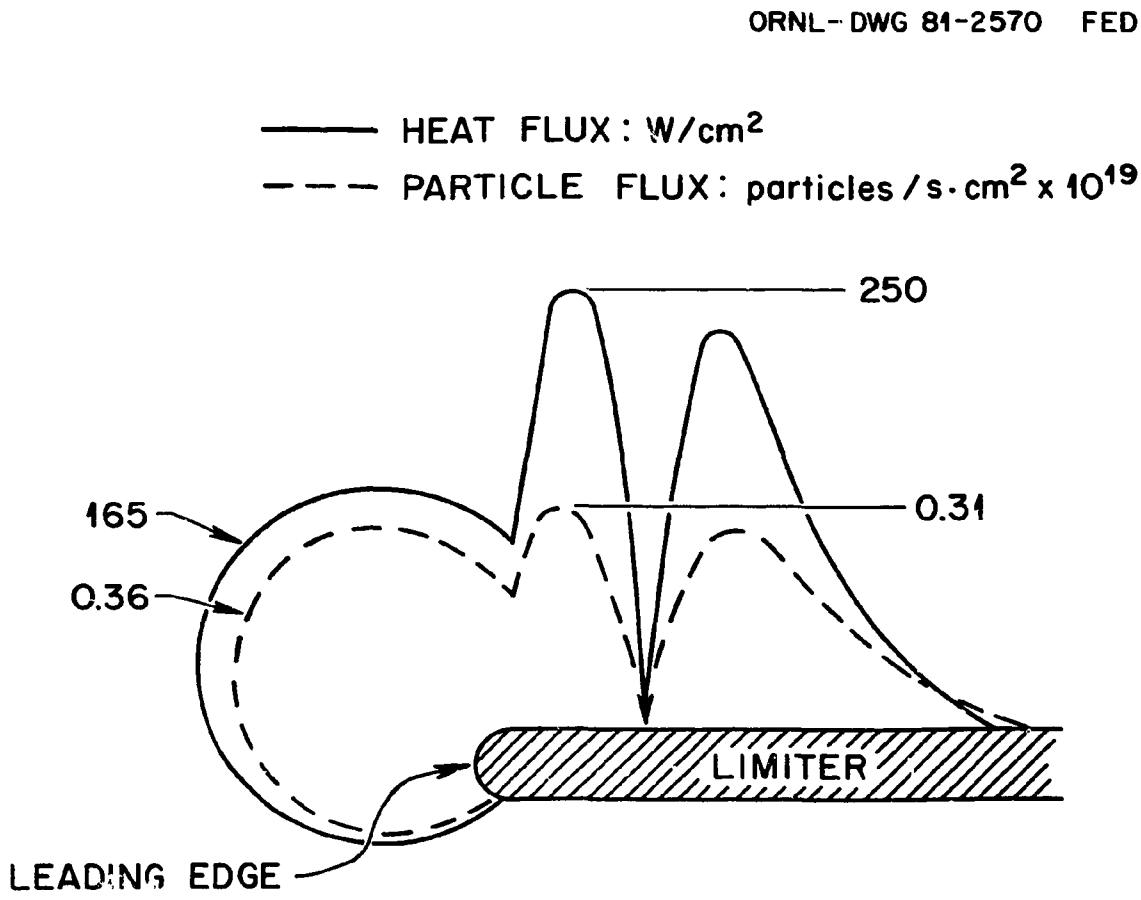

Fig. 6.17. Limiter heat flux and particle flux distribution.

Coolant outlet pressure	0.73 MPa (110 psi)
Coolant passage	Rectangular, 0.3 cm × 1.0 cm
Flow velocity	5.1 m/s
Total coolant flow	560 kg/s

Several types of graphite tile erosion mechanisms will combine to limit the life of the limiter. These erosion mechanisms are physical sputtering from charged particles leaving the plasma and from charge exchange neutral particles, chemical sputtering caused by the reaction of graphite with hydrogen to form methane, and sublimation caused by the intense heating during plasma disruptions. For this preliminary evaluation of the limiter life, the chemical erosion was estimated to be equal to the physical sputtering. The total thickness of graphite eroded during each phase of operation is identified in Table 6.5. Assuming that the available thickness of graphite for erosion is 1.0 cm, the frequency of replacement for each phase was computed and is presented in Table 6.6. As indicated, the replacement frequency, based on the present methodology and assumptions, is 1-2 months during the various phases of FED operation.

Loads on the limiter include internal coolant pressure and plasma disruption electromagnetic forces. Additionally, thermal stresses occur during operation and also result from fabrication processes, such as brazing. The coolant pressure of 1.0 MPa (150 psi) can be handled by appropriate internal rib spacing. For the FED baseline limiter structural thickness of 0.30 cm (near the tip), a rib spacing of 0.8 cm results in a 35-MPa (5-ksi) bending stress. Thermal stresses in the copper structure near the limiter tip are approximately 70 MPa (10 ksi) during reactor operation, assuming that the limiter is constrained from bending in the toroidal direction. Electromagnetic loads from plasma disruption are approximately 0.4 MPa (60 psi) normal to the limiter surface. This load on the cantilevered limiter requires increasing limiter depths and structural thicknesses with increasing distance from the tip.

A structural thickness of 1.3 cm is required for the 20-cm limiter depth at the shield support point. This assumes a 280-MPa (40-ksi)

Table 6.6. Limiter replacement frequency

Phase	Replacement frequency (months)
I	2
II	1.5
III	1.5
IV	1

Table 6.5. Limiter erosion

Phase	Duration (years)	Number of pulses	Erosion[a]			
			Physical sputtering[b] (cm)	Chemical erosion (cm)	Sublimation during disruptions (cm)	Total (cm)
I	0-1	16,000	2.3	2.3	1.1	5.7
II	1-3	46,000	6.6	6.6	3.2	16.4
III	3-4	23,000	3.2	3.2	0.6	7.0
IV	4-10	276,000	40.0	40.0	0.7	80.0

[a] No design factors included.

[b] Includes erosion from charged particle flux and charge exchange neutral flux.

allowable stress level, which could easily be attained in high strength, cold-worked copper. The effects of vibrations induced by plasma disruptions remain to be analyzed, and fracture mechanics techniques will be employed to predict their impact on lifetime. The applicability of cold-worked copper must be assessed with regard to fabrication considerations. In any event, since the limiter is to be filled with shielding material (steel), no problem is seen in attaining adequate bending strength to accept the presently defined electromagnetic loads.

6.4.5 Conclusions and Recommendations

Design and analyses efforts have led to the baseline limiter design described above. It is recommended at this time that the concept be carried as a baseline. Analyses have shown that the heat loads are acceptable, that some adjustment in leading edge heat load and pumping is possible by plasma positioning, and that a reasonable removal and replacement scheme is possible.

The key issue in determining the feasibility of using a pump limiter is the life expectancy, calculated to be on the order of 1-2 months for the baseline design at an availability of 10-20%. Because erosion of high Z materials is approximately a factor of 100 lower than the baseline low Z material, use of these high Z materials would increase limiter life to approximately that of the device. It is, therefore, recommended that further analysis and consideration be given to the surface material selection and to the effects of the predicted life on overall operations.

6.5 SUMMARY

The major conclusions of the Nuclear Systems analyses are summarized below.

1. Torus Sector Design. Technically feasible approaches have been conceptually developed for the key aspects of the torus sector design. The torus consists of a spool structure and ten shield sectors, each of which is capable of direct radial extraction between the outer legs of the TF coils. The sectors are supported by a thin-skinned (high resistance) spool structure. The outer face of each sector is defined as a single

planar surface to simplify the vacuum sealing problem. The sector-to-spool structure vacuum seal consists of a single convoluted metal bellows.

2. First Wall Design. A first wall baseline design for FED has been developed and analyzed. The design comprises three regions: (1) an actively cooled stainless steel wall on the outboard and 45° facets; (2) passively cooled graphite armor bands on each side of a mechanical pump limiter located at the bottom of the plasma chamber; and (3) passively cooled graphite armor bands on each side of the limiter. Analysis of these first wall surfaces in the FED operating environment, considering all normal and disruption loads, indicates that these surfaces will last the ten-year machine life. The total erosion is less than 2.6 cm of the 5-cm-thick graphite armor tiles. No redeposition of the sputtered material was considered, nor has any accounting for the sputtered material been addressed in these studies. Three key issues remain that can significantly influence the overall first wall surface performance and require effort in the fusion community. These are (1) better understanding and definition of plasma-wall interaction phenomena, including self-sputtering; (2) better understanding of disruption effects, including response of the melt layer; and (3) better understanding of the fate of sputtered material from first wall surfaces surrounding the plasma.

3. Limiter Design. A baseline concept has been developed for a mechanical pump limiter and incorporated into the FED design. A single limiter located at the bottom of the plasma chamber was selected as the baseline based primarily on maintenance considerations. However, location of the limiter on a 45° facet of the chamber wall was also examined and represents an alternate option. The limiter extends around the entire torus and consists of ten removable segments, each weighing about 15 tonnes. The limiter surface is flat in both the toroidal and poloidal directions. Analyses of the limiter indicate that the heat loads can be accommodated and that some adjustment in leading edge heat load and pumping is possible by plasma positioning. A feasible removal and replacement scheme has been identified. The lifetime throughout the postulated operating sequence of FED, assuming the use of low Z surface materials, is approximately 1-2 months. If use of high Z materials can be demonstrated to be acceptable from the standpoint of plasma performance,

then the reduced levels of erosion of such materials would result in a limiter life approximately equal to the assumed device life of ten years. These key issues must continue to be pursued.

REFERENCES

1. C. C. Baker et al., *Starfire — A Commercial Fusion Tokamak Power Plant Study*, ANL/FPP-80-1, Argonne National Laboratory (1980).
2. R. W. Conn, S. P. Grotz, R. J. Taylor, and M. Ulrickson, *Limiter Pumping Considerations for ETF/INTOR*, INTOR/PHY/8-13 (ETF-R-80-PS-024), Engineering Test Facility Design Center (July 1980).
3. Y-K. M. Peng, R. R. Parker, and D. Overskei, *An Option of Limiter Pumping Approach in ETF*, ETF-R-80-PS-023, Engineering Test Facility Design Center (July 1980).
4. M. L. Xue et al., "Oscillating Limiter Concepts," paper presented at the Non-magnetic Divertor Workshop, Massachusetts Institute of Technology, Cambridge, Massachusetts, October 16-17, 1980.
5. K. H. Burrell, "Simple Method of Removing Helium Ash and Impurities from Fusion Reactors," paper presented at the Non-magnetic Divertor Workshop, Massachusetts Institute of Technology, Cambridge, Massachusetts, October 16-17, 1980.
6. J. Schultz, "Limiter Pumping; Implications for FED, Materials Selection, and New Topologies," seminar presented at Fusion Engineering Design Center, ORNL, Oak Ridge, Tennessee, November 1980.
7. D. O. Overskei et al., "Mechanical Divertor Proposals," Physics Task Team Report, December 1980.

7. ELECTRICAL SYSTEMS

J. G. Murray*

W. D. Nelson[†] S. L. Thomson[♣]

G. E. Gorker[†] G. Bronner[§]

D. H. Metzler[†] H. Vogel[‖]

7.1 INTRODUCTION

The FED electrical systems include ac power, energy storage, power conversion equipment, plasma heating equipment, fueling systems, standard and feedback controls, instrumentation, and data acquisition. Previous reports on the Engineering Test Facility (ETF) and the International Tokamak Reactor (INTOR) by the FED Electrical Systems Branch provided basic data on these areas. This section focuses on those issues considered most critical to the current phase of FED concept development. These critical issues include (1) design of the plasma heating systems, consisting of rf startup assist systems, the baseline ion cyclotron resonance heating (ICRH) bulk heating system, and the alternate neutral beam injection (NBI) bulk heating system, (2) implications of alternate startup options, (3) impact and handling of disruption-induced eddy currents, and (4) requirements and limitations of plasma position control.

---

*Fusion Engineering Design Center/Princeton Plasma Physics Laboratory.

†Fusion Engineering Design Center/General Electric Company.

♣Fusion Engineering Design Center/Bechtel Corporation.

§Princeton Plasma Physics Laboratory.

‖Los Alamos National Laboratory.

7.2 RF HEATING SYSTEMS

7.2.1 Introduction

Several rf heating regimes appear to be attractive for potential application in FED. The experimental success that has been achieved so far and the potential technological advantages that may be realized have been the basis for suggesting that rf heating be seriously examined in FED. Accordingly, this mode of heating has been adopted as the baseline for the present studies, admittedly to provide a more in-depth examination of the key issues such a selection raises. Nevertheless, considerable additional experimental and theoretical advances remain to be achieved to demonstrate that rf heating systems represent viable options for FED operation.

Relative to rf heating, neutral beam heating has a significantly more reliable physics and technology basis for application to FED and remains a strong alternative for bulk heating.

7.2.2 Purpose

The principal purpose of this effort is to develop rf heating subsystem concepts. By evaluating the impact on these concepts of changes in requirements, the effort also supports the trade studies carried out by the FED physics task teams. A listing of the more salient problems includes investigating the use of hardened launchers for reactor-relevant designs, matching these launchers to the plasma, making provisions for operating on different frequencies, and investigating the feasibility of current drive.

7.2.3 Major Assumptions and Constraints

Table 7.1 shows a listing of the parameters and requirements for the heating subsystems extracted from the FED parameter list. Constraints include developing heating subsystems compatible with the ten toroidal field (TF) coils of the tokamak design, the facilities, and the program schedule of FED. The last constraint manifests itself in the selection of technology available in the FED program's time frame.

Table 7.1. RF heating subsystem parameters

Startup	
Type of heating (rf assist)	ECRH
Initiating voltage, with rf assist	25 V
Current rise time	6 s
Time duration of rf assist	
Preheating	0.2 s
Current ramp	0.2 s
Startup rf power	1 MW
Frequency	~80 GHz
Bulk heating	
Type of heating	ICRH
Species/harmonic	D^+/second
Pulse length	$\geq$106 s
Initial	6 s
Burn	$\geq$100 s
Power	
Initial	50 MW
Burn	36 MW
Frequency (B = 3.62 T)	~54 MHz

7.2.4 Description of Design Effort

An iterative approach is used as the method of development. The departure point was the earlier ETF configuration. At the outset, some changes were made to reflect the emphasis on rf heating as the first choice for the auxiliary heating system over the NBI approach. Without the complexity of both NBI and rf heating, the concept is made easier from a remote maintenance standpoint. Most of this study effort is on the ICRH equipment, because the electron cyclotron resonance heating (ECRH) subsystem requirements are a simplified version of the previous effort.

When configuring the heating subsystems, a conservative approach was taken toward technology. In general, either technology in the current Department of Energy/Office of Fusion Energy (DOE/OFE) plans for

the next five years or off-the-shelf components are used in the concepts.

7.2.5 Design Description

Figure 7.1 shows the ECRH subsystem used to initialize the plasma and assist the ohmic heating (OH) subsystem during startup. Ten launchers (one per torus sector) are mounted in the top wall on the high field side. Each launcher is supplied by a gyrotron power oscillator with an output of ∿200 kW at the tube. This concept is constrained by the available technology. It would be preferable to have coherent amplifiers combined to supply higher power to fewer launchers. Present development plans call for a 200-kW cw gyrotron oscillator at a frequency of ∿100 GHz to be available about 1986, but there are no plans for high power, long pulse amplifiers. Some consideration is being given to a 1-MW tube, but it would not be available before late 1989.

The requirement to launch a wave (extraordinary mode) from the high field side is a difficult one to meet on a reactor-relevant machine like FED. Feasibility issues associated with remote maintenance of such a launcher were raised at the Remote Maintenance Workshop in January 1981.

Figure 7.2 shows the ICRH system concept. The changes made to the design developed for ETF application include an increase in power from a demonstration level of 10 MW on ETF to the 36 MW required for sustained heating on FED. A ridge-loaded waveguide launcher replaces the simple waveguide because the frequency is generally lower for the smaller toroidal field flux density of FED.

The rf generator is the same basic concept proposed for ETF, except that more power modules are required to meet the higher power level. These high power amplifiers use currently available vacuum tubes. A more efficient design is possible if high power (>>1-MW) tubes are developed.

The impact of varying the operating frequency is under discussion. This is desirable to support early phase testing at lower values of TF-B and/or to do selective species heating for different parts of the operating cycle (i.e., plasma initiation, bulk heating, drive, etc.).

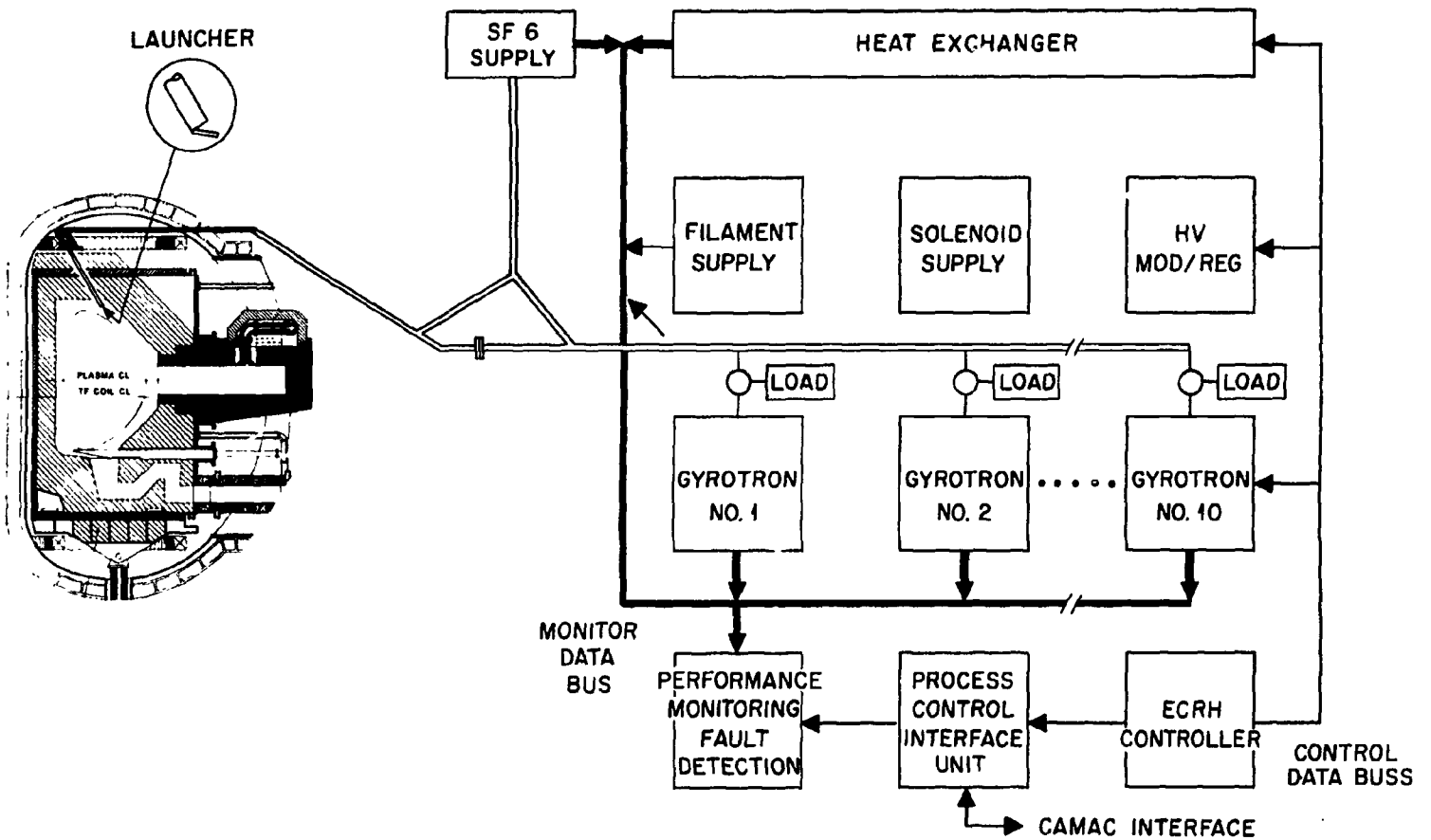

Fig. 7.1. ECRH subsystem components.

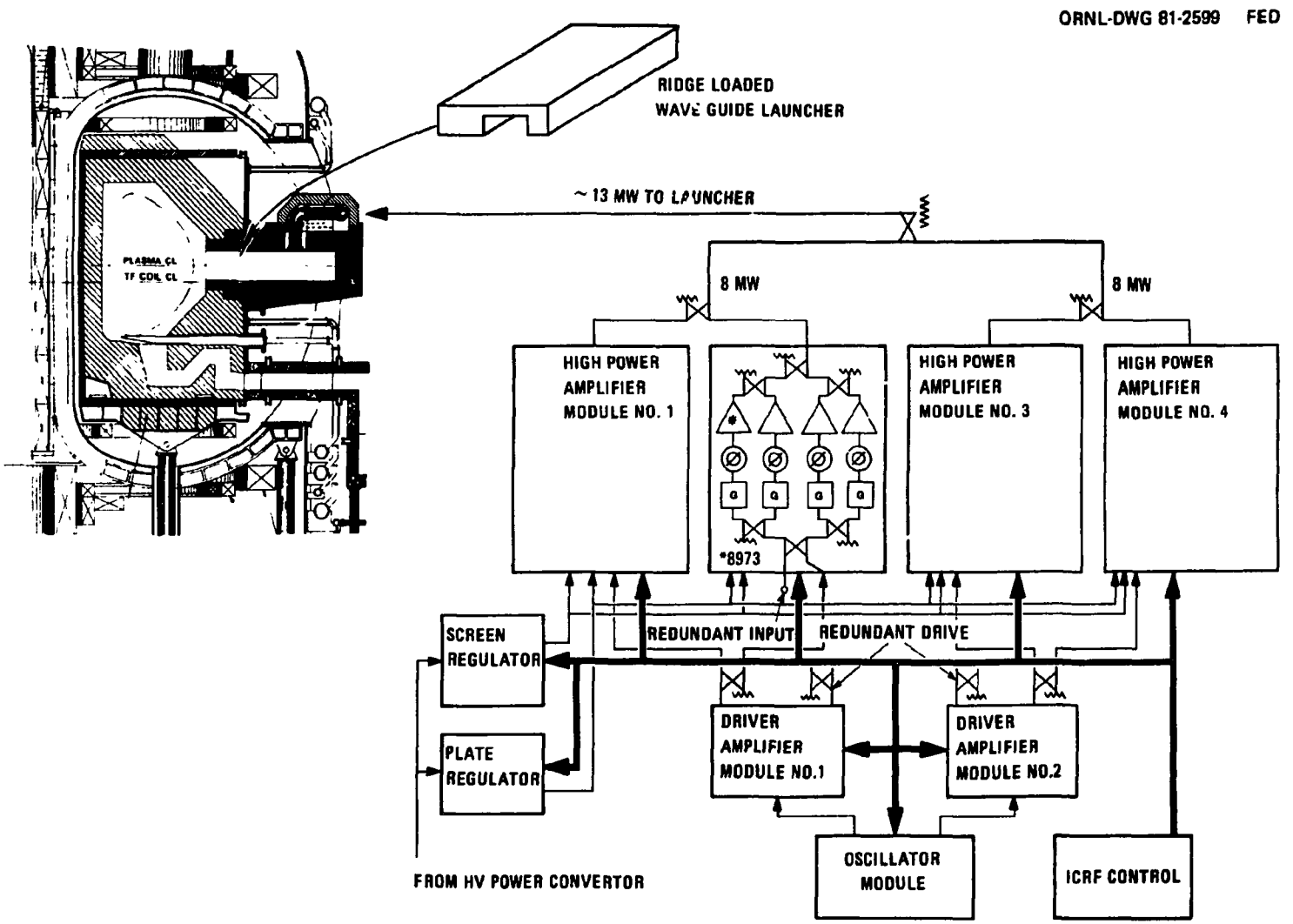

Fig. 7.2. ICRH concept.

A multiple frequency system that would meet this need is significantly more complex. High power resonators must be switched. Launchers may require multiple feed points or switchable matching sections. More launchers may be required to handle the same amount of power. Thus far, only preliminary thoughts have been given to the multiple frequency system.

7.2.6 Conclusions and Recommendations

A viable rf bulk heating concept has been developed for FED application. In this concept, a conservative approach was taken in selection of technology approaches to be used. As a result, the necessary rf components represent feasible, available designs in the FED timeframe. Remote maintenance is perceived as a problem for the ECRH launcher. Launcher designs for a reactor-relevant device require more effort. Modeling the effectiveness of waveguide launchers requires development and is being pursued at Princeton Plasma Physics Laboratory (PPPL) by P. Colestock. A cooperative effort between the Design Center and PPPL is being pursued. This modeling effort should produce trade-off information useful in developing the launcher design. Some feasibility issues may arise from this modeling development. Development needs should be examined after the requirements for FED have been better defined. Continuation of the multiple frequency operation system concepts is recommended. Finally, if current drive on FED is needed or desired, concepts must be developed.

7.3 NBI HEATING SYSTEMS

7.3.1 Purpose

Neutral beam injection (NBI) is an alternate heating approach for FED. This effort studies the impact of retaining the option of NBI heating should the rf heating results prove disappointing. The effort also includes investigation of the impact of the long pulse requirement (operation for 106 out of 152 s) on the beam line design. Finally, the

current drive function, even when relegated to a demonstration level, requires high energy injection, thus necessitating a look at the technology available for candidate solutions.

7.3.2 Major Assumptions and Constraints

The major assumptions are (1) the FED parameters are used (see Table 7.2), (2) the ETF NBI configuration is the starting point, and (3) the driving of plasma current (I_p) by the auxiliary (neutral beam) heating systems is a function to be demonstrated and is not essential to the basic operation.

The design effort is constrained by (1) the ten TF coils of the FED configuration, (2) the FED schedule, and (3) the findings of the OFE Technical Management Board (TMB) NBI Task Committee.

7.3.3 Study Effort

A baseline iteration approach is used in this effort to assess the impacts of assumption and constraint changes. Configuration performance and operation are evaluated using the ETFNB code.[1] Using this code, one can trade off source and beam line size, cost, wall heat loading, efficiency, etc. The TMB NBI Task Committee effort complemented this effort. In general, technology status and limits are investigated by the committee, and design or design application studies are performed by the Design Center.

7.3.4 Study Results

The NBI Task Committee's preliminary conclusion is that positive ion source beam line technology is sufficient to ensure meeting the FED scheduled operational date of 1990 for the plasma heating function. However, higher energy beams than are currently available are required for the current drive function. At present, negative ion source beam lines are the most promising, but they lag their positive ion equivalents in development by 3-5 years.

Table 7.2. NBI requirements

Functional requirements	Bulk heating Power drive Current drive Impurity control Fueling augmentation
Performance requirements	
Heating	
Energy	150 keV
Power	
Bulk heating	45-50 MW
Steady state	36 MW
Injection angle[a]	20°
(to normal at magnetic axis, equivalent to 16° at plasma edge)	
Species mix (by current after neutralization)	
Full	60
Half	24
Third	16
Pulse length	
Bulk heating	6 s
Steady state	t_{burn}
Current drive	
Energy	400 keV
Power	40-45 MW
Injection angle	53°
(to normal at magnetic axis, equivalent to 41° at plasma edge)	

[a]Capable of quasi-tangential injection at up to 35°.

The Design Center investigated the impact of long pulse operation. There are four general areas of concern: (1) neutron fluence damage, (2) surface heating in the beam line, (3) availability, and (4) life cycle cost (LCC). Briefly, neutron fluence damage limits the life of organic insulators (such as G10 in the bending magnets) to about 10^4 pulses. Surface temperatures are four times higher without active cooling for accelerator stacks and beam dumps (although the use of direct recovery mitigates the beam dump problem). To first order, availability is reduced because cryopump regeneration must be done each day for a long pulse NBI system instead of once a week as in ETF. The refrigeration LCC for operation in the long pulse mode increases by ~$150,000/year. All of these problems are amenable to straightforward engineering solutions, but the driven situation is more costly and less reliable and has higher development risks.

A summary of the FED NBI parameters is shown in Table 7.3. (This pertains only to the plasma heating configuration.) The salient changes from ETF are (1) lower power sources, (2) elimination of the neutron shutter, and (3) more nuclear shielding. Injection angles from perpendicular up to 35° (quasi-tangential) are possible when interfacing with the ten TF coils of FED. Figure 7.3 shows elevation and plan views of the NBI interface.

7.3.5 Conclusions and Recommendations

Neutral beam injection heating is a feasible, practical alternative to rf heating on FED. There are no significant problems with keeping this option open.

Aside from a continuum of iterations of the NBI heating design to respond to changes in requirements, the most important remaining effort is addressing the availability questions. This entails carrying out a detailed design to a point at which maintenance actions could be delineated step by step, components could be listed with failure rates estimated and scaled, and remote maintenance equipment requirements could be identified. Cost estimates would be better if this detailed design were available.

Table 7.3. NBI parameters for heating

Interface	
Number of injectors	4
Drift duct, H × W × L	1.2 × 1.0 × 3.3 m
Average power density	∿1.4 kW/cm^2
Beam crossover	Drift duct center
Injection angle	0-35°
Shielding thickness	
Nuclear borated concrete	1 m
Magnetic ingot iron	0.15 m
Injector	
Energy	150 keV
Power	
Full energy	32 MW
All energies	50 MW
Ion fraction	
Full	0.8
Half	0.12
Third	0.08
Pulse length	106 s
Divergence	1.5°
Efficiency	
Full energy	26
All energies	41
Current per source	59 A
Source size, W × H	0.14 × 0.28 m
Sources per injector	6
Direct recovery efficiency	0.6
Cryogenic pumping	
Area 1, drift region	∿50 m^2
Area 2, gas cell region	∿25 m^2
Dimensions	
Box, W × H × L	6 × 8 × 4 m
Transition section, W × H × L	(1-2.5) × (1.2-2.7) × 3.2 m

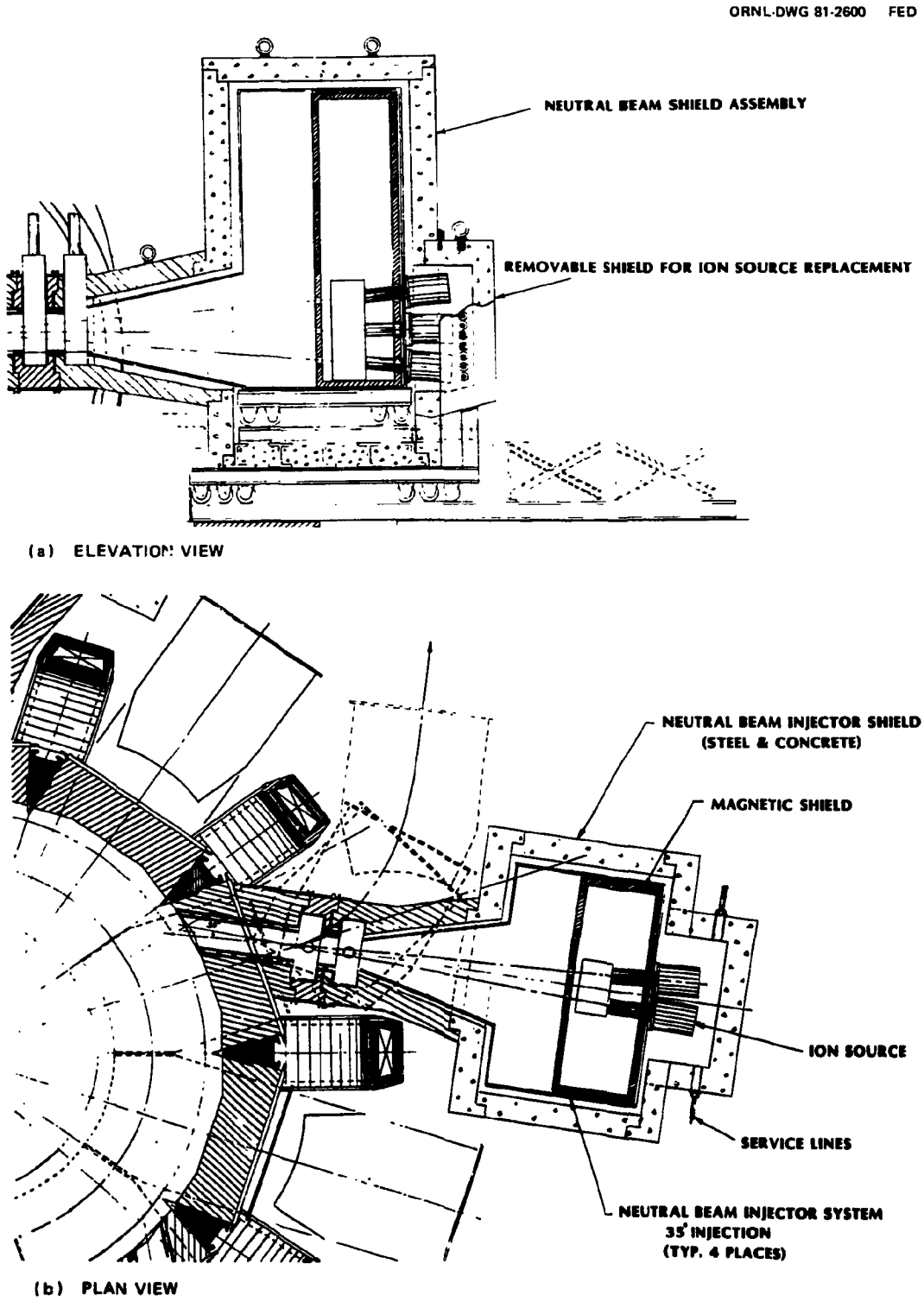

Fig. 7.3. NBI interfaces: (a) elevation view and (b) plan view.

Some technology developments should be pursued, specifically direct recovery for positive ion beams and general component development for high energy beams. Obviously, there is much to do on the high energy beam line design for current drive, but the technology must be developed first.

7.4 STARTUP

7.4.1 Purpose

The present baseline method of initiating plasma startup in FED involves ionizing the fill gas and heating electrons to approximately 100 eV using ECRH prior to initiating a plasma current with the OH system.[2] Under these conditions, there is no need for a high voltage (100 V) OH pulse and the resulting high currents in the vacuum enclosure. The rf-assisted startup also allows the design of a relatively low impedance plasma vacuum chamber consisting of ten removable segments of armor and coolant pipes as well as the neutron shielding and the outer spool structure. This forms the chamber boundary, which can be made of heavy material. A thicker metal wall chamber is more reactor-relevant because it can more reliably withstand disruption-induced currents than a thin, highly resistive chamber.

This startup method is not now used on existing machines; hence, further experimental testing is needed to demonstrate that rf assist can satisfactorily provide plasma startup with a low voltage, equivalent to approximately 10-20 V, on the plasma in FED. Preliminary test results from the Impurity Study Experiment (ISX-B) and WT-1 are given in Refs. 3 and 4.

The implementation of an ECRH-assisted design option for FED will impose the following requirements:

1. The rf power must successfully heat a small localized volume of plasma to electron temperatures of approximately 100 eV.
2. There must not be an influx of impurities from the wall of the vacuum vessel that would be detrimental to plasma startup.

3. The plasma must be confined long enough to allow the low voltage OH system to build up the plasma current to a value consistent with the desired safety factor.
4. The high frequency (100-GHz) gyrotrons must be developed in time for FED.

To provide a backup to the ECRH-assisted startup, two other methods of initiating a plasma are being considered. (Initiating a plasma is defined as producing a 60-kA plasma current in approximately 100 ms with a ramp rate of 600 kA/s.) The first method involves increasing the rf power from 1 MW to at least 20 MW, using lower hybrid resonance heating (LHRH), ICRH, or ECRH; the second method uses the control coils (blip coils) to provide a plasma loop voltage of 100 V for 100 ms.

7.4.2 Assumptions and Guidelines

As noted above, the baseline method assumes that a small volume of plasma, localized at the upper hybrid resonance (UHR), can be heated to high enough temperatures that radiation losses due to low Z impurities no longer dominate. In the UHR zone, electrons are heated to approximately 100 eV in 100-200 ms with $\lesssim$1 MW. Because of the high plasma conductivity, the plasma current can be induced without the need for a high plasma voltage.

The scenario adopted as the first backup to ECRH-assisted startup assumes the use of ICRH to provide "brute force" heating of the full bore plasma to approximately 100 eV. For this backup option, it was assumed that 50 MW of ICRH would be used to provide the bulk heating to raise the plasma temperature to the burn state. Therefore, the same equipment could be used to provide the startup power. In addition to the concern that the ICRH will not be effective in initially heating the gas, there is some concern that injecting significant amounts of ICRH power during startup may result in an influx of impurities from the wall. There is also the possibility of installing smaller microwave horns in the vacuum vessel for using LHRH or ECRH if either of these proves more advantageous.

The second backup procedure assumes that blip coils can be installed just outside the vacuum chamber shield and could also be used for horizontal and vertical position feedback control. For this high voltage startup, it is assumed that the impurity control will be sufficient to allow a satisfactory startup with only 100 V induced around the plasma for 100 ms.

7.4.3 Design Description

To size the blip coil, a computer program was developed to account for the eddy currents and voltages induced in structures and in the poloidal field (PF) windings. It assumes a starting plasma 20 cm in diameter with a resistance $R_p(t)$, given by

$$R_p(t) = \begin{cases} \alpha t^{-1}, & t \leq 0.01 \text{ s} \\ \beta t^{-1.6674}, & t \leq 0.01 \text{ s} , \end{cases}$$

where $\alpha = 150\ \mu\Omega$ and $\beta = 6.94\ \mu\Omega$.

From the blip coil computer program, it was determined that a vacuum chamber with stainless steel walls 1 cm thick would require four external coils to provide the 0.5-1.5 MAT necessary for startup initiation (see coils 41 and 42 on Fig. 7.4). The analysis also showed that the vacuum chamber walls cause a 90-ms delay in the plasma current buildup, and hence the volts per turn on the blip coil had to remain at a value of 137 V per turn for 190 ms to provide for the initiation.

In completing this study, the losses in the structures were determined (Table 7.4). The total ampere-turns and energy requirements were determined as a function of the vacuum chamber resistance (Fig. 7.5). The currents and voltages required in the PF coils as a function of time are shown in Figs. 7.6 and 7.7. It can be seen that the voltages induced in the PF coils due to blip coil operation are low (<30 V per turn). This is about the same voltage that results from a 20-ms disruption. The delay of the plasma current rise due to the vacuum vessel

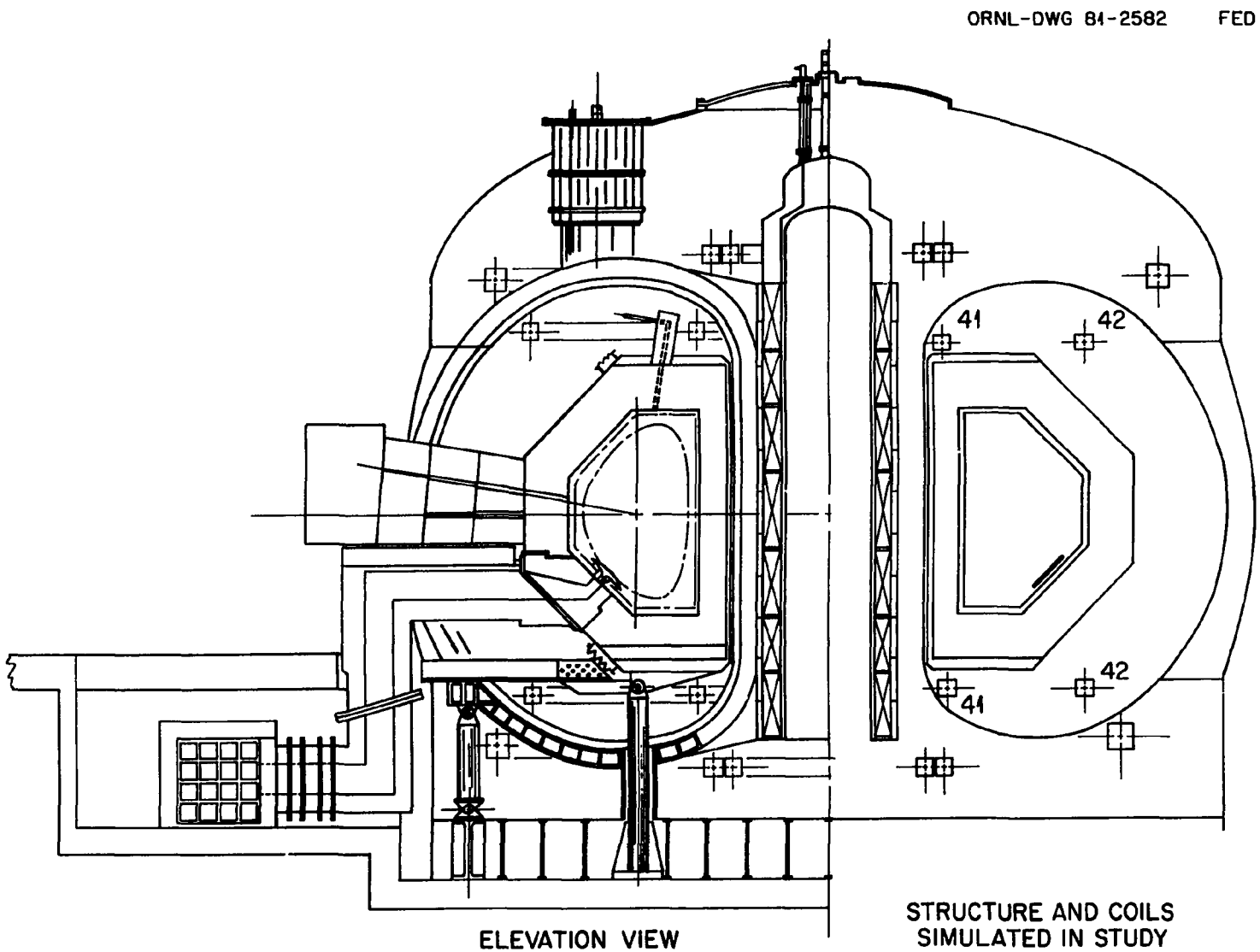

Fig. 7.4. Structure and coils simulated in study.

Table 7.4. Startup energy losses

Element designation	Loss (kJ)
Plasma (20-cm radius)	174
Bucking cylinder	199
TF cryostat	1486
Spool	327
Inner wall	374
Spool top, shell top	4520
Plasma shell	408
Graphite	21.1
Water pipe	153
Breeder blanket	145
Outer shell	361
OH coil	0
EI coil	0
EO coils	0
Blip coils	8280
OH cryostat	8.8

walls can be seen in Fig. 7.7. A summary of conclusions regarding the selection of the vacuum chamber structure is given in Table 7.5.

7.4.4 Conclusions and Recommendations

The testing of rf-assisted startup on ISX-B needs to be continued. If the results are satisfactory, then ECRH tubes should be developed before the final design configuration is required for FED.

The feasibility of startup using LHRH or ICRH needs to be tested on the Princeton Large Torus (PLT). If the tests are successful, a design value for the power needed for FED should be determined.

The physics effort should be continued to determine the minimum voltage and time required to reliably start up the FED, using an OH system (blip coils) and impurity levels consistent with those achievable in FED.

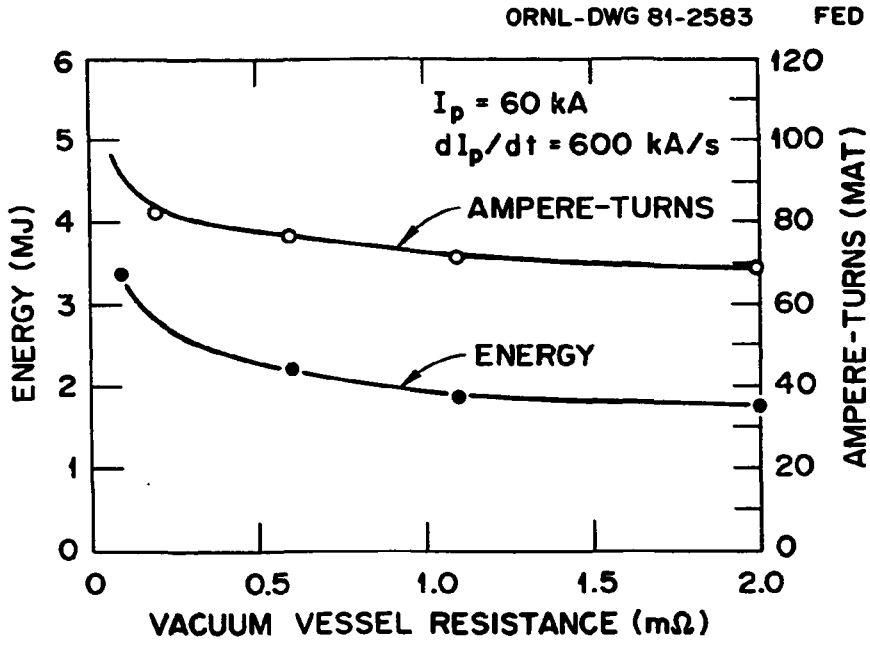

Fig. 7.5. Energy and ampere-turns to provide initial startup with blip coils.

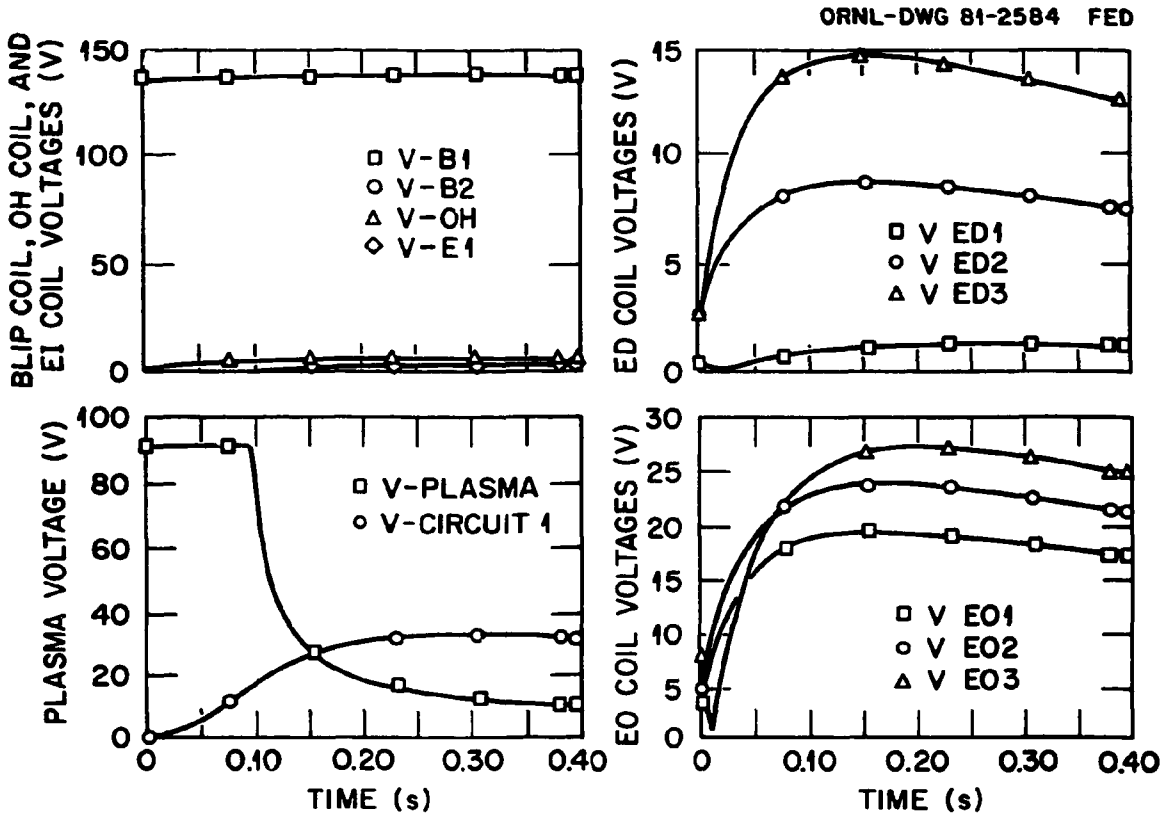

Fig. 7.6. Voltages in PF coils and plasma during startup.

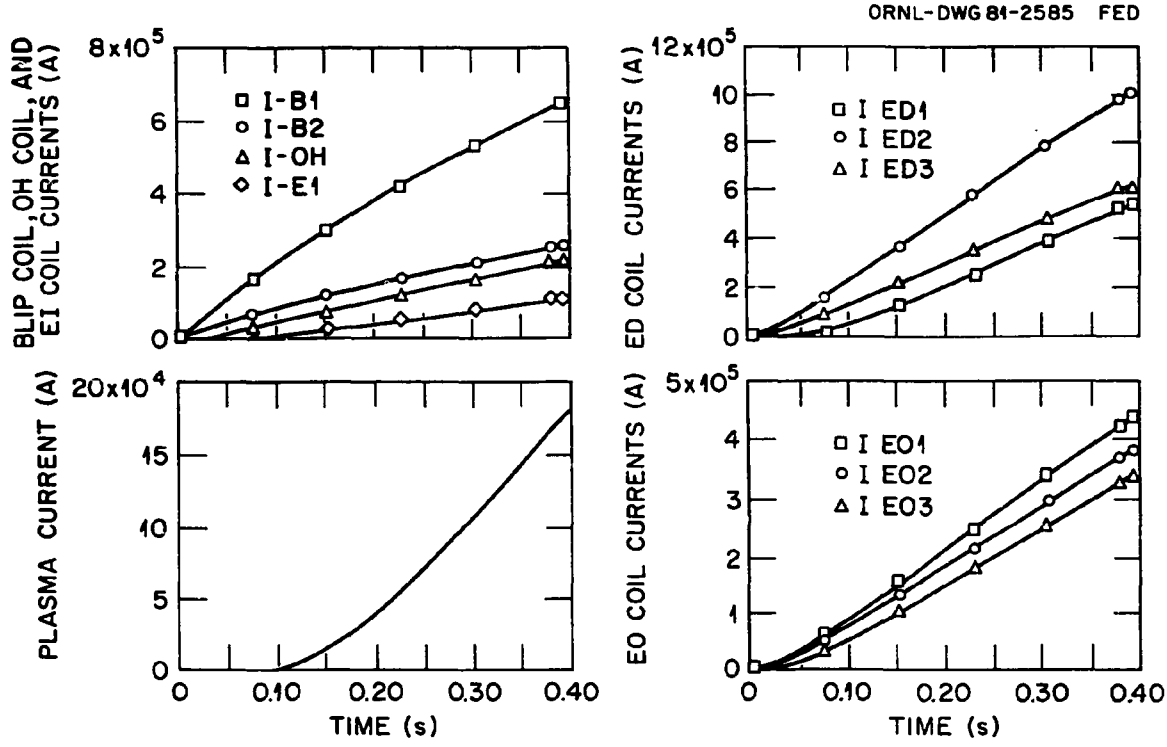

Fig. 7.7. Currents in PF coils and plasma during startup.

Table 7.5. Selection of vacuum chamber structures

Conducting liner or wall near plasma
Segment walls: should use 1-cm-thick stainless steel with internal connections
First wall: can be either carbon blocks and/or stainless steel coolant pipes with electrical connections to the segment walls to eliminate arc voltages
External walls of vacuum vessel
Should have relatively high toroidal resistance for external shells
Should use laminated neutral shield material
External structures
Blip coils should be located above and below vacuum vessel
Dewar for superconductors should have no insulating breaks
External poloidal coil case should be limited to approximately 50-ms time constants

The use of a small amount of ECRH ($\sim$1 MW) for plasma initiation appears to be the most efficient and perhaps the most relevant for future reactors. Thus, the development required to prove this method of startup should be pursued.

There is a high probability that rf heating, either ICRH or LHRH, will be most advantageous for bulk heating. If these rf power sources are available it may be more advantageous to use them instead of ECRH for plasma initiation, even if they are less efficient for the initation phase of startup.

7.5 DISRUPTION-INDUCED EDDY CURRENT STUDIES

7.5.1 Purpose

During a plasma disruption, large eddy currents are induced in the reactor structure. These currents can result in electric arcs between structures, with consequent surface erosion. The eddy currents are induced toroidally (in the plasma current direction) and interact with

the poloidal magnetic field to cause J × B forces on the structures. If the structure is designed so that radial current paths are required to complete the eddy current circuits, then the radial currents will also interact with the toroidal field to cause much larger J × B forces on the structures. The eddy currents also cause resistive heating in the structures, which is of concern for those structures that are cryogenically cooled. Another effect of a plasma disruption is that electric potentials are induced in the PF coils, and these induced voltages constrain the coil design. The analysis of these electromagnetic effects resulting from plasma disruptions was undertaken to determine the reactor design characteristics required to withstand or reduce the induced currents, voltages, and forces.

7.5.2 Assumptions and Guidelines

The disruption is simulated by assuming that the plasma remains fixed in space and that the plasma current decays linearly to zero over a period of 20 ms. The disruption time for the FED baseline is 10 ms, and this value will be used in future studies. The currents induced in the first wall will be greater (but by less than a factor of 2) than those reported here for a 20-ms disruption. The reactor structures and magnets for the present analysis are modeled after the ETF design 2 configuration of July 1980 and are representative of the current FED baseline. The characteristic frequency of the disruption is low enough that skin currents can be neglected. The skin depth in a steel conductor is 3 cm for a characteristic time of 1 ms or 15 cm for a characteristic time of 20 ms, while the thickness of the structures is typically 1 cm.

7.5.3 Description of Analysis

The reactor structure and PF coils are modeled as a set of mutually coupled toroidal circuits of rectangular cross section (Fig. 7.8). The self-inductance and mutual inductance of these circuits are calculated by a numerical integration code. The set of equations representing the circuits,

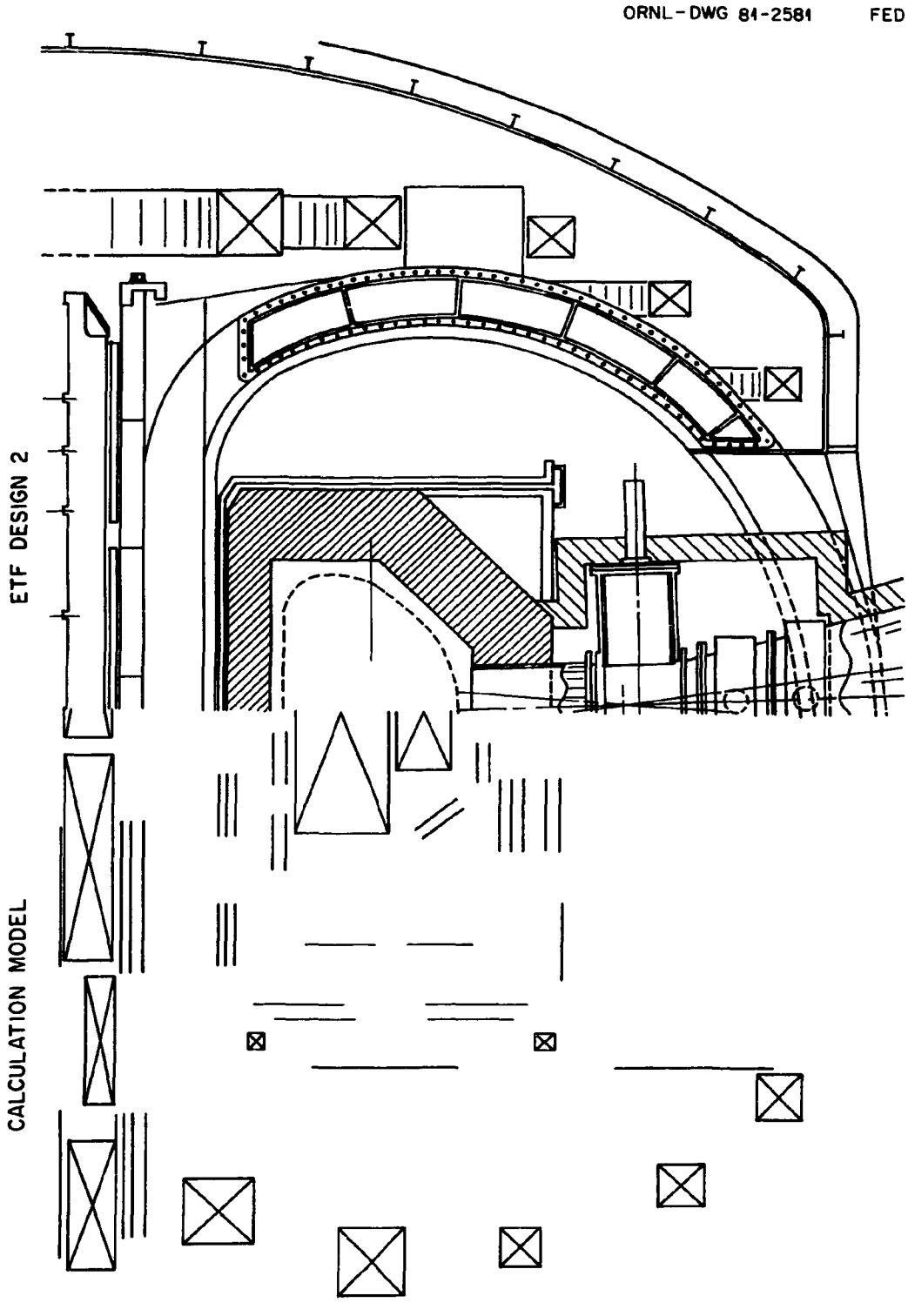

Fig. 7.8. Model of reactor configuration.

$$V_i = M_{ij}\dot{I}_j + L_i\dot{I}_i + R_iI_i \ ,$$

where L and M are the circuit self-inductance and mutual inductance and V, I, and R are the voltage, current, and resistance, respectively, is solved by iteration, subject to the forcing function on the plasma current. Using the calculated currents, the poloidal magnetic field and the electromagnetic forces on the structures as functions of space and time are calculated. The analysis has been performed for cases with and without electrical connections between the torus shield sectors at the first wall, for designs with and without toroidal insulating breaks, and for different structural materials.

7.5.4 Results

The directions of the magnetic fields and induced currents at the first wall of a torus shield sector are shown in Fig. 7.9. The toroidal current and vertical field cause a J × B force on the first wall, directed toward the plasma. This force is equivalent to a surface force of 0.2-0.5 MPa. If the shield sectors are not electrically connected to each other at the first wall, radial current paths exist between the front and back walls of the sector. The radial currents and toroidal field cause J × B forces on the side walls of 3-5 MN. These forces cause a twisting force on the sector because they make the sector side walls attempt to rotate in opposite directions. The sector must be designed to withstand these loads, but they do not impose a serious design constraint.

The potential induced in the PF coils is much less if the shield sectors are electrically connected at the first wall (Table 7.6). Two of the coils in this configuration require additional shielding to meet the nominal design criteria of 25 V/turn.

The current densities calculated for the structural paths when the first wall is electrically connected are shown in Table 7.7. The temporal peak current density is the maximum sum of the currents in all of the conductors used to simulate a surface divided by the actual surface

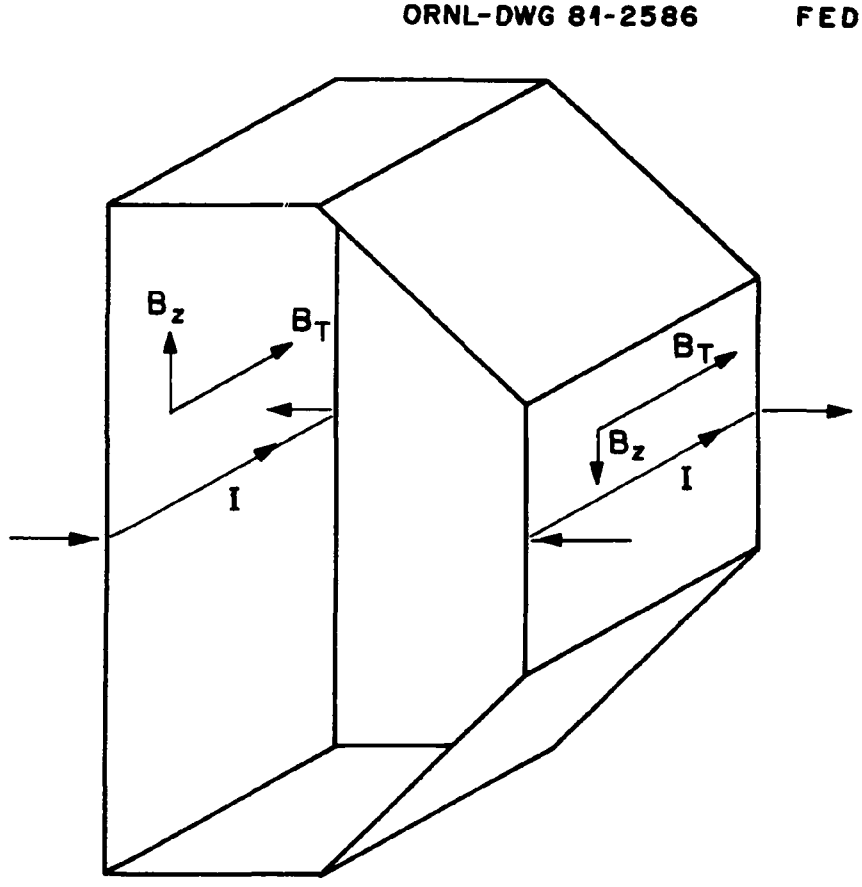

Fig. 7.9. Eddy current and magnetic field directions on torus shield sector first wall.

Table 7.6. Induced voltages during disruption

Coil	Case with conducting vessel		Case with electrical break
	Volts/turn	Peak (kV)	Peak (kV)
EI	22.0	14.0	31.0
ED1	0.25	0.1	8.8
ED2	5.8	2.1	33.0
ED3	14.0	4.0	22.0
EO1	23.0	2.6	10.0
EO2	37.0	5.0	7.0
EO3	82.0	11.0	48.0
OH	3.1	2.2	80.0

Table 7.7. Maximum current densities

Surface	Total surface maximum ms	Total surface maximum A/cm^2	Local maximum A/cm^2
Inside wall			
Inboard			
Graphite	20	200	520
Shield	20	2800	7300
Outboard			
Pipes	20	1600	4500
Shield	21	1300	4000
Top	20	1200	3800
Divertor	150	2600	8200
Outside shield wall			
Inboard	25	800	2800
Outboard	45	470	1200
Top	40	420	830
Spool	38	420	2500
TF dewar	40	260	2300
Bucking cylinder	120	50	180

cross-sectional area. The local maximum is the maximum current in a given conductor divided by the area of that conductor. The inner surface currents peak at 20 ms, and the outer torus surfaces peak at about 40 ms. The limiter, which is equivalent to the divertor collection plate in the model, is copper, and the current does not peak during the 150-ms time interval used in the calculation (Fig. 7.10). The maximum current density that must be carried between either the inboard or outboard sector inside walls is approximately 8000 A/cm^2 (Table 7.7).

If the shield sectors are not connected near the first wall to form a continuous toroidal current path, then arcs will develop between the sectors and cause erosion of the surface material. The amount of material eroded is on the order of 1 g for the steel first wall and 10 g for the copper limiter plate. Since the arcing will be localized, this erosion may result in failure of coolant passages. If low resistance materials are used (e.g., aluminum first wall pipes), the current will concentrate in these conductors and the arc erosion will be greater. If insulating breaks are used in the toroidal current paths, then the voltages induced in the poloidal coils will be greater.

The mechanical design of contacts required to connect the first walls is a key issue. Preliminary analyses show that the walls must be connected across 50-100% of the gap with a contact pressure on the order of 7 MPa to prevent melting at the contact surface. This pressure can be provided by mechanical or electromagnetic forces. Figure 7.11 is a conceptual design of a compressible metal seal contact, which relies mainly on the elasticity of the metal to provide the contact pressure. Stress relaxation due to neutron radiation will limit the life of such a contact. The electromagnetic forces induced by the disruption can also supply contact pressure. Figure 7.12 represents a conceptual design that makes use of these forces both to close the contact and to provide the pressure. The preliminary concepts identified here will be developed further in future work.

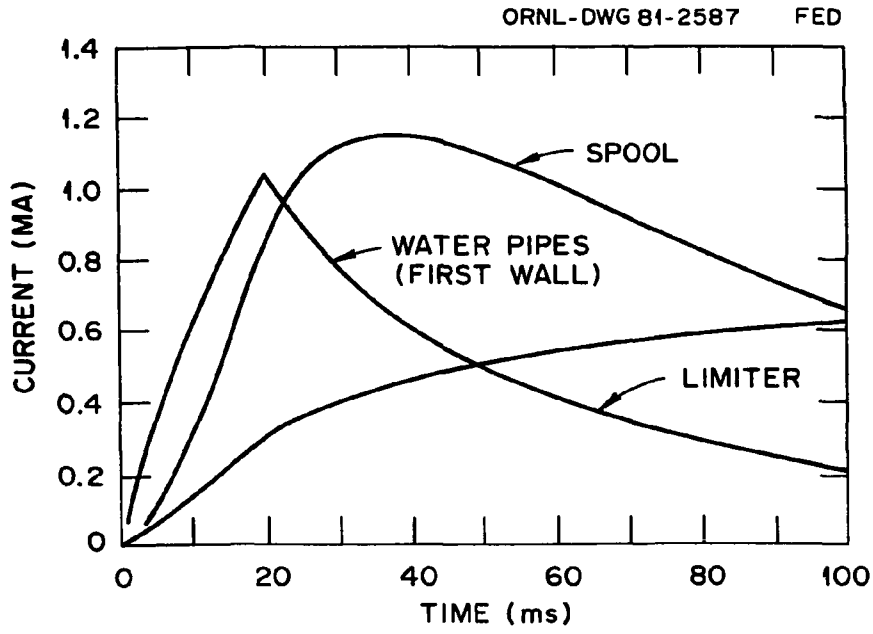

Fig. 7.10. Currents in structures.

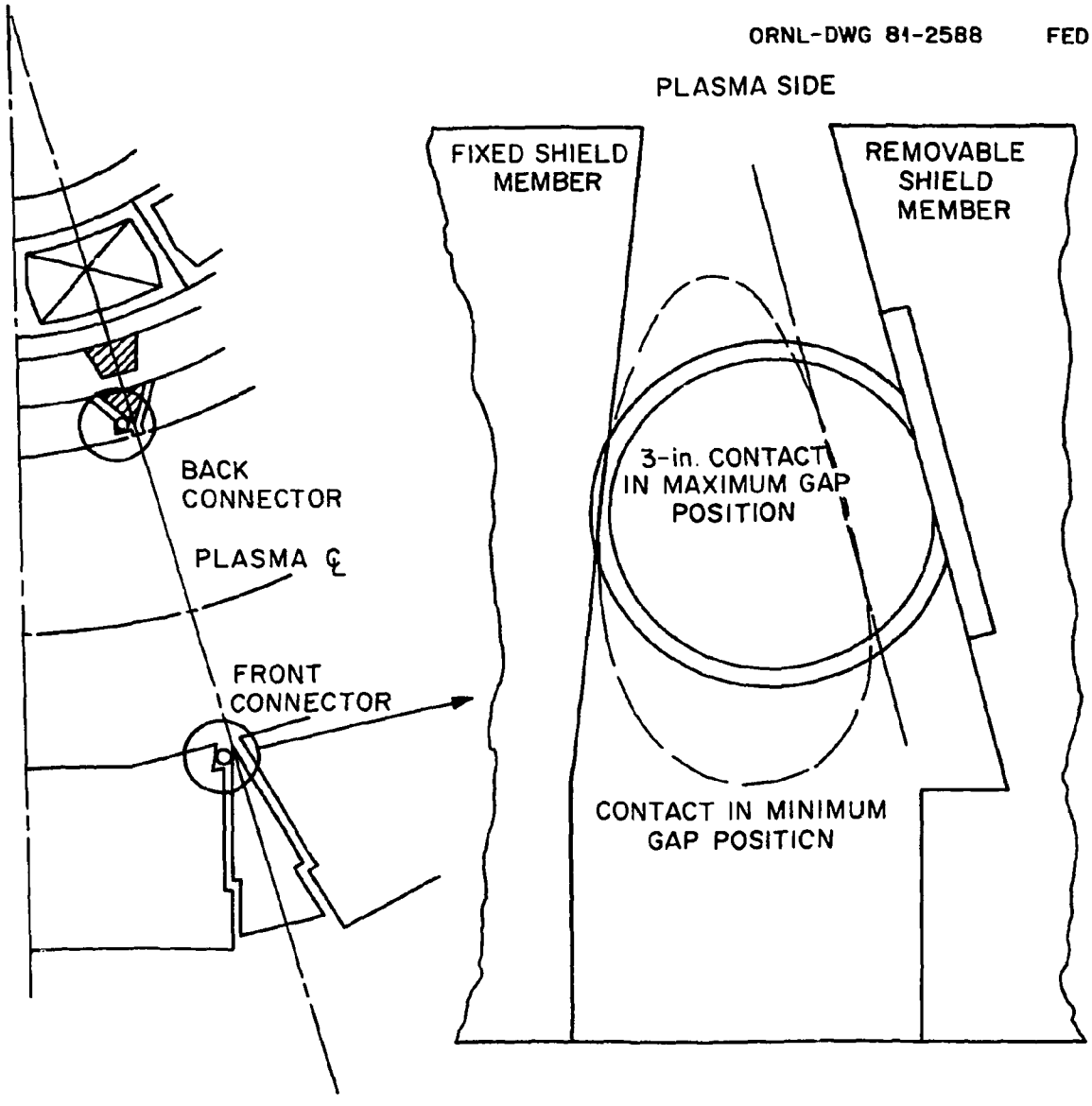

Fig. 7.11. Compressible metal seal contact.

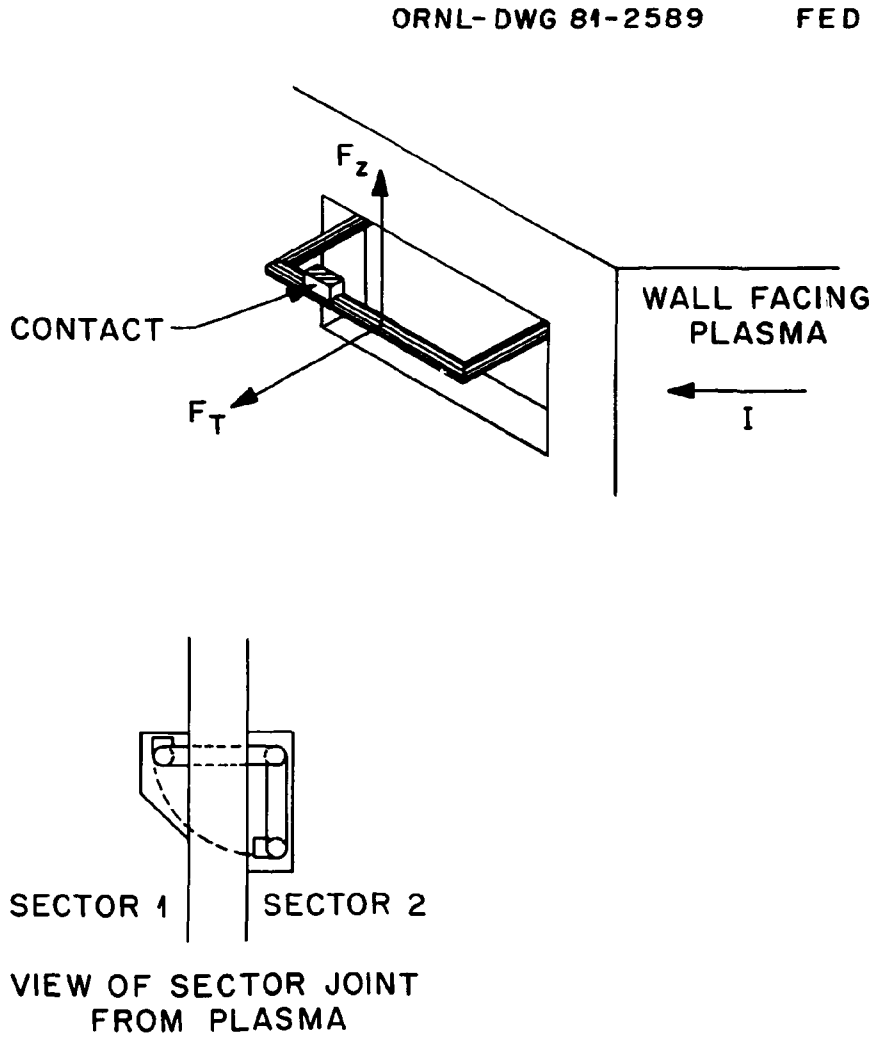

Fig. 7.12. Contact operated by electromagnetic forces.

7.5.5 Conclusions and Recommendations

The shield sectors should be electrically connected to each other at or near the first wall to form a continuous toroidal current path without arcs. Toroidal insulating breaks in the structures should not be used, and the use of low resistance materials, such as copper or aluminum, should be minimized and carefully engineered with respect to eddy currents. An electromagnetic analysis of the reference design, following these recommendations, will be performed for the updated FED configuration.

7.6 PLASMA POSITION CONTROL

7.6.1 Purpose

This study was performed to provide guidance for establishment of control coil power requirements. These requirements relate to a thick torus wall that would be used in a reactor design. Relationships between plasma time constant, plasma movement, and plasma current are investigated. The results indicate feasibility of position control in the presence of large step changes in the plasma time constant.

7.6.2 Assumptions

The assumptions made for this study are:

1. Plasma current distribution is assumed to be approximately parabolic and can be modeled with six segments, each with uniform current distribution.
2. Current distribution inside the plasma does not change, but current magnitude does.
3. Plasma moves with constant cross section.
4. Toroidal field effects on plasma position or current are not included.
5. Plasma pressure effects are not included.
6. The plasma moves without hitting limiter or wall.

7. The torus, mechanical support structures, and PF coils are simulated with 72 annular conductors.
8. The control coil position, the error sensing system, and the gain control were arbitrarily selected and not optimized.
9. Plasma movement is related to changes in magnetic energy.
10. Change of mutual inductances between plasma and structure or coils is approximated with linear interpolation.

7.6.3 Description of Study

The study effort began with a specified tokamak configuration that was representative of FED. This configuration was modeled with 72 mutually coupled circuits simulating the PF coils and structural plates. A mutual inductance matrix was generated using the physical sizes, shapes, and locations of the conductors. Equations were derived to relate changes in stored energy in the conductor set to plasma movement in the radial (R) and vertical (Z) directions. Using these equations, relationships between coil energy, plasma time constant, plasma current, and plasma position were investigated.

This investigation generally followed the route of assuming that the plasma is at equilibrium at $t = 0$ with the plasma center located at $R = 0$, $Z = 0$. Displacement of the plasma in the radial and vertical directions is measured from this equilibrium position. The plasma is then given a selected instantaneous change in time constant ($L_p/R_p = \tau_p$). This causes changes in plasma current (I_p) and plasma position (R and Z), as well as changes in the other coil currents. Sensing of plasma shift is assumed to be via detecting eddy currents in the inner wall of the torus. This sensed signal is amplified with a selected gain G and fed back to the control coils. The system is diagrammed in Fig. 7.13. Plots of the changes in plasma current, plasma radius, plasma vertical position, and control coil power are generated as a function of time for the given values of plasma time constant and gain.

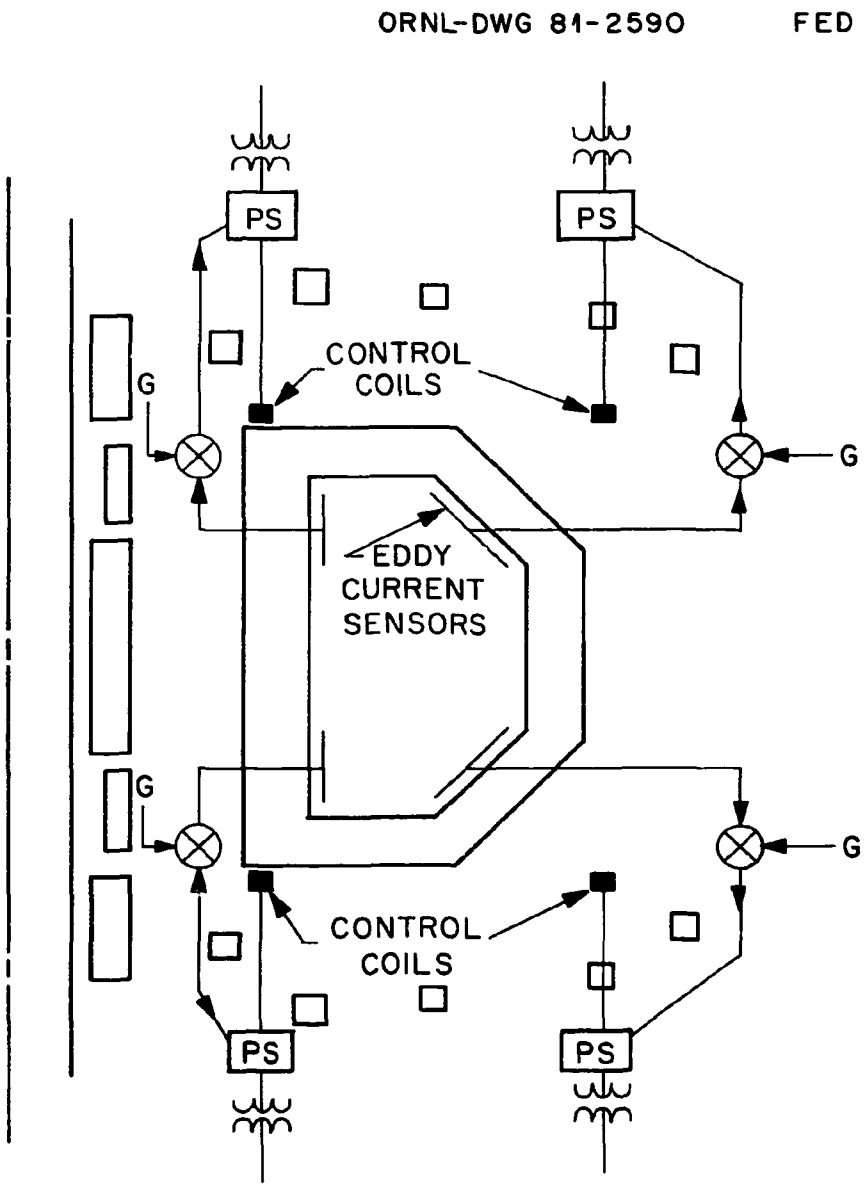

Fig. 7.13. Plasma position control diagram.

7.6.4 Results

Figure 7.14 is representative of the plots of I_p, R, Z, and control coil power vs time for given values of τ_p and G. In the plots shown, τ_p = 40 s and G = 30. Maximum values of R and Z are identified as R_m and Z_m, with the time that the maxima occur identified as t_m.

Figure 7.15 shows how the radial displacement and recovery time vary for a simple feedback system with G = 30 when the magnitude of the plasma time constant is varied from 20 to 100 s. During normal operation, the plasma time constant is nearly 1000 s, so using τ_p = 20 s represents a 50:1 change from normal. We note that the radial displacement is held to less than 1.3 cm over this range.

Figures 7.16 and 7.17 show radial and vertical plasma displacement for G = 20 with the plasma time constant varied from 20 to 100 s. In these cases the maximum radial displacement is about 1.4 cm and the maximum vertical displacement was slightly greater than 2 cm.

Figure 7.18 shows the control coil energy requirements for G = 20. The curves are marked to show energy at the point where the plasma has reached maximum displacement and begins to return to its original position.

7.6.5 Conclusions and Recommendations

In none of the cases shown did the control power exceed a total of 25 MW for the four coils before the plasma returned to the R = 0, Z = 0 position. It would be possible to increase the gain for the longer plasma time constants so as to further decrease the maximum control power and plasma displacement, while also decreasing the time required to return the plasma to its original position.

For plasma time constant changes as large as 50:1 from normal plasma conditions, the plasma radial movement is held to less than 2 cm with reasonable loop gains in a simple feedback system. Power requirements are on the order of 25 MW for four control coils when the plasma begins to return to its original position. Work remains to be done in optimizing control coil locations, selecting the method of feedback,

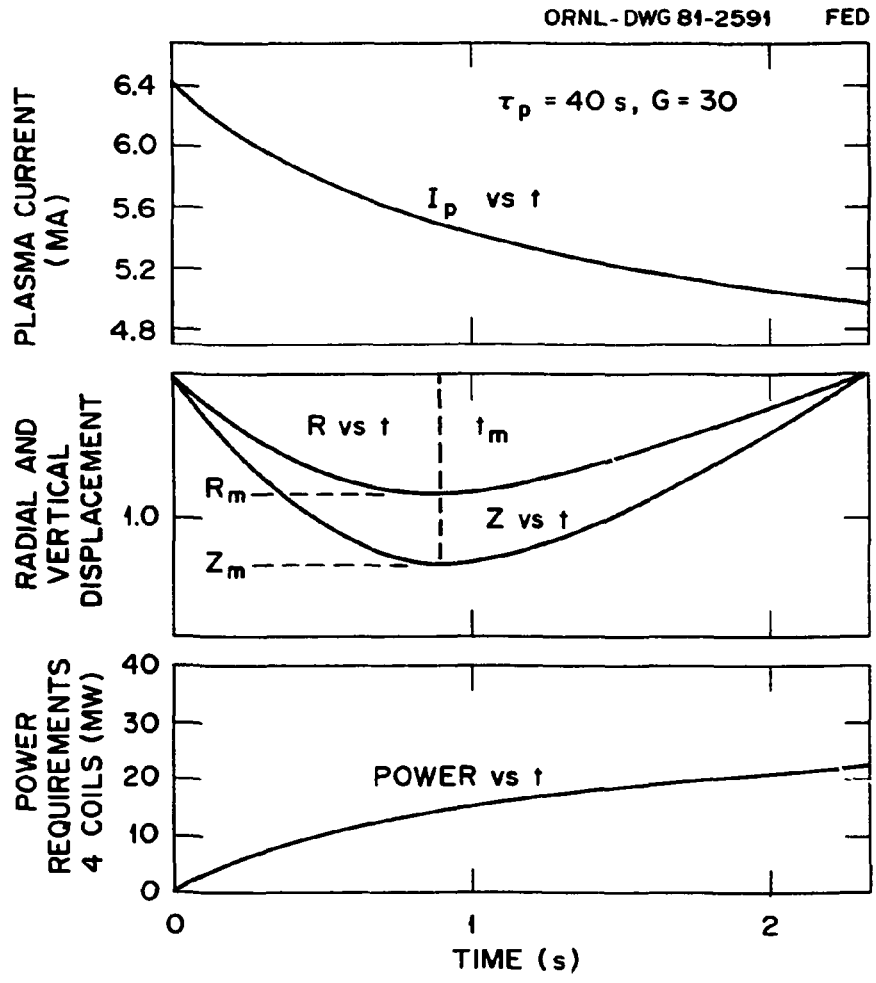

Fig. 7.14. Plasma current, position, and control power for 25:1 change in plasma time constant.

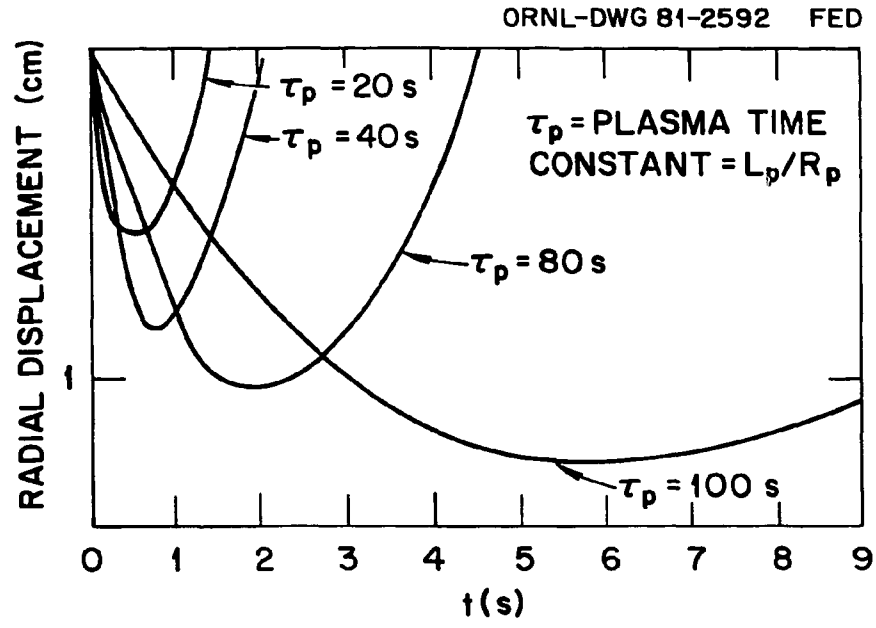

Fig. 7.15. Radial plasma displacement (G = 30).

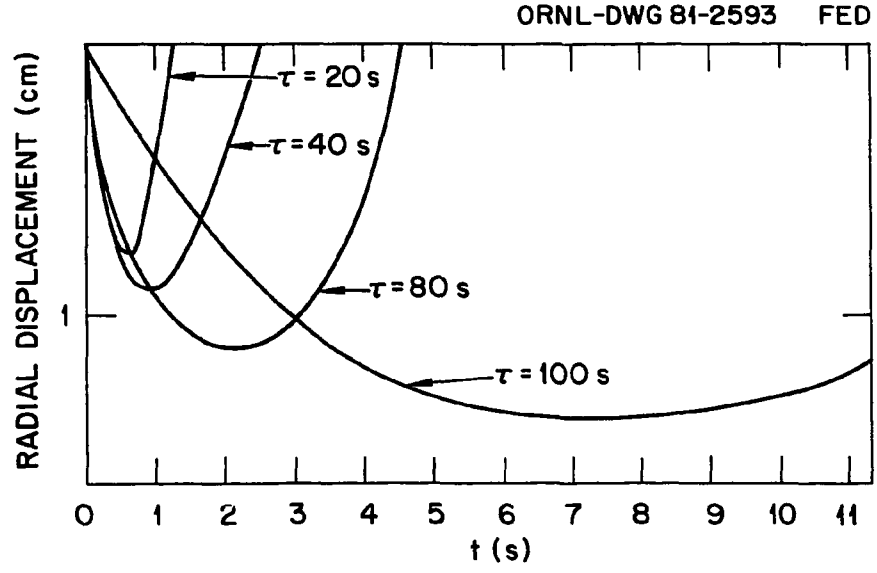

Fig. 7.16. Radial plasma displacement (G = 20).

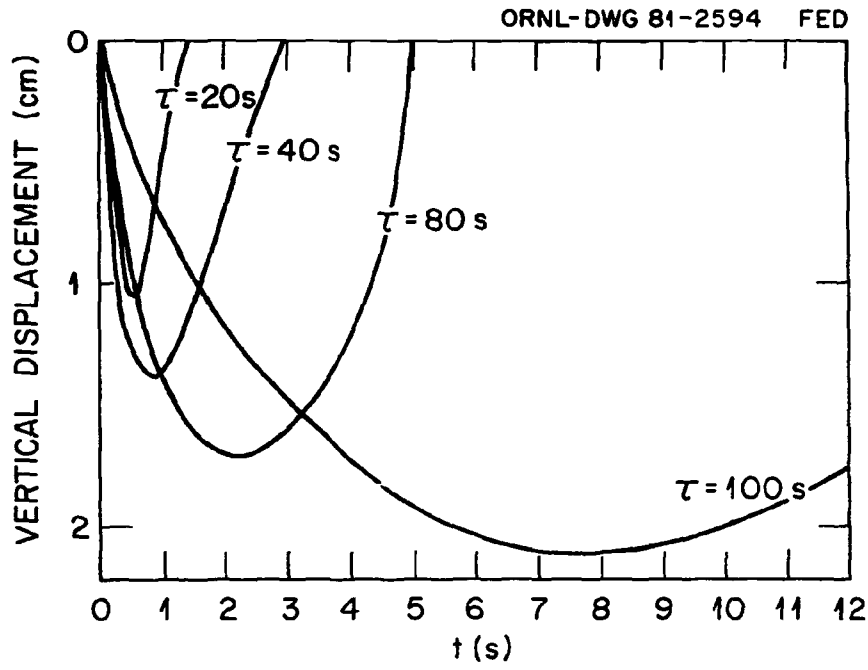

Fig. 7.17. Vertical plasma displacement (G = 20).

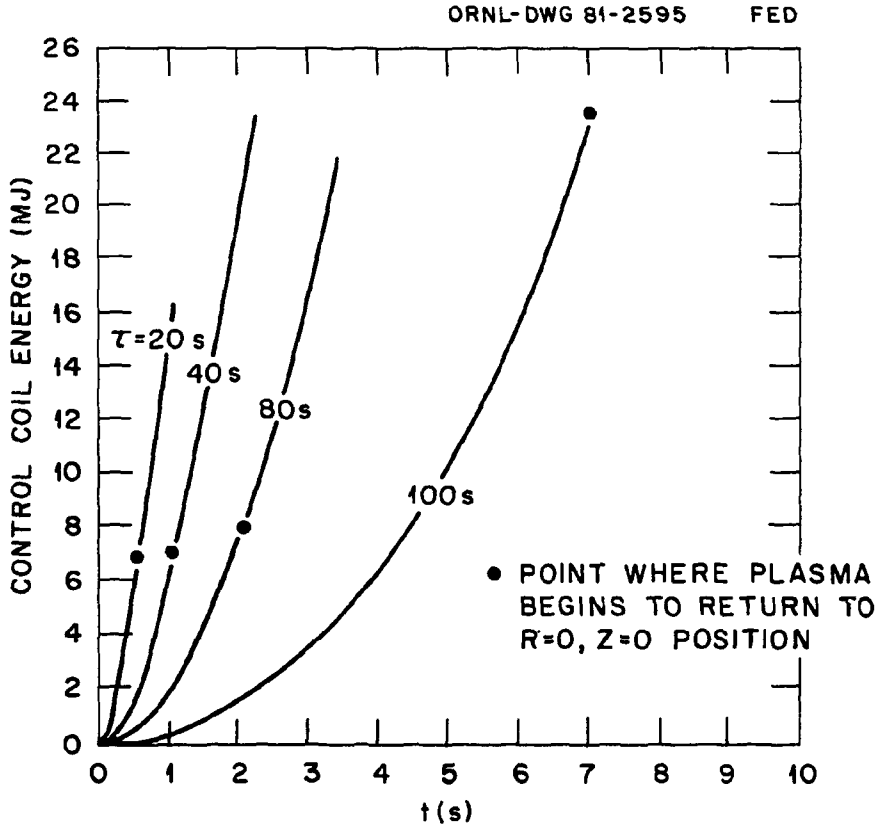

Fig. 7.18. Control energy requirements (G = 20).

determining sensors to detect the plasma movement, and determining allowable plasma movement. In addition, the analysis should be extended by removing or modifying some of the simplifying assumptions.

7.7 SUMMARY

The major conclusions of the electrical systems analyses are summarized below.

1. Heating Systems. A viable rf bulk heating concept has been developed for FED application. However, launcher designs for a reactor-relevant machine require more effort. Neutral beam injection appears to be a feasible, practical alternative to rf bulk heating in FED.

2. FED Startup Options. The use of small amounts of ECRH ($\sim$1 MW) for plasma initiation appears to be most efficient and may be most relevant for reactors. Thus, the development required to prove this method of startup should be pursued. There is a high probability that rf heating, either ICRH or LHRH, will be most advantageous for bulk heating. If these rf power sources are available it may be more cost-effective to use them rather than ECRH for plasma initiation, even if they are less efficient for the initiation phase of startup. The physics effort should be continued to determine the minimum voltage and time required to reliably start up the FED using an OH system (blip coils) and impurity levels consistent with those achievable in FED.

3. Disruption-Induced Eddy Current Studies. In order to mitigate the effects of disruption-induced eddy currents, the shield sectors should be electrically connected to each other at or near the first wall to form a continuous toroidal current path. Toroidal insulating breaks in the structures should not be used, and the use of low resistance materials, such as copper or aluminum, should be minimized and carefully engineered with respect to eddy currents. An electromagnetic analysis of the reference design, following these recommendations, will be performed for the updated FED configuration.

4. Plasma Position Control Studies. For plasma time constant changes as large as 50:1 from normal plasma conditions, the plasma radial movement is held to less than 1 cm with reasonable loop gains in

a simple feedback system. Power requirements are on the order of 25 MW for four control coils when the plasma begins to return to its original position. Work remains to be done in optimizing control coil locations, selecting the method of feedback, determining sensors to detect the plasma movement, and determining allowable plasma movement. In addition, the analysis should be extended by removing or modifying some of the simplifying assumptions.

REFERENCES

1. L. Stewart (Exxon Nuclear Corporation) and J. Kamperschroer (General Atomic Company), ETFNB, computer code for the Engineering Test Facility Neutral Beam analysis.
2. Y-K. M. Peng, S. K. Borowski, and T. Kammash, Nucl. Fusion 18, 1489 (1978).
3. T. Cho, S. Kubo, M. Ikeda, T. Saito, Y. Terumichi, Y. Hamada, and S. Tanaka, Phys. Lett. 77A(5) 318 (1980).
4. R. M. Gilgenbach et al., *Electron Cyclotron/Upper Hybrid Resonant Preionization in the ISX-B Tokamak,* NRL Memorandum Report 4248, Naval Research Laboratory (June 1980).

8. SYSTEMS ENGINEERING*

T. E. Shannon[†]

G. E. Smith[‡] R. L. Reid[†]

R. J. Barrett[§] W. T. Reiersen[‡]

C. A. Flanagan[‖] K. F. Wu[†]

8.1 INTRODUCTION

On October 30, 1980, the Design Center issued an initial set of parameters to provide a preliminary characterization of the FED. These parameters have served as a point of departure for a series of trade studies, design investigations, and systems analyses directed toward further definition of the FED.

This section summarizes the results of a number of system-level trade studies and analyses carried out over the past four months. These studies were performed to gain further insight into the manner in which device cost and performance are affected by variation of basic machine parameters. In the same vein, studies directed toward facility cost drivers have also been performed. The studies performed and summarized in this section are:

- Variation in plasma minor radius (Sect. 8.2).
- Increase in neutron wall loading (Sect. 8.3).
- Variation in inboard shield thickness (Sect. 8.4).
- Variation in fusion power (Sect. 8.5).

---

*The authors gratefully acknowledge contributions to this section made by E. H. Diamond and R. E. Nygren.

[†]Fusion Engineering Design Center/Oak Ridge National Laboratory.

[‡]Fusion Engineering Design Center/Grumman Aerospace Corporation.

[§]Fusion Engineering Design Center/Burns and Roe, Inc.

[‖]Fusion Engineering Design Center/Westinghouse Electric Corporation.

- Estimate of the number of full field pulses over the device lifetime (Sect. 8.6).
- Device size and cost sensitivity to number of pulses (Sect. 8.7).
- Description of the FED facility (Sect. 8.8).
- Tokamak test cell cost sensitivity to size, proportions, and over-pressure requirements (Sect. 8.9).

Results are summarized in Sect. 8.10.

8.2 PLASMA MINOR RADIUS VARIATION

8.2.1 Purpose

The purpose of this study was to investigate the impact of variation in plasma minor radius on tokamak performance and cost if neutron wall loading were held constant.

8.2.2 Assumptions and Guidelines

This trade study was conducted about a fixed neutron wall loading of 0.44 MW/m^2 (the present FED value) under the following assumptions. The maximum field at the toroidal field (TF) coil was held at 8.0 T. Beta was varied inversely with aspect ratio from a base value of 6% at an aspect ratio of 3.7. The inboard shield thickness was held constant at a value of 0.70 m. The ohmic field swing was from +7 T to -7 T.

Note that imposing the requirements of both fixed neutron wall loading and fixed field at the TF coil yields a unique combination of values for aspect ratio and field on axis for a given plasma minor radius.

8.2.3 Description of Analysis Results

Table 8.1 shows performance, cost, and burn time as functions of the plasma minor radius. Decreasing the plasma minor radius from the base value of 1.3 m to 1.1 m (with an associated increase in both field on axis and aspect ratio) yields an increase in burn time to approximately 1000 s for a 6% increase in cost. Performance is degraded in that Q decreases from 5.3 to 4.0. In essence, enhanced burn time is traded for

Table 8.1. Trade studies about a neutron wall loading of 0.44 MW/m^2

a (m)	R_o (m)	A	B_T (T)	β (%)	I_p (MA)	Q	P_{fusion} (MW)	P_{aux}[a] (MW)	t_{burn} (s)	Cost (relative)
1.1	5.3	4.8	4.3	4.6	4.5	4.0	170	43	1040	1.06
1.2	5.0	4.2	3.9	5.3	5.3	4.5	170	38	520	1.02
1.3	4.8	3.7	3.6	6.0	6.2	5.3	180	34	100	1.00
1.4	4.8	3.4	3.4	6.5	7.0	6.2	195	31	-[b]	1.04

[a] Amount of injected power required to maintain plasma at the specified operating point.

[b] Insufficient volt-seconds to achieve current startup.

lower Q. Increasing the minor radius from 1.3 m to 1.4 m (with an associated decrease in both field on axis and aspect ratio) results in a tokamak configuration that has insufficient volt-seconds to achieve current startup. Disregarding the startup limitation, this configuration achieves a slight increase in performance (Q increases from 5.3 to 6.2) for a 4% increase in cost.

Decreasing the plasma minor radius, as indicated, results in increased burn capability for a fixed ohmic heating (OH) flux swing of +7 T to -7 T. If a constant burn of 100 s were desired at reduced plasma minor radius, the flux swing could be decreased (OH solenoid sized for lower field), except for the tokamak with the 1.4-m minor radius. This configuration requires an OH flux swing from +8.4 T to -8.4 T, which violates the 7-T limit imposed on the OH solenoid. For the criterion of constant burn time, cost is seen to achieve a shallow minimum at a minor radius of 1.2 m as shown in Table 8.2.

8.2.4 Conclusions and Recommendations

For the constraints considered in this trade study, it is concluded that reducing the plasma minor radius from 1.3 m to 1.2 m (with an associated increase in aspect ratio and field on axis to 4.2 and 3.9 T, respectively) has some positive cost benefit impact. This configuration would achieve an increase in burn time of approximately 400 s for essentially the same cost but at a reduction in Q of 15%.

8.3 NEUTRON WALL LOADING

8.3.1 Purpose

The purpose of this study was to determine the impact of neutron wall loading on FED performance and cost.

8.3.2 Assumptions and Guidelines

This study was conducted subject to the following constraints: Beta was held fixed at 6%. The maximum field at the TF coil was maintained

Table 8.2. Trade studies about a neutron wall loading of 0.44 MW/m^2 (B_{OH} = variable)

a (m)	R_o (m)	A	B_T (T)	β (%)	I_p (MA)	Q	P_{fusion} (MW)	P_{aux}[a] (MW)	t_{burn} (s)	Cost (relative)
1.1	5.3	4.8	4.3	4.6	4.5	4.0	170	43	100	1.02
1.2	5.0	4.2	3.9	5.3	5.3	4.5	170	38	100	0.99
1.3	4.8	3.7	3.6	6.0	6.2	5.3	180	34	100	1.00
1.4	4.8	3.4	3.4	6.5	7.0	6.2	195	31	100	1.04

[a]Amount of injected power required to maintain plasma at the specified operating point.

at 8.0 T. Aspect ratio was set at a value of 3.7, the current FED value. Inboard shield thickness was varied from 0.67 m to 0.80 m as a function of neutron wall loading in order to maintain approximately the same heat load to the TF coils. Burn time per pulse was maintained at approximately 100 s. Maximum flux swing of the OH coil was limited to +7 T to -7 T.

8.3.3 Description of Analysis Results

The results of this study, normalized to present FED values and presented in Fig. 8.1, show that capital cost varies almost linearly with neutron wall loading. A change of ±20% in neutron wall loading results in a ±10% change in cost. At each value of wall loading, the plasma minor radius and the field on axis were determined consistent with constant values of aspect ratio and maximum toroidal field. The field in the OH solenoid was selected consistent with a burn time of approximately 100 s but was not allowed to exceed 7.0 T. Table 8.3 presents additional parameters for some of the points that make up the curve of Fig. 8.1. As previously indicated, cost decreases with decreasing values of neutron wall loading. However, fusion power also decreases while plasma heating power increases, resulting in lower values of Q. The minimum value of neutron wall loading consistent with the constraints of this study is approximately 0.3 MW/m^2, imposed by limitations on the volt-second capability of the OH coil. As wall loading decreases to this value, the self-consistent plasma minor radius is 1.16 m. When coupled with the fixed aspect ratio of 3.7, this value produces just enough volt-seconds to provide 100 s of burn. A further reduction in wall loading and plasma minor radius would result in a tokamak configuration that would burn for less than 100 s.

8.3.4 Conclusions

The capital cost and performance of FED are dependent on the selected value of neutron wall loading. The minimum-cost FED is therefore dependent on the minimum neutron wall loading and the lowest value of Q deemed necessary to achieve the goals of a FED.

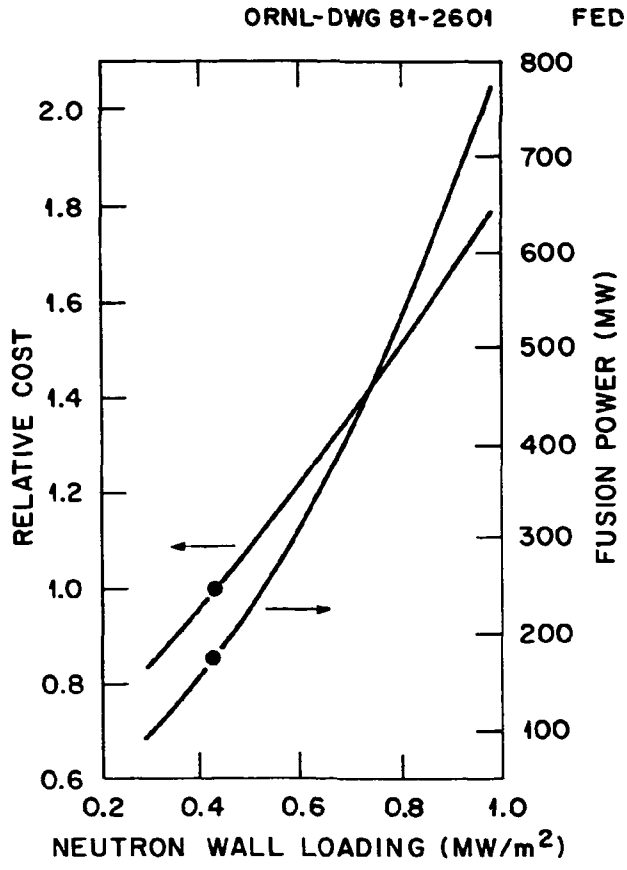

Fig. 8.1. Capital cost and fusion power vs neutron wall loading (A = 3.7, β = 6%, B_m = 8 T, t_{burn} = 100 s).

Table 8.3. Key parameters for selected points used to develop the curves in Fig. 8.1

Parameter	Case 1	Case 2	Case 3	Case 4	Case 5
L_w (MW/m^2)	0.30	0.44	0.50	0.70	1.00
a (m)	1.16	1.30	1.36	1.55	1.80
A	3.7	3.7	3.7	3.7	3.7
R_o (m)	4.3	4.8	5.1	5.7	6.6
B_t (T)	3.4	3.6	3.7	3.9	4.1
I_p (MA)	5.2	6.2	6.6	7.9	9.7
P_{fusion} (MW)	97	180	225	405	780
Q	2.4	5.3	7.6	46	∞
P_{htg}[a] (MW)	43	36	34	34	39
P_{aux}[b] (MW)	41	34	30	9	0

[a] Maximum heating power to get to the operating point.

[b] Heating power to sustain the operating point.

8.4 INBOARD SHIELD THICKNESS

8.4.1 Purpose

The purpose of this study was to determine the effect of varying inboard shield thickness on capital cost, TF coil dose rate, performance, and unit capital cost [$/kW(t)].

8.4.2 Assumptions and Guidelines

The study was conducted for the following fixed parameters:

Plasma minor radius, a	1.3 m
Maximum TF field, B_m	8 T
Beta, β	6%
Burn time, t_{burn}	100 s
OH field, B_{OH}	±7 T
Number of cycles, N	3.5×10^5

8.4.3 Description of Analysis Results

The results of varying the inboard shield thickness from 0.5 m to 0.8 m are shown in Figs. 8.2-8.5. Figure 8.2 shows that capital cost variation with shield thickness is slight, approximately 1.0% relative to the base FED cost at a shield thickness of 0.7 m. The capital cost decreases with decreasing shield thickness down to ∿0.6 m and then increases as shield thickness is further decreased. Values of aspect ratio and field on axis are also shown in Fig. 8.2 as a function of shield thickness. The minimum in capital cost as a function of shield thickness occurs when cost associated with decreased tokamak size, indicated by aspect ratio in Fig. 8.2, is compensated for by increased TF coil refrigeration cost due to the thinner shields, as shown by the system cost summary presented in Table 8.4. Figure 8.3 shows that fusion power and neutron wall loading increase as shield thickness decreases. The result is a decrease in unit cost [$/kW(t)] with decreasing shield thickness, as shown in Fig. 8.4. Q, shown in Fig. 8.5, is enhanced as the result of decreased shield thickness. Increased Q and decreased

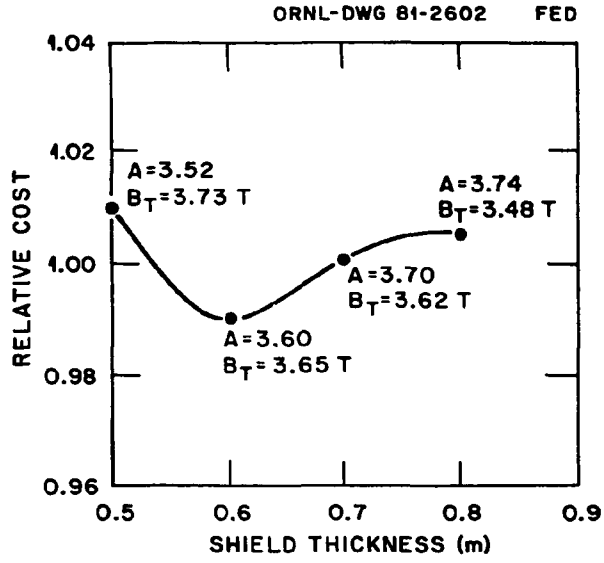

Fig. 8.2. Capital cost vs shield thickness (a = 1.3 m, β = 6%, B_m = 8 T, t_{burn} = 100 s).

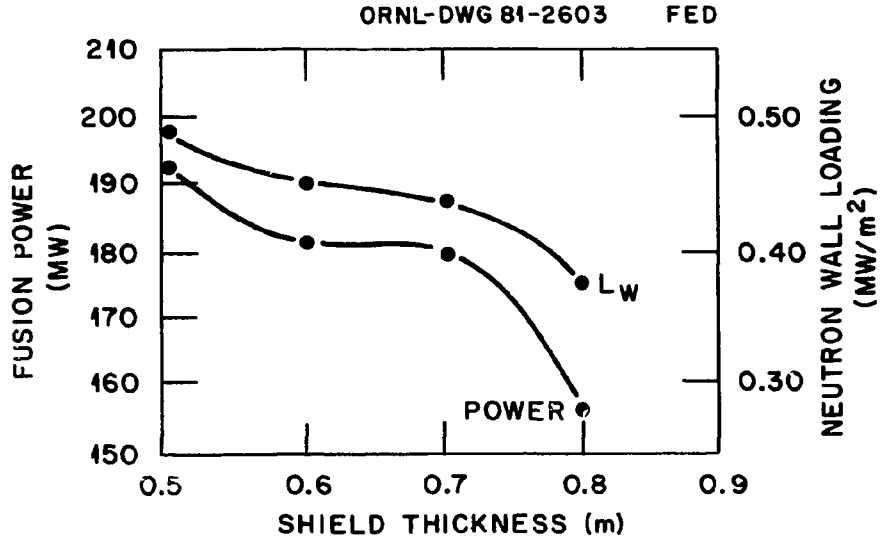

Fig. 3.3. Performance vs shield thickness (a = 1.3 m, β = 6%, B_m = 8 T, t_{burn} = 100 s).

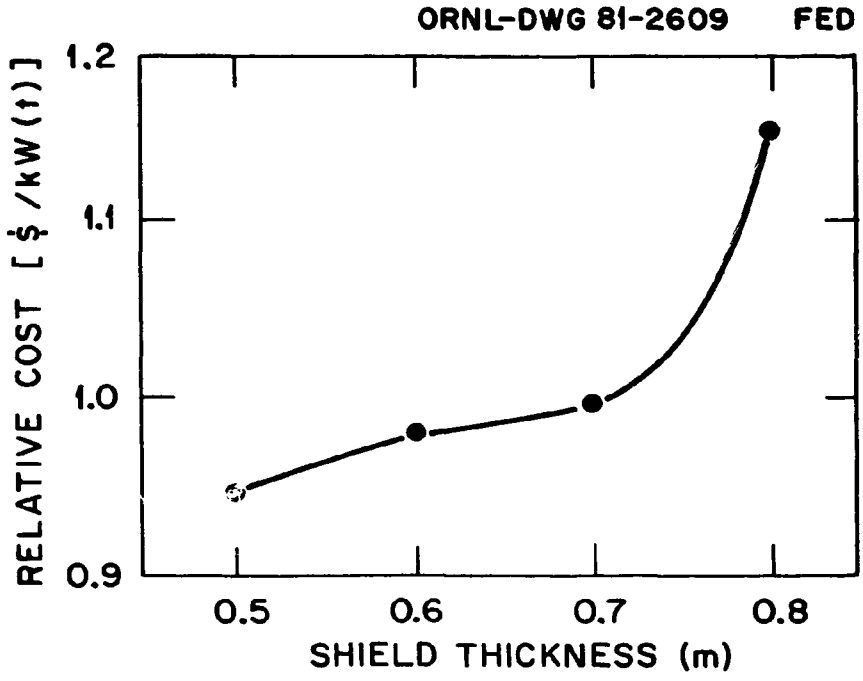

Fig. 8.4. Relative power costs vs shield thickness (a = 1.3 m, β = 6%, B_m = 8 T, t_{burn} = 100 s).

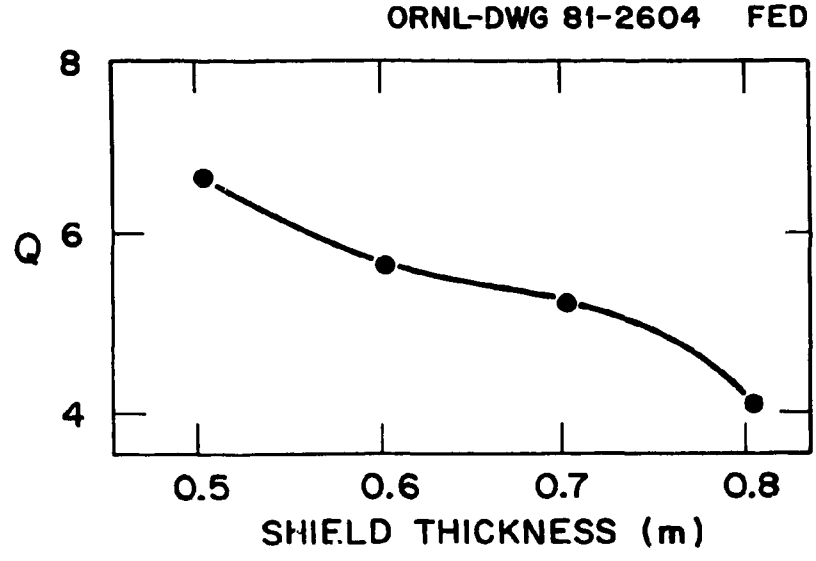

Fig. 8.5. Q vs shield thickness (a = 1.3 m, β = 6%, B_m = 8 T, t_{burn} = 100 s)

unit cost are important considerations for fusion reactors but are of less significance for FED as it is currently envisioned. For FED, there is more concern with total capital cost, which is shown to be a weak function of inboard shield thickness.

Instantaneous refrigeration requirements for the TF coils increase as the shield thickness is decreased, as shown in Table 8.4. These values are associated with nuclear heating only. For costing purposes, cycle average nuclear heating requirements were used and a constant value of 35 kW was included to account for ac losses. At a shield thickness of 0.5 m, the nuclear heating in the TF coil is approximately 200 kW, which appears excessive and suggests that a shield thickness greater than 0.5 m should be used.

The radiation dose to the TF coil insulation is also shown in Table 8.4. The dose increases as shield thickness decreases and exceeds the imposed limit of 1×10^9 rad for a shield thickness of 0.5 m. The dose is dependent on accumulated burn time. For this study, 3.5×10^5 cycles at 100 s per cycle were used. A substantial margin for increased number of cycles exists for the thicker shields (i.e., 0.7 m and 0.8 m), but little margin on dose is available for the 0.6-m shield configuration.

Table 8.4. TF coil refrigeration and radiation dose

Shield thickness (m)	0.5	0.6	0.7	0.8
Refrigeration[a] (kW)	200	53	14	4
Dose[b] (rad)	4.5×10^9	9.1×10^8	1.9×10^8	3.9×10^7

[a]Nuclear heating only. Instantaneous value.

[b]Based on 3.5×10^5 cycles at 100 s per cycle.

8.4.4 Conclusion

Inboard shield thickness over the range of values investigated has a minimal influence on FED cost. A value of shield thickness of at least 0.6 m is required to avoid radiation damage to the TF coil insulation.

8.5 VARIATION IN FUSION POWER

8.5.1 Purpose

It is recognized that the fusion power produced by a fixed FED device could be greater or less than the FED baseline value of 180 MW because of the uncertainties associated with the physics performance of the plasma (confinement, beta, safety factor, etc.). If the physics performance should be better than expected, then the device should be able to take advantage of the improved performance. If the physics performance should be worse than expected, then the device should still be able to deliver the established objectives. To meet either of these postulated circumstances, the affected systems of FED should be designed from the outset to permit operation over some range of fusion power output.

In recognition of these possibilities, a study was performed using the FEDC systems code (see the Appendix) to determine which systems are most impacted by such considerations and to determine the associated capital cost impact for postulated ranges of fusion power output.

8.5.2 Assumptions and Guidelines

The study was performed using the baseline parameters given in Table 8.5.

The scope of the study is indicated in Fig. 8.6. Two basic options were considered — either better performance (resulting from postulated better energy confinement or from higher beta) or worse performance (resulting from postulated worse energy confinement or from lower beta). As indicated, the postulated better performance could result in ignition, and for this circumstance two situations were examined: in the first case the fusion power remains at the baseline value (resulting from improved confinement) and in the second the fusion power is assumed to be twice the baseline value (resulting from increased beta). The postulated worse performance leads to a requirement that the device be operated in a driven mode, and again two situations were examined: in the first case the fusion power is equal to the baseline (improved

Table 8.5. Baseline parameters

Minor radius (m)	1.3
Elongation	1.6
Major radius (m)	4.8
Maximum field at winding (T)	8.0
Field on axis (T)	3.6
Fusion power (MW)	180
Q	5
Average beta (%)	6

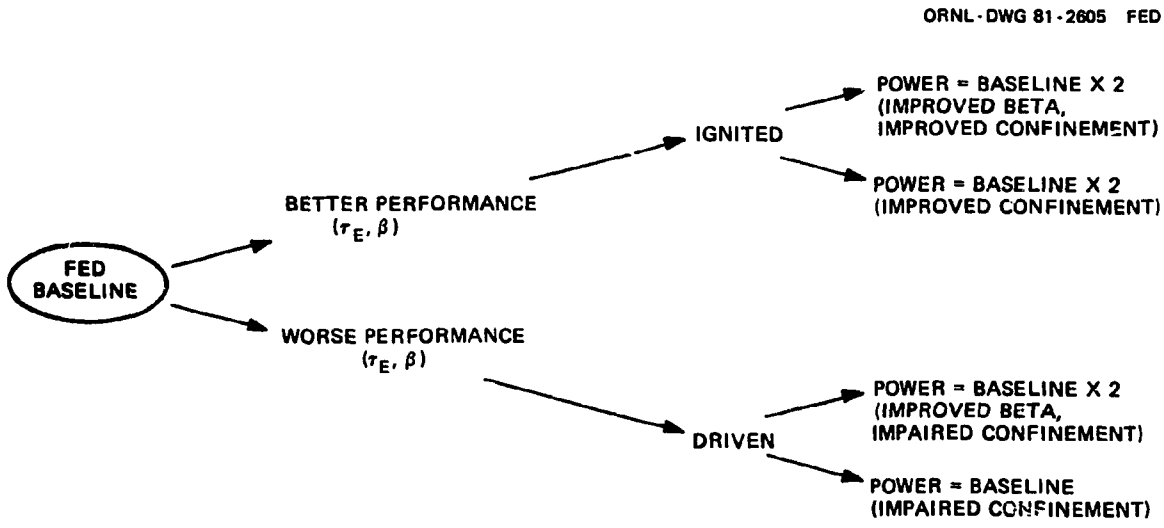

Fig. 8.6. Nature of cases examined.

confinement is assumed) and in the second a doubling of the baseline power is postulated (increased beta is assumed). These four cases represent a range in potential performance that in general encompasses the variation in plasma physics parameters and considerations described in Sect. 4 and listed in Table 4.2.

8.5.3 Description of Analysis Results

Table 8.6 characterizes the engineering implications resulting from the postulated variations in performance. For each of the four cases the following points are noteworthy.

Case 1

This case achieves ignition. It results from a postulated improvement in confinement by a factor of 2 and assumes the average beta is held constant at 6%. In this case, the sustaining auxiliary heating power requirement is reduced to zero, but auxiliary heating is required to achieve ignition. As a consequence, there is a net reduction in the particle and heat flux to the first wall components (first wall, armor, and limiter). Otherwise, there are no engineering implications, since the fusion power remains the same and the auxiliary power required is no greater than the baseline case.

Case 2

This case is driven, with the total fusion power equal to the baseline case. Confinement is assumed to be only half as good as the baseline case and the value of Q decreases from 5 to 2. To maintain the same total fusion power requires a significant increase in auxiliary heating. Average beta is held at 6%. The systems most affected are the primary heating systems, the first wall and limiter (to handle the increased surface heat loads), the ac power systems, the heat dissipation systems, and the tritium processing systems.

Case 3

This case assumes that the total fusion power is doubled. To achieve this, the average value of beta must increase from 6% to 8.5% with energy confinement as given by modified Alcator scaling. Ignition is achieved. The systems most affected are the first wall and limiter

Table 8.6. Parameters characterizing engineering implications of postulated changes in plasma performance

		Power same as baseline		Double baseline power	
	FED baseline	Increased confinement (Case 1)	Decreased confinement (Case 2)	Baseline confinement (Case 3)	Decreased confinement (Case 4)
D-T fusion power (MW)	180	180	180	360	360
Q	5	Ignition	2	Ignition	10
Beta (%)	6	6	6	8.5	8.5
Plasma current (MA)	6.2	6.2	6.2	6.2	6.2
τ/τ_{ALC}	1.0	2.1	0.53	1.1	0.66
Power distribution					
• Sustained heating (MW)	36	0	91	0	36
• Alpha heating (MW)	36	36	36	72	72
Total to first wall/ limiter (MW)	72	36	127	72	108
• Neutron power (MW)	144	144	144	288	288
Required ac power (MW)	197	117	355	142	222
Cooling tower heat load (MW)	400	325	545	567	640
TF refrigeration (kW)	44	44	44	61	61

(to handle the increased surface heat load), the shield (to handle the increased neutron power), the heat dissipation system, the refrigeration system, and the tritium processing system.

Case 4

This case also assumes that the fusion power is doubled but that relative to Case 3 the energy confinement is decreased by 50%. The result is Q = 10 at an average beta of 8.5%. The systems most affected are the same as those in Case 3.

As indicated above, only a few systems are significantly impacted by postulated variations in plasma performance. These are those impacted by the level of fusion power and by the changes in heating requirements.

The systems code was also employed to examine the associated capital cost impact. The results for the four cases and the baseline are given in Table 8.7. This table indicates the system capital cost for those systems which are impacted by the postulated changes in performance. Also given is the total capital cost, which in all cases is expressed as twice the total direct cost. As indicated, the changes in systems costs are small and the largest change in total capital cost is less than 10%. In addition, if all of the changes indicated for these four cases were to be accommodated in one design, the total capital cost would be approximately 15% greater than the baseline.

8.5.4 Conclusions

When the FED concept is selected, it will be necessary to make a decision on the degree of flexibility that should be incorporated into the design to accommodate a range of device performance resulting from uncertainty in the physics performance. The results of the present study suggest that considerable engineering flexibility can be provided at modest cost ($\leq$15%) by designing selected systems to accommodate a range of device performance.

Table 8.7. Capital cost impact

	FED baseline	Power same as baseline: Increased confinement (Case 1)	Power same as baseline: Decreased confinement (Case 2)	Double baseline power: Baseline confinement (Case 3)	Double baseline power: Decreased confinement (Case 4)
Systems cost[a,b]					
Heating	49	35	90	43	57
Refrigeration	14	14	15	18	18
Heat transport	10	9	13	13	14
Fuel handling	11	11	12	12	12
AC power	13	11	19	11	15
Buildings	135	135	135	139	139
Total capital cost	1230	1192	1338	1240	1278

[a] Only systems where differences result are shown.

[b] All costs in millions of 1980 dollars.

8.6 NUMBER OF FULL FIELD PULSES IN FED

8.6.1 Purpose

A key item in engineering the design of various components in FED is the number of full field [TF and poloidal field (PF)] pulses. The design of the metallic structural components of the FED magnet systems must preclude fatigue failure due to the repetitive application of loads that could ultimately lead to fracture. In the Engineering Test Facility (ETF) design effort, the number of pulses was 5×10^5 and the peak magnetic field strength at the toroidal field winding was 11.4 T. In order to designate a less highly stressed design, the peak magnetic field strength in the current FED design studies was reduced to 8 T and consideration was given to reducing the number of full field pulses by as much as an order of magnitude. Accordingly, studies reported in this document have examined the impact of varying the number of full field pulses over the range from 10^4 to 10^6.

The purpose of this study was to develop an operating sequence for FED over its postulated lifetime of at least ten years and to develop an estimate of the number of full field pulses that might reasonably be required to conduct the proposed operations. The subsequent engineering design of FED will be based on the recommended values resulting from this study.

8.6.2 Assumptions and Guidelines

It was assumed that scheduled operations of FED would occur six days a week with two shifts a day. The third shift would be used (at least in the early phases of operation) for modifications, maintenance, and preparation for the next day's operations.

Assumptions were made about the frequency of pulses and scheduled maintenance time; these vary with the phases of operation. The burn length of each pulse was assumed to be 100 s and the time between burns was assumed to be a minimum of 52 s to accommodate startup, shutdown, and pumpout. Although it was assumed that a pulse would occur, on average, once every 10 min during the early phases of operation and

once every 5 min during the later phases, it should be noted that particularly during the D-T engineering testing phase, it will be necessary to have extended periods of performance (days to weeks) in which the device operates with repetitive pulses every 152 s.

The operating lifetime for FED was assumed to be ten years. Several discussions with ORNL senior experimentalists were useful in developing the assumptions and guidelines and in ensuring that these estimates are consistent with recent tokamak practice.

8.6.3 Description of Operating Sequence Phases

Table 8.8 summarizes the proposed phases of the FED operating schedule. Four phases are identified. The first three years are devoted to systems checkout and hydrogen/deuterium operation. The last seven years represent deuterium-tritium (D-T) operation with the first year devoted to developing an operational understanding of D-T plasma burn; the remaining six years are dedicated to engineering testing.

8.6.4 Estimated Number of Pulses in Each Phase of FED Operations

Table 8.9 summarizes the number of pulses estimated to occur in each phase of FED operations.

Limited full field operation is assumed in Phases I and II; 75% of all pulses will be with the TF system operating at $\leq$6 T and 25% will be at the full rated field of 8 T. In Phases III and IV, all operations are assumed to occur at the full rated toroidal magnetic field strength of 8 T.

During Phase I, it is anticipated that there will be frequent requirements for equipment modifications or repair, equipment checkout/testing, general exploration of what is required to accomplish successful machine operation, and maintenance. For these reasons, it has been assumed that on the average there will be two weeks per month when no scheduled operations will occur, and when operations do occur a pulse will be no more frequent than one every 10 min on average.

During Phases II, III, and IV it has been assumed that, on average, scheduled maintenance and modification will require only one week per

Table 8.8. FED operating sequence phases

Phase	Description	Duration
I	Integrated systems checkout: Major machine systems operation including discharge cleaning, diagnostics shakedown, systems and subsystems shakedown/integration, and limited hydrogen operation	1 year
II	Hydrogen (deuterium) operation: Hydrogen (0.5 year) — cleanliness and feedback position control, startup and runup of I_p, initial disruption control, preliminary shaping, fueling, preliminary heating Deuterium into hydrogen (1.5 year) — beta, heating, elongation, mechanical divertor, impurity control, fueling experiments	2 years
III	D-T plasma burn: Exploration of long pulse, D-T operation, exploration of plasma performance under varying conditions under operator control	1 year
IV	D-T engineering testing: Nuclear and plasma engineering testing with machine operated confidently and reliably with good repeatability	6 years

Table 8.9. Number of pulses during FED operations (pulse burn length = 100 s)

Phase	Duration (years)	Description	Peak toroidal field	Operating assumptions	Number of pulses	Number of full field pulses
I	0-1.0	Integrated systems checkout	≤6 T (75%) 8 T (25%)	6 days/week 2 shifts/day 1 pulse/10 min Downtime of 2 weeks/month	16,000	4,000
II	1.0-3.0	Hydrogen (deuterium) operation	≤6 T (75%) 8 T (25%)	6 days/week 2 shifts/day 1 pulse/10 min Downtime of 1 week/month	46,000	11,500
III	3.0-4.0	D-T plasma burn	8 T	Same as Phase II	23,000	23,000
IV	4.0-10.0	D-T engineering testing	8 T	Same as Phase II, except 1 pulse/5 min	276,000	276,000
				Total	361,000	314,500

month. Pulses will continue to be no more frequent than every 10 min in Phases II and III but will increase in frequency to one every 5 min (on average) in Phase IV.

The table shows that for the indicated assumptions, the total number of pulses is 3.6×10^5; of these, about 3.1×10^5 would be full field pulses.

8.6.5 Conclusions and Recommendations

For the present FED baseline pulse burn time of 100 s, an operating schedule has been developed for an assumed ten-year operating lifetime. Based on the stated assumptions in this operating sequence, the total number of pulses is 3.6×10^5 and of these about 3.1×10^5 are estimated to occur with full field conditions.

It is recommended that 3.5×10^5 full field pulses be used as the baseline value for all future FED design studies.

More detailed development of an operating schedule is required, including specification of the details of the engineering testing that will be required in Phase IV. Such a test program schedule could result in some modification in the number of full field pulses that might be required. In addition, it may prove feasible and desirable to increase the pulse burn time to 200-500 s, which would decrease the number of full field pulses.

8.7 DEVICE SIZE AND COST SENSITIVITY TO NUMBER OF PULSES

8.7.1 Purpose

The purpose of this study was to examine the sensitivity of device size and cost to the number of pulses applied over the lifetime of the machine. Specifically, sensitivity was determined for pulse levels of 5×10^4, 1×10^5, 5×10^5, and 1×10^6.

8.7.2 Assumptions and Guidelines

FED performance was fixed by holding the following parameters constant:

Plasma radius	1.3 m
Field on axis	3.62 T
Average beta	6%
TF ripple	0.83%
Safety factor, q	2.5
Q	5.3
Neutron wall loading	0.44 MW/m^2
Burn time	100 s

Parameter values used in the study were taken from the initial FED parameter list. The revised parameter list (in Sect. 3) reflects current parameters that are in some cases slightly different from those used here; e.g., a TF ripple of 0.78% and a safety factor of 3.2.

The number of pulses in a fixed total time (e.g., 10 or 15 years) affects requirements for radiation shielding of the inboard TF coil leg. The inboard shield was sized to limit the dose to the inboard TF coil leg to a maximum of 10^9 rad while restricting nuclear heating of the TF coils to a maximum of 60 kW (to avoid excessive refrigeration costs).

As discussed in Sect. 5.2, the number of pulses is a significant factor in the design of the TF coil case and support structure. The FEDC systems code does not directly account for out-of-plane TF coil loads or intercoil structural requirements. Structural analysis of TF coil design is required to reasonably reflect the impact of number of pulses on TF design and cost. For this study, the systems code was used; inputs were developed that resulted in coil case weights consistent with those indicated in Sect. 5.2.

FED design requirements on utilization (defined as the ratio of operating time to calendar time) were assumed to be 0.13 for less than 10^5 pulses, 0.35 at 5×10^5 pulses, and 0.60 at 10^6 pulses. Increased utilization is required with an increased number of pulses to allow the completion of more extensive test plans within a reasonable period of time (<15 years).

8.7.3 Description of Trade Study

The FEDC systems code was used to develop design parameters and capital costs for pulse requirements of 5×10^4, 1×10^5, 5×10^5, and 1×10^6. Inputs were developed to fix the performance and burn time of the device while accommodating changes required by varying the number of pulses.

In the trade study, only implications on capital cost were considered. It should be recognized that development costs and operating and support costs can also be expected to increase with an increased number of pulses. However, insufficient information has been gathered to date to quantify these costs.

8.7.4 Results of Trade Study

In varying the design life from 5×10^4 to 1×10^6 pulses, while holding performance constant, the systems code indicated a required increase in machine size (major radius) of 4.5% and an attendant increase in capital cost of 5.4% (see Tables 8.10 and 8.11). It should be noted that characteristic parameters and capital cost estimates did not change appreciably between 5×10^4 and 1×10^5 pulses; such changes only became significant between 1×10^5 and 1×10^6 pulses. The changes in total capital cost were largely attributable to changes in the capital cost of the TF coil system, the shield, the refrigeration system, the building, and the fuel processing system.

The change in TF coil system capital cost is directly related to TF coil structural requirements, which are discussed in detail in Sect. 5.2. Over the range of 5×10^4 to 1×10^6 pulses, TF coil case weight doubled and TF coil system capital costs increased by 22%.

The mechanical properties of TF coil conductor insulation and the resistivity of the copper stabilizer are affected by the fluence to the TF coils. A maximum exposure of 10^9 rad was assumed for the insulating material. For the copper stabilizer, exposure was limited to 2.4×10^{-4} displacements per atom (dpa). However, two anneals were allowed over the life of FED, which effectively eliminated constraints due to displacement damage of the copper stabilizer.

Table 8.10. Characteristic FED parameters vs number of pulses

	5×10^4	1×10^5	5×10^5	1×10^6
Aspect ratio	3.59	3.60	3.67	3.75
Major radius (m)	4.67	4.68	4.77	4.89
Fusion power (MW)	175	175	179	183
Inboard shield (m)	0.59	0.59	0.62	0.66
TF power deposition (kW)	60	60	42	26
TF coil dose rate (rad)	1.5×10^8	3.0×10^8	10^9	10^9
TF coil case weight (kG)	4.8×10^4	5.6×10^4	7.4×10^4	9.5×10^4
Maximum field (T)	7.90	7.88	7.82	7.80

Table 8.11. Relative FED system costs vs number of pulses

	Relative cost[a]			
System	5×10^4	1×10^5	5×10^5	1×10^6
Shield	0.131	0.132	0.135	0.139
TF	0.144	0.148	0.160	0.175
Refrigeration	0.038	0.038	0.033	0.027
Fuel processing	0.023	0.023	0.029	0.034
Reactor cell	0.115	0.116	0.119	0.122
FED Total	0.993	1.000	1.025	1.054

[a] Relative cost = cost/total cost for 1×10^5 pulses.

Fluence to the TF coils (inboard leg) is limited by the thickness of the inboard shield. At 1×10^6 pulses, a shield thickness of 0.66 m is required to limit the fluence to 10^9 rad; at 5×10^5 pulses, the required shield thickness is 0.62 m. Reducing the shield thickness results in a smaller device in a smaller building, with attendant cost benefits. Below 10^5 pulses, however, the benefits of further reducing the inboard shield thickness tend to be offset by increased refrigeration requirements due to increased nuclear heating of the TF coils. This finding is consistent with the discussion in Sect. 8.4.

It may be seen in Table 8.10 that the outboard shield thickness is not sensitive to number of pulses. The outboard shield is sized for a biological dose rate of 2 mR/h 24 hr after shutdown. In the systems code, the outboard shield thickness is a function of the neutron flux and is independent of the number of pulses, because the dose rate after 24 h is largely determined by radionuclides with short half-lives, which are in saturated concentration after relatively few pulses.

Another system that appeared sensitive to the number of pulses is the fuel processing system. Increased utilization is required with an increased number of pulses. Conceptually, increased utilization requires that fuel be processed at a faster rate, resulting in increased capital costs. However, this would not necessarily be true if the fuel processing system was sized for a specified period of sustained operation at lower levels of utilization. In order to accurately assess the impact of number of pulses on fuel processing system costs, more detailed specifications are required.

The capital cost figures shown in Table 8.10 do not reflect the cost of availability enhancements that would be required in order to achieve the utilization required at an increased number of pulses. The availability characteristics of FED have not yet been established. However, based on previous analyses performed on similar tokamak designs [ETF and the International Tokamak Reactor (INTOR)], the cost of availability enhancements should not be appreciable below 1×10^5 pulses. However, as the number of pulses approaches 1×10^6, the cost of availability enhancements can be expected to become increasingly substantial.

8.7.5 Conclusions

FED operations at up to 2-4 × 10^5 pulses can be accomplished in a reasonable period of time (<15 years) without major capital cost impact. More extensive test plans requiring a larger number of pulses would encounter increasingly severe availability constraints and capital cost impacts.

In evaluating changes in pulse requirements, attention should be focused on

1. the TF coils,
2. the inboard shield,
3. the refrigeration system,
4. the reactor cell, and
5. the fuel processing system.

For pulse operations exceeding 1 × 10^5 pulses, attention should also be focused on availability implications.

8.8 FED FACILITIES DESCRIPTION

8.8.1 Purpose

The task of defining the FED facilities is just beginning. The initial thrust of this study has been toward defining the options and major factors influencing the selection of tokamak cell and hot cell areas. The ultimate product of this task will be a consistent preconceptual description of the FED facilities.

8.8.2 Assumptions and Guidelines

The basic guideline used in identifying facilities options is that all the facilities must provide the necessary functions and support for the FED and its operation. Since the FED design is not yet fully established, the facilities to support FED are also not fully determined. However, possible options can be suggested and studied to lay the groundwork for later design decisions. The suggested options should be kept as flexible as possible to allow for the variety of machine, maintenance, and operating options currently being considered for FED.

8.8.3 Description of Analysis

Several facilities and buildings are needed to support FED. These facilities may require a variety of construction techniques, which can be broadly grouped into three categories: special, conventional, and open construction. Each of these categories is briefly outlined in Table 8.12, together with a preliminary list of facilities expected to be in each category. Other facilities will probably be required and will be added as their needs are identified. Note that the special construction category deals with the prevention of radioactivity releases and is subdivided into two subcategories: containment and confinement. Containment implies the capability to isolate the building and any contained radioactivity from the environment; confinement implies the use of ventilation techniques to control and reduce radioactive releases.

The initial FED facility investigations have been directed primarily toward the tokamak cell and hot cell facility configurations. One study was performed to identify some aspects of machine design and maintenance operations that could affect the tokamak cell size. Currently, a number of machine design and maintenance options are being considered. In some cases, the impact of these options on the tokamak cell may influence the selection among various options.

The several options considered in this study are grouped into two categories: machine options and maintenance options, as outlined in Table 8.13. All these options were considered both individually and in combination. The overhead crane for maintenance transport has the advantage of being able to lift components over other components, but this may also be viewed by some as a disadvantage because it exposes other components to possible damage from crane failure. Several techniques may be possible to enable the use of the overhead crane. One configuration would move the components with the overhead crane to the hot cell entrance where the load would be placed on a rail car shuttle to take it into the hot cell. Surface transportation requires surface rights-of-way around other components to get to the hot cell entrance. The requirements for cryostat or PF coil laydown areas, either in the tokamak cell or elsewhere, have not yet been established. For example, the cryostat dome

Table 8.12. Construction categories for FED facilities

Category	Description	Buildings and facilities
Special construction	Restricts radioactivity release	
Containment	Isolatable, very low leakage, withstands overpressure, internal and external missiles, high level seismic events	Tokamak cell Tritium processing
Confinement	Uses ventilation to control radioactivity releases, withstands some missiles and high level seismic events	Hot cell facility Radioactive waste treatment Ventilation systems Heat exchanger building (depends on potential tritium leakage)
Conventional construction	Houses machines and people, basically conforms to Uniform Building Code, may have special requirements depending on equipment needs; e.g., special ventilation, seismic consideration for machine mounting, and extra protection for safety-related systems	Electrical equipment building Control room Administration building Mockup and fabrication shop Cryogenic building
Open construction	Exposes machines to the elements, allows air cooling and greater spacing between components	Cooling towers Electrical switchyard Transformers

Table 8.13. Configuration options

Machine design options
Reference FED design (rf bulk heating, pump limiter)
Basic machine with neutral beam injectors for bulk heating[a]
Basic machine with bundle divertor for impurity control[a]
Maintenance options
Crane transport
Surface transport (e.g., wheels, tracks, rollers, airfloats)
Cryostat dome or PF coil laydown area, with or without removal of other equipment

[a]Although the current FED baseline employs ICRH and a pump limiter, these facilities studies have also considered the potential impact if NBI and a bundle divertor were to be used.

may be fabricated in segments and might be capable of disassembly should it need to be removed. An unlikely possibility is that the PF coils might be wound in place so that their removal might be accomplished by unwinding the coils and disassembling the coil cases. Alternatively, various configurations and maintenance approaches have been suggested which would provide laydown areas for these components outside the tokamak cell. In this study, laydown areas were not assumed to be required for the PF coils or the cryostat dome. If an area is provided for the cryostat dome, it is assumed that the PF coils can be stacked over the cryostat dome, thereby eliminating the need for additional laydown area.

Only cylindrical tokamak cells were considered to allow for possible overpressure design. Additional discussion of overpressure considerations is given in Sect. 8.9. An overhead crane was assumed to be required even if it was not the primary means of maintenance transportation. Two types of movement were assumed in removing components from the device: (1) radial motion to clear the TF coil outer leg and (2) movement by either overhead crane or surface transportation (e.g., rails, rollers, or airfloats) from the machine to the hot cell or hot cell entrance. All movements by either crane or surface were assumed to require 2 m of clearance from other major components and the cell walls. The only exception to this assumption was when transport was by overhead crane and the component could be lifted straight up from its normal operating position. In these cases, no allowance was made for clearance between the component being moved and the component to which it would normally be attached. However, wall clearance was provided in all cases.

The height of the cell is dominated by the crane clearance requirements. Since all the options assumed that an overhead crane would be necessary, even if it were not the primary mode of transport, all the cell heights were taken to have an effective height of 64 m. A review of the crane clearance requirements suggests that more than one-half of the cell height is required for crane operation.

More than forty combinations of these options were examined and minimum radius cells were estimated that could satisfy the needs of each configuration. In several cases, the minimum radius cell resulted in asymmetric arrangements where the center of the FED did not coincide with the center of the cell. The results from these studies are summarized in Table 8.14. As shown in the table, the cell size could be between about 22 m and 37 m, depending on the options selected. The approximate increments in size required for several maintenance options are given as ranges, since the actual values depend somewhat on the machine design options assumed. If the overhead crane is used for transport and no PF or cryostat laydown area is provided, the different machine design options have a negligible effect on cell radius. Providing surface transportation rights-of-way or laydown areas for PF coils or cryostat dome significantly increases the building radius. The combination of surface transportation with laydown area adds the effect of each option.

Figure 8.7 schematically shows the relative sizes of three possible tokamak cells resulting from selection of three different sets of options. The largest cell radius results from selection of all possible options, i.e., a basic machine with four neutral beam injectors and a bundle divertor, rights-of-way for surface transportation, and a cryostat laydown area. The smallest cell results from only considering the basic machine; however, addition of neutral beam injectors and a bundle divertor does not significantly affect this estimated size. The third case is representative of several possible intermediate cases with approximately the same radius. This particular cell size results from the basic machine with four neutral beam injectors, a bundle divertor, and crane transport, without either cryostat or PF coil laydown area.

This study shows that maintenance options and operations have a large influence on tokamak cell size, with the maintenance options having a much larger influence than the machine design options. The tokamak cell is expected to be the most expensive building of the FED facility because it will require the most expensive construction techniques and will have the most stringent requirements. Thus, the results of this study have suggested that methods of providing the space required by

Table 8.14. Tokamak cell sizes

Description	Approximate radius (m)
Basic machine with any combination of machine design options and crane transport	22
Increment for surface rights-of-way	+ 5 to 8
Increment for PF coil laydown area	+ 4 to 5
Increment for cryostat laydown area	+ 5 to 7
Increment for not removing shielded pump duct (or not using alternate stacking procedure)	+ 2
Minimum radius with all options	37
Minimum radius with all options but no laydown area for PF coil or cryostat	30

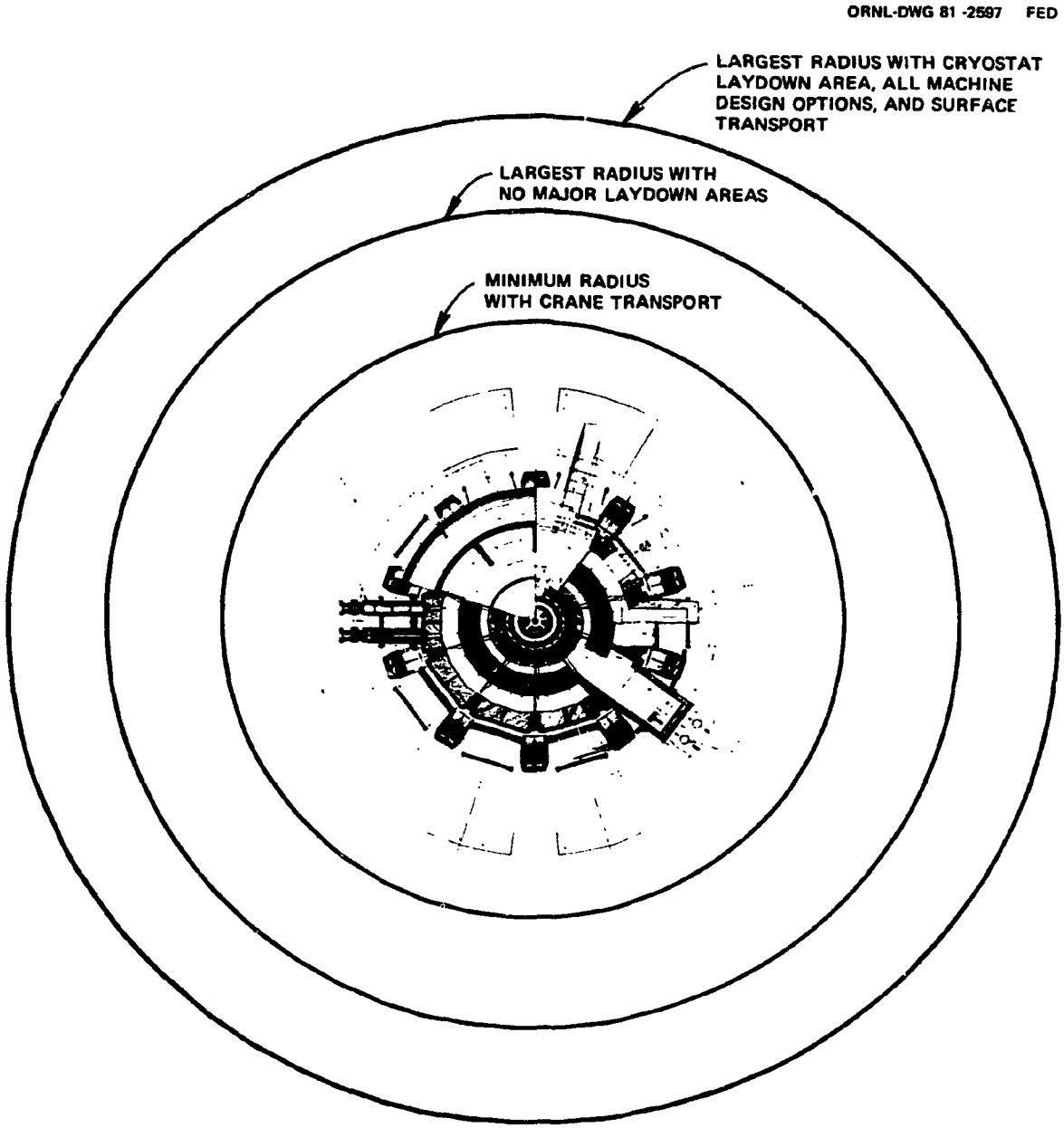

Fig. 8.7. Schematic representation of feasible tokamak cells.

maintenance options and operations in other buildings or of reducing the required space should be explored. A configuration which combines the tokamak cell and hot cell facilities has been developed to accommodate these suggestions. Plan and elevation views of this combined configuration are shown in Figs. 8.8 and 8.9.

A second configuration was based on a more conventional configuration in which the tokamak cell is in a large building and a separate hot cell is attached to one side. Plan and elevation views of a possible configuration using this philosophy are given in Figs. 8.10 and 8.11.

The combined configuration offers a potential advantage of reduced tokamak cell size. This is accomplished by postulating the use of the overhead crane for component transport, by providing a cryostat dome laydown area outside the tokamak cell, and by providing most of the necessary crane operating space and clearance in the hot cell building. In effect, this transfers substantial space from the tokamak cell into the hot cell. Since the hot cell is expected to have less stringent construction criteria, it will cost less per unit volume than the tokamak cell building. This combined arrangement requires only one large capacity crane, as opposed to two for the configuration with a separate tokamak cell and a separate hot cell. A key disadvantage may be the design and construction of the cell top closure, because the smaller size of the cell could substantially increase the overpressure expected from cryogen releases. The hot cell in this combined configuration has been developed for a low plant availability. Two large general-purpose hot cells would be used to disassemble major components, while smaller components would be maintained in smaller general-purpose cells.

The configuration with a separate tokamak cell and hot cell offers the advantage of conventional construction techniques. In addition, less construction interference is expected than may result in the previous arrangement. The size of the tokamak building will be influenced by the machine options, size, and maintenance requirements. For the particular case shown in Figs. 8.10 and 8.11, the configuration included four neutral beam injectors, a bundle divertor, a laydown area for the cryostat dome, and rights-of-way for surface transportation (e.g., rail

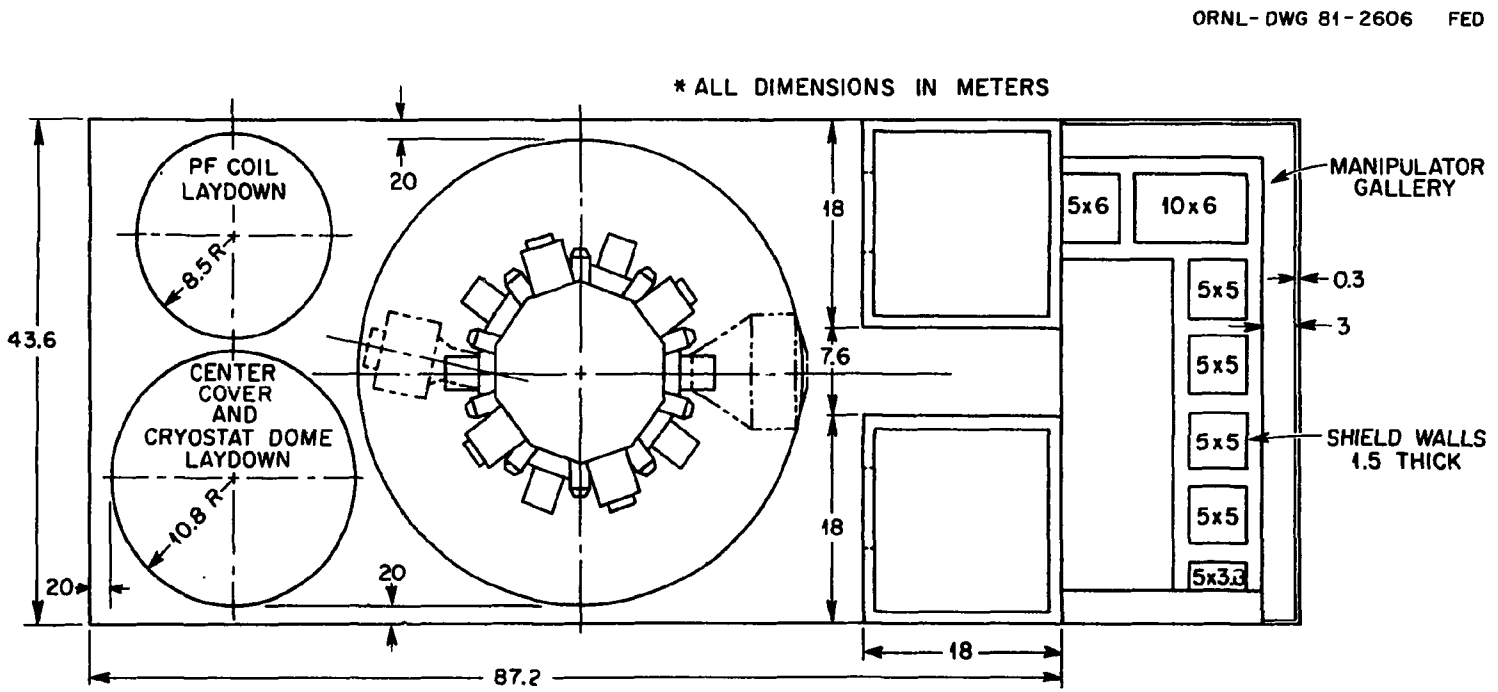

Fig. 8.8. Plan view of combined tokamak cell and hot cell.

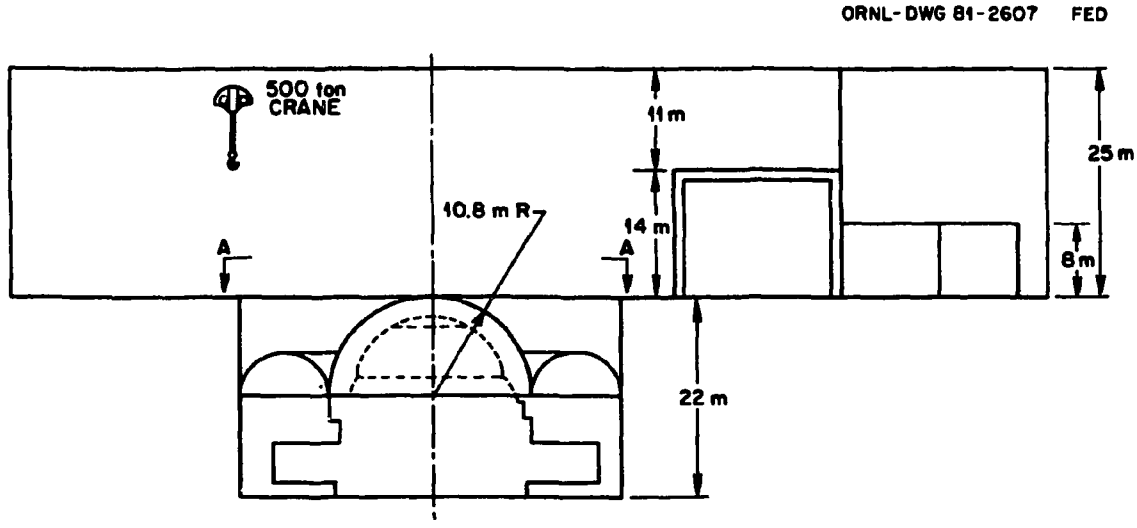

Fig. 8.9. Elevation view of combined tokamak cell and hot cell.

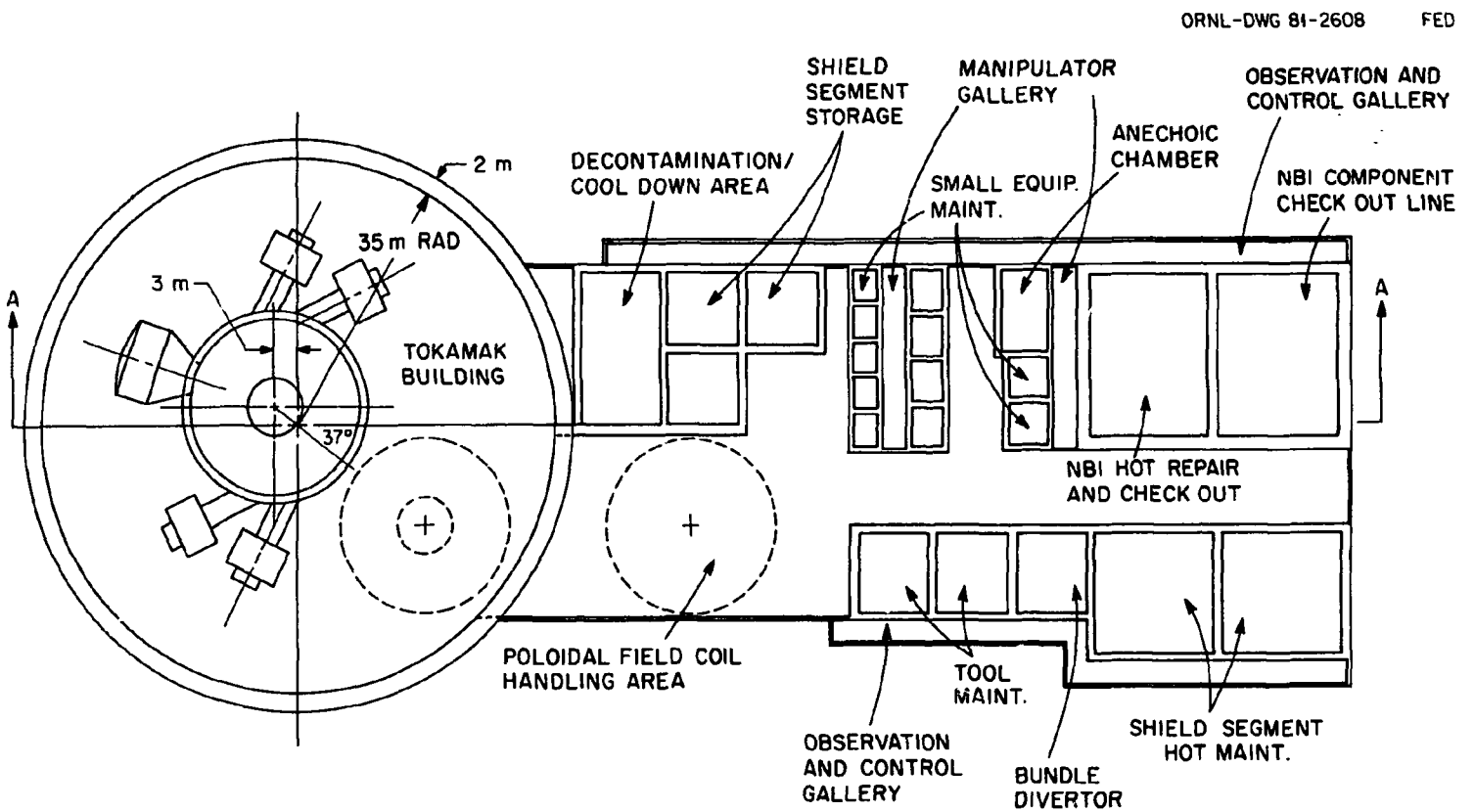

Fig. 8.10. Plan view of separate tokamak cell and hot cell.

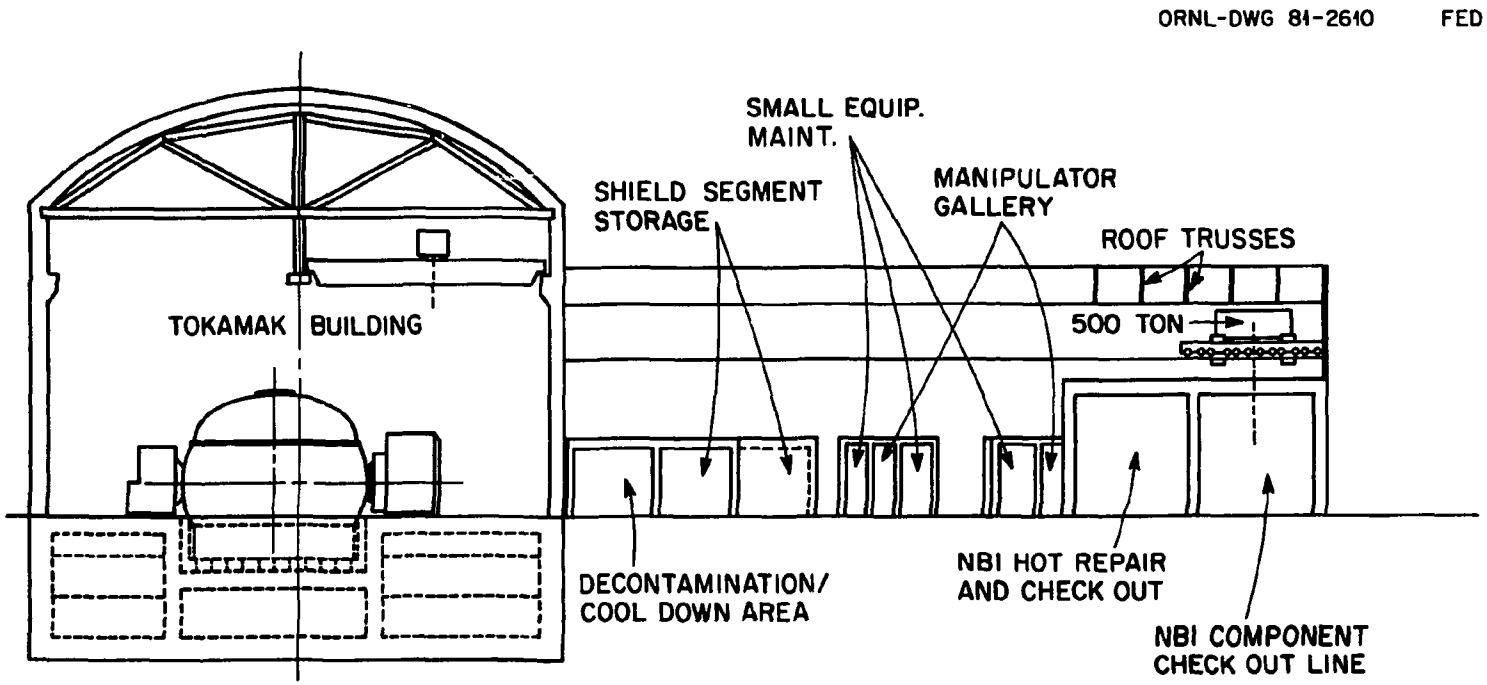

Fig. 8.11. Elevation view of separate tokamak cell and hot cell.

or airfloats). The hot cell arrangement was developed to support a high plant availability by including dedicated maintenance cells for each major equipment type.

8.8.4 Description of Analysis Results

The study of possible FED facilities has identified several facilities and buildings that will probably be required to support FED. Two possible tokamak cell and hot cell arrangements are being studied to identify the key features that will influence later design decisions.

8.8.5 Conclusions and Recommendations

Preliminary studies have identified feasible options for the FED facilities. Effort should continue to more fully develop the facility characteristics. There must be a constant interplay with the design process to ensure that the support facilities meet the needs of the developing FED design. The facilities need to remain flexible to be able to adapt quickly to the improving knowledge of the FED requirements.

Very important areas affecting facilities design will be safety and environmental considerations. For example, one unknown in tokamak cell design is the required overpressure criteria. The cell overpressure criteria will be directly influenced by safety and environmental criteria used to preclude the release of tritium and activated material.

8.9 TOKAMAK CELL COST SENSITIVITY

8.9.1 Purpose

Current estimates of FED tokamak cell cost depend on the volume of the cell. As design options are identified, it becomes increasingly important to identify and estimate the cost impact of the design options and associated design criteria. One criterion that is expected to have a significant impact on cell cost is the overpressure that the cell must be designed to withstand. The relative proportions of the cell may also have a significant cost impact. The purposes of this study were to

develop a cost model that would incorporate these effects and then to use the model to assess the possible magnitude of these effects. The results of this study are expected to be useful in selecting from among various cell design options.

8.9.2 Assumptions and Guidelines

The current tokamak cell cost model expresses cell cost as proportional to cell volume to the 0.7 power. This is a rule of thumb developed to give an approximate cost estimate for large nuclear reactor-related buildings and is based on practical experience for large buildings with some overpressure capabilities. However, this dependency does not account for anticipated variation due to overpressure requirements, nor does it reflect any changes due to the relative proportions of the building except through the changes in volume.

Safety criteria may require the FED tokamak cell to withstand a specific overpressure. Significant amounts of tritium will be handled and used within FED. As a result, a potential exists for accidental release of tritium in amounts possibly large enough to exceed accepted standards for tritium release. Therefore, the facility design must preclude the release of tritium. FED operation will also result in activation of several materials that might also represent some possibilities for undesirable radioactive release unless precluded by facility design. A confinement philosophy is necessary to deal with such postulated radioactive releases. One confinement philosophy calls for isolation of the outside environment from the cell or building containing radioactivity whenever any event occurs that could release undesirable amounts of radioactivity. In order to maintain this isolation of outside environment from the cell, it is often necessary for the building structure to be designed to withstand significant overpressures resulting from postulated concurrent release of gases and energy. In the FED situation, a postulated total release of all cryogens, i.e., liquid helium and liquid nitrogen, could cause significant overpressure of the tokamak cell if isolation is to be maintained. Accordingly, a containment building capable of withstanding significant overpressures appears to be prudent.

Other techniques may be available for mitigating the consequences of radioactivity release without a containment building. However, until such design solutions are developed, it appears appropriate to assume the need for a containment building.

To develop a more refined cost model for a containment building, it was necessary to make some assumptions concerning the type of structure to be used. One common approach to construction of pressure-containing buildings is to use a freestanding cylindrical steel shell to meet the pressure requirements. It is assumed that the top would be elliptical. Both these techniques allow the steel to be placed in hoop stress and reduce or eliminate bending stresses, allowing thinner steel cross sections to be used. (Other techniques for pressure-containing buildings have been used successfully but have not been addressed in this study.)

Several other reasons support the use of a steel shell. A steel building liner may be advisable to reduce the amount of tritium absorption if tritium should accidentally be released to the building. A steel liner would also offer advantages for decontamination operations after accidental release of activated materials. A steel shell is often useful in preventing flying concrete chips caused by spalling if missiles were to strike the exterior of the building, and it may also be beneficial for shielding against stray magnetic fields and rf signals. Based on these benefits, a steel shell has been assumed for the analysis performed in this study.

In addition to the steel shell, 2 m of ordinary reinforced concrete completely surrounds the building. This concrete is needed for neutron and gamma shielding during operation and maintenance activities. It also serves as external missile protection and as a major part of the foundation system.

Excavation is likely to be required by any building design; however, preliminary estimates of excavation costs show that these would be negligible unless unusual site conditions were encountered.

The unit costs were estimated based on discussions with civil engineers involved in the design and construction of similar building structures. These costs are typical. Steel was assumed to cost \$13,800 per ton (\$15.20/kg) as fabricated steel liner. Another \$1,580/m^2 of

cell surface area was used to estimate the cost of installing and testing the cell liner. The cost of reinforced concrete was taken as $350 per cubic y ($458/m^3), including placement and form work. In addition to thes basic materials, a large fraction of any building cost is required for incidental items such as internal partitions, paint, stairways, lights, heating, air conditioning, ventilation, electrical distribution, etc. The cost for these incidentals is often estimated to be equal to the cost of basic construction materials and erection. However, in this study, this approach yielded greatly increased incidental cost with increasing overpressure. even when the cell size remained the same. To avoid this apparent difiiculty, the cost of incidentals was assumed to be proportional to cell volume. The constant of proportionality was estimated so the cell costs would approximately agree with earlier cost estimates for low overpressure (∿1 atm). This resulted in about $120/m^3 for incidentals. While this estimate is somewhat arbitrary, it was not a major factor in determining the general building cost trends and was judged to be of the right order of magnitude.

8.9.3 Description of Analysis Effort

The cell cost model was developed by using the expression for hoop stress relationship to determine the required thickness of steel. The steel thickness was then multiplied by the cell surface area to determine the amount of steel required. To simplify the expression, the height was taken as the effective height of a right circular cylinder, which allowed simpler expressions for surface area and volume, rather than accounting explicitly for the effects of the elliptical top.

The development of the cell cost expression is outlined in Table 8.15. The resulting expression was used to investigate ranges of values for cell radius, height, and overpressure. Part of the study was devoted to investigating the release of a fixed amount of cryogen, regardless of the size of the cell. While the basic FED design could be accommodated by a wide range of cell sizes, the FED is expected to have approximately the same quantity of cryogens regardless of cell size. For this study the maximum possible liquid helium release was estimated to be 224,000 ℓ

Table 8.15. Development of tokamak cell cost model

Steel costs (thickness × cell surface area × density × unit cost)
+ installation costs (cell surface area × unit cost)
+ concrete costs (thickness × cell surface area × unit cost)
+ incidental costs (cell volume × unit cost)
= Total tokamak cell costs

of liquid helium (the expected amount of liquid helium in the tokamak cell to cool the superconducting PF and TF coils). This is not necesarily all the cryogens in the cell, since substantial amounts of liquid nitrogen are also expected. Also, the probability of such a release has not been addressed. Once a fixed cryogen release is assumed, then the overpressure criterion depends on the total volume of the cell.

8.9.4 Description of Analysis Results

Before discussing specific results, several general trends can be anticipated. The cell cost is expected to increase with any increase in radius, height, or overpressure. For fixed cell dimensions, the cost is a linear function of overpressure. For a fixed radius and overpressure, the cost is a linear function of height. However, for a fixed height and overpressure, the cost is a rather complex cubic function of radius. For a fixed cryogen release the radius, height, and overpressure are related in a more complex fashion, and the trends are not easily anticipated.

Specific results have been normalized to the FED tokamak cell currently estimated by the FEDC systems code, which has a radius of 27 m, an effective height of about 60.5 m, and an overpressure design criterion of about 1 atm. The minimum tokamak cell size that can be optimistically anticipated has a minimum radius of about 20 m and a minimum height of about 20 m. From these minima, the possible cell dimensions may be as large as a radius of 40 m and a height of 70 m. For this range of cell sizes, the overpressure resulting from the postulated fixed cryogen release ranges from about 0.7 atm for the largest cell to about 7.0 atm for the smallest cell.

Figures 8.12-8.14 show the results of some example calculations. These examples indicate how cell cost varies with overpressure, radius, and height, respectively. The figures also show what happens in the case of the postulated fixed cryogen release. The figures support the trends anticipated by inspection of the cost expression and also show that cell costs are much more sensitive to overpressure and radius than to cell height. The material and installation costs for steel quickly dominate the cell cost as the overpressure is increased.

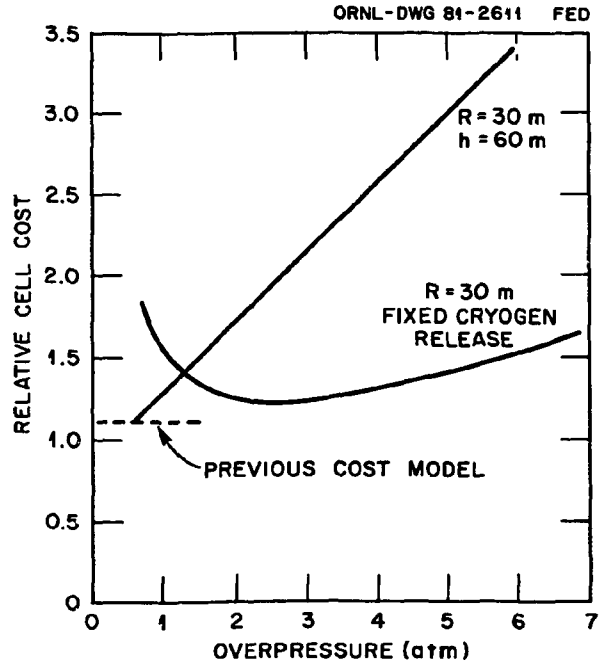

Fig. 8.12. Cell cost variation due to changes in overpressure criteria.

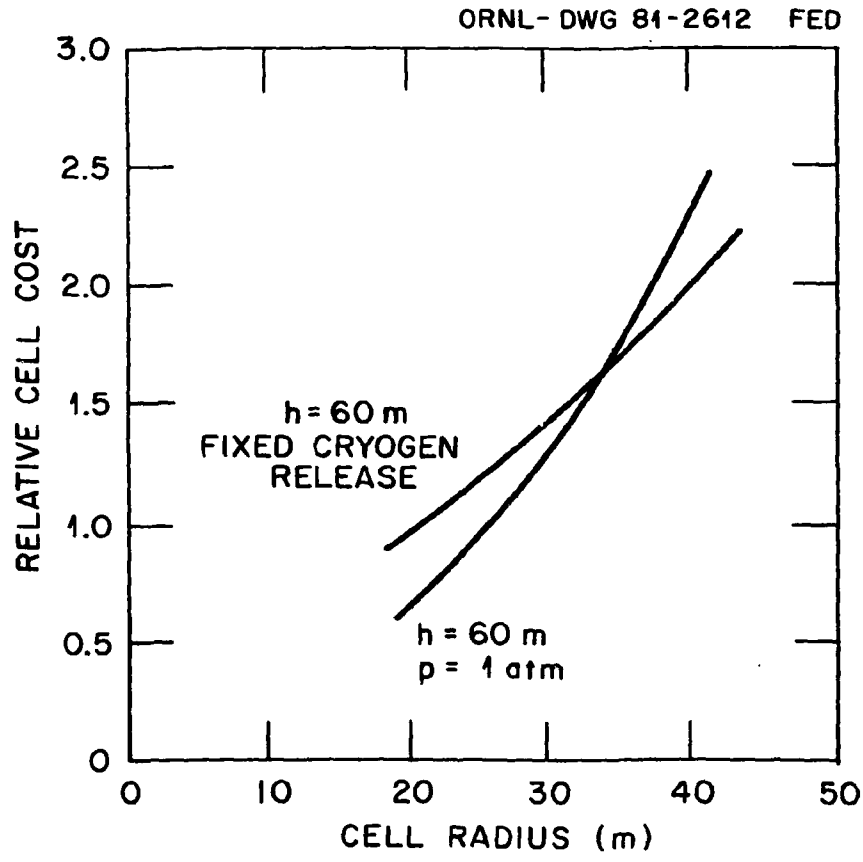

Fig. 8.13. Cell cost variation due to changes in cell radius.

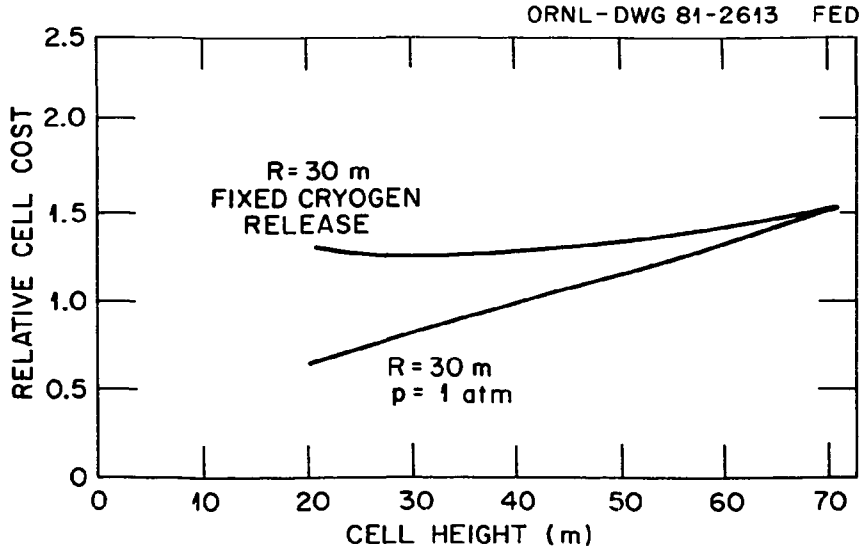

Fig. 8.14. Cell cost variation due to changes in cell height.

For the situation with fixed cryogen release, overpressure, radius, and height are not independent. When two parameters are specified, the third parameter is uniquely determined. As the overpressure is decreased, the cell volume must increase. On the other hand, as the overpressure is increased, the steel thickness must increase to contain the additional pressure. These effects are responsible for the relative minima which appear in Figs. 8.12 and 8.14. When the cell is very large at low overpressures, the cell costs are very large. When the overpressure is very high, the steel costs are large. In between these two effects, a minimum cell cost occurs between overpressures of 2 and 3 atm or between cell heights of 20 and 30 m. The locations of the minima would shift slightly if the base parameters were changed. Figure 8.13 would also exhibit a minimum cell cost if the radius were extended to lower values, but these lower values are below the practical minimum radius for FED and therefore not feasible.

8.9.5 Conclusions and Recommendations

The selection of tokamak cell size, shape, and overpressure for FED is likely to be a function of many variables. Cost will be only one of these factors. However, based on this preliminary study of cell cost, some desirable cell features can be outlined. The cell radius and associated overpressure should be kept as low as practical. On the other hand, cell height has less effect on cell cost and thus is not as important to minimize. If a fixed cryogen release must be contained in the cell, then there may be a minimum cell cost for a specific set of cell parameters that should be considered in selecting cell dimensions.

Additional effort will be needed to identify other important factors and to estimate their impact on cell design. The cost model developed in this study does not account for possible tokamak cell influence on the cost of other facilities and machine designs and, thus, does not give a complete cost picture, even for the parameters studied. For example, increased cell radius will cause increased length of electrical leads and service pipes, which would be an increased cost factor. On the other hand, decreasing the radius may result in reduced maintenance

space, which in turn would require more sophisticated and expensive maintenance equipment.

8.10 SUMMARY

The major conclusions of the FED systems engineering analyses are summarized below.

1. Plasma Minor Radius Variation. Variation in plasma minor radius (with fixed values of neutron wall loading, maximum toroidal field, beta, OH coil flux swing, and inboard shield thickness) exerts a significant effect on burn time and a less pronounced impact on cost and performance (Q). Reduction of the plasma minor radius from 1.3 m to 1.2 m doubled burn time for approximately the same cost. Performance decreases slightly with decreasing plasma minor radius and, conversely, improves slightly with increasing plasma minor radius.

2. Neutron Wall Loading. Capital cost varies almost linearly with neutron wall loading. If it were desired to double the neutron wall loading relative to the baseline, then the capital cost would increase by approximately 80%. For the assumptions adopted here, there appears to be a lower limit on the wall loading imposed by volt-second requirements.

3. Inboard Shield Thickness. Variation in inboard shield thickness over a range of 0.5 m to 0.8 m was found to have very little (approximately 1%) impact on device capital cost. It was determined that while the total radiation dose to TF coil insulation could be held below a level of 10^9 rad with an inboard shield thickness of 0.5 m, refrigeration requirements climbed sharply as the shield thickness dropped below 0.6 m. It was recommended, therefore, that an inboard shield thickness of at least 0.6 m be incorporated in the FED design.

4. Engineering Design Flexibility. The cost penalty of incorporating the design flexibility necessary to (1) take advantage of better than assumed physics performance and/or (2) meet planned objectives in the face of lower than expected physics performance was determined to be approximately 15% relative to the baseline capital cost. The systems most affected are the primary heating systems, the first wall and limiter,

the ac power systems, the heat dissipation systems, and the tritium processing systems. The study indicates that a significant degree of flexibility can be achieved at a moderate increase in capital costs.

5. Number of Full Field Pulses. The number of pulses that FED might sustain over its projected lifetime of ten years is a significant driver in the design of the machine structure. To estimate the number of pulses which the device might be required to sustain, (1) a four-phase program was hypothesized, (2) ground rules for machine utilization were determined for each phase, and (3) the total number of pulses for each phase was established. The total number of pulses (at all field strength levels) was estimated to be 3.6×10^5, with full field pulses totaling approximately 3.1×10^5. On the basis of these results, the study recommendation is that a value of 3.5×10^5 full field pulses be used as the baseline value for all future FED design studies.

A related study aimed at establishing the sensitivity of device size and cost to number of pulses was also carried out. The FEDC systems code was used to develop design parameters and capital costs for pulse requirements from 5×10^4 to 1×10^6. Machine performance parameters and burn time were held fixed. Other device characteristics were varied as required to sustain the specified number of pulses. Study results showed little change in cost or machine characteristics as the number of pulses increased from 5×10^4 to 1×10^5. Above this point, however, total capital cost increased, with the TF coils and associated support structure exhibiting the most significant single cost gain. The study concluded that FED operations requiring from 2×10^5 to 4×10^5 pulses could be accomplished in a reasonable time period (<15 years) without incurring major capital costs. Based on these findings, the recommended design value of 3.5×10^5 full power pulses appears to be reasonable.

6. Facility Options. The initial thrust of the FED facilities study is directed toward (1) definitions of the options and major factors influencing the design of tokamak cell and hot cell areas and (2) an assessment of the design and cost impact imposed by these options. Machine options to be accommodated include: the FED baseline (pump limiter and ICRH bulk heating), substitution of neutral beam injectors

for bulk heating, and substitution of a bundle divertor for the pump limiter. On the facilities side, options include types of construction and their potential application to specific building types, options for the handling of major components during maintenance operations, and options for building configuration and layout. At this stage of the facilities study effort, several feasible approaches have been established. Their development will continue in close coordination with the design of the basic machine.

APPENDIX

FEDC Systems Code

R. L. Reid*

SYSTEMS CODE SUMMARY DESCRIPTION

The FEDC systems code is composed of 26 independent modules executed by a driver program. Each module determines performance, cost, and configuration for a major tokamak component or function. The modular approach was chosen because it allows independent modeling of the various tokamak systems by more than one author and also allows refinement of the modules as long as input and output files remain compatible. An iteration loop is provided to size the shield thickness based on the limiting constraints of nuclear heating in the superconducting toroidal field (TF) coil, displacements per atom (dpa) damage to the copper matrix, radiation dose to the insulation, or provisions for hands-on maintenance within a given time after shutdown. The TF coil bore is sized for the most stringent requirement of ripple consideration or for the minimum size to encircle the plasma plus shield. Coil radial build is determined from consideration of magnetic field, major radius, conductor current density, calculated stresses, and an allowable strain rate. Options for a Moses & Young constant tension coil shape or an arbitrary coil shape are provided. An iteration loop ensures adequate space between TF coils for neutral beam penetration. An option is available for varying the aspect ratio to obtain a given pulse length or for fixing the aspect ratio to determine the maximum pulse length. Pulsed electrical power supplies are modeled as solid-state rectifier/converters buffered from the utility grid by motor-generator (MG) flywheel sets. The reactor cell is modeled as a cylindrical building with a dome.

*Fusion Engineering Design Center/Oak Ridge National Laboratory.

A.1 PHYSICS MODEL

The physics model presently used in the systems code is zero-dimensional (0-D). However, temperature profile effects have been estimated based on normalization to results from a one-and-one-half-dimensional (1-1/2-D) transport code. The density profile across the plasma radius is assumed to be flat. The normalization was done about the plasma parameters specified for the Engineering Test Facility (ETF) design of June 1980. The effects of temperature profile were accounted for on the reactivity $\langle\sigma v\rangle$, on Alcator scaling of confinement time, and on bremsstrahlung radiation in the following manner:

$$\langle\sigma v\rangle \propto [1.4 - 0.3(T_i - 11.6)] \times f(T_i) ,$$

$$\tau \propto [2.1 - 0.042(T_e - 12.40)] \times f(a^2\eta_e) ,$$

$$P_{rad} \propto [1.3 + 0.0084(T_e - 12.4)] \times f(\eta_e^2 Z_{eff}\sqrt{T_e}) ,$$

where

$\langle\sigma v\rangle$ = reactivity,
τ = confinement time associated with conduction and convection losses,
P_{rad} = bremsstrahlung radiation,
a = plasma minor radius,
η_e = electron density,
T_e = electron temperature,
T_i = ion temperature, and
Z_{eff} = effective Z.

Alcator scaling is used for both ion and electron transport. Maximum heating requirements during startup are based on a plasma temperature ramp from the ohmic plasma regime up to the operating temperature while maintaining a constant plasma density. Typical input to the physics module includes: field on axis, aspect ratio, plasma

minor radius, plasma elongation, plasma temperature, beta, and safety factor. Output includes ion and electron densities, fusion power, auxiliary power at the operating point (if any), plasma current, fueling rates, and volt-seconds required for startup.

The physics module is in the process of being updated. A 1-1/2-D code is being streamlined for application in the systems code.

A.2 COST MODEL

Costs are estimated for some components by multiplying the total quantity of material, volume, electrical power, etc., for a given component as determined by the relevant FED systems code modules by appropriate unit cost value (i.e., \$/kg, \$/kW, \$/m^3). For some components, costs are obtained by applying algorithms instead of a single unit cost value. The projected costs are for buildings and equipment only and do not include costs associated with engineering, contingency, etc. Table A.1 presents the major unit cost values and assumptions currently used in the systems code.

Table A.1. Unit cost values and algorithms

Component	Unit cost	Comments
TF coils		
NbTi conductor	$90/kg	
Nb_3Sn conductor	$225/kg	
Stainless steel structure	$26/kg	
PF coils		
Superconducting	$50/kg	
Copper	$30/kg	
Shield		
Stainless steel	$26/kg	
Plasma heating		
Neutral beams	Algorithm	Based on costing 16 subsystems
Ion cyclotron resonance heating	Algorithm	Based on power levels
Electron cyclotron resonance heating	Algorithm	Based on power levels
Vacuum system		
Pumps, valves	Algorithm	Based on pumping speed and duct size; $300/($m^3$/s) for D-T and $750/($m^3$/s) for helium
Tritium		
Fuel processing and emergency detritiation systems	Algorithm	Based on tritium flow rate, containment volume, cleanup time required, etc.

Table A.1 (continued)

Component	Unit Cost	Comments
Electrical		
Pulsed power supplies	Algorithm	Based on cost of converters, protection equipment, bus work, instrumentation
MG sets	Algorithm	Cost is based on megavolt-amperes and stored energy of the MG set
TF power conversion (for superconducting coils)	Algorithm	Based on the cost of four subsystems: dc circuit breakers, dump resistors, power supplies, busing
Substation		
Transformers and circuit breakers	Algorithm	Typically scales as $(MVA)^{0.8}$. Normalized cost is \$25/kVA for FED
Heat transport	Algorithm	Cost scales as $(power)^{0.7}$. Normalized costs for FED are \$20/kW for heat transfer loops and \$20/kW for cooling towers
Refrigerator	Algorithm	Cost is scaled as (cycle-average refrigerator required power)$^{0.7}$. Normalized cost is \$660/kW for FED
Buildings		
Reactor cell	Algorithm	Scales as $(volume)^{0.7}$. Normalized cost is \$500/m^3 for FED

Table A.1 (continued)

Component	Unit Cost	Comments
Hot cell	$270/m^3	
Auxiliary building	270	
Rad waste building	270	
Control building	270	
Administration building	$ 80/m^3	
Service building	80	
Energy storage building	80	
Diesel generator building	80	
Instrumentation and control		A constant value of $36 million is used
Maintenance equipment		A constant value of $25 million is used